AD-A082 494 AIR FORCE AVIONICS LAB WRIGHT-PATTERSON AFB OH F/G 17/7
GRAVITY MODEL EVALUATION FOR PRECISE TERRESTRIAL INERTIAL NAVIG--ETC(U)
DEC 79 R M EDWARDS
UNCLASSIFIED AFAL-TR-79-1231 NL

SECURITY CLASSIFICATION OF THIS PAGE (When Data Entered)

REPORT DOCUMENTATION PAGE

READ INSTRUCTIONS BEFORE COMPLETING FORM

1. REPORT NUMBER: AFAL-TR-79-1231	2. GOVT ACCESSION NO.
3. RECIPIENT'S CATALOG NUMBER	
4. TITLE (and Subtitle): Gravity Model Evaluation for Precise Terrestrial Inertial Navigation: A System Accuracy Approach	5. TYPE OF REPORT & PERIOD COVERED: Final Report, for Period 17 Dec 76 — 15 Dec 79
6. PERFORMING ORG. REPORT NUMBER	
7. AUTHOR(s): Robert M. Edwards, Major USAF	8. CONTRACT OR GRANT NUMBER(s)
9. PERFORMING ORGANIZATION NAME AND ADDRESS: Avionics Laboratory (AFAL/RWA), AF Wright Aeronautical Laboratories, AFSC, Wright-Patterson AFB, Ohio 45433	10. PROGRAM ELEMENT, PROJECT, TASK AREA & WORK UNIT NUMBERS: 16 6095 1514 17 15
11. CONTROLLING OFFICE NAME AND ADDRESS	12. REPORT DATE: December 1979
	13. NUMBER OF PAGES: 292
14. MONITORING AGENCY NAME & ADDRESS (if different from Controlling Office): 12 285	15. SECURITY CLASS. (of this report): UNCLASSIFIED
	15a. DECLASSIFICATION/DOWNGRADING SCHEDULE

16. DISTRIBUTION STATEMENT (of this Report)

Approved for public release; distribution unlimited.

17. DISTRIBUTION STATEMENT (of the abstract entered in Block 20, if different from Report)

18. SUPPLEMENTARY NOTES

Presented to the Faculty of the School of Engineering of the Air Force Institute of Technology Air University in partial fulfillment of the Requirements for the Degree of Doctor of Philosophy.

19. KEY WORDS (Continue on reverse side if necessary and identify by block number)

Gravity	Geopotential Modeling	Upward Continuation
Gravitation	Vertical Deflections	Navigation
Geopotential	Gravity Anomaly	Inertial Navigation
Gravity Modeling	Geodesy	Cruise Missile
Gravitational Modeling	G&C ASALM	ALCM

20. ABSTRACT (Continue on reverse side if necessary and identify by block number)

Inertial navigation has evolved to the point that the traditional gravity model is a principle error source in precise systems. Since future systems may require a more accurate gravity model, a statistical performance evaluation is needed to compare candidate models on realistic scenarios.

The present methods of model evaluation are Monte Carlo, which is computationally costly, and linear state space covariance

DD FORM 1 JAN 73 1473 EDITION OF 1 NOV 65 IS OBSOLETE

SECURITY CLASSIFICATION OF THIS PAGE (When Data Entered)

Ø1-1670

analysis, which has troublesome trajectory and statistical model restrictions. This research developed a new statistical analysis technique based on a double integral expression of the navigation system error covariance. Numerical algorithms were formulated to approximate the covariance, and the accuracy and efficiency of these algorithms were compared using a simple Schuler Loop example analysis. An algorithm based on a pair of nested, single integrals (Nested Integrals) was shown to be more efficient than direct approximation of the covariance double integral and was selected for further development. This Nested Integrals method was verified against linear state space covariance analysis results on a great circle trajectory and against Monte Carlo results on a hypothetical trajectory for an air-launched strategic missile. A 30:1 computational efficiency advantage over Monte Carlo was demonstrated. The errors of linear state space analysis were demonstrated by violating the trajectory restriction. In a final development, the Nested Integrals algorithm was modified to account for Kalman filter updates of navigation estimates based on external measurements. In summary, a new gravity model evaluation method, more efficient than Monte Carlo and more flexible than linear state space covariance analysis, was developed and verified.

FOREWORD

This report describes in-house effort conducted by personnel of the Reference Systems Branch (RWA), Reconnaissance and Weapon Delivery Division (RW), Air Force Avionics Laboratory, Wright-Patterson Air Force Base, Ohio, under Project 6095, "Inertial Reference and Guidance Technology", Task 609515, "Reference System Software Development and Evaluation", Work Unit 60951514, "Gravity Modeling for Precise Terrestrial Inertial Navigation". This report is, in essence, a dissertation submitted by Maj Robert M. Edwards to the School of Engineering, Air Force Institute of Technology, Wright Patterson Air Force Base, Ohio, in partial fulfillment of the requirements for the degree of Doctor of Philosophy.

The work reported herein was performed during the period 17 December 1976 to 15 December 1979, under the direction of the author, Maj Edwards (AFAL/RWA-3), project engineer. The report was released by the author in December 1979.

A number of individuals have contributed to this research by direct assistance and by offering encouragement or advice. I wish to gratefully acknowledge this support. Dr. James Negro, now with the Charles Stark Draper Laboratory, was initially the principle advisor, and his advice and guidance led to a clear definition of the research project. Several individuals and organizations contributed to the definition of the problem. Principle contributors were: Dr. Don Eckhardt, Mr. Bela Szabo, and Mr. George Hadgigeorge of the Air Force Geophysics Laboratory; Dr. Tom Davis of the Naval Oceanographic Office; Mr. Ed Roof of the Army Engineer Topographic Laboratories; Mr. Lou Decker of the Defense Mapping Agency Aerospace Center; Dr. Ray Nash, Dr. Stanley Jordan, and Dr. Warren Heller of The Analytic Sciences Corporation; Mr. Morris Bennett of Geodynamics Corporation; Mr. Ken Fertig, Dr. Gervasio Prado, and Mr. Bill Robertson of the Charles Stark Draper Laboratory; and Dr. Richard Rapp of Ohio State University. Major Gary Reid accepted the responsibility of principle advisor and has provided valuable support and guidance. Dr. Peter Maybeck, a committee member, and Mr. Stanton Musick have provided advice and general support throughout the effort. For their critical review of the dissertation, I thank Dr. David Lee and Captain William Weisel, both members of my doctoral committee. I am grateful to Mr. William Shephard of the Air Force Avionics Laboratory for both

material and moral support. Mrs. Libby Ditmer deserves credit for her careful review of the draft dissertation. Mr. David Kaiser has provided timely advice on the difficult computational issues that this research raised. Mrs. Shirley Suttman has provided support throughout this research. Mr. Kenneth Cunningham and Mrs. Clarenda Jackson were invaluable in producing the graphical results for the dissertation.

Contents

Contents

Contents

List of Figures

List of Figures

List of Figures

List of Tables

Notation

Over 200 symbols or acronyms appear in this work. The most important of these are listed below with a short description and with a reference page. Vectors, physical or mathematical, are underlined. Vectors are usually lower case Greek or Roman characters (exceptions: $\underline{G}$ and $\underline{G}_m$); whereas, matrices are always upper case Greek or Roman characters. Scalars are usually lower case Greek or Roman characters (without underline). The list of symbols and acronyms is divided by font into (1) lower case Roman, (2) upper case Roman, (3) lower case Greek, (4) upper case Greek, (5) script, and (6) other.

Lower case Roman

Symbol	Description	Page
$\underline{a}$	total acceleration vector	2
c_n	anomaly degree variance	138
d	correlation distance or parameter	71
d	depth to anomalous potential white noise process	130
e	subscript - east horizontal axis	90
$\underline{f}$	specific force	2
g	magnitude of gravity	95
h	altitude	95
i	great circle earth-relative inclination	94

Symbol	Description	Page
n	subscript - north horizontal coordinate	90
n	superscript - navigation coordinate *frame (east-north-vertical)*	90
$\underline{q}$	vector of white gaussian noises for gravity disturbance model	16
$\underline{r}$	position vector	2
s_n	integrand weighting in discrete summation	40
t	time	11
t_o	initial time	26
$\underline{u}$	geodetic error driving terms	11
$\underline{v}$	velocity vector	2
$\underline{v}$	measurement noise	150
$\underline{w}_f$	white noise for filter model	149
$\underline{x}$	navigation error state vector	11
$\underline{x}_a$	augmented system state vector	17
$\underline{x}_g$	*gravity shaping filter state* vector	16
$\underline{x}_f$	filter model state vector	149
z	subscript - vertical (up) axis	90
$\underline{z}$	vector of measurements	150

Upper case Roman

A	parameter in c_n definition	138
B	parameter in c_n definition	138

Symbol	Description	Page
C_g	gravity shaping filter output matrix	17
CEP	circular-error-probable	1
D	intermediate matrix in Nested Integrals	33
F	Navigation error propagation matrix	11
F_a	augmented system propagation matrix	17
F_g	gravity shaping filter propagation matrix	16
F_f	filter model propagation matrix	149
$\underline{G}$	gravitational acceleration	2
G	navigation error distribution matrix	11
G_a	augmented system distribution matrix	17
G_f	filter model distribution matrix	149
G_g	gravity shaping filter distribution matrix	16
$\underline{G}_m$	gravitational model	2
H	measurement matrix	150
I	identity matrix	19
INS	inertial navigation system	18
K	matrix of Kalman gains	151
N	undulation (or height) of the geoid	116
P	navigation error covariance matrix	26

Symbol	Description	Page
P_a	augmented state covariance matrix	17
P_f	filter model covariance matrix	150
P_g	gravity shaping filter state covariance matrix	83
Q	geodetic error correlation matrix function	31
Q_f	filter model noise strength	149
Q_g	gravity shaping filter noise strength	17
Q_v	filter model velocity channel noise strength	157
Q_ϵ	filter model attitude channel noise strength	157
R	radius of sphere approximating earth surface	130
R	measurement noise strength	151
R_e	earth radius	95
T	anomalous potential	32
T	superscript - transpose matrix	17
U	gravitational potential	135
V	horizontal velocity component	71
$\underline{V}$	earth-relative horizontal velocity (ground speed)	228
X	vector cross product	230
Lower case Greek		
α	heading angle	218
β	feedback gain	73
γ	resolvent angle in CEP calculation	241

Symbol	Description	Page
δ	Dirac delta function $\delta(x) = 0$ for all $x \neq 0$ $\int_{-\epsilon}^{+\epsilon} \delta(x)dx = 1$ for all $\epsilon > 0$	17
δ_n	integrand weighting function	54
$\delta\underline{g}$	gravity disturbance vector	4
$\overline{\delta\underline{g}}$	ensemble vector of gravity disturbances	118
$\delta\underline{r}$	position error	15
$\delta\underline{v}$	velocity error	90
$\delta\lambda$	longitude error	90
$\delta\phi$	latitude error	90
$\underline{\epsilon}$	attitude error	90
ζ	damping coefficient	81
η	prime deflection of the vertical	32
θ	arbitrary element of Θ	26
θ_o	design mission or trajectory	26
λ	longitude	136
μ	crossrange (transverse) deflection of the vertical	116
$\mu_\oplus$	earth gravitational constant	136
ν	intermediate quantity	81
ξ	meridional deflection of the vertical	32
σ_g^2	anomaly variance	95
σ_r^2	variance of measurement error	158

Lower case Greek

Symbol	Description	Page
τ	downrange (inplane) deflection of the vertical	116
ϕ	latitude	213
ϕ_{gg}	anomaly correlation function	101
ϕ_{TT}	correlation of T	174
ψ	central angle	100
$\underline{\omega}$	inertial angular velocity	3
ω_{ie}	earth rotation rate	95
ω_s	Schuler angular velocity	70

Upper case Greek

Δg	gravity anomaly	101
Δt	time increment for integration approximation	40
Θ	mission sample space	26
Φ	navigation error state transition matrix	28
Φ_a	augmented system state transition matrix	17

Script

$\mathscr{e}$	exponential	71
$\mathscr{E}$	expectation operator	17
$\mathscr{l}$	downrange (inplane) deflection of the vertical	116
$\mathscr{M}$	mean operator	243

Other

Symbol	Description	Page
o	subscript for initial time	26
0	matrix zero	55
∇	gradient operator	136

I. Introduction

Inertial navigation has evolved to the point that the traditional gravity model is a principle error source in advanced, precise systems. Future autonomous strategic systems, such as the cruise missile, will likely require a more accurate gravity model. Mission success depends on navigation system accuracy not gravity model accuracy per se. So an improved gravity model should be judged by system-level performance expressed, for example, as circular-error-probable (CEP). The objective of this research is to develop a new computational technique whereby alternative gravity models can be compared by expected navigation system accuracy on realistic mission scenarios.

This section presents a discussion of the background and motivation for the research. The role of the gravity model and the navigation system errors induced by this model are interpreted for this study. The need for a statistical evaluation is explained, and the present methods for performing such analyses are discussed. The shortcomings of these present statistical evaluation methods are given as motivation for the research.

1.1 The Role of the Gravity Model in Inertial Navigation

The gravity model in an inertial navigation system is a subsystem or component providing one part of the information required for navigation position, velocity and

attitude estimates (see Figure 1). The exact role of the gravity model, the nature of modeling errors, and the effect of such errors on navigation estimates must be understood to appreciate the impetus for gravity model improvements.

An inertial navigation system senses the vehicle dynamics and applies the laws of physics to estimate position, velocity and attitude. The inertial navigation system performs two fundamental tasks. First, the vehicle rotational velocity $\underline{\omega}$ is measured and used to track attitude. Second, position $\underline{r}$ and velocity $\underline{v}$ are computed by integrating an estimate of acceleration $\underline{a}$.

The total vehicle acceleration cannot be sensed, since the gravity field acts on both the vehicle and the accelerometers. The total acceleration is given by

$$\underline{a} = \underline{f} + \underline{G} \tag{1}$$

where $\underline{f}$ is the specific force (force per unit mass) from contact forces such as aerodynamic drag and $\underline{G}$ is gravitational acceleration due to mass attraction acting on the vehicle. The estimate of acceleration is made by

$$\hat{\underline{a}} = \tilde{\underline{f}} + \underline{G}_m(\hat{\underline{r}}) \tag{1a}$$

where "^" indicates navigation estimates, "~" indicates measured data, and $\underline{G}_m(\cdot)$ is the gravitation model.

The gravity model term in (1a) introduces error by

a. Modeling errors, and

b. Evaluation errors

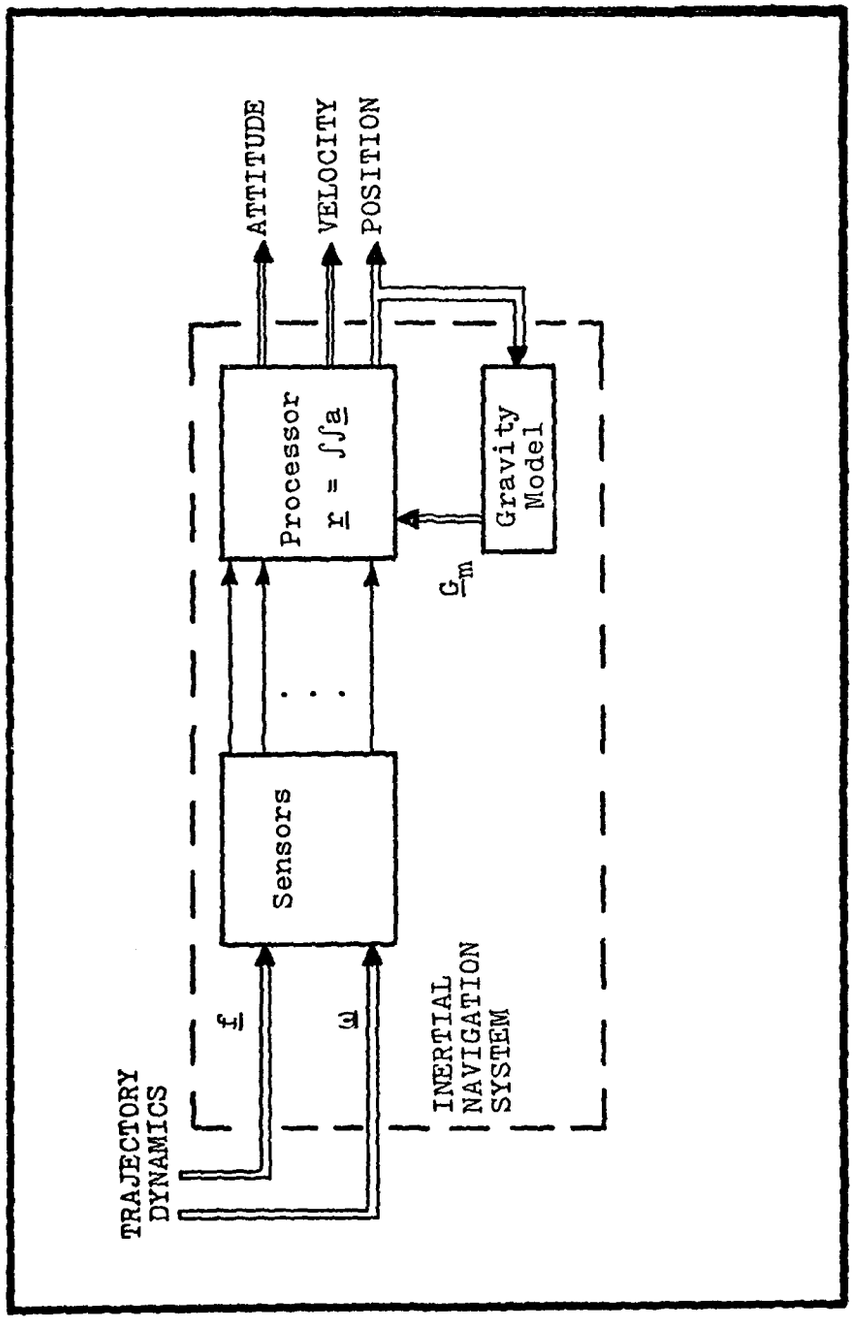

Figure 1. Role of the Gravity Model in Inertial Navigation

The evaluation errors come from evaluating gravitation at an erroneous position $\underline{r}$. This evaluation error is responsible for the principle navigation system error mode - the Schuler mode. The evaluation error is not an error induced by the model and is therefore considered part of the inertial navigation error propagation. The modeling error can be stated as a gravity disturbance

$$\delta\underline{g}(\underline{r}) = \underline{G}_m(\underline{r}) - \underline{G}(\underline{r}) \qquad (2)$$

given perfect position information. This error of (2) introduced by (1a) creates the navigation system errors which are the subject of this work.

1.2 The Traditional Gravity Model

The gravity model used in most present operational inertial navigators is based on a gravity field perpendicular ("normal" field) to an ellipsoid which approximates the mean sea-level equipotential surface called the geoid. In some instances, zonal spherical harmonic or spheroidal equipotential surface models are used as a basis for the gravity model. The associated simple gravity models are within 400 mgal* of measured gravity values.

The use of such simple models has been prevalent for two reasons. First, computational resources are limited for the on-line application. Second, the presence of other system error sources has, in the past, reduced the incentive

---

* 1 mgal = 10^{-3} galileo = 10^{-3}cm/sec^2 = 10^{-5}m/sec^2 $\approx$ 1μg

for a more complex and accurate model. Kayton [Ref 1] in 1960 suggested that these simple models are sufficient for system with accelerometer uncertainty greater than 20 mgal -- an estimate at that time of gravity disturbance standard deviation.

1.3 Impetus for Model Improvement

Since the late 1940's, inertial navigation design has progressed to a fine art. Refinements have been concentrated principally in inertial instrument design and calibration with other basic concepts essentially intact. The error levels of periodically recalibrated inertial components have reached the point that the traditional gravity model is now a principle error source in overall system accuracy. It is easy to understand why a detailed new model might be used in a flight test environment where data purity is important. However, one could question the need on-line for model refinements since the errors induced are not unacceptable for most navigation applications. The impetus comes from the potential military application -- where the impetus for inertial navigation originated. In the autonomous delivery of weapons, any error significantly diminishes weapon systems's effectiveness, so these gravity induced errors cannot be ignored. The self-contained nature of inertial navigation virtually assures a continued military application even with advanced radiometric navigation systems available. The evolution of strategic forces to

include cruise missile concepts provides the prime motivation for the increased emphasis on refining the traditional gravity modeling used in on-line inertial navigation.

1.4 The Need for Model Performance Evaluation

The need for an improved gravity model may be met using existing data base and on-line modeling methods [Ref 2]. While future research may refine and make them more efficient, several methods of computing gravity exist today. These methods are primarily based on Green's and Stoke's theorems [Ref 3] which require data over a closed surface (approximately) encompassing all earth mass. Heretofore, data limitations over vast ocean expanses have diminished the accuracy of these models. Recent satellite altimetry measurements give an estimate of the anomalous potential* over much of these regions. These new data can be combined with existing gravity data using heterogeneous data processing techniques [Ref 4]. This increased data base can then be used to identify parameters of a more precise model for on-line application.

The gravity models which might be used on-line have many forms. The canonical form is the Legendre function expansion based on a Fourier series representation of the geoid. This spherical harmonic series can theoretically be expanded to any degree and order required to yield a residual

---

* See Reference 3 and Appendix A for definitions of anomalous field quantities.

field below some arbitrary magnitude [Ref 3]. Measurement errors and computational costs argue against carrying such modeling to the extreme, however. This form of globally applicable functional approximation is countered by other methods which seek to describe gravity in a smaller region using interpolating functions [Ref 5]. The rationale is that fewer coefficients, hence fewer calculations, may be required for the same accuracy within a restricted region. The point mass grid of the MINUTEMAN launch region gravity model [Ref 6] is a compromise between these extremes. While this model is a globally valid approximation, it has more detail and greater accuracy in the critical launch region. The Poisson integral, Stoke's integral, and the coating method [Ref 2:39-54] give a more direct link between measured data on one hand and gravity estimates on the other. Approximations of field theory integrals constitute alternate forms of gravity modeling.

1.5 Present Methods for Evaluating Alternative Gravity Models

An abundance of modeling methods exists then. What is lacking is a consistent way of comparing models and specifically evaluating the error contribution to inertial navigation performance corresponding to each candidate model. There are two fundamentally different methods of calculating a system accuracy measure: deterministic and statistical. In a deterministic analysis a complex gravity

model is used as the "truth" model. The design mission is simulated, and the resulting inertial navigation estimates are compared to the true position, velocity and attitude. This deterministic study yields error as a function of time. The resulting error profile is only valid for that particular mission and, hence, should be considered one (simulated) sample out of the set of possible missions. Since the truth model is limited in scope (it still has errors of omission) and has an inherently inaccurate data base (errors of commission cannot be avoided), some residual uncertainty remains in even this result.

The statistical approach, on the other hand, frankly admits these model uncertainties at the outset and proposes to project these model errors in terms of navigation performance. To this end, the statistics of the residual field (correlation function) coupled with a model of either the inertial navigator per se or of the error propagation in the inertial navigator are used to produce estimates of inertial navigation error statistics. The general strategy of statistical analysis is presented in Figure 2.

1.6 Trajectory Models

The trajectory model includes all environmental, dynamic and ambient condition data required for analyses. Usually, position, velocity, specific force, and attitude are sufficient. Other conditions such as temperature may influence the operation of the inertial system enough

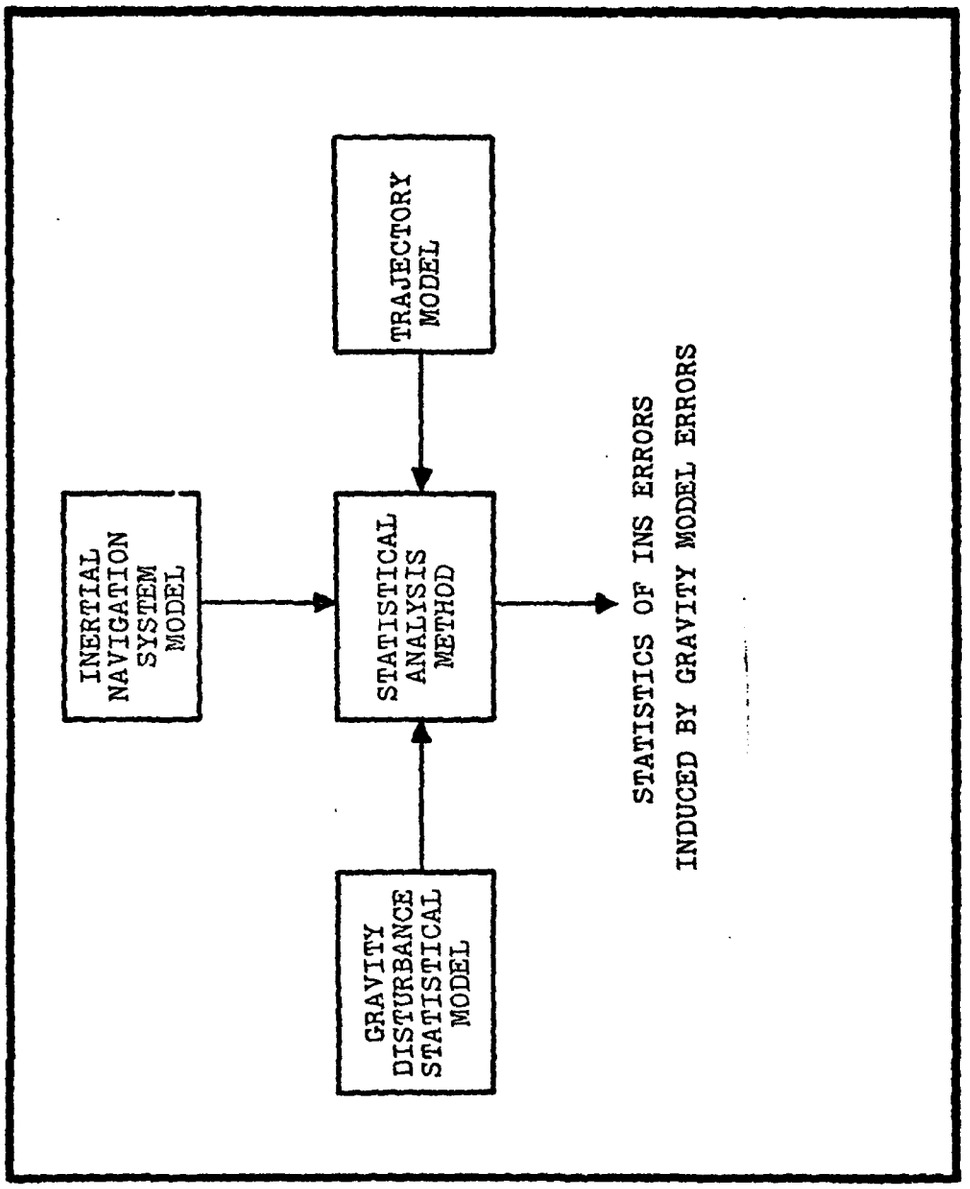

Figure 2. General Strategy of Statistical Analysis

to warrant modeling. For the basic problem of providing trajectory information, two clear methods exist.

For relatively simple trajectories, closed-form mathematical expressions can be derived and offer a computationally efficient manner of providing the required data. Examples of this type of model are used in Section IV studies.

While complex trajectories could theoretically be decomposed into a finite number of simple segments, deriving closed-form expressions becomes an onerous burden. Computer approximation based on the kinematic relationships of such segments can be programmed and offers a flexible method of generating the design mission data. The PROFGEN [Ref 7], profile generator, program developed by Musick is an excellent example of this approach. The program accepts mission phase specifications as inputs. The results for contiguous segments are abutted, and the overall mission trajectory is the output.

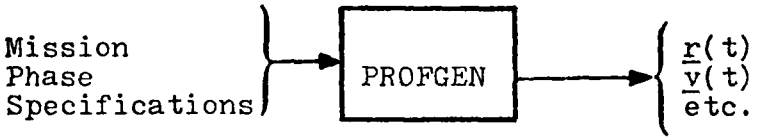

Adequate methods exist to furnish the trajectory information required in the statistical analysis. The great flexibility of these methods should handle any conceivable navigation mission. Examples are presented in later sections using both closed-form trajectories and PROFGEN approximations.

1.7 Inertial Navigation System Model

The inertial navigation system has been modeled by two methods which should be adequate for any statistical analysis: whole-valued simulation and error propagation model. The navigation system model used may be dictated by the analysis method, but analyses have been conducted with both of these model types.

The whole-valued simulation is a direct simulation of the inertial navigation algorithm. Errors are simulated in the input data to the algorithm and are observed in the output navigation estimates. In modern navigation systems, the algorithm is already in the form of a digital computer program, so the operational algorithm may be used directly. More generally, the double integration of acceleration may be used as a generic navigation system model with no direct link to an existing system.

The second method is simply a first-order approximation of the propagation of errors through the inertial navigation system. Only the errors and not the whole-valued estimates are modeled. Britting has shown that this first-order error model can be formulated in a general manner [Ref 8]. This formulation can be cast in the form of a first-order, vector differential equation [Ref 9: Equation 3-1, p22]

$$\dot{\underline{x}}(t) = F(t)\underline{x}(t) + G(t)\underline{u}(t) \qquad (3)$$

where

$\underline{x}(t)$ is an n-state mathematical vector of navigational errors in position, velocity, and attitude estimates

$F(t)$ is an nXn error propagation matrix relating error rate to present state;

$\underline{u}(t)$ is an m-dimensional vector of gravity disturbance quantities; and

$G(t)$ is an nXm distribution matrix.

Note that for this work, $\underline{u}(t)$ contains only those terms associated with geodetic errors. For example, $\underline{u}(t) = \delta\underline{g}(t)$. Other system error sources such as accelerometer bias and gyroscopic drift are assumed to be zero, so the results obtained here will reflect the effects of geodetic errors alone.

The whole-valued simulation contains nonlinearities which the error propagation model loses by the first-order expansion. The error propagation model has, however, been widely accepted since it accurately models navigation system behavior observed in flight tests. Either of these methods, then, will sufficiently model the inertial navigation errors to support the statistical analysis.

1.8 Gravity Disturbance Statistical Models

The statistics of the disturbance field for a particular gravity model can be summarized in one scalar correlation function (see Appendix A). With this function as a

basis, all other auto- and cross-correlations of anomalous gravity terms can be derived [Ref 4]. Field theory provides the functional interrelationships between these terms [Ref 3]. Models for these basic functions have been developed -- primarily using gravity anomaly autocorrelation function as a basis. Three of the fully developed models are:

a. Linear state space based on a Gauss-Markov process,

b. Anomaly degree variance based on a spherical harmonic expression of the correlation function, and

c. Attenuated white noise based on a subterranean white noise process for anomalous potential.

Details of these models will be presented in examples of Sections IV, V, and VI. For now, the point is that adequate models exist to support the statistical evaluation.

1.9 Present Methods of Statistical Analysis

The central element (Figure 2) of the general strategy is the analysis method. This method combines the three models just discussed to produce an estimate of the navigation system error statistics caused by the errors in modeling gravity. Two distinct approaches have been taken in the past: Monte Carlo and linear state space covariance analysis. These methods differ considerably and must be explored separately to appreciate the inherent strengths and weaknesses of each.

1.9.1 Monte Carlo Method

First, the Monte Carlo method takes a direct mission simulation approach (Figure 3). It is, in fact, an ensemble of deterministic cases corresponding to an ensemble of residual field realizations. The gravity disturbance profiles are produced in such a way that in the limit they match the correlations given by the residual field correlation function. These simulations may be either of the navigation equations directly (whole-valued simulation) or of navigation error propagation. In either case, the ultimate output of these simulations is an ensemble of error-time histories from which means, standard deviations, covariances, and other sample statistics can be calculated. Since histograms can be formed for any particular error at any point in time, a frequency function can be approximated. This feature is not of significant importance to this work since second order statistics are usually sufficient to specify system accuracy.

The significant cost of the Monte Carlo method is the computation time required to simulate the trajectories. Enough cases must be run to yield statistics of high confidence. In a recent advanced cruise missile study, Chatfield [Ref 10] used 90 simulations to produce the desired circular-error-probable statistic.

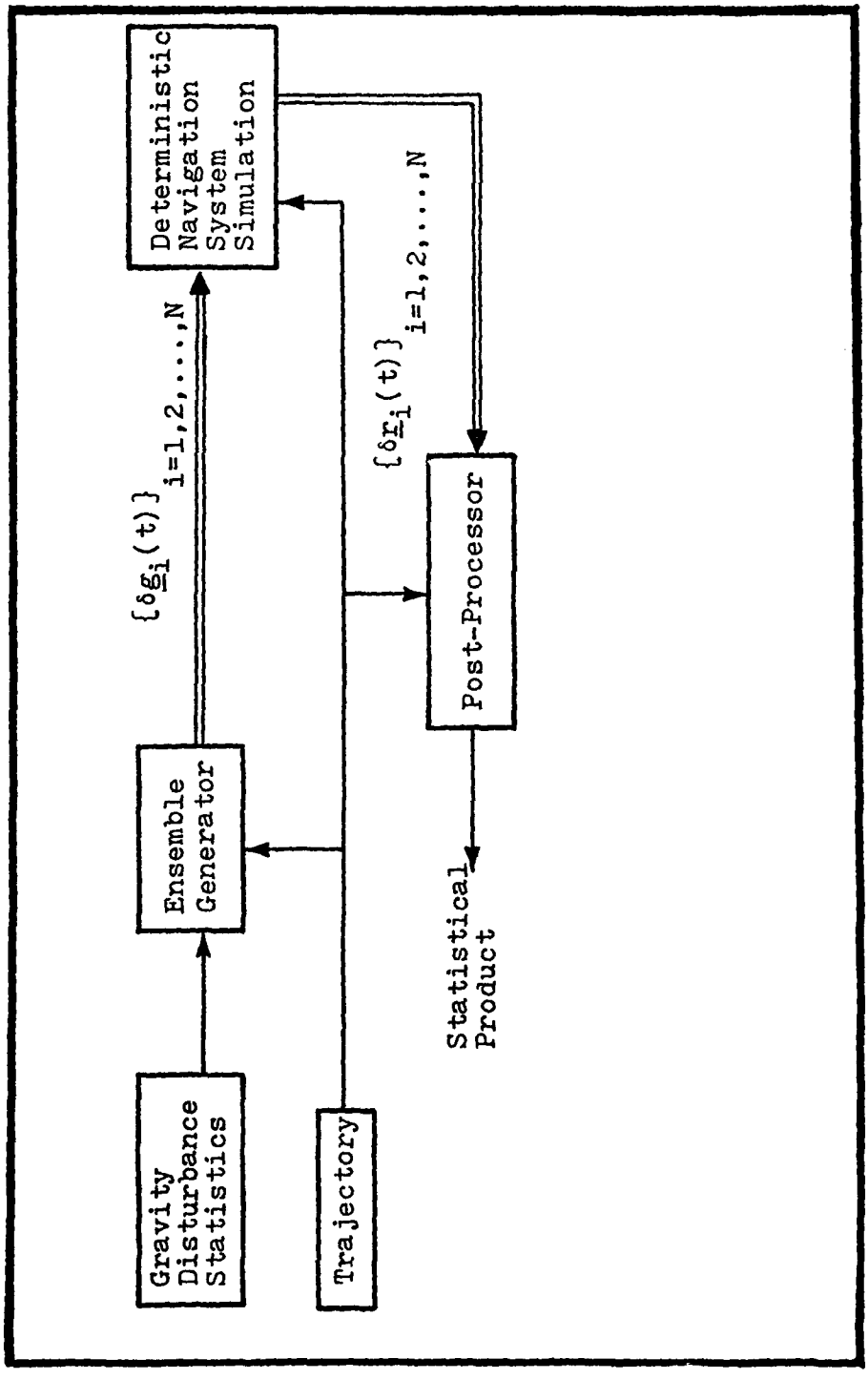

Figure 3. Monte Carlo Method

While this cost is considerable, the fact that the analysis could be performed demonstrates the flexibility of this method. The Monte Carlo restrictions on trajectory are minor, being essentially limited to the ones imposed by the trajectory simulator. In addition to this scenario flexibility, considerable freedom exists in the functional form of the correlation model. The gravity disturbance profiles are produced using the residual field correlation function. While the residual field is dependent on the gravity model, there are, as noted above, several developed functional models to summarize the correlations of the residual field. The Monte Carlo method imposes no limitation on the functional form of the correlation model.

1.9.2 Linear State Space Covariance Analysis

The linear state space covariance approach was formulated by Levine and Gelb in a landmark paper [Ref 11] in 1968. This method and the attendant stochastic gravity model have been refined to be consistent with most of the field theory impositions [Ref 12].

The gravity disturbance terms, $\underline{u}$, are modeled as the output of a linear filter driven by white, gaussian, independent noise sources. The state vector model of this linear filter is

$$\dot{\underline{x}}_g(t) = F_g(t)\underline{x}_g(t) + G_g(t)\underline{q}(t) \qquad (4)$$

where $\underline{q}(t)$ is a white gaussian noise process.

The output equation to form the disturbance terms is

$$\underline{u}(t) = C_g(t)\underline{x}_g(t) \tag{5}$$

The white noise terms, $\underline{q}(t)$, are modeled to have correlation

$$\mathcal{E}[\underline{q}(t)\underline{q}^T(p)] = Q_g(t)\ \delta(p-t) \tag{6}$$

where $\delta(\cdot)$ is the Dirac delta function. An augmented state (see Figure 4) can now be defined as

$$\underline{x}_a(t) = \begin{Bmatrix} \underline{x}(t) \\ \cdots\cdots \\ \underline{x}_g(t) \end{Bmatrix} \tag{7}$$

The augmented state vector differential equation is

$$\dot{\underline{x}}_a(t) = F_a(t)\underline{x}_a(t) + G_a(t)\underline{q}(t) \tag{8}$$

where

$$F_a(t) = \left[\begin{array}{c:c} F(t) & G(t)C_g(t) \\ \cdots\cdots & \cdots\cdots\cdots \\ 0 & F_g(t) \end{array}\right] \tag{9}$$

and

$$G_a(t) = \begin{bmatrix} 0 \\ \cdots\cdots \\ G_g(t) \end{bmatrix} \tag{10}$$

With this augmented form the system covariance integral becomes

$$P_a(t) = \int_{t_o}^{t}\int_{t_o}^{t} \Phi_a(t,p)G_a(p)Q_g(p)\delta(q-p)G_a^T(q)\Phi_a^T(t,q)\,dpdq \tag{11}$$

where

$$\dot{\Phi}_a(t,t_1) = F_a(t)\Phi_a(t,t_1) \tag{12a}$$

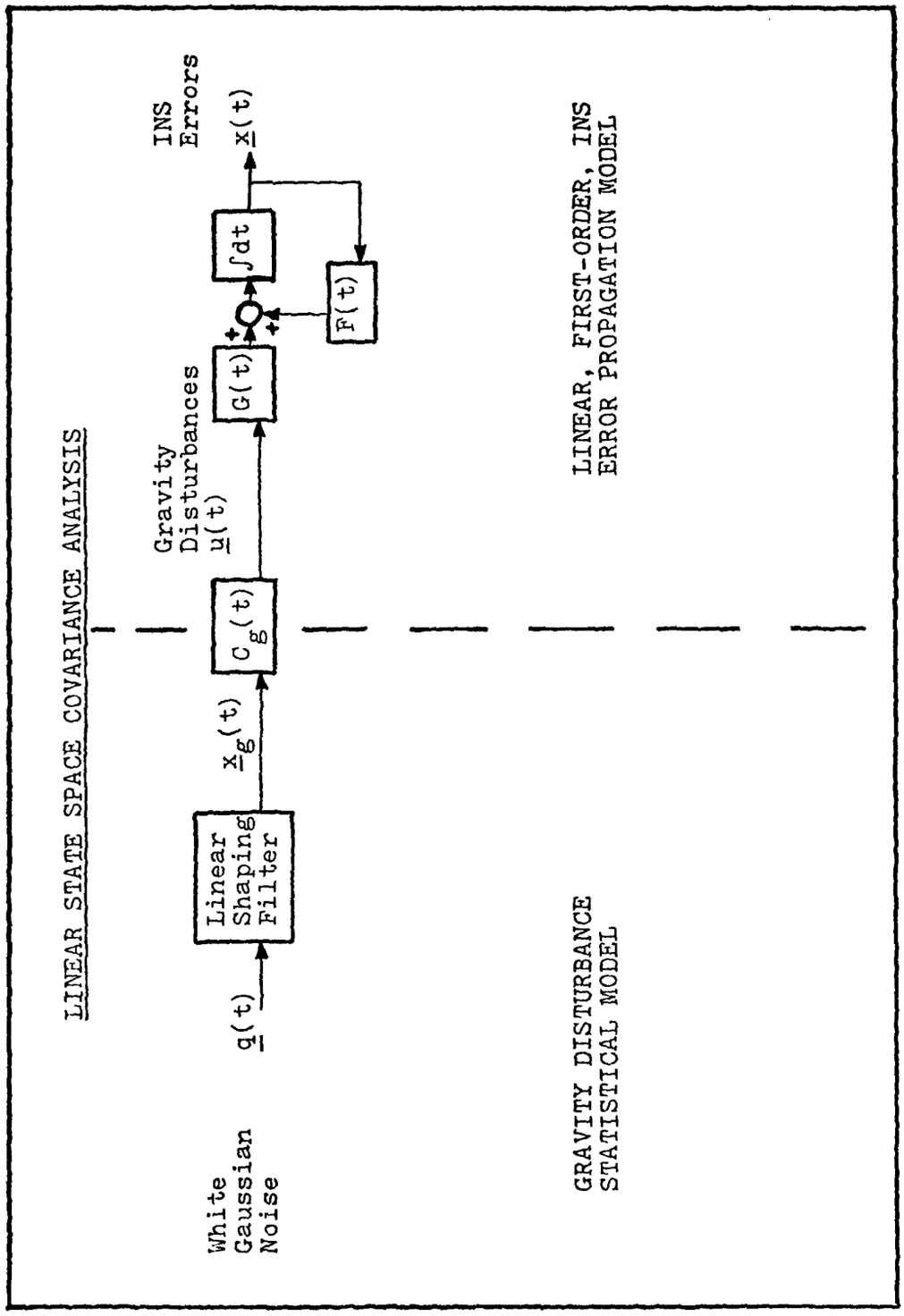

Figure 4. Linear State Space Covariance Method Model Interface

subject to

$$\Phi_a(t_1, t_1) = I \tag{12b}$$

The delta function allows a reduction to

$$P_a(t) = \int_{t_o}^{t} \Phi_a(t,p) G_a(p) Q_g(p) G_a^T(p) \Phi_a^T(t,p)\, dp \tag{13}$$

Applying Leibnitz' rule now yields

$$\dot{P}_a(t) = F_a(t)P_a(t) + P_a(t)F^T(t) + G_a(t)Q_g(t)G_a^T(t) \tag{14}$$

This equation can be solved numerically by a number of powerful and efficient numerical integration techniques. The fact that the solution can be cast in this mold is the most persuasive argument for using linear state space methods.

The key to this efficiency is the delta function which allows one level of integration to be solved directly without approximation. The Gauss-Markov model which produced this advantage is the root of errors that can result when linear state space covariance analysis is used on complex trajectories.

Obviously, the linear state space covariance analysis restricts the gravity disturbance statistical model form to one compatible with linear state space description. This restriction, while undesirable, is much less serious than the loss of trajectory generality which accompanies the time-domain use of the Gauss-Markov model. Gravity disturbance is a spatial function and hence the statistical representation is a spatial process. The conversion from

spatial to a temporal representation of the statistical process, symbolized in Figure 5, causes the resulting model to err when the trajectory varies from a particular form.

The details of the spatial to temporal model conversion are presented in Appendix B. To understand why this conversion creates error, one need only consider the variables involved. The spatial model has central angle, ψ, as an independent variable. Central angle is not a scalar since, in general, the total central angle change is not equal to the sum of the central angle changes along mission segments. Time is a scalar and the conversion to the time independent variable means that the underlying relationship is mismodeled, in general. For the special case of a great circle trajectory, the total central angle change is the sum of the segment changes and the conversion is also only strictly valid for great circle missions with non-decreasing central angle of less than 180^{o}.

Another trajectory restriction is imposed by the original spatial Gauss-Markov model. This formulation does not treat changes in altitude, and therefore, the model is only valid for constant altitude trajectories as well. Equivalent statistics may be calculated from the original at other altitude levels [Ref 13]; however, combining these into a linear system format requires some improvisation.

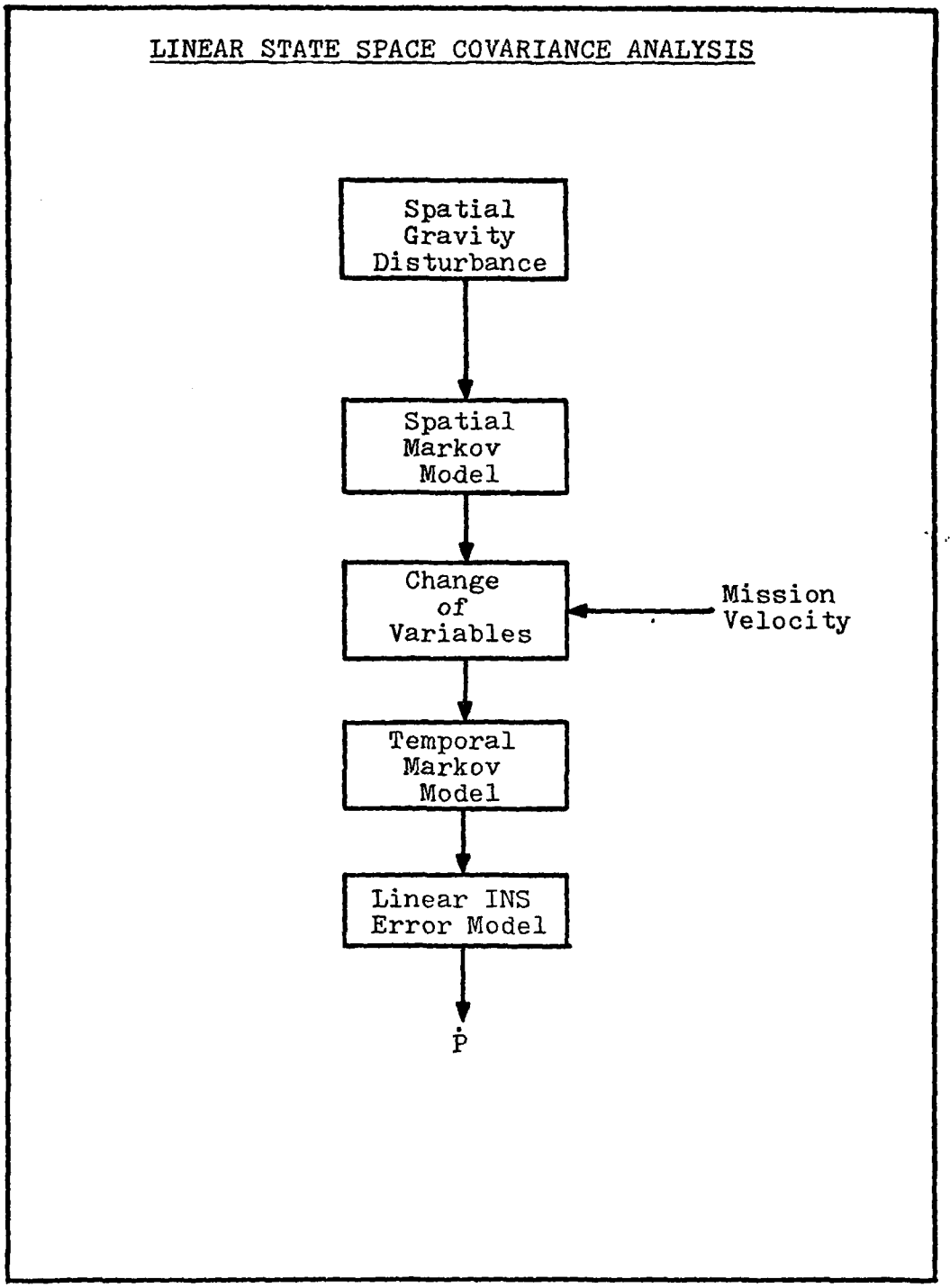

Figure 5. Linear State Space Covariance Analysis Genealogy

In summary then, the only trajectory for which the linear state space covariance analysis is valid is a constant altitude, great circle case with a monotonically non-decreasing central angle of less than 180^{o}. So, the considerable computation efficiency achieved through (14) has the severe trajectory limitations as a price. Although the trajectory restrictions of the Gauss-Markov model are well-known, the extent of errors induced when the trajectory restrictions are violated is not known. Numerical examples will be presented in Section IV to explore this area.

1.10 Motivation for Research

Adequate models exist for trajectory, for navigation system, and for gravity disturbance statistics, but the two present methods of statistical analysis have serious disadvantages which limit their usefulness. The Monte Carlo method has virtually no restrictions, but the requirement to produce samples until the statistics stabilize is often costly. On the other hand, the trajectory restrictions of the linear state space covariance method significantly limit the usefulness of this method. The gravity disturbance statistical model is also limited to a particular Gauss-Markov form for the linear state space method, and this constraint might limit the utility of this evaluation method on some alternative on-line gravity models such as a truncated spherical harmonic model.

An alternative to these methods is needed which is more flexible than linear state space covariance analysis and which is more efficient than Monte Carlo. To develop such an alternative is the objective of this research.

1.11 Overview of the Research

The following sections document the research to develop, verify and demonstrate the alternative statistical analysis method. Section II presents the theoretical development and Section III the numerical method. The new method is compared to the linear state space method in Section IV and to Monte Carlo in Section V. These comparisons constitute a thorough verification of both the theoretical and numerical aspects of the new analysis technique. Demonstrations are then presented (Sections VI, VII, and VIII) which show the flexibility of this new analysis method to treat a variety of gravity models and gravity disturbance statistical modeling methods. In a final development, the effects of Kalman filter updates on gravity induced navigation error statistics are included (Section IX) in the analysis algorithm, and this update process is verified. In all, a new statistical analysis technique is presented to evaluate the system errors induced by gravity modeling errors.

II. Development of a Gravity Model Performance Measure Based on an Inertial Navigation Error Covariance Integral

In Section I, the present methods of statistical analysis were reviewed. The Monte Carlo method, while flexible, has significant computational cost. The linear state space covariance analysis is computationally efficient but has unacceptable trajectory restrictions associated with the Gauss-Markov gravity disturbance statistical model. To develop an efficient yet flexible alternative analysis method, a line of development is suggested which is parallel to the linear state space (Figure 5) but which avoids the dependence on the Gauss-Markov statistical model. The purpose of this section is to present the theoretical development of the covariance integral as a candidate alternative statistical analysis method.

2.1 General Approach

The genealogy of the linear state space covariance analysis method (portrayed symbolically in Figure 5) and the parallel approach to be taken here are shown in Figure 6. The crucial change-of-variables (from central angle ψ to time t) does not occur in this new "covariance integral" formulation; the spatial dependence of the correlations is retained. This approach does not exclude the Gauss-Markov gravity disturbance statistical model from use. But, it does mean that the gravity disturbance correlations from

that model are used directly, and not the temporal linear filter model of gravity disturbance (4). As a consequence, the integral expression of the navigation error covariance will not contain a simplifying Dirac delta function as in (11). The covariance integral becomes, then, the end object of the theoretical development. The final analysis will be simply a numerical approximation of this integral. Theoretical development of the new "covariance integrals" statistical evaluation method is made in the next subsection.

2.2 The Covariance Integral Theoretical Development

The sample space definition is the key to any statistical analysis. The view taken here is that the desired error statistics represent, in a performance index sense, the expected performance over some range Θ of possible missions. Then to produce statistics representative of missions in Θ, the statistical expectation must be over all $\theta \in \Theta$. A mission θ is simply a position-time history or trajectory and corresponds to one sample from the space Θ. For each θ, a navigation propagation characteristic is defined and a gravity disturbance is generated. This disturbance is implicitly a function of time being explicitly dependent on the $\underline{r}(t)$ dictated by θ. Then the navigation error dynamics (3) may be written as

$$\dot{\underline{x}}(t;\theta) = F(t;\theta)\ \underline{x}(t;\theta) + G(t;\theta)\ \underline{u}(t;\theta) \qquad (15)$$

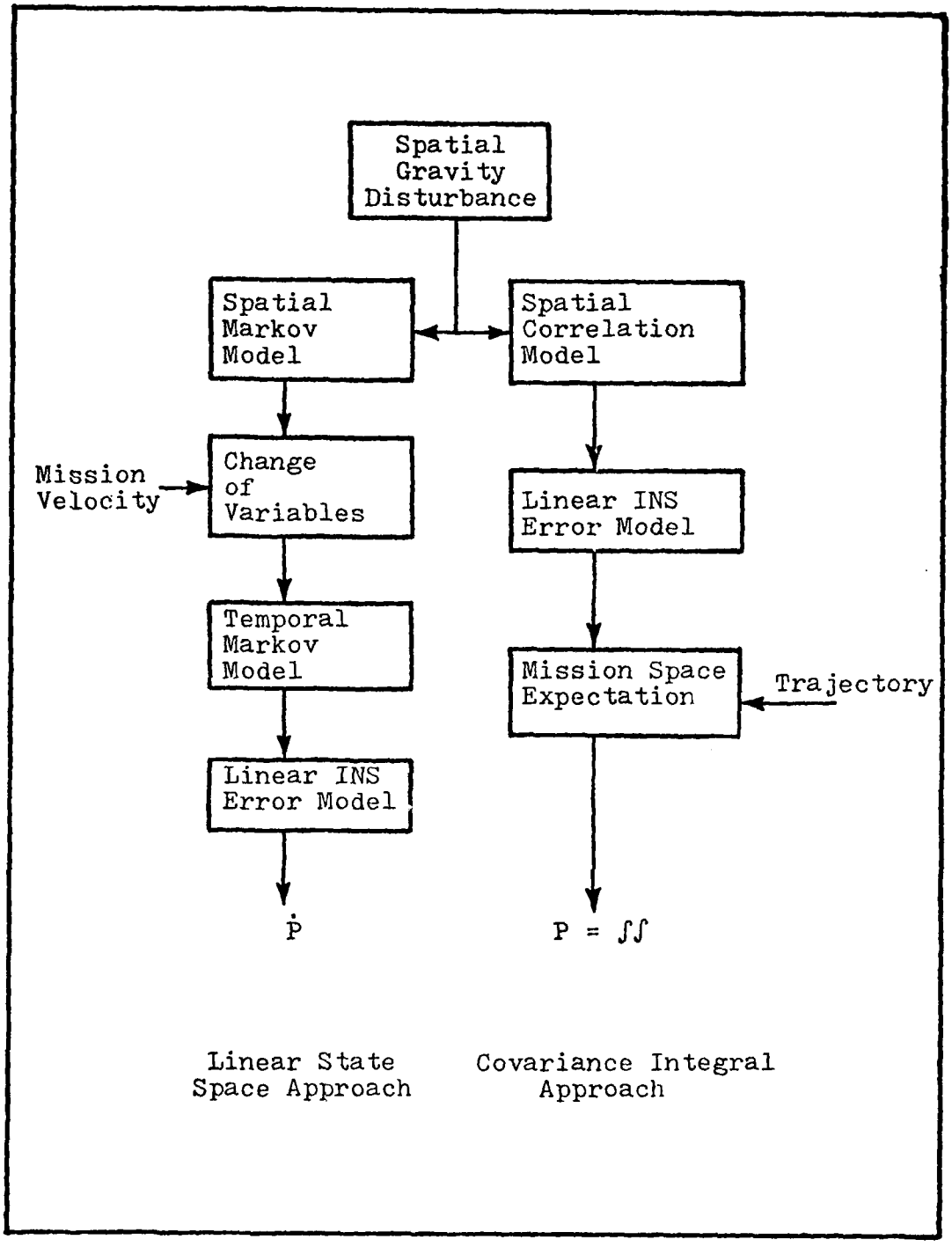

Figure 6. Covariance Integral Genealogy

with initial error state $\underline{x}(t_o;\theta)$ which will be retained in the development for generality.

Since (15) is a linear system, there exists a state transition matrix $\Phi(t,t_1;\theta)$ which satisfies

$$\dot{\Phi}(t,t_1;\theta) = F(t;\theta)\ \Phi(t,t_1;\theta) \tag{16}$$

and

$$\Phi(t,t;\theta) = I \tag{17}$$

This matrix also satisfies the semigroup property

$$\Phi(t_3,t_1;\theta) = \Phi(t_3,t_2;\theta)\ \ \Phi(t_2,t_1;\theta) \tag{18}$$

which will be essential in the upcoming numerical analysis. For now these properties allow the solution of (15) to be cast in the form

$$\underline{x}(t;\theta) = \int_{t_o}^{t} \Phi(t,p;\theta)\ G(p;\theta)\ \underline{u}(p;\theta)\ dp + \Phi(t,t_o;\theta)\underline{x}(t_o;\theta) \tag{19}$$

The next step toward forming the covariance matrix is to produce the outer product

$$\begin{aligned}\underline{x}(t;\theta)\underline{x}^T(t;\theta) = {} & \int_{t_o}^{t}\int_{t_o}^{t} \Phi(t,p;\theta)G(p;\theta)\ [\underline{u}(p;\theta)\underline{u}^T(q;\theta)] \\ & G^T(q;\theta)\Phi^T(t,q;\theta)\,dpdq \\ & + \left\{\Phi(t,t_o;\theta)\ \int_{t_o}^{t}[\underline{x}(t_o;\theta)\underline{u}^T(p;\theta)]\ G^T(p;\theta)\right. \\ & \left.\Phi^T(t,p;\theta)\,dp\right\} \\ & + \left\{\Phi(t,t_o;\theta)\ \int_{t_o}^{t}[\underline{x}(t_o;\theta)\underline{u}^T(p;\theta)]\ G^T(p;\theta)\right. \\ & \left.\Phi^{\ T}(t,p;\theta)\,dp\right\}^T \\ & + \Phi(t,t_o;\theta)\ [\underline{x}(t_o;\theta)\underline{x}^T(t_o;\theta)]\ \Phi^T(t,t_o;\theta)\end{aligned} \tag{20}$$

The navigation error state covariance P(t) is defined as the expectation of this outer product over all mission θ within the mission region Θ. That is,

$$P(t) = \mathop{\mathscr{E}}_{\theta \in \Theta} \left[\underline{x}(t;\theta) \underline{x}^T(t;\theta) \right] \tag{21}$$

Now to cast the problem in a form for which computer solution is practical, assume that the mission region Θ has been selected sufficiently small that one mission, the design mission θ_o, can represent the mission geometries and the navigation error dynamics throughout that region (Figure 7). The disturbance, $u(t,\theta)$, varies more with geographic variations; hence, is retained in that form. The design mission θ_o defines an occurrence of a position-time history $\underline{r}(t)$ for $t \epsilon (t_o, t_f)$. The present assumptions mean the following approximation replacements can occur as defined below

$$F(t;\theta) \leftarrow F(t) = F(t;\theta_o) \tag{22}$$

$$G(t;\theta) \leftarrow G(t) = G(t;\theta_o) \tag{23}$$

$$\Phi(t,t_1;\theta) \leftarrow \Phi(t,t_1) = \Phi(t,t_1;\theta_o) \tag{24}$$

This replacement will simplify taking the expectation since F(t), G(t), and $\Phi(t,p)$ are not changed over the range of Θ. Without such a simplification, the expectation expressed by (21) would be extremely difficult to approximate by other than Monte Carlo analysis. Applying (21) to (20) then yields

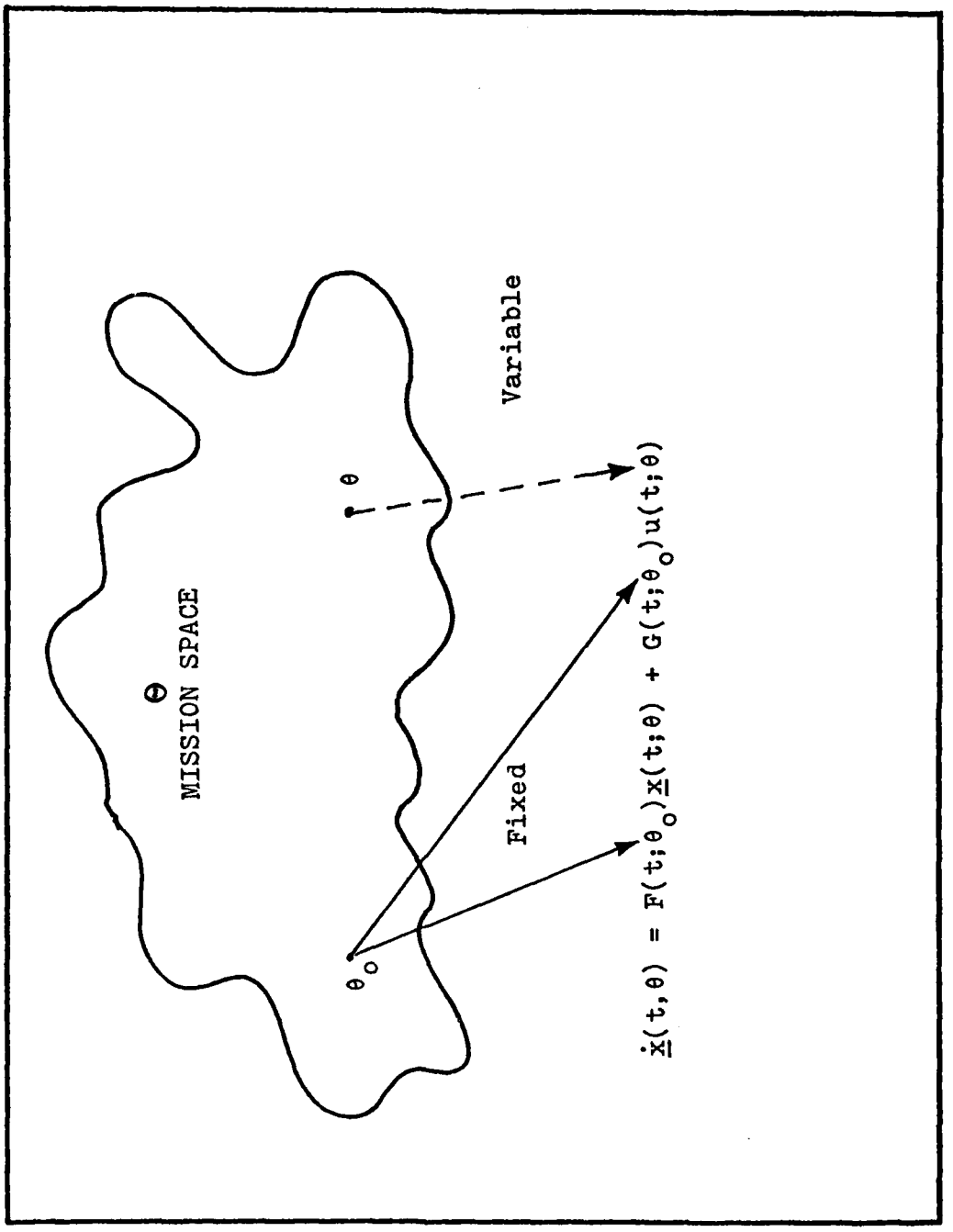

Figure 7. Covariance Integral Mission Sample Space Interpretations

$$P(t) = \int_{t_o}^{t} \int_{t_o}^{t} \Phi(t,p)G(p) \underset{\theta \in \Theta}{\mathscr{E}} \left[\underline{u}(p;\theta)\underline{u}^T(q;\theta)\right] G^T(q)\Phi^T(t,q)\,dpdq$$
$$+ E(t) + E^T(t) + \Phi(t,t_o)P(t_o)\Phi^T(t,t_o) \qquad (25)$$

and

$$E(t) = \Phi(t,t_o)\int_{t_o}^{t} \underset{\theta \in \Theta}{\mathscr{E}} \left[\underline{x}(t_o;\theta)\underline{u}^T(p;\theta)\right] G^T(p)\Phi^T(t,p)\,dp \qquad (26)$$

The initial covariance, $P(t_o)$, and hence, $\underline{x}(t_o;\theta)$, will be modeled as identically zero for the following development. A perfect initial condition is thus assumed. The penalty for this simplification is that calibration and alignment errors which are geodetic in origin cannot be included as initial conditions. Should it become important to include such terms with the gravity modeling error evaluation, some additional development will be required to approximate (26). Alternatively, calibration and alignment can be included as part of the design mission. The navigation error propagation model and the trajectory must reflect this fact.

By the above simplifying assumptions, the last three terms in (25) are removed yielding

$$P(t) = \int_{t_o}^{t} \int_{t_o}^{t} \Phi(t,p)G(p)Q(p,q)G^T(q)\Phi^T(t,q)\,dpdq \qquad (27)$$

where

$$Q(p,q) = \underset{\theta \in \Theta}{\mathscr{E}} \{\underline{u}(p;\theta)\underline{u}^T(q;\theta)\} \qquad (28)$$

This geodetic error correlation function $Q(p,q)$ summarizes the statistical relations between gravity errors at time p with those at time q. Since $\underline{u}(p,\theta)$ is, in

reality, $\underline{u}[\underline{r}(p)]$ for $\underline{r}(p)$ defined by θ, it is more correct to express this function in terms of positions (i.e., $Q[\underline{r}(p),\underline{r}(q)]$). Again, θ_o yields the required position history, and $\underline{r}(p)$ and $\underline{r}(q)$ are defined by θ_o for evaluations of the correlation function model.

The elements of the Q-matrix are auto- and cross-correlation functions which, as previously discussed, can be derived from one scalar correlation function model [see Appendix A]. For this work it suffices to note that a body of theory exists on the relationships of the correlation of anomalous gravity disturbance vector δg and undulation of the geoid N. Related terms are vertical deflections, η and ξ, gravity anomaly Δg, and anomalous potential T. These anomalous gravity terms are defined in Appendix A. One purpose here is to develop a scheme general enough to allow a correlation modeling choice.

Equation (27) is the desired expression of navigation error covariance as an integral involving the trajectory, error propagation, and correlation function models. Numerical methods will be derived in the next section to approximate (27) directly. Another formulation is suggested by the linear state space methods.

Equation (27) is similar to (11) of the linear state space statistical analyses. Computational advantage is gained in that development when Leibnitz' rule is applied. Following this example yields

$$\dot{P}(t) = F(t)P(t) + P(t)F^T(t) + G(t)D(t) + D^T(t)G^T(t) \quad (29a)$$

where

$$D(t) = \int_{t_o}^{t} Q(t,p)G^T(p)\ \Phi^T(t,p)\,dp \quad (29b)$$

Since time appears as an argument of $Q(\cdot,\cdot)$ differentiation of (29b) will not yield a simple form in general. Combining (29b) with the integral form of (29a) yields a pair of nested single integrals which can be approximated, instead of directly approximating (27). Approximations based on this nested integrals approach will also be developed in the next section.

2.3 Comparisons to Present Statistical Analysis Methods

The objectives of this "covariance integral" evaluation method are efficiency and flexibility advantage over existing methods of gravity model statistical evaluation. The efficiency of a numerically approximated covariance integral is compared to Monte Carlo in Section V. This comparison must wait until then because first the development of numerical methods for approximating the covariance integral must be accomplished. These numerical methods are developed in Section III. However, the flexibility comparisons can be made at this point.

Flexibility, as used here, is the facility to process a variety of models in either of the three categories: trajectory, navigation system, and disturbance statistics.

The model flexibility for the new covariance integral formulation is presented in Table I along with the two current analysis methods. This new method is, as desired, more flexible than the linear state space covariance analysis.

The trajectory flexibility is the major concern with the linear state space method. The formulation of (27), or the equivalent (29), impose no special constraint on $\underline{r}(t)$, the trajectory. As long as the Q-matrix and F-matrix can be evaluated using $\underline{r}(t)$, the covariance integral offers a means of evaluating the system performance of the gravity model on any trajectory.

The linear state space evaluation approach is forced to use the Gauss-Markov gravity disturbance statistical model. This restriction is not, of itself, a major concern, but it is a definite limitation. On the other hand, the new formulation requires only that the disturbance correlations be modeled as spatially dependent quantities for which $\underline{r}(p)$ and $\underline{r}(q)$ from the design mission will serve as inputs. This flexibility allows the analyst options in this modeling which may simplify the overall task. A demonstration using three different model forms for the gravity disturbance statistics is presented in Section VI.

The navigation model is restricted in this new formulation. The linear state space navigation error propagation model shared by linear state space and the covariance integral

Table I

Statistical Analysis Methods Model Flexibility Comparisons

Statistical Analysis Method	Trajectory	Gravity Disturbance Correlations	Inertial Navigation Model
Linear State Space Covariance Analysis	Great Circle@	Gauss-Markov	Linear State Space Error Propagation
Covariance Integral	*	*	Linear State Space Error Propagation
Monte Carlo	*	*	*

* indicates a freedom of choice -- model is not dictated by the method

@ monotonically non-decreasing central angle of less than 180°

formulations is not considered a serious drawback because the model is widely-accepted as a valid system description.

The covariance integral approach gives the desired model flexibility. The promise of greater efficiency than Monte Carlo can be shown only after a numerical approximation algorithm is developed and proven.

III. Numerical Approximation the Covariance Integral

In Section I, the motivation was given for developing a new statistical method to evaluate system accuracy performance of gravity models. The theoretical basis for the covariance integral (27), presented in Section II, offers considerable freedom in model selections. Except for pathologically simple cases, a closed-form expression for covariance integral cannot be expected, so a means of approximating the integrations is needed. The main purpose of this section is to investigate alternative approximation procedures and to select one procedure for futher verification, demonstration, and development. Approximating the covariance integral is straightforward, but computational cost becomes prohibitive for realistic problems. Therefore, this section also addresses the data logistics issue which is critical in forming an economically feasible analysis method.

Two general lines can be followed to approximate the covariance integral. A direct approximation can be made by replacing the double integration of (27) with finite double summations. An alternative, referred to as the Nested Integrals method, is to approximate the integrals of (29b) and (29a) in that order. Recursive algorithms will be developed along both these theoretically equivalent lines after the common computational problems are

addressed. Both the accuracy and efficiency of these candidate algorithms will then be assessed in order to select one method for further study.

The next three subsections are devoted to the computational details of these algorithms. The reader not interested in these matters may wish to proceed to subsection 3.4 where the comparison of the developed algorithms begins.

3.1 Common Computational Problems

The theoretical work of this research could be covered without discussing the techniques used in producing numerical results. Such treatment would neglect an issue critical to the use of the covariance integral statistical method. In developing computer programs to execute the approximations of (27) and (29), considerable study and experiment went into the data flow and algorithmic structure. This subsection presents the details of these software design decisions, because the solution reached in this study may be applicable to other studies.

Several arbitrary decisions must be made in designing software for a general requirement like "Evaluate (27) with a numerical approximation over a wide range of trajectory, error propagation, and gravity disturbance models." Other general specifications include efficiency and accuracy requirements. Factors which influence these decisions are:

a. The specific problem to be solved. The strategy used on simple problems like the Schuler loop examples, which are presented later in this section, is certainly different from that used on the full-scale problems presented in the following sections.

b. Computing system capacities. Available computer core, input-output efficiency, and throughput are examples of the capacities of a specific computational facility which should be considered.

c. Available support software. Computer file record management and subroutine libraries should be exploited.

d. General user environment. Priority is established at most large computing facilities based on many factors, and this general environment influences the nature of the software design.

The decisions made in preparing software for this study were based on using a CDC CYBER 74 computing facility in an environment which encourages short multi-step processes over long computation time jobs. The following decisions were influenced by this environment and this inherent bias should be remembered. With this warning, the following discussion gives one example of a solution to the computational burden associated with approximating the covariance integral.

Either a direct approximation of (27) or the Nested Integrals approximation of (29) requires $\underline{r}(t)$ and $\Phi(p,q)$

data. Methods for producing $\underline{r}(t)$ exist [Ref 7] for trajectories too complex for closed-form mathematical expressions. The Φ-matrices can be produced using (16) and (17) by ordinary differential equation, predictor-corrector methods [e.g. Ref 14]. Once produced, the logistics of supplying these data must be resolved. This issue is treated first because the algorithmic forms are influenced by the data flow. Since the Nested Integrals data requirements are practically the same as the direct approximations, the direct method will be used as an example in the following discussion.

The direct integral approximations will be based on a finite double summation replacing (27). That is,

$$P(n) = \sum_{i=0}^{n} \sum_{j=0}^{n} \Phi(n,i)G(i)Q(i,j)G^{T}(j)\Phi^{T}(n,j)\,\Delta t_i \Delta t_j s_n(i,j) \tag{30}$$

where $s_n(i,j)$ is the quadrature weighting associated with the integrand evaluation at $(p,q) \equiv (i\ ,j\ )$. Details of the weighting factor are covered later in the algorithm developments. Attention will now be given to the nature of the data and to the manner in which it is produced.

Fundamental to the formation of (30) is a discretization of the time interval (t_o, t_n). One can view the integrals of (27) as a process applied to a signal, the integrand. With this approach, the time steps should be small enough to give at least adequate representation of the integrand as specified by Shannon's sampling theorem.

The frequency spectrum of the integrand is affected by all three analysis models. The trajectory affects both the Φ and Q matrices. The inertial navigation error propagation model along with the design mission trajectory model define the F matrix used in computing Φ. The gravity disturbance correlation model is embodied in Q, which has position arguments defined by the trajectory. The dynamics of the trajectory, the dynamics of the error propagation model, and the spatial spectrum of the gravity disturbance correlation model must all be considered in subdividing the time interval.

Once a proper time partition is defined, the integrand must be evaluated for every pair (t_i, t_j) such that both t_i and t_j are in the set $\{t_o, t_1, \ldots, t_N\}$. This Φ-matrix data need is a critical computational issue which will be addressed at length.

If n_s is the number of error states, the integral summation can also be reduced from n_s^2 terms to $\frac{1}{2}n_s(n_s+1)$ because P(t) is symmetric. This symmetric property, as will be shown later, can be used to decrease the number of $\Phi(i,j)$ matrices. That is, the only $\Phi(i,j)$ matrices required are for (i, j) pairs such that $0 \leq j \leq i \leq N$. Since $\Phi(i,j) = I$ when $i=j$, the true requirement is for (i, j) pairs such that $0 \leq j < i \leq N$. For example, $\Phi(4,7)$ need not be calculated, whereas $\Phi(7,4)$ is required. The number of Φ-matrices required is $\frac{1}{2}(N+1)(N+2) - (N+1) = \frac{1}{2}N(N+1)$. To demonstrate the magnitude of this data burden,

consider a 500-point time partition and 9X9 Φ-matrices. The 12,250 Φ-matrices would require 10,145,250 words of storage.

Clearly, the logistics of these data must be carefully planned to make this analysis method economically feasible. The semi-group property, equation (18), can be used to reduce this data storage, but at a cost in computation time. For discussion purposes, let N=3. The approximation stated in (30) requires $\Phi(1,0)$, $\Phi(2,1)$, $\Phi(2,0)$, $\Phi(3,2)$, $\Phi(3,1)$, and $\Phi(3,0)$. All of these can be produced from $\Phi(3,2)$, $\Phi(2,1)$, and $\Phi(1,0)$ using (18). To see this, note that

$$\Phi(1,0) = \Phi(1,0) \tag{31a}$$

$$\Phi(2,1) = \Phi(2,1) \tag{31b}$$

$$\Phi(2,0) = \Phi(2,1)\ \Phi(1,0) \tag{31c}$$

$$\Phi(3,2) = \Phi(3,2) \tag{31d}$$

$$\Phi(3,1) = \Phi(3,2)\ \Phi(2,1) \tag{31e}$$

$$\Phi(3,0) = \Phi(3,2)\ \Phi(2,1)\ \Phi(1,0) \tag{31f}$$

For N=3, then, the storage requirement can be reduced from six to three Φ-matrices. In general, this technique requires only N Φ-matrices as opposed to the $\frac{1}{2}N(N+1)$ needed for (30). For the 500-point example with 9X9 Φ -matrices, the storage requirement decreases from 10,145,250 to 40,500 words.

Note that the production of $\Phi(3,0)$ above, requires two matrix multiplications. This computational cost is offset by the fact that $\Phi(3,0)$ is not produced by solving (16) initialized with $\Phi(0,0) = I$. Note that although the product sequence runs backward in time, each $\Phi(i+1,i)$ results from a forward-time integration from the initial condition $\Phi(i,i) = I$. Questions of numerical stability must be asked concerning the possibly hundreds of matrix multiplications which full-scale problems might require. For the studies presented in this and later sections, a simple test was performed to test this Φ-matrix production technique. $\Phi(N,0)$ was produced by two methods. First, the $\Phi(i,i-1)$ matrices were calculated using (16) and (17). From these,

$$\Phi(N,0) = \Phi(N,N-1)\ \Phi(N,N-2)\ \ldots\ \Phi(2,1)\ \Phi(1,0) \qquad (32)$$

was calculated. Then, $\Phi(N,0)$ was produced by integrating (16) initialized with $\Phi(0,0) = I$. The elements of these two alternative $\Phi(N,0)$ matrices were individually compared. The differences observed were on the order of the computer word accuracy limit and this technique was judged accurate enough for the studies which follow.

These test results are unique to the computing system and model choices. For other applications, a test similar to the one above is advised prior to conducting an analysis using the technique of repeated multiplications.

It should be clear from (31) that a preferred order of computation exists. Repetitious calculations can be avoided, for example, if $\Phi(3,1)$ is calculated and used prior to $\Phi(3,0)$. The associative and commutative properties of matrix addition permit the summation of (30) such that $\Phi(3,2)$ comes before $\Phi(3,1)$ which comes before $\Phi(3,0)$. In general, an algorithmic form is desired in which $\Phi(n,n-1)$, $\Phi(n,n-2)$, ..., $\Phi(n,0)$ are required in that order. The second index decreases -- moves backward in time. This order of summation is therefore backward from the way the sum would normally be formed. Explicit reference to this reverse-chronological order will be made at those points in the algorithm developments where the summations are modified to this desired order.

Another data logistics issue is whether to produce the Φ-matrices in parallel with P computations or to produce all the data before computing any P values. The parallel production method means $\Phi(n,n-1)$ would be produced and stored just prior to the P(n) computation. All previous Φ-matrices would have been produced on previous steps and stored for retrieval. This approach, therefore, almost forces a chronologically sequential Φ-matrix storage. This storage mode would be prohibitively costly in computer input-output time if the reverse-chronological summation form is used. Another disadvantage is that the trajectory model which supports Φ computation would either have to

reside in computer core with the P calculation or be overlayed iteratively with the P calculation. Except for simple analyses, the computer core requirements would be a severe disadvantage on one hand or the peripheral processing would be costly on the other.

If the parallel computing structure has disadvantages, the serial design has distinct positive attributes. First, the trajectory generation and state transition matrix calculation form a natural partition for the analysis. These two data sets provide all the data for (30) except that associated with the correlation model. The Φ-matrix calculation requires the trajectory model already, so a parallel calculation imposes no additional computer core costs. The data from both trajectory and Φ calculations can be generated in a natural ascending time order, and the data order can be reversed in an inexpensive data processing step. Once these data have been produced and filed, they can be used repetitively, if needed, without the cost of regeneration.

Now, attention must turn to the data retrieval costs. For reasonably sized problems like the examples in later sections, a straightforward approach to retrieving these data for the required computation could require several hours of peripheral processing time due to the input-output operations involved. This cost is likely to be the dominant factor in designing any software to approximate the covariance integral. To understand the magnitude of this

prospective cost, consider the following. To compute $P(1)$, $\Phi(1,0)$ is needed; to produce $P(2)$, $\Phi(2,1)$ and $\Phi(1,0)$ are required; and to form $P(N)$ a total of N matrices are retrieved. In computing $P(1)$, $P(2)$, ..., $P(N-1)$, and $P(N)$, a total of $\frac{1}{2}N(N+1)$ Φ-matrix fetch operations must be performed. In later sections, example problems are treated for which $N=408$. For such problems, a total of 83,436 fetch operations are required. Since these matrices cannot all reside in computer core, the input-output time can be substantial.

Methods of reducing this computational burden must be considered. Even though all Φ-matrices cannot be in core simultaneously, certainly several may be. To the existing data processing step, a task can be added to pack the Φ-matrices. Several chronologically contiguous Φ-matrices could be packed into each record. Then, several matrices would be brought into core with each fetch operation. If k matrices are packed into each record and if N/k is an integer, the number of record retrievals is decreased from $\frac{1}{2}N(N+1)$ to $\frac{1}{2}N(N/k+1)$. With $N=408$ and with $k=4$, the 83,436 record fetches are reduced to 21,012. Even though more data is transferred, a savings of input-output time is realized from the avoided fetch operations.

The cost in core storage for this input-output efficiency is modest. Instead of storing one Φ-matrix in core at a time, k of them must be stored. The computer

core storage increases from n^2 to kn^2. The necessary trade-off between core storage and input-output costs is a subjective decision influenced primarily by the computing environment priority system. The method of packing records offers one means of lowering input-output time should such economy be desirable. If the experience of these studies is a general indicator, this issue will be crucial in using a covariance integral statistical analysis.

The records used in these studies were placed in reverse chronological order, and four nascent records were packed into one record prior to the filing step. The type of file structure has not been addressed in the previous discussions. The filing suggested is sequential, but a simple sequential file structure was not used. Three file structures were considered: sequential, random access or indexed, and indexed-sequential. The decision to use the indexed-sequential structure was based partly on experience and partly on experiment. To clarify the rationale for this choice, these file structures will be discussed in terms of how the integral approximation would proceed using each different structure.

a. Sequential file. This file structure is probably the most familiar since the normal FORTRAN read and write operations use and create sequential files. Record retrievals are sequential and usually proceed one record at a time. For the application here, the Φ-matrices would be

stored in reverse chronological order -- each record being packed with k data sets. To calculate P(n), the first record retrieved should contain the $\Phi(n,n-1)$ matrix. The following operations would occur: rewind file, skip forward $\frac{N-n}{k}$ records, read in the next record which contains $\Phi(n,n-1)$, and read and process the remaining records sequentially. The last record contains $\Phi(1,0)$.

b. Indexed or random access file. For this file structure, each record is identified by a key. This key is assigned at the time the record is filed, and it can be simply the integer of the highest index in the record (e.g. key = j for the record containing $\Phi(kj,kj-1)$). As each record is filed, the record key and the record address are stored in a dictionary for later address retrieval. Since the key uniquely identifies the record, the file chronological order does not have to be reversed, just the order in which keys are produced in file retrievals. The operations to calculate P(n) are: calculate key for the record containing $\Phi(n,n-1)$, find record address in key dictionary, retrieve record, process this record, and continue this cycle in a reverse chronological order until the $\Phi(1,0)$ matrix is used. The key calculation can be simply key = integer $(\frac{n+k-1}{k})$. For this keying system, the j-th record contains $\Phi(kj,kj-1)$ through $\Phi(kj-k+1,kj-k)$ data.

c. Indexed-sequential file. This file structure is designed for efficient operation in either a random access or a sequential mode. Each record is assigned a key and filed like an indexed file. The records are contiguous in storage, so once the initial record is located by key search, the next and subsequent records can be retrieved by sequential mode operations. The fact that every record retrieved does not require a key search is a significant savings in some applications. To calculate P(n); the file containing $\Phi(n,n-1)$ is found by calculating the key and consulting the dictionary; remaining records are read into core sequentially until the final record containing $\Phi(1,0)$ is processed. The key for the reversed chronological file ascends as time descends. This key could be simply: key = N+1 - integer $(\frac{n+k-1}{k})$. The j-th record would then contain the $\Phi(N-jk+k,N-jk+k-1)$ through $\Phi(N-jk+1,N-jk)$ data.

The sequential file structure was not used because the file rewind and record skip operations were expected to use a prohibitive amount of input-output time. Some simple experiments with random access files indicated that several hours of input-output time would be needed for one of the 408-point examples of Section IV. When the indexed-sequential file structure was used on these problems, the input-output time required was only 1600 seconds -- less than $\frac{1}{2}$ hour. The indexed-sequential file structure seems uniquely in harmony with the data retrieval desired in these analyses. In the studies performed during this

research, this file structure afforded substantial computational costs savings over the other structures.

The savings associated with indexed-sequential file structure are offset somewhat by increased core requirements to accommodate the system software which manages the record storage and retrieval. If a sequential file structure were used, these same operations would be required in the program explicitly, however. Additional savings with indexed-sequential files are gained by providing a buffer in core for several records to come in simultaneously. For the examples analyzed in this study, this increased core storage requirement was judged to be acceptable in order that the input-output time requirement be acceptably low.

In summary, four distinct methods were used to solve the Φ-data logistics problem:

a. Only $\Phi(i,i-1)$ matrices are produced prior to the $P(t)$ calculations,

b. Φ-matrices are stored in reverse chronological order for subsequent retrieval,

c. Several Φ-matrices are packed into each record of the data file to decrease the number of record retrievals, and

d. Indexed-sequential files are used for efficient retrieval.

These methods essentially trade-off computer core increases for lower input-output time.

Attention has been focused on the need to supply Φ-data to the finite summations, but a similar need for $\underline{r}$-data exists in the Q-matrix evaluations. The integrand evaluations can be organized such that these two data needs are parallel. While the $\Phi(n,n-1)$ to $\Phi(n,0)$ matrices are being calculated and used, the pairs $(\underline{r}_n,\underline{r}_{n-1})$ through $(\underline{r}_n,\underline{r}_o)$ are needed for the associated Q evaluations. The $\underline{r}$-data can be stored with the Φ-data by grouping $\underline{r}(i)$ with $\Phi(i,i-1)$. This pairing of $\underline{r}$ and $\Phi$is convenient since the coupled trajectory and Φ computations will naturally yield this set at the same time. Time data may similarly be required for Δt_i calculation. For this study, the record structure was:

$$\left(\frac{N}{k} - m + 1\right),$$

$$\underline{r}(mk),\ \underline{r}(mk-1),\ \ldots,\ \underline{r}(mk-k+1),$$

$$\Phi(mk,mk-1),\ \Phi(mk-1,mk-2),\ \ldots,\ \Phi(mk-k+1,mk-k),$$

$$t_{mk}, t_{mk-1}, \ldots, t_{mk-k+1}$$

where $m = 1,2, \ldots, \frac{N}{k}$. The record-unique key is the integer $\frac{N}{k} - m + 1$. In the examples of Section IV, a four-element representation of $\underline{r}$ was used and four (k) data sets per record. This record format requires 345 words per record versus the 87 words per record with $k = 1$. An additional 1300-word buffer was provided for the record manager system software. These computer core costs were judged to be modest in comparison to the input-output time

savings.

These computational considerations seem mundane compared to the theoretical aspects of this work. But for full-scale and realistic problems, attention to these details will probably be the deciding factor in whether or not the analysis will be done. The procedures outlined above solved this problem within the budgetary constraints of this research project. The analyses performed for Sections IV through IX would have been unacceptably expensive had the data logistics not been organized efficiently. These methods should be useful in other covariance integral approximations. Whether to use any or all of these data logistics methods should be determined on a case-by-case basis. Diverse factors which are problem and computer facility unique will certainly need to be considered.

The algorithmic forms will be developed in the next subsections. The issues discussed here which influence the choices in algorithmic form are:

a. Decision to produce P(n) recursively, and

b. The efficiencies of reverse chronological summation.

These factors should be recalled in the algorithmic developments which follow.

3.2 Two Dimensional Direct Integral Approximations

With these data handling issues concluded, the direct approximation of (27) can be addressed. The task is to

produce the entire sequence of the time history {P(0), P(1), ..., P(N)}, not just one element. So, a sequential algorithm is suggested.

To begin this development, a general discrete approximation of Eq (27) can be written as

$$P(n) = \sum_{i=0}^{n} \sum_{j=0}^{n} \Phi(n,i)G(i)Q(i,j)G^T(j)\Phi^T(n,j) \cdot \cdot \Delta t_j \, \Delta t_i \, s_n(i,j) \qquad (30)$$

where

1) Δt_i and Δt_j are time intervals associated with the i-th and j-th data points.

2) $s_n(i,j)$ is a discrete weighting function which depends on the index n. A different function $s_n(\cdot,\cdot)$ will be defined for each integration rule.

Note that for proper weighting

$$\sum_{i=0}^{n} \sum_{j=0}^{n} s_n(i,j) \, \Delta t_i \, \Delta t_j = (t_n - t_o)^2 \qquad (33)$$

The simplest choices for s_n functions correspond to rectangular and trapezoidal integration rules. Others can certainly be developed, but these simple rules will yield the least cumbersome recursion relationships. The improvements from rectangular to trapezoidal will give insight into the incentive for higher order development.

3.2.1 Rectangular Integration Approximation Algorithm

The rectangular integration approximation gives equal weighting to all evaluation points. The formulation here is a slight modification of the usual rectangular rule, but the essential character of the method is retained.

In one dimensional integration approximation, the integral is calculated using n integration steps and n integrand evaluations. In the following development n+1 integrand evaluations are assumed to bracket the integration interval. Each integrand evaluation in the finite sum is adjusted by a weighting factor of n/n+1 to account for this change. In this subsection, this simple one-dimensional integral approximation rule will be extended to two dimensional (double) integrals. This rule will be interpreted with (30) to form a recursion which yields the sequence $\{P(i)\}$.

The one-dimensional weighting of integrand evaluations can be expressed as a sequence of functions. The generic element is defined for $n \geq 1$ by

$$\delta_n(i) = \begin{cases} 0 & i < 0 \quad \text{or} \quad i > n \\ \frac{n}{n+1} & 0 \leq i \leq n \end{cases} \tag{34}$$

This sequence weighting function gives the weight assigned to the i-th integrand evaluation for $i = 0,1,2, \ldots, n$. The extension to two dimensions is simply

$$s_n(i,j) = \delta_n(i)\ \delta_n(j)$$

$$= \begin{cases} \left(\frac{n}{n+1}\right)^2 & \text{for both } 0 \leq i \leq n \text{ and } 0 \leq j \leq n \\ 0 & \text{otherwise} \end{cases} \tag{35}$$

Note that $\sum_{i=0}^{n} \sum_{j=0}^{n} s_n(i,j) = n^2$, so this constant weighting

will satisfy (33) as long as $\sum_{i=0}^{n} \Delta t_i = t_n - t_o$. A constant step size was used in this work with $\Delta t_i = \Delta t = (t_n - t_o)/n$ for $0 \leq i \leq n$. A more general variable step size approach might prove more efficient on missions with a wide range of dynamics. This generalization is not required for the verifications and demonstrations of this work, but a suggestion for future research along this line is given in Section XI.

With $s_n(i,j)$ defined by (35), the direct approximation of (27) could proceed according to (30) for each value of n. A recursion is more efficient when a sequence of answers is desired. The solution of the homogeneous form of (27) is well-known [Ref 15: Equation (4-114) on page 165 with $Q(\tau) = 0$]. With some algebraic manipulations, the term, $\Phi(n,n-1)\ P(n-1)\ \Phi^T(n,n-1)$, appears within the P(n) summation and forms the basis for the recursive relationship.

To develop this recursive relationship, write (30) as

$$P(n) = S_1 + S_2 + S_3 + S_4 \tag{36}$$

where

$$S_1 = \sum_{i=0}^{n-1} \sum_{j=0}^{n-1} \Phi(n,i)G(i)Q(i,j)G^T(j)\Phi^T(n,j)\ \Delta t_i\ \Delta t_j s_n(i,j) \tag{37}$$

$$S_2 = \sum_{j=0}^{n-1} \Phi(n,n)G(n)Q(n,j)G^T(j)\Phi^T(n,j)\ \Delta t_n\ \Delta t_j s_n(n,j) \tag{38}$$

$$S_3 = \sum_{i=0}^{n-1} \Phi(n,i)G(i)Q(i,n)G^T(n)\Phi^T(n,n)\ \Delta t_i\ \Delta t_n s_n(i,n) \tag{39}$$

$$S_4 = \Phi(n,n)G(n)Q(n,n)G^T(n)\Phi^T(n,n)\ \Delta t_n^2 s_n(n,n) \tag{40}$$

Some obvious simplifications can be made since $\Phi(n,n) = I$. A decomposition of (37) should yield P(n-1), and the factored form is obtained using

$$\Phi(n,i) = \Phi(n,n-1)\Phi(n-1,i) \tag{41}$$

which yields

$$S_1 = \Phi(n,n-1)\left\{ \sum_{i=0}^{n-1} \sum_{j=0}^{n-1} \Phi(n-1,i)G(i)Q(i,j)G^T(j)\Phi^T(n-1,j)\ \Delta t_i\ \Delta t_j s_n(i,j)\right\} \cdot\Phi^T(n,n-1) \tag{42}$$

Note that the indices of summation in (42) are such that $s_{n-1}(i,j)$ is $(n-1)^2/n^2$ throughout the ranges. Since $s_n(i,j)$ is $n^2/(n+1)^2$, a replacement can be made using

$$s_n(i,j) = \frac{n^4}{(n^2-1)^2}\, s_{n-1}(i,j) \tag{43}$$

for both $0 \le i \le n-1$ and $0 \le j \le n-1$. With this relationship

$$S_1 = \frac{n^4}{(n^2-1)^2}\ \Phi(n,n-1)\left\{ \sum_{i=0}^{n-1} \sum_{j=0}^{n-1} \Phi(n-1,i)G(i)Q(i,j)G^T(j)\Phi^T(n-1,j)\ \Delta t_i\ \Delta t_j s_{n-1}(i,j)\right\} \Phi^T(n,n-1)$$

$$= \frac{n^4}{(n^2-1)^2}\ \Phi(n,n-1)\ P(n-1)\Phi^T(n,n-1) \tag{44}$$

The homogeneous solution is, in this case, modified by a factor which reflects the change in weighting from t_{n-1} to the t_n evaluation point. S_2, S_3, and S_4 represent the

change in P over the t_{n-1} to t_n interval due to new disturbances entering the problem. In that sense, S_2, S_3, and S_4 represent the current time effects while S_1 represents the past time effects. This type of interpretation is important later in applying these algorithms to more complex trajectory and correlation models than those which follow in this section.

Equation (44) establishes the basic recursive relationship with (36). Some additional interpretations will ease the computational burdens associated with S_2 and S_3. First, from the definition of Q, (28), it should be clear that

$$Q(i,j) = Q^T(j,i) \tag{45}$$

Using this relationship, it follows that

$$S_3 = S_2^T \tag{46}$$

This relationship affords a considerable computational savings since these summations are the major part of the calculations required on each recursion.

These "current time" contributors to P(n) have a strong similarity to the D function of Nested Integrals, (29). At this point, the S_2 and S_4 terms will be redefined in a way which will enhance one's appreciation of the likeness. Define

$$D_a(n) = S_2 = G(n) \sum_{i=0}^{n-1} Q(n,i)G^T(i)\Phi^T(n,i)\ \Delta t_n\ \Delta t_i s_n(n,i) \tag{47}$$

$$D_b(n) = S_4 = G(n)Q(n,n)G^T(n)\ \Delta t_n^2 s_n(n,n) \tag{48}$$

Now, equation (41) can be restated as

$$P(n) = \frac{n^4}{(n^2-1)^2}\,\Phi(n,n-1)P(n-1)\Phi(n,n-1) + D_a(n) + D_a^T(n) + D_b(n) \qquad (49)$$

The recursion is defined by (47), (48), and (49), but the summation of (47) must be properly interpreted to yield the reverse chronological form. To make this point explicit,

$$D_a(n) = G(n) \sum_{i=1}^{n} Q(n,n-i)G^T(n-i)\Phi^T(n,n-i)\,\Delta t_n\,\Delta t_{n-i}\,s_n(n,n-i) \qquad (47a)$$

Summing in the order prescribed by (47a) requires $\Phi(n,n-1)$, $\Phi(n,n-2)$, ..., $\Phi(n,1)$, and $\Phi(n,0)$ in that order. This arrangement allows the data logistics economies discussed in subsection 3.1. Figure 8 presents the algorithmic structure which executes the summation of (47a). Note that at the top of the DO loop the local variable $\Phi_{Temp} = \Phi(n,j)$, and note that the multiplication at the bottom of the loop requires only $\Phi(j,j-1)$ as new data. Since there is no $\Phi(0,-1)$, the $\underline{r}_o$ evaluation point is treated separately. The READ operations should not be taken literally. Recall that several data sets may be packed in one record; therefore, READ means "locate" which may or may not require an actual READ operation. The sequential data retrieval within the loop is initialized by the $\underline{r}(n)$ data retrieve upon entry to the algorithm. Again, these data handling techniques are not the only solution, but algorithms formed in this manner allowed this work to proceed.

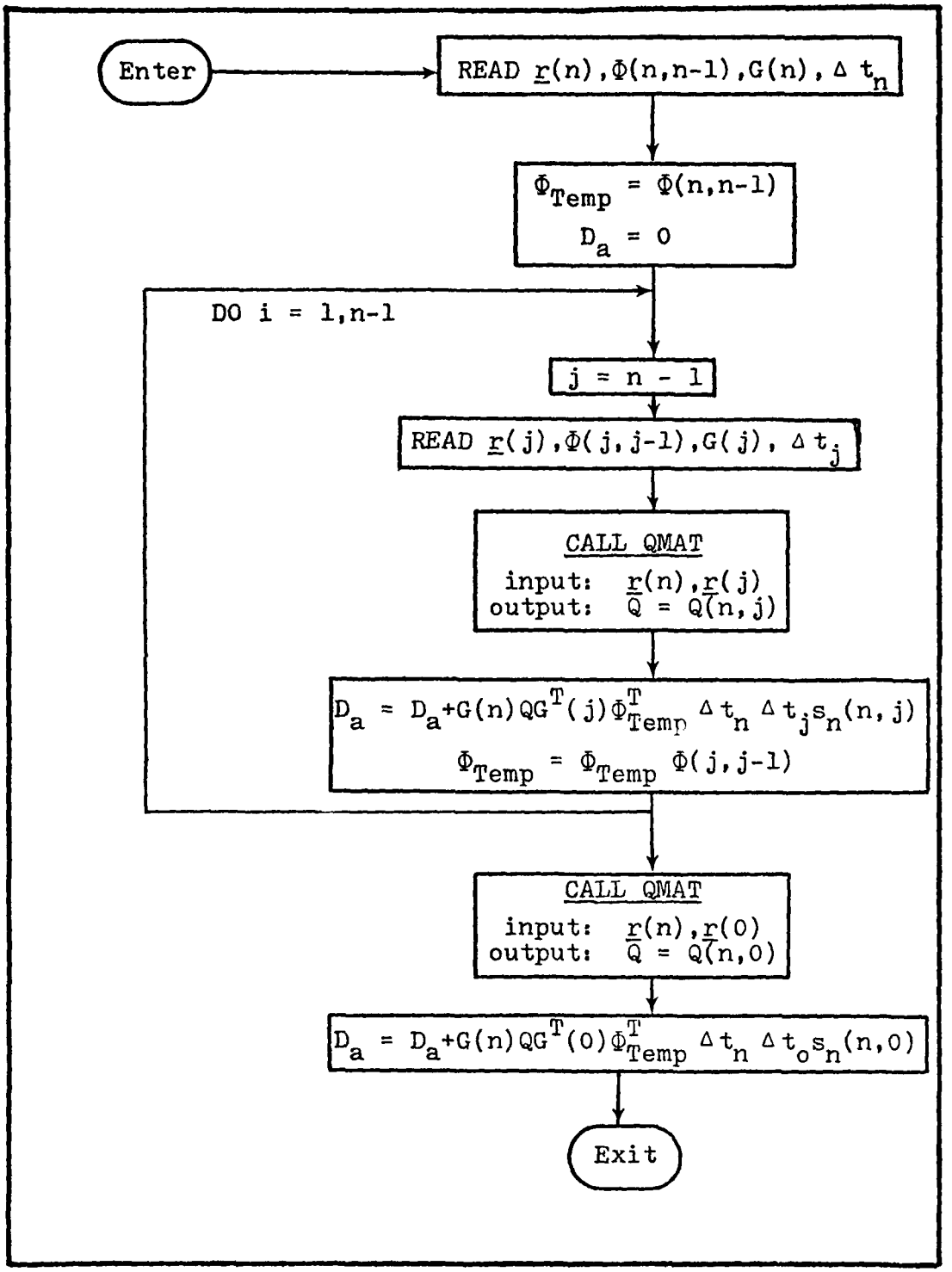

Figure 8. Rectangular Algorithm D(n) Computation

The recursion of (49) applies for $n \geq 2$ because of the obvious singularity at n=1. Since P(0) is identically zero by previous assumptions, one might make the mistake of using the last three terms of (49) to produce P(1). This would neglect the $D_b(0)$ term which occurs in (30) evaluated for n=1. This term adds the effects of disturbances near the start of the mission. The first step, then, can be calculated by executing (30) for n=1.

$$P(1) = \Phi(1,0)D_b(0)\Phi^T(1,0) + D_a(1) + D_a^T(1) + D_b(1) \tag{50}$$

The algorithm is completely defined by (47a), (48), and (49) for the recursion and by (47a), (48), and (50) for the first step. The algorithmic procedure is straightforward except for the $D_a(n)$ computation shown in Figure 8. For each iteration after t_1, $D_a(n)$ and $D_b(n)$ are computed. Then, P(n) is computed by (49) using the $\Phi(n,n-1)$ which is on file.

3.2.2 Trapezoidal Integration Approximation Algorithm

The Trapezoidal algorithm will next be developed in a manner similar to the Rectangular development. First, a weighting function will be specified, and then, recursion and initialization relationships will be formed.

The weighting function for one-dimensional integration approximation by the trapezoidal rule is

$$\delta_n(i) = \begin{cases} 0 & i < 0 \quad \text{or} \quad i > n \\ \frac{1}{2} & i = 0 \quad \text{or} \quad i = n \\ 1 & 1 \leq i \leq n-1 \end{cases} \tag{51}$$

Extending this to two dimensions, define

$$s_n(i,j) = \delta_n(i)\delta_n(j)$$

$$s_n(i,j) = \begin{cases} 0 & (i,j) \ni (i<0 \text{ or } j<0 \text{ or } i>n \text{ or } i>n) \\ \frac{1}{4} & (i,j) \in \{(0,0),(0,n),(n,0),(n,n)\} \\ \frac{1}{2} & (i,j) \in \{(0,k),(k,0),(n,k),(k,n) \ni 1 \le k \le n-1\} \\ 1 & (i,j) \ni (1 \le i \le n-1 \text{ and } 1 \le j \le n-1) \end{cases} \tag{52}$$

The rule expressed by (51) applies to equal subintervals [Ref 16:144] which will apply in the analyses following. This form can be used for non-uniform step sizes but care must be taken to satisfy the constraint of (33).

An alternative for nonuniform step sizes is to give unity weighting to all integrand evaluations and to compute step size as a function of n by

$$t_i(n) = \begin{cases} \frac{1}{2}(t_1 - t_o) & i = 0 \\ \frac{1}{2}(t_{i+1} - t_{i-1}) & 1 \le i \le n-1 \\ \frac{1}{2}(t_n - t_{n-1}) & i = n \end{cases} \tag{53}$$

For this development $s_n(i,j)$ is retained since it aids the development of a recursive relationship.

In the development of the Rectangular recursion, use was made of the constant ratio between $s_n(i,j)$ and $s_{n-1}(i,j)$ over a restricted range of (i,j). In the Trapezoidal case, a similar useful property exists only this time it is the difference of the two weighting functions. Note that $s_n(i,j) - s_{n-1}(i,j)$ is zero except for the cases of either i or j equal to either n or n-1.

j \ i	0	1	2	. . .	n-2	n-1	n	n+1
n+1	0	0	0	. . .	0	0	0	0
n	$\frac{1}{4}$	$\frac{1}{2}$	$\frac{1}{2}$	. . .	$\frac{1}{2}$	$\frac{1}{2}$	$\frac{1}{4}$	0
n-1	$\frac{1}{4}$	$\frac{1}{2}$	$\frac{1}{2}$	. . .	$\frac{1}{2}$	3/4	$\frac{1}{2}$	0
n-2	0	0	0	. . .	0	$\frac{1}{2}$	$\frac{1}{2}$	0
.	.	.	.	.	.	.	.	.
.	.	.	.	.	.	.	.	.
.	.	.	.	.	.	.	.	.
2	0	0	0	. . .	0	$\frac{1}{2}$	$\frac{1}{2}$	0
1	0	0	0	. . .	0	$\frac{1}{2}$	$\frac{1}{2}$	0
0	0	0	0	. . .	0	$\frac{1}{4}$	$\frac{1}{4}$	0

$$s_n(i,j) - s_{n-1}(i,j)$$

The weighting functions are the same over indices ranging from 0 to n-2. Over the range of 0 to n-2 of one index with the other fixed at n-1, $s_{n-1}(i,j)$ is exactly one-half of $s_n(i,j)$. The n-1 corner element shows a 4:1 ratio of $s_n(n-1,n-1):s_{n-1}(n-1,n-1)$. With these relationships in mind, the summation of (30) is partitioned by

$$P(n) = S_1 + S_2 + S_3 + S_4 + S_5 + S_6 + S_7 \qquad (54)$$

where for this Trapezoidal development the 0 to n-2 sub-block gives

$$S_1 = \sum_{i=0}^{n-2} \sum_{j=0}^{n-2} \Phi(n,i)G(i)Q(i,j)G^T(j)\Phi^T(n,j)\ \Delta t_i\ \Delta t_j s_n(i,j) \qquad (55)$$

The elements of the sum with n-1 index in one position give

$$S_2 = \sum_{i=0}^{n-2} \Phi(n,n-1)G(n-1)Q(n-1,i)G^T(i)\Phi^T(n,i)\ \Delta t_i\ \Delta t_{n-1}$$
$$s_n(n-1,i) \qquad (56)$$

Using (45) again the next term can be stated as

$$S_3 = S_2^T \qquad (57)$$

And the (n-1,n-1) corner element is given by

$$S_4 = \Phi(n,n-1)G(n-1)Q(n-1,n-1)G^T(n-1)\Phi^T(n,n-1)\ \Delta t_{n-1}^2$$
$$s_n(n-1,n-1) \qquad (58)$$

The elements with n as the first index are included in

$$S_5 = \sum_{i=0}^{n-1} \Phi(n,n)G(n)Q(n,i)G^T(i)\Phi^T(n,i)\ \Delta t_i\ \Delta t_n s_n(n,i) \qquad (59)$$

Using (45), the other n-index elements are given by

$$S_6 = S_5^T \qquad (60)$$

The (n,n) corner element is

$$S_7 = \Phi(n,n)G(n)Q(n,n)G^T(n)\Phi^T(n,n)\ \Delta t_n^2 s_n(n,n) \qquad (61)$$

The $s_n(n-1,i)$ of (56) can be replaced by $2s_{n-1}(n-1,i)$ using the relationship discussed previously. Similarly, $s_n(n-1,n-1)$ in (58) can be replaced by $4s_{n-1}(n-1,n-1)$. Using these changes and factoring out $\Phi(n,n-1)$, yields

$$S_1 + \tfrac{1}{2}S_2 + \tfrac{1}{2}S_2^T + \tfrac{1}{4}S_4 = \Phi(n,n-1)P(n-1)\Phi^T(n,n-1) \qquad (62)$$

With this result, (54) can be restated as

$$P(n) = \Phi(n,n-1)P(n-1)\Phi^T(n,n-1) + \tfrac{1}{2}S_2 + \tfrac{1}{2}S_2^T + (3/4)S_4$$
$$+ S_5 + S_5^T + S_7 \qquad (63)$$

With the definitions,

$$D_a(n) = S_5 = \sum_{i=0}^{n-1} G(n)Q(n,i)G^T(i)\Phi^T(n,i)\ \Delta t_i\ \Delta t_n s_n(i,j) \qquad (64)$$

$$D_b(n) = S_7 = G(n)Q(n,n)G^T(n)\ \Delta t_n^2 s_n(n,n) \tag{65}$$

the following identifications can be made

$$\tfrac{1}{2}S_2 = \Phi(n,n-1)D_a(n-1)\Phi^T(n,n-1) \tag{66}$$

$$(3/4)S_4 = 3\Phi(n,n-1)D_b(n-1)\Phi^T(n,n-1) \tag{67}$$

Drawing all of these terms together yields the desired recursion

$$P(n) = \Phi(n,n-1)\ \{P(n-1) + D_a(n-1) + D_a^T(n-1) + 3D_b(n-1)\}$$
$$\Phi^T(n,n-1) + D_a(n) + D_a^T(n) + D_b(n) \tag{68}$$

Again the main computational burden is the D_a computation and the reverse chronological order is implemented by

$$D_a(n) = \sum_{i=1}^{n} G(n)Q(n,n-i)G^T(n-i)\Phi^T(n,n-i)\ \Delta t_n\ \Delta t_{n-i} s_n(n,n-i) \tag{64a}$$

The Trapezoidal algorithm recursion is defined by (64a), (65), and (68). The P(1) calculation of the Rectangular method is used for the first step since for $n=1$ the two methods are equivalent. Figure 8 is a valid description of the Trapezoidal algorithm except the past value of D_a must be saved.

3.3 Nested Integrals Approximation Algorithm

As an alternative to these two direct approximations of (27), an algorithm based on the sequential solution of two one-dimensional integrals is suggested. This nested pair of integrals results when one takes the derivative of

(27) with respect to time, t. The resulting algorithm is similar to those in the direct integral approximations by rectangular and trapezoidal rules. This new form permits the use of powerful ordinary differential equation techniques to produce the final result.

The first step in the development is an application of Liebnitz' rule to (27):

$$\dot{P}(t) = G(t) \int_{t_o}^{t} Q(t,q)\, G^T(q)\Phi^T(t,q)\,dq + \int_{t_o}^{t} \Phi(t,p)G(p)Q[\underline{r}(p),\underline{r}(t)]dp\; G^T(t) + F(t)\,P(t) + P(t)F^T(t) \qquad (69)$$

Defining

$$D(t) = \int_{t_o}^{t} Q(t,p)G^T(p)\Phi^T(t,p)\,dp \qquad (29b)$$

and noting from (45) that

$$Q(t,p) = Q^T(p,t) \qquad (45a)$$

results in

$$\dot{P}(t) = G(t)D(t) + D^T(t)G^T(t) + P(t)F^T(t) + F(t)P(t) \qquad (19a)$$

The differential equation in (29a) together with its associated equation (29b) comprise the nested integrals pair.

To solve these equations, first, approximate a solution to (29b) for D(t) over the full span of mission time for which P(t) is required. A completely new integral occurs for each t_n since $\underline{r}(t_n)$ occurs as an argument to $Q(\cdot,\cdot)$ for the first time in the n-th integral of the sequence.

$$D(n) = \int_{t_o}^{t_n} Q[\underline{r}(t_n),\underline{r}(p)]G^T(p)\Phi^T(t_n,p)\,dp \qquad (70)$$

Since $\{D(1),D(2), \ldots, D(N)\}$ must be produced, let the approximation take the form of a simple quadrature formula. Using the reverse chronological form,

$$D(n) = \sum_{i=0}^{n} Q[\underline{r}(n),\underline{r}(n-i)]G^T(n-i)\Phi^T(n,n-i) \cdot \Delta t_{n-i}\, s_n(n-i) \qquad (71)$$

One could develop $s_n(i)$ for an involved quadrature form. To keep the computations simple, lower the time-step increments to reduce integral approximation error to an acceptable level. So, define

$$s_n(i) = \begin{cases} \frac{1}{2} & i = 0 \\ 1 & 1 \le i \le n-1 \\ \frac{1}{2} & i = n \end{cases} \qquad *(72)$$

corresponding to trapezoidal integration. Then evaluating (71) for n=1,2, ..., N will yield a sequence $\{D(0),D(1), \ldots, D(N)\}$ which can be used in solving (29a).

One can treat (29a) with a multitude of ordinary differential equation methods. For the following numerical examples, a predictor-corrector [Ref 14] was employed,

---

* As previously discussed, this weighting could also be viewed as an alteration or redefinition of Δt_i. The form presented here makes such weighting explicit for clarity.

* because $\dot{P}$ is a function of P. Since evaluations of (29b) are required at points other than $\{t_0, t_1, \ldots, t_N\}$, a simple linear interpolator was used on D(t), F(t), and G(t). The overall Nested Integrals algorithm is a hybrid integration method using trapezoidal quadrature for D(t) and predictor-corrector methods for P(t).

Here, one should note that the Nested Integrals algorithm requires F(t) data explicitly, whereas the direct integral approximations did not. The data flow is somewhat altered by this need. The flow, including the indexed sequential file step (subsection 3.1), is diagrammed in Figure 9. The D(n) computation is quite similar to the $D_a(n)$ computation portrayed in Figure 8. Obvious changes are the (n,n) point and the deletion of G(n) and Δt_n terms.

3.4 Comparison Rationale

One can speculate about the relative merits of these three algorithms: Rectangular, Trapezoidal, and Nested Integrals. The spatial spectrum of the anomalous gravity correlation functions and the temporal spectrum of the inertial navigation error propagation are the principal concerns in selecting step size for any method. Nevertheless, all three methods are expected [Ref 17:382-384] to yield

---

* The specific predictor-corrector was variable-order, variable-step-size Adams-Pecce algorithm described in Ref 14. Other predictor-corrector formulations of comparable order should give comparable results.

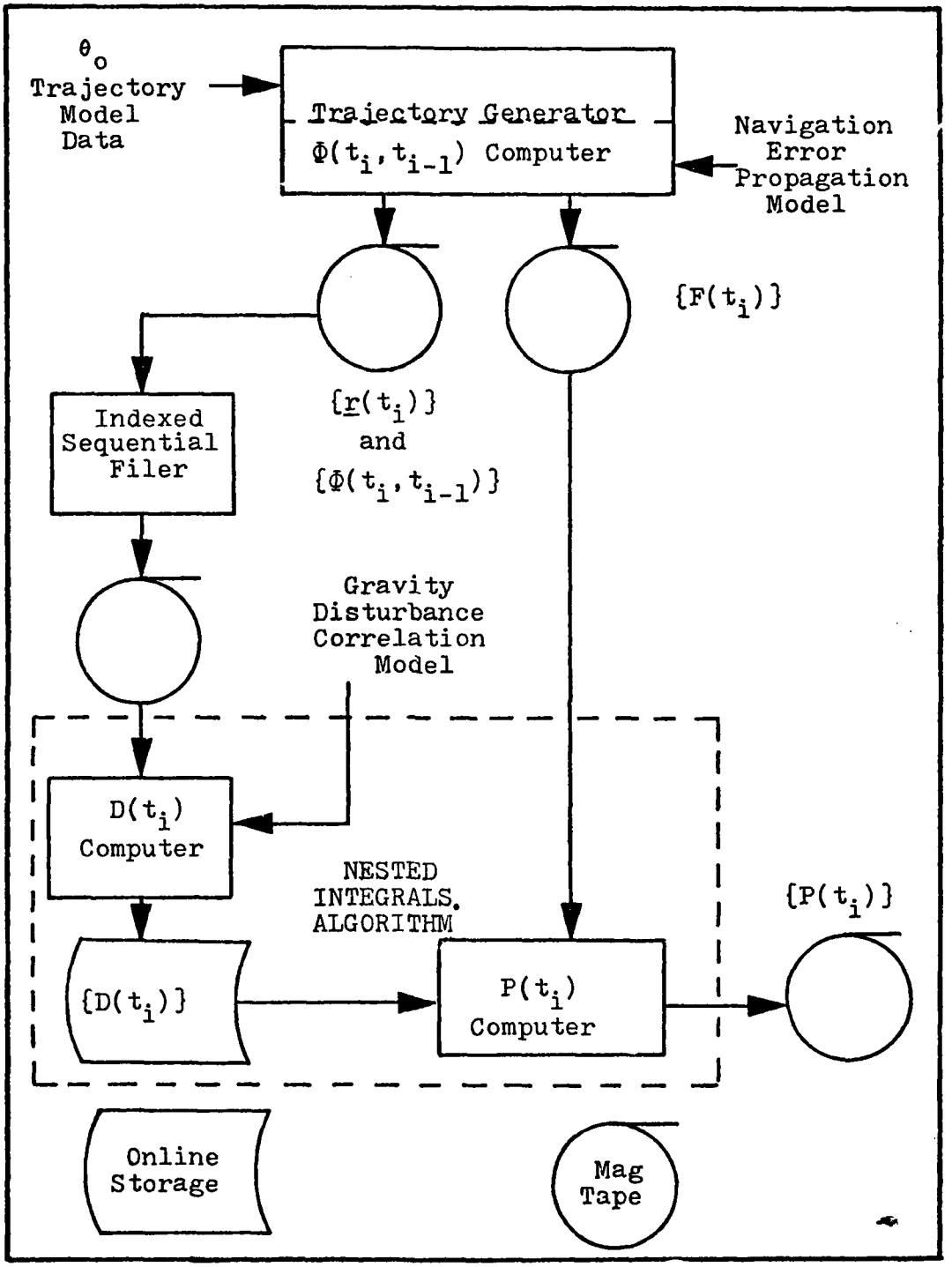

Figure 9. Nested Integrals Information Flow

acceptable accuracy when both the products of t_i with F(t) eigenvalues are small compared to 1 and $|\underline{r}(t_i) - \underline{r}(t_{i-1})|$ is small compared to correlation distances in Q(·,·). The Trapezoidal algorithm should be somewhat more accurate than the Rectangular, because a higher order interpolating polynomial represents the function between evaluation points.* The amount of improvement here will indicate the productivity of more complex direct approximations. The predictor-corrector P(t) computation in the Nested Integrals algorithm should give an accuracy advantage but will undoubtedly cost in computer storage and execution time.

Accuracy and efficiency will be used to select one of the alternatives for further development and study. To quantify the differences for this selection, a simple test case is proposed. This example should be in the form of the problem type that these algorithms are intended to solve, but it should be simple enough for an indisputable comparison to the true solution.

3.5 Undamped Schuler Loop Driven by Exponentially Correlated Noise

A simple model of an inertial system horizontal channel is the Schuler loop. In its purest form, this model is an

---

* Hildebrand [Ref 18:93-94] has shown that for interpolating functions of order 2n and 2n+1 the approximation error is bounded by a term involving Δt^{2n+3}.

undamped, second-order feedback loop. The feedback signal represents, to first order, the corrective influence of the gravity model, given position errors [Ref 2 : Appendix B]. The feedback weighting is the squared Schuler frequency, $\omega_s^2 = \frac{g}{R_e}$.

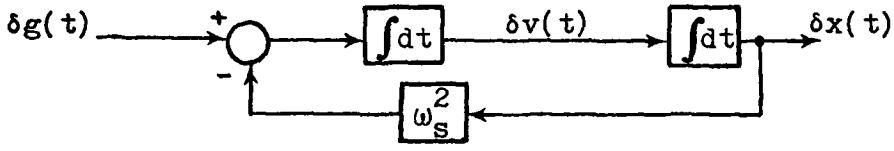

As diagrammed above, this loop is driven by the gravity model error term δg which corresponds to the vertical deflection in the +x direction multiplied by g.

This double integration with negative feedback forms a pure oscillator with fundamental frequency ω_s.

Defining state variables as integrator outputs yields

$$\begin{Bmatrix} \delta\dot{x} \\ \delta\dot{v} \end{Bmatrix} = \begin{bmatrix} 0 & 1 \\ -\omega_s^2 & 0 \end{bmatrix} \begin{Bmatrix} \delta x \\ \delta v \end{Bmatrix} + \begin{Bmatrix} 0 \\ 1 \end{Bmatrix} \delta g \qquad (73)$$

For the algorithms, identify

$$F(t) = F = \begin{bmatrix} 0 & 1 \\ -\omega_s^2 & 0 \end{bmatrix} \qquad (74)$$

$$G(t) = G = \begin{bmatrix} 0 \\ 1 \end{bmatrix} \qquad (75)$$

$$\underline{x} = \begin{Bmatrix} \delta x \\ \delta v \end{Bmatrix} \qquad (76)$$

$$\underline{u} = \{\delta g\} \qquad (77)$$

From (74), one can derive

$$\Phi(t,p)=\Phi(t-p) = \begin{bmatrix} \cos\omega_s(t-p) & \frac{1}{\omega_s}\sin\omega_s(t-p) \\ -\omega_s \sin\omega_s(t-p) & \cos\omega_s(t-p) \end{bmatrix} \tag{78}$$

Levine and Gelb [Ref 11] suggest a simple exponential correlation for such a δg. The correlation is spatial since the gravity model error is a spatial function.

$$\mathcal{E}\left[\delta g(x_1)\ \delta g(x_2)\right] = \sigma^2 e^{\frac{|x_2-x_1|}{d}} \tag{79}$$

where σ^2 is the variance and d is the correlation distance.

From (79), form the required gravity correlation function

$$Q[\underline{r}(t_1),\underline{r}(t_2)] = Q[x(t_1),x(t_2)] = \sigma^2 e^{\frac{|x(t_2)-x(t_1)|}{d}} \tag{80}$$

Only the design mission remains to be specified. Again, simplicity is desired, so a constant velocity trajectory is selected

$$x(t) = V \cdot t \tag{81}$$

Now,

$$|x(t_2)-x(t_1)| = V \cdot |t_2-t_1| \tag{82}$$

in (80) above. For the numerical example, data is specified by Table II. These data correspond to values for horizontal gravity modeling errors [Ref 12] and a bomber cruise mission. The intent is to form only a representative case, so precision in these data is not an issue.

Table II

Schuler Cases Data

Quantity	Symbol	Value, Units
Initial time	t_o	0 sec
Velocity	V	615 ft/sec
Disturbance Variance*	σ^2	1273 $(\text{mgal})^2$
Correlation Distance	d	20 n m
Schuler Frequency	ω_s	$1.24 \times 10^{-3} \frac{\text{rad}}{\text{sec}}$

* Corresponds to a 36 μg root-mean-square which is equivalent to 7.5 arc sec rms.

1 mgal = 10^{-3} cm/sec^2 = 10^{-5} m/sec^2.

3.5.1 Closed Form Solution

The information to perform the integral approximations is now completely specified. Now P(t) must be produced in closed form to study and compare algorithm errors.

The problem can be solved using a straightforward approach based on stochastic linear system theory. The model for gravity error, δg, is the output of a linear filter driven by white, gaussian noise. The block diagram below shows the basic relationship between the noise $q_x(x)$ and the disturbance $\delta g_x(x)$.

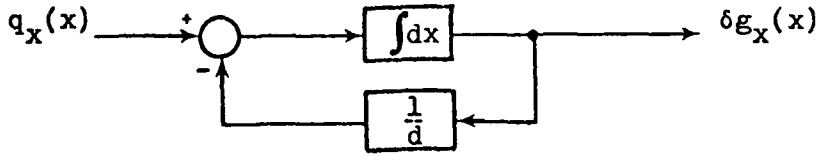

where

$$\mathcal{E}[q_x(x_1)q_x(x_2)] = \frac{2\sigma^2}{d}\,\delta(x_2-x_1) \tag{83}$$

Also, the filter is modeled at steady state,

$$\mathcal{E}[\delta g_x(x)^2] = \sigma^2 \tag{84}$$

This spatial model is converted to temporal by the velocity. Simply replace dx by V·dt, and the block diagram can be converted to

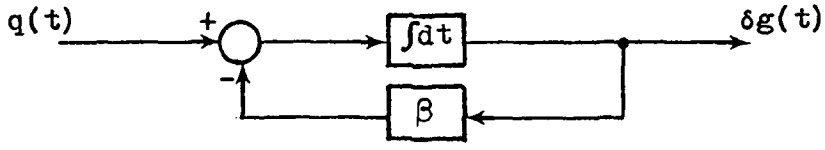

with

$$\beta = \frac{V}{d} \tag{85}$$

The noise process satisfies

$$\mathcal{E}[q(t_1)q(t_2)] = 2\beta\sigma^2\,\delta(t_2-t_1) \tag{86}$$

Combining the Schuler loop with this model yields one linear system driven by q(t). An augmented state equation can now be formed

$$\begin{Bmatrix} \delta\dot{x} \\ \delta\dot{v} \\ \hline \delta\dot{g} \end{Bmatrix} = \left[\begin{array}{cc:c} 0 & 1 & 0 \\ -\omega_s^2 & 0 & 1 \\ \hdashline 0 & 0 & -\beta \end{array}\right] \begin{Bmatrix} \delta x \\ \delta v \\ \hline \delta g \end{Bmatrix} + \begin{Bmatrix} 0 \\ 0 \\ \hline 1 \end{Bmatrix} q(t) \tag{87}$$

$\underline{x}_a(t)$, F_a, and G_a are given by (7) through (10). Then,

$$\dot{P}_a(t) = F_aP_a(t) + P_a(t)\,F_a^T + G_aQ_gG_a^T \tag{14}$$

where Q_g comes from (6) as

$$Q_g = [2\beta\,\sigma^2] \tag{88}$$

Define

$$P_a = \begin{bmatrix} P_{11} & P_{12} & P_{13} \\ P_{12} & P_{22} & P_{23} \\ P_{13} & P_{23} & P_{33} \end{bmatrix} \tag{89}$$

and note that

$$P_a(0) = \left[\begin{array}{cc:c} 0 & 0 & 0 \\ 0 & 0 & 0 \\ \hdashline 0 & 0 & \sigma^2 \end{array}\right] \tag{90}$$

Now define

$$h = \beta/\omega_s \tag{91}$$

$$A = \frac{1}{\beta^2+\omega_s^2} \tag{92}$$

Then solving (14) yields

$$P_{11}(t) = \frac{\sigma^2 A}{\omega_s}\{ht - \frac{1}{2\omega_s}[h \sin 2\omega_s t + 1 - \cos 2\omega_s t] + 2A\omega_s[1-e^{-\beta t}(h \sin\omega_s t + \cos\omega_s t)]\} \tag{93}$$

$$P_{12}(t) = \frac{\sigma^2 A}{\omega_s}\{\tfrac{1}{2}[h(1-\cos 2\omega_s t) - \sin 2\omega_s t] + e^{-\beta t} \sin\omega_s t\} \tag{94}$$

$$P_{22}(t) = \sigma^2 A\{\beta t + \tfrac{1}{2}(h\sin\omega_s t - \cos 2\omega_s t + 1) - 2\omega_s \beta A[h + e^{-\beta t}(\sin\omega_s t - h \cos\omega_s t)]\} \tag{95}$$

$$P_{13}(t) = \sigma^2 A\{1-e^{-\beta t}[\cos\omega_s t + h \sin\omega_s t]\} \tag{96}$$

$$P_{23}(t) = \sigma^2 A\{\beta + e^{-\beta t}[-\beta \cos\omega_s t + \omega_s \sin\omega_s t]\} \tag{97}$$

$$P_{33}(t) = \sigma^2 \tag{98}$$

Now (93), (94), and (95) give the true answers against which the algorithms' performance can be judged. Note that the position and velocity variance terms have ramp components. The results (96) and (97), incidentally, give the correlation of position and velocity errors with present gravity error. Equation (98) merely confirms the problem specification in (84).

3.5.2 Numerical Comparisons

Trapezoidal and Rectangular algorithm solutions were formed using (75), (78), (80), and (81). The Nested Integrals algorithm also required (74). For each of the three methods, a fixed integration step size was used throughout an analysis case. Six different integration step size cases were considered: 3.75, 7.5, 15, 30, 60, and 120 seconds. The errors in P(t) elements for each of these 18 cases are plotted against a common scale for comparisons. The position and velocity variance results are presented in Figures C-1 through C-6 . The position-velocity covariance results are presented in Figures C-7 through C-9. All of these graphical results are located in Appendix C. These graphs verify that each approximation technique is accurate, given a small enough integration step size, Δt. The variance approximation errors grow with time, but the variances being approximated have ramp terms as seen in (93) and (95) above. A better

perspective is gained if these errors are expressed in a percent of the true value. The results for percent position variance error are presented in Figures C-10, C-11, and C-12 for the three candidate methods. The only significant errors, from a practical viewpoint, are the initialization errors associated with the Rectangular and Trapezoidal algorithms. The absolute error may grow, but the percent errors fall to clearly acceptable levels for small Δt.

Obviously, for all methods, some catastrophic failure awaits the unwary user who increases Δt beyond the largest value (120 seconds) used in this study. The explanation is found in applying Shannon's sampling theorem to the choice of integration step size, and a digression on this point is needed before the accuracy comparison is conducted.

Shannon's sampling theorem dictates that $\frac{1}{\Delta t}$ be at least twice the highest frequency [Ref 15:295] which affects the integrand of (27). This integrand is affected by the error propagation model, the trajectory, and the correlation function. The trajectory is not reflected in the simple error propagation model, but it affects the correlation function through its arguments. The frequency characteristics of the propagation model and of the trajectory-driven error of propagation function should therefore be investigated.

The Schuler loop of this example acts as a low pass filter to the gravity disturbance input. The filter

dynamics are adequately modeled when Δt is less than one-tenth the Schuler period. This imposes the constraint that integration step size be less than 8.4 minutes - clearly met by all values of Δt considered. The input correlation function then, must, be the key to the problem for the greater Δt values.

The correlation function is spatial, but, as seen, velocity converts this process into the time domain. The correlation time,

$$t_c = \frac{1}{\beta} = d/V, \qquad (99)$$

is 198 seconds in this case. Adequate sampling dictates that Δt be less than 99 seconds ($\frac{1}{2}$ t_c), and common practice [Ref 15:295] indicates one should select Δt as low as 20 seconds ($t_c/10$). A 99-second step size corresponds to 4.7 or the logarithmic integration step size scale in Figures C-1 through C-12, and a 20-second step size corresponds to 2.4. The sampling theorem violation for the 120-second (5 on the logarithmic scale) case explains the significant increase in error for that case. The 60 second (4 on the logarithmic scale) case is near this violation. The results for 60 seconds and 120 seconds, therefore, do not represent the algorithm performance and should be eliminated prior to comparing the results for the three alternative algorithms.

AD-A082 494 AIR FORCE AVIONICS LAB WRIGHT-PATTERSON AFB OH F/G 17/7
GRAVITY MODEL EVALUATION FOR PRECISE TERRESTRIAL INERTIAL NAVIG--ETC(U)
DEC 79 R M EDWARDS
UNCLASSIFIED AFAL-TR-79-1231 NL

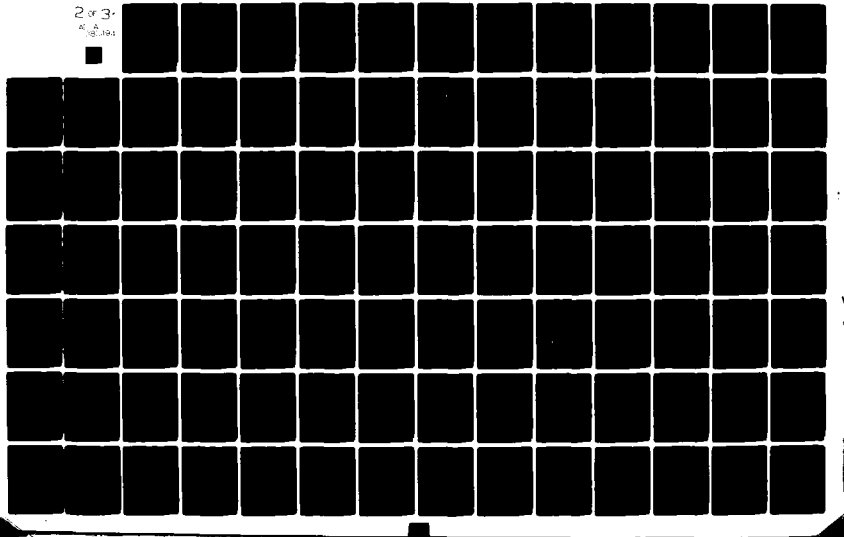

The results for position and velocity variance error were replotted, then, for the four lowest integration step sizes. These results are shown in composite form in Figures C-13 and C-14. This format facilitates the direct comparison of approximation results.

Schuler rate undulations stand out in the Rectangular algorithm results. The lack of predominant Schuler rate errors in the Nested Integrals and Trapezoidal must be attributed to the higher order representation of the integrand. Recall that Nested Integrals has a trapezoidal rule approximation for D(t), so the similarity of these results is not so surprising. The generally lower and less perturbed Nested Integrals and Trapezoidal computation error gives these methods a decided edge over the Rectangular alternative. The Trapezoidal maximum error (sup norm) in velocity variance is slightly lower than Nested Integrals. The Nested Integrals is slightly better in the position variance calculation by the same judgment criteria.

Accuracy is not the only concern. The computational burden should also be considered in the final selection. The input-output computer costs were practically the same for all three methods. The computer memory required for Nested Integrals was only 2000 words more than the alternatives, which is not a major consideration. The computation time did vary, and these times, normalized to the smallest value, are given in Table III.

Table III

Normalized Computation Time

Δt SEC	RECTANGULAR	TRAPEZOIDAL	NESTED INTEGRALS
3.75	1485	1556	449
7.5	370	387	114
15.	94	100	29
30.	24	25	8
60.	6.3	6.5	2.4
120.	1.9	1.9	1.0

Note that for all three methods, halving the integration step size doubles the number of points, and increases the computation time by approximately 2^2. This reflects the underlying two-dimenstional integration which is being approximated.

The surprising result of the computation time comparison is that the Nested Integral method is more efficient than the other methods by a ratio of almost three to one.

The Nested Integrals method is more efficient than either the Rectangular or the Trapezoidal method. The Nested Integrals results were as accurate as the Trapezoidal results and substantially superior to the Rectangular results. Based on these accuracy and efficiency comparisons, the Nested Integrals method was selected for further development and study.

A trapezoidal integration approximation rule limits the accuracy of both the Nested Integrals and Trapezoidal algorithms. An accuracy improvement is anticipated in either case if the integration is approximated using Simpson's rule. [Ref 18:93-94] The classical debate of whether to decrease step size or increase integration order can be raised. For the problem considered here and probably for other more complex navigation scenarios, the sampling theorem compels the selection of step size. Even though a substantial improvement is obtained when the rectangular rule is replaced by the trapezoidal, the trapezoidal algorithm leaves little error to improve on when integration step size is well below the Shannon rate. For this reason, an extension to Simpson's rule for the D(t) computation in the Nested Integrals algorithm was not made. The trapezoidal rule D(t) approximation is the basis for the Nested Integrals results presented in the following sections.

3.6 Damped Schuler Case

The previous undamped Schuler loop example, however, leaves something to be desired in terms of giving insight into practical problems. In this test case, the variance being approximated grew with time; therefore, the absolute error could also grow with time while the percent error fell. In a practical case, the Schuler loop would

probably be damped by measurements. The question, then, is whether or not the Nested Integrals method still gives valid results when the system is damped.

To answer this question, two chages are made in the problem formulation. First, a damping term corresponding to continuous velocity measurement and feedback is added to the Schuler Loop model

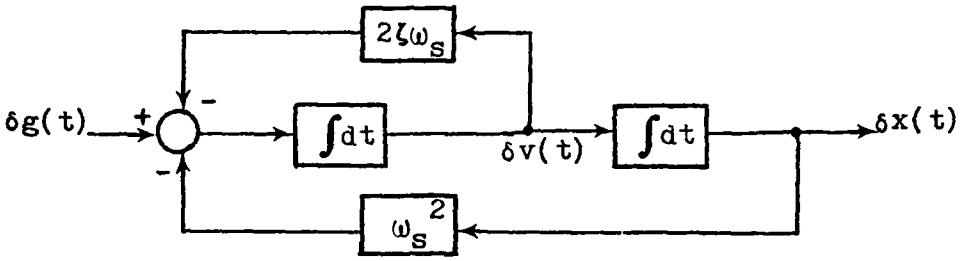

where ζ is the damping factor. For this numerical example, ζ is set to 0.3, which corresponds to an underdamped system. The F matrix

$$F = \begin{bmatrix} 0 & 1 \\ -\omega_s^2 & -2\zeta\omega_s \end{bmatrix} \tag{100}$$

yields a state transition matrix

$$\Phi(t,p) = e^{-\zeta\omega_s(t-p)} \begin{bmatrix} (\cos\omega t + \zeta\nu \sin\omega t) & (-\frac{1}{\omega}\sin\omega t) \\ (-\omega_s\nu \sin\omega t) & (\cos\omega t - \zeta\nu \sin\omega t) \end{bmatrix} \tag{101}$$

where

$$\omega = \omega_s\sqrt{1-\zeta^2} \qquad \nu = 1/\sqrt{1-\zeta^2}$$

Second the gravity disturbance model is increased in complexity by forming a second-order filter. This gravity disturbance yeilds a more realistic correlation function. The two-state correlation is rounded, as empirical data reflects, at zero shift rather than peaked at zero shift as is the correlation for the previous one-state model. The second order, stochastic model for gravity disturbance

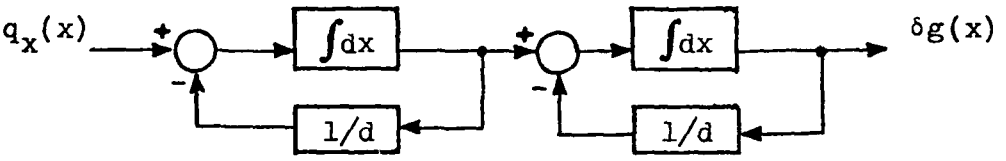

gives an autocorrelation function

$$\mathcal{E}[\delta g(x_1)\delta g(x_2)] = \sigma^2 e^{-\frac{|x_2-x_1|}{d}} \left(1 + \frac{|x_2-x_1|}{d}\right) \quad (102)$$

The parameter d is no longer the distance at which correlation is $1/e$ of the zero shift value. The term "correlation distance" of Table II should be loosely interpreted for this case. Applying (82) and (86) yields

$$Q[\underline{r}(t_1),\underline{r}(t_2)] = \sigma^2 e^{-\beta|t_2-t_1|} \left(1+\beta|t_2-t_1|\right) \quad (103)$$

Constant velocity is again used to convert the spatial correlation model to temporal:

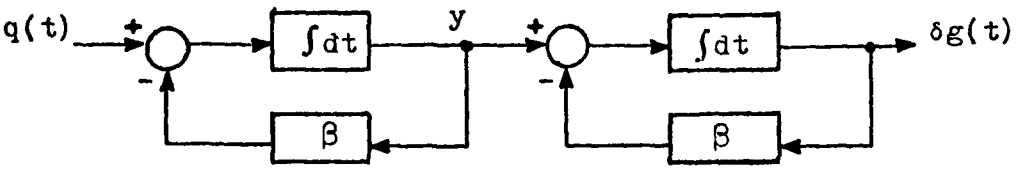

Let

$$P_g(t) = \mathscr{E}\begin{bmatrix} \delta g^2 & \delta g\, y \\ y\delta g & y^2 \end{bmatrix} = \begin{bmatrix} \sigma^2 & \beta\sigma^2 \\ \beta\sigma^2 & 2\beta^2\sigma^2 \end{bmatrix} \tag{104}$$

for filter at steady state.

An augmented system can again be formed to yield a system for which a closed-form solution is possible. Let

$$\underline{x}_a = \begin{Bmatrix} \delta x \\ \delta v \\ \hline \delta g \\ y \end{Bmatrix} \tag{105}$$

Then

$$\dot{\underline{x}}_a(t) = \left[\begin{array}{cc:cc} 0 & 1 & 0 & 0 \\ -\omega_s^2 & -2\zeta\omega_s & 1 & 0 \\ \hdashline 0 & 0 & -\beta & 1 \\ 0 & 0 & 0 & -\beta \end{array}\right] \underline{x}_a(t) + \left\{\begin{array}{c} 0 \\ 0 \\ \hline 0 \\ 1 \end{array}\right\} q(t) \tag{106}$$

Let F_a and G_a be defined from (106), then (14) is again valid. Now,

$$Q_g = [4\beta^3\sigma^2] \tag{107}$$

and from (67)

$$P_a(0) = \sigma^2 \begin{bmatrix} 0 & 0 & 0 & 0 \\ 0 & 0 & 0 & 0 \\ 0 & 0 & 1 & \beta \\ 0 & 0 & \beta & 2\beta^2 \end{bmatrix} \tag{108}$$

For numerical results, the data of Table II was again used along with the 0.3 value for ζ.

Theoretically, (14) can be solved in closed form using (106), (107), and (108). For this example, however, the true solution was found by solving (14) using a predictor-corrector integration algorithm [Ref 14].

Using (100), (101), (103), and (75), the Nested Integrals results for position and velocity variance were produced (Figures D-1 through D-4). Figures for the Damped Schuler case are located in Appendix D. Since these approximation results were generally more accurate than for the undamped case, an additional integration step size case with Δt of 240 seconds (6 on the logarithmic scale) was also included. The approximation algorithm apparently does solve (29) for the damped Schuler case in a satisfactory manner. The percent position variance error (Figure D-3) would be acceptable for most practical situations, and the fact that this error stabilizes and does not grow is reassuring. The percentage results for the undamped Schuler case, therefore, were not dependent on the presence of a ramp term in the variance solutions.

3.7 Conclusions from Schuler Loop Cases

Three alternate algorithms were produced which demonstrated the ability to solve the covariance integral. Each method had acceptable small error in calculating P(t)

given small enough integration step size Δt. The Trapezoidal algorithm was more accurate than the Rectangular algorithm. The improvement was not sufficient to warrant developing even higher order integration algorithms. On the other hand, the Nested Integrals algorithm is superior to Trapezoidal in computation efficiency and roughly equivalent in accuracy. The Nested Integrals approach was selected for further development and study.

The undamped Schuler loop used in this method's comparison left some doubt. A damped Schuler loop case was conducted with Nested Integrals to demonstrate that the results did not depend on the undamped model instability. The results in both of these Schuler loop cases verify that the Nested Integrals concept is a valid means of producing navigation error covariances.

The total navaigation system error propagation includes more than a Schuler loop, and the gravity disturbance is also multidimensional. A more realistic verification is required, then, to demonstrate the performance with a complete navigation system model.

IV. Nested Integrals Versus Linear State Space Covariance Analysis

In the last two sections, a new covariance analysis algorithm, Nested Integrals, was developed and demonstrated. The demonstrations of Section III were one-dimensional. In this section, an analysis of a complete navigation system is presented to verify further the validity of this method. As in the Schuler loop cases, the demonstration will be compared to a linear state space covariance result. Since Nested Integrals represents an alternative to the linear state space covariance analysis, it is instructive to demonstrate not only where the methods agree, but also where they yield different answers. This section presents both the full-scale verification and the point of departure by comparing Nested Integrals results to those produced by linear state space methods on a range of trajectories.

The full-scale verification is performed using a great circle trajectory. On this trajectory, the linear state space covariance analysis theoretically yields the correct result, and Nested Integrals answers are compared to those results as further proof of this new method. Two minor circle trajectories are, next, selected to violate the linear state space method's restrictions. The Nested Integrals method properly accounts for correlations in these minor circle instances, and these results should, therefore, be valid. So the difference between the two methods will

be the error induced in linear state space covariance analysis on the non-great circle trajectories. This parametric study gives insight into the extent of mission trajectories for which linear state space results might be acceptable.

To conduct these studies, models for the trajectories mentioned must be formed. Also, a full-scale gravity disturbance model which can be cast in a linear state space format must be defined. With a definition of the navigation error propagation model, then, the study can begin.

4.1 Modeling Choices

The model requirements for both types of analysis are similar. The form in which the gravity-disturbance statistical model enters the analysis is the principal difference. The details of the navigation error propagation, gravity disturbance, and trajectory models are provided in Appendices E through H. The following brief descriptions provide additional background and model interface detail.

These details come into focus when the needs of the two analyses are reviewed. Looking first at the linear state space covariance analysis, recall the structure of this method from Section II:

The error propagation model is in the form

$$\dot{\underline{x}}(t) = F(t)\underline{x}(t) + G(t)\underline{u}(t) \qquad (3)$$

The gravity disturbance is modeled as a Gauss-Markov process by

$$\dot{\underline{x}}_g(t) = F_g(t)\underline{x}_g(t) + G_g(t)\underline{q}(t) \qquad (4)$$

The disturbance input to the navigation errors is

$$\underline{u}(t) = C_g(t)\underline{x}_g(t) \qquad (5)$$

subject to,

$$\mathcal{E}[\underline{q}(t)\underline{q}^T(p)] = Q_g(t)\delta(t-p) \qquad (6)$$

The augmented state is defined by

$$\underline{x}_a(t) = \begin{Bmatrix} \underline{x}(t) \\ \cdots\cdots \\ \underline{x}_g(t) \end{Bmatrix} \qquad (7)$$

so,

$$\dot{\underline{x}}_a(t) = F_a(t)\underline{x}_a(t) + G_a(t)\underline{q}(t) \qquad (8)$$

where

$$F_a(t) = \left[\begin{array}{c:c} F(t) & G(t)\,C_g(t) \\ \cdots\cdots & \cdots\cdots\cdots \\ 0 & F_g(t) \end{array}\right] \qquad (9)$$

and

$$G_a(t) = \begin{bmatrix} 0 \\ \cdots\cdots \\ G_g(t) \end{bmatrix} \qquad (10)$$

The covariance of the augmented state satisfies

$$\dot{P}_a(t) = F_a(t)P_a(t) + P_a(t)F_a^T(t) + G_a(t)Q_g(t)G^T(t) \qquad (14)$$

Solving (14) yields the linear state space results

The state $\underline{x}$ and $\underline{x}_g$ must be defined and then the components of each associated model given. The navigation error propagation model of (3), for this study, is that of Widnall and Grundy [Ref 9 :26-27]. The vertical channel

is modified to represent a stable system based on altimeter aiding as suggested by Britting [Ref 8]. The navigation error state vector of the Widnall-Grundy model has nine elements

$$\underline{x}(t) = \begin{Bmatrix} x_1(t) \\ \vdots \\ x_9(t) \end{Bmatrix} \tag{109}$$

which are defined as follows:

x_1 is $\delta\lambda$, error in longitude

x_2 is $\delta\phi$, error in latitude

x_3 is δh, error in altitude

x_4 is δv_e, error in east earth-relative velocity

x_5 is δv_n, error in north velocity

x_6 is δv_z, error in vertical velocity

x_7 is ϵ_e, orientation error about the east axis (local level)

x_8 is ϵ_n, orientation error about the north axis (local level)

x_9 is ϵ_z, orientation error about the vertical axis.

The modified Widnall-Grundy F-matrix for (3) is provided in Appendix E. Consistent with the east-north-vertical coordinate frame of the navigation error states, the gravity disturbance is defined

$$\underline{u}(t) = \delta\underline{g}^n(t) = \begin{Bmatrix} \delta g_e(t) \\ \delta g_n(t) \\ \delta g_z(t) \end{Bmatrix} \tag{110}$$

where the n superscript indicates the physical vector is mathematically represented in n-frame (east-north-vertical or "navigation" frame) coordinates. These $\delta\underline{g}^n$ terms drive the respective $\delta\dot{\underline{v}}^n$ terms in (3).

$$\underline{G} = \begin{bmatrix} 0 \\ \cdots \\ I \\ \cdots \\ 0 \end{bmatrix} \tag{111}$$

where the partitions are each 3X3 matrices.

Since a linear state space covariance analysis is to be performed, a statistical model for gravity disturbances in the form of (4) must be provided. To complement the full-scale navigation error model, an eight-state gravity disturbance model is selected [Ref 19]. This linear shaping filter has been the subject of much research [Ref 12] aimed at producing a model which replicates empirically derived anomaly correlations and which yields auto- and cross-correlations of other disturbance terms consistent with gravitational field theory. The filter can be viewed as three separate linear systems each driven by an element of $\underline{q}$. Stationary statistics were assumed in the model development [Ref 19], so the noise strength Q_g is constant. A linear combination of the filter states, $\underline{x}_g$ elements, form gravimetric deflections and anomaly. The details of the $C_g(t)$ output matrix of (5) along with the F_g and G_g matrices of (4) are provided in Appendix F. Q_g is also described in Appendix F.

With these elements of the analysis defined, the F_a and G_a can be formed. Thus, $\dot{P}_a$ can be evaluated by (14) and numerical solutions for P_a attained.

The initial condition must be supplied to start the solution process. Even though the navigation error covariance is zero initially, the augmented state covariance is non-zero, because the modeled gravity process is assumed to be stationary, hence must be initialized in its steady state condition. To model this in-process situation, the gravity disturbance covariance is assumed to be at steady state P_g. This initial condition leads to

$$P_a(t_o) = \begin{bmatrix} 0 & \vdots & 0 \\ \cdots & \vdots & \cdots \\ 0 & \vdots & P_g \end{bmatrix} \tag{112}$$

where the zero matrices are of required dimension. The P_g initial condition for the gravity disturbance state's covariance is specified in Appendix F.

Now, turning to the Nested Integrals analysis, the pertinent equations from Section II are:

$$\dot{\underline{x}}(t) = F(t)\underline{x}(t) + G(t)\underline{u}(t) \tag{3}$$

From (28),

$$Q(p,q) = \mathcal{E}\{\underline{u}(p)\underline{u}^T(q)\} \tag{28a}$$

From (16),

$$\dot{\Phi}(t,t_i) = F(t)\Phi(t,t_i) \tag{16a}$$

for $t \geq t_i$, and with initial condition $\Phi(t_i,t_i) = I$.

$$\dot{P}(t) = G(t)D(t) + D^T(t)G^T(t)+P(t)F^T(t)+F(t)P(t) \qquad (29a)$$

$$D(t) = \int_{t_o}^{t} Q(t,p)G^T(p)\Phi^T(t,p)dp \qquad (29b)$$

Solving (29) yields the Nested Integrals result.

F(t), G(t), and $\underline{u}(t)$ are described above. The Q(p,q) correlation matrix function is the form of the gravity disturbance statistical model for Nested Integrals.

Q(p,q) is formed from the same model used in linear state space analysis. Equation (4) for the linear state space method is the temporal form of a spatial statistical process (see Appendix B). The correlations of $\underline{x}_g$ are solved in this spatial domain and the output matrix of (5) applied to yield the elements of Q(p,q). This matrix function is provided in Appendix F with the method for producing the central angle and heading associated with the $\underline{r}(p)$ - $\underline{r}(q)$ pair.

Solution of (29) can commence with the specification of zero initial condition for P(t) as discussed in Section II.

The linear state space and Nested Integrals analyses described above need a trajectory model to evaluate F(t), $C_g(t)$, Q_g, P_g, F_g, and Q(p,q). The great circle trajectory is described in Appendix G and the minor circle trajectory in Appendix H. A constant altitude profile is modeled for both the great circle and minor circle trajectories. This flight path avoids upward continuing [Ref 13] the gravity statistics. For convenience, the velocity is also held

constant at a value consistent with a bomber or transport aircraft cruise. The algorithm generating the great circle flight path (Appendix G) differs from the minor circle (Appendix H) in that an inclination can be specified. The inclination given in Table IV forces the great circle path off a cardinal direction and, thus, insures that all navigation channels are exercised in this study. The flights are all modeled to occur in the same geographic area, so minor circle results can be compared directly to great circle results. With these trajectory models, the modeling structures for both the great circle and the minor circle cases are set, and the studies themselves can be addressed.

4.2 Great Circle Case

The data required by the trajectory model of Appendix G and the gravity disturbance statistical model for the great circle case are given in Table IV , below. These data will be used in several studies in Sections VI through IX. Also, the minor circle trajectories will use the same data set with two exceptions; inclination, i, is unused and the initial circle angle, Λ_o, has a different meaning which is explained in Appendices G and H. The Nested Integrals integration step size is also provided in Table IV.

As proposed, both Nested Integrals and linear state space covariance analyses are performed on the great circle case. Since the trajectory does not violate the linear

TABLE IV - Great Circle Case Data

Quantity	Symbol	Value	Units
Final time	t_f	12240	seconds
Initial time	t_o	0	seconds
Initial circle angle†	Λ_c	0	degrees
Inclination angle†*	i	45	degrees
Velocity magnitude*	V	615	ft/sec
Earth radius	R_e	20925640	ft
Altitude	h	0	ft
Gravity magnitude	g	32.174	ft/sec^2
Earth rotation rate	ω_{ie}	$7.2921 \cdot 10^{-5}$	rad/sec
Anomaly variance	σ_g^2	1800	$(mgal)^2$
Correlation parameter	d	20	n m
Nested Integrals step size	Δt	30	sec

† Meaning varies. See Appendix G for great circle and Appendix H for minor circle interpretations.

* Earth relative terms

‡ Applies to great circle only.

state space constraints, those results should be correct and offer a benchmark against which Nested Integrals performance can be judged on this full-scale case. The covariance results by both methods at 200 minutes into the mission are provided in Table V. All 45 independent elements of the covariance matrix are given in lower tri-

TABLE V - COVARIANCE COMPARISON: GREAT CIRCLE CASE, MISSION TIME 200. MIN.

NESTED INTEGRALS SOLUTION

.5094E-08								
-.1784E-08	.4486E-08							
-.3589E-01	-.2800E-01	.2514E+07						
.6074E-05	.1764E-04	.9020E+03	-.2805E+01					
-.2321E-04	.5626E-05	.7037E+03	-.1096E+01	.2807E+01				
-.4516E-04	-.3739E-04	.4741E+02	-.1049E+01	-.8238E+00	.3487E+01			
.1784E-08	-.4486E-08	.2800E-01	-.1764E-04	-.5626E-05	.3739E-04	.4486E-08		
.4940E-08	-.1730E-08	-.3480E-01	.5890E-05	-.2251E-04	-.4476E-04	.1730E-08	.4790E-08	
.1244E-08	-.4358E-09	-.8766E-02	.1483E-05	-.5669E-05	-.1127E-04	.4358E-09	.1207E-08	.3039E-09

LINEAR STATE SPACE SOLUTION

.5096E-08								
-.1785E-08	.4485E-08							
-.3586E-01	-.2800E-01	.2515E+07						
.6068E-05	.1773E-04	.9015E+03	-.2805E+01					
-.2333E-04	.5625E-05	.7048E+03	-.1096E+01	.2807E+01				
-.4612E-04	-.3745E-04	.4736E+02	-.1048E+01	-.8240E+00	.3488E+01			
.1785E-08	-.4485E-08	.2800E-01	-.1773E-04	-.5625E-05	.3745E-04	.4485E-08		
.4942E-08	-.1731E-08	-.3477E-01	.5884E-05	-.2262E-04	-.4472E-04	.1731E-08	.4792E-08	
.1245E-08	-.4360E-09	-.8758E-02	.1482E-05	-.5698E-05	-.1126E-04	.4360E-09	.1207E-08	.3040E-09

PER CENT DIFFERENCE

-.4278E-01								
-.5294E-01	.2545E-01							
.9760E-01	-.6949E-02	-.2638E-01						
.9409E-01	-.5326E+00	.6246E-01	-.3348E-01					
-.5002E+00	.1916E-01	-.1604E+00	-.1396E-01	.2459E-01				
.7889E-01	-.1425E+00	.1052E+00	.9494E-01	-.2875E-01	-.2391E-01			
-.5294E-01	.2545E-01	-.6949E-02	-.5326E+00	.1916E-01	-.1425E+00	.2545E-01		
-.4278E-01	-.5294E-01	.9760E-01	.9409E-01	-.5002E+00	.7889E-01	-.5294E-01	-.4278E-01	
-.4278E-01	-.5294E-01	.9760E-01	.9411E-01	-.5002E+00	.7889E-01	-.5294E-01	-.4278E-01	-.4278E-01

UNITS

RAD**2								
RAD**2	RAD**2							
FT	FT	FT**2						
FT/SEC	FT/SEC	FT**2/SEC	(FT/SEC)**2					
FT/SEC	FT/SEC	FT**2/SEC	(FT/SEC)**2	(FT/SEC)**2				
FT/SEC	FT/SEC	FT**2/SEC	(FT/SEC)**2	(FT/SEC)**2	(FT/SEC)**2			
RAD**2	RAD**2	FT	FT/SEC	FT/SEC	FT/SEC	RAD**2		
RAD**2	RAD**2	FT	FT/SEC	FT/SEC	FT/SEC	RAD**2	RAD**2	
RAD**2	RAD**2	FT	FT/SEC	FT/SEC	FT/SEC	RAD**2	RAD**2	RAD**2

angular format. Using the linear state space answers as a base, the differences in the results are expressed in percent in Table V. The largest difference between the two methods at 200 minutes is only one-half of one percent.

Table V gives assurance that all elements are being calculated correctly at one time. Next, circular-error-probable is calculated throughout the mission to demonstrate that the solutions agree over all time. The circular-error-probable (CEP) summarizes the horizontal position covariances into one well-accepted figure of merit. This statistic is calculated by an approximation for a multi-dimensional normal distribution [Ref 20]; the calculation details are presented in Appendix I.

The circular-error-probable results for the great circle case are displayed in Figure 10. Agreement between the two analysis methods is so close that the curve markers must be offset to clarify that two curves are plotted. These results, together with Table V, clearly demonstrate the validity of the Nested Integrals analysis on a full-scale problem.

In this case, the results are equivalent, but Nested Integrals required approximately three times the computation time as did linear state space. The input/output time for Nested Integrals was nearly twice the computation time because of the 21,012 file GET operations; whereas,

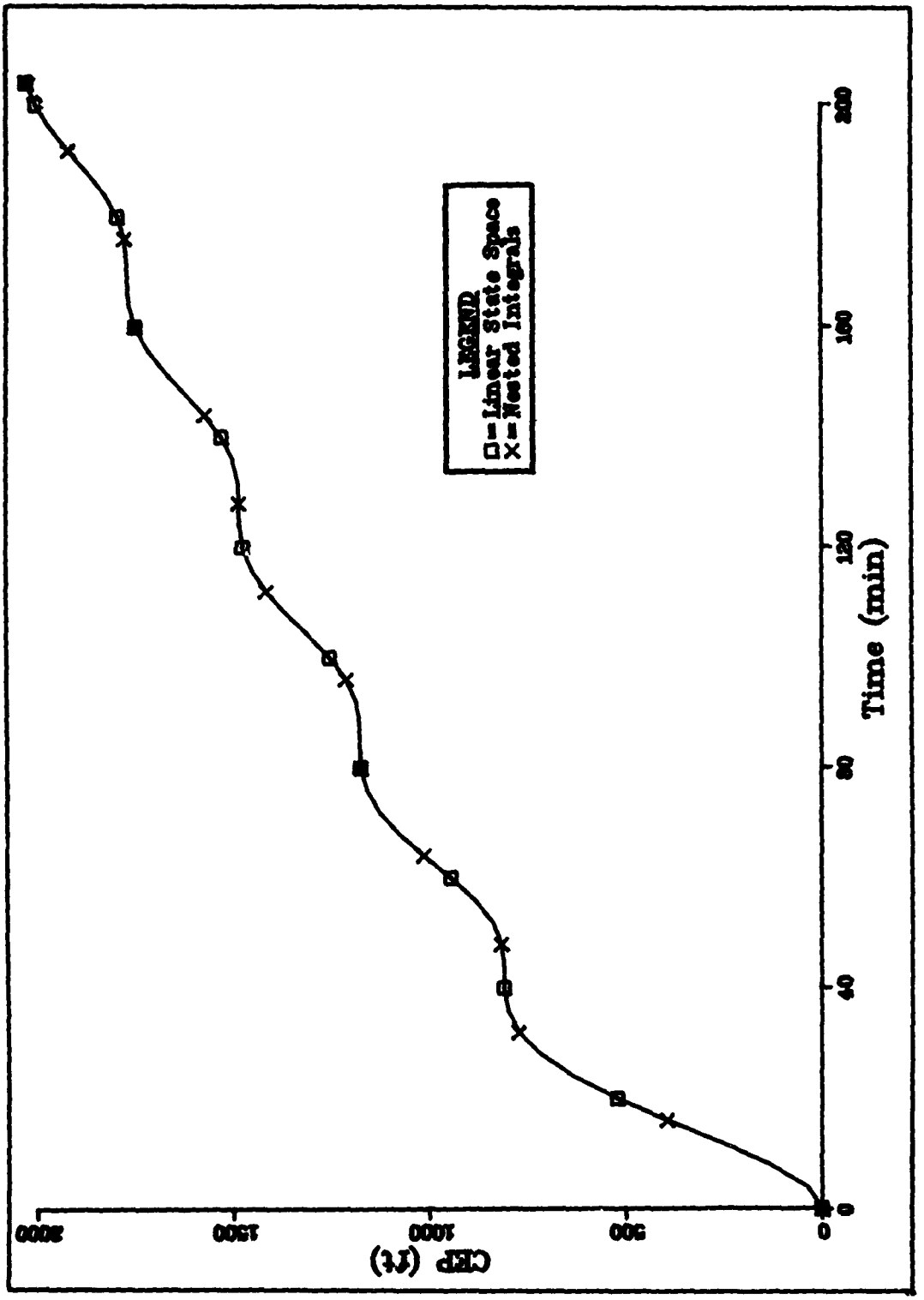

Figure 10. Circular-Error-Probable: Great Circle Case Comparison

the linear state space input/output time is virtually nil. While no efforts were made to minimize computer resource costs, it is clear that a substantial penalty is paid when Nested Integrals is used in place of the linear state space covariance analysis; therefore, the errors produced by linear state space analysis on other than great circle trajectories must be considered.

4.3 Minor Circle Cases

Precisely this consideration prompts the minor circle trajectory study. The great circle case, viewed as a 3444 n m minor circle radius case, has shcwn exact comparisons between Nested Integrals and linear state space covariance analyses. Two other minor circle cases are proposed here to scan parametrically the trajectory restriction effects. Minor circle cases are defined by the radius of the closed flight path in a planar sense. The details of the minor circle trajectory are provided in Appendix H. The parametric range should include trajectories for which linear state space analysis is expected to err significantly.

Intuitively, one expects little error on cases where the minor circle radius is much larger than the correlation parameter. Of course, any trajectory that completes a minor circle is expected to elicit some error when using the linear state space method since the linear state space modeling grossly misrepresents the correlations along such a path. More pronounced effects should be observed on

cases where the minor circle radius is of the same order of magnitude as the correlation parameter. To cover this range of effects, additional minor circle cases of 197 nm and 20 nm radii are studied. The 197 nm case completes exactly one circuit in the 204 minutes of simulated flight. This radius is approximately five times the 20 nm correlation parameter, so this case should represent a transition to trajectories with significant errors. To evoke some definite errors, the final trajectory is a relatively tight turn of 20 nm radius. This radius equals the correlation parameter, and this case completes nearly ten circuits during the 204-minute flight.

The parameteric scan of this study, then, includes trajectories of 3444, of 197, and of 20 nm minor circle radii. Before reviewing the covariance results, consider the effect this set of trajectories has on central angle and, therefore, on correlations. The central angle $\psi(t,t_o)$ between $\underline{r}(t_o)$ and $\underline{r}(t)$ will serve as the example. For the minor circle cases (see Appendix H for derivation),

$$\psi(t,t_o) = \cos^{-1}\left\{\frac{R_e^2 - r_c^2[1-\cos\{(t-t_o)V/r_c\}]}{R_e^2}\right\} \qquad (113)$$

where r_c is minor circle radius as defined in Appendix H. From (113), it follows that the great circle case, $r_c=R_e$, yields

$$\psi(t,t_o) = |t-t_o|\ V/r_c \qquad (114)$$

subject to $0 \leq \psi \leq 180^{o}$. This central angle to the original point is presented, for all three cases, in Figure 11. With this example it is clear that only the great circle case gives the same results for $\psi(t_2,t_1) + \psi(t_1,t_o)$ as for $\psi(t_2,t_o)$ -- a matter discussed at the end of Section II regarding the trajectory restriction.

This spatial variation is reflected in the correlations of anomalous gravity terms. For illustration, consider the correlation of anomaly at t_o with anomaly at t throughout the flights. The model anomaly correlation function for this study specifies that [Ref 19]

$$\phi_{gg}(\psi) = \sigma_g^2 \left[1 + M - \tfrac{1}{2}M^2\right] e^{-M} \qquad (115)$$

where

$$M = r\,\psi/d \qquad (116)$$

and

r is position vector radius,

d is correlation parameter, and

σ_g^2 is anomaly variance.

All three quantities are defined and background on (115) is given in Appendix F. The correlation of $\Delta g(t_o)$ with $\Delta g(t)$ for all three minor circle cases are presented in Figure 12. The strong effects of trajectory on correlation are clear. On every complete circuit, the anomaly correlation with the initial point becomes the anomaly variance again. The linear state space covariance analysis forces the great circle correlation rule regardless of

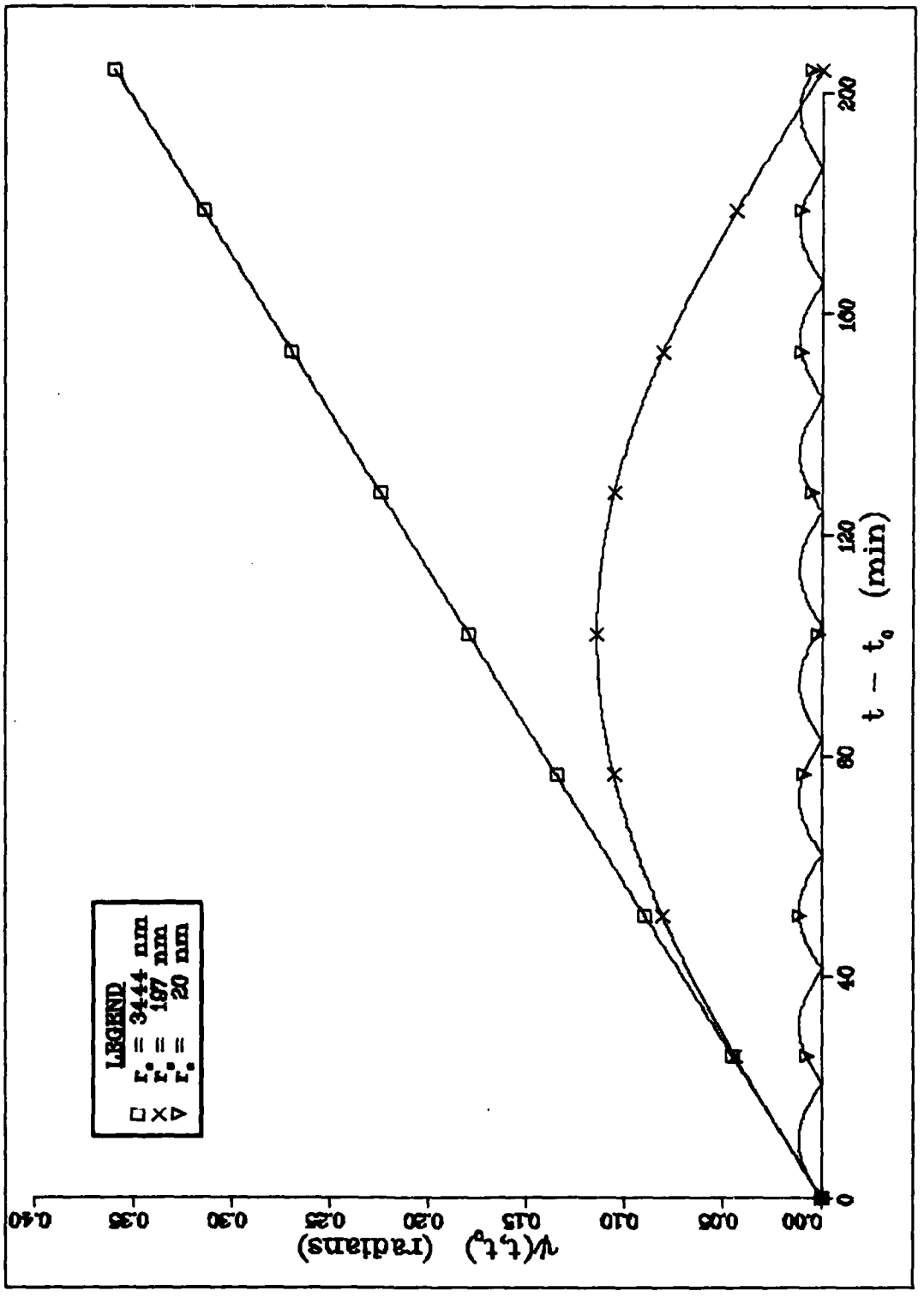

Figure 11. Minor Circle Cases: Central Angle Comparison

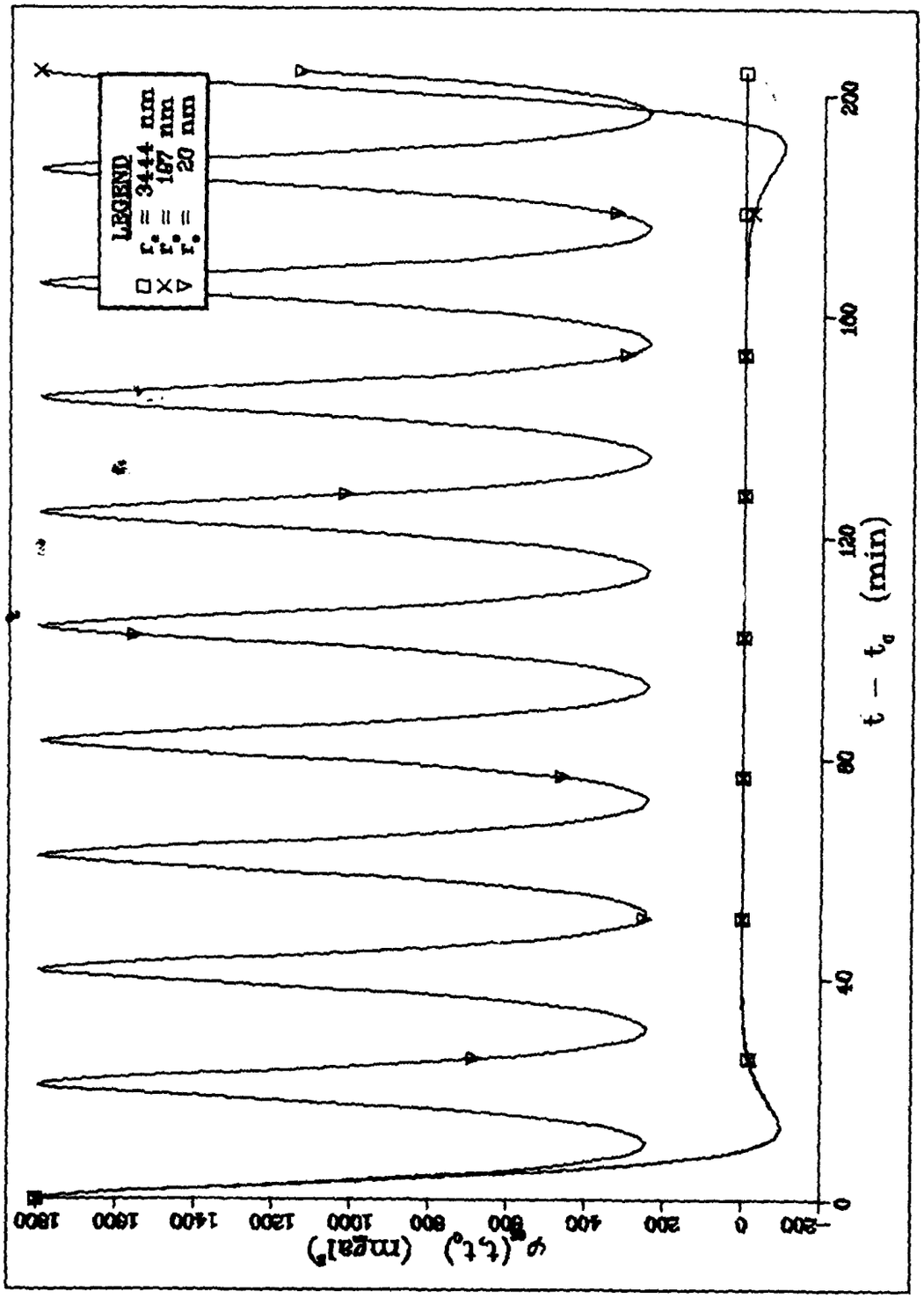

Figure 12. Minor Circle Cases: Anomaly Correlation Comparison

trajectory and, hence, introduces error.

With this understanding of the underlying correlation mismodeling, the results should come as no surprise. The 3444 nm case results were presented previously in Figure 10. The 197 nm case results are presented in Figure 13, and the 20 nm results are shown in Figure 14. The 197 nm case shows a close agreement between the two analysis methods over the first half of the flight, as one would expect from the apparent match between the great circle and the 197 nm minor circle correlations shown in Figure 12. The correlation curves diverge when the minor circle closes, and a slight divergence is seen in the circular-error-probable results toward the end of the 204-minute mission. The results by linear state space on the 197 nm case appear close enough to the current Nested Integrals results for practical applications. The substantial computational advantage of linear state space would motivate the acceptance of such minor errors on this mission.

The 20 nm circle results match well for one half of the minor circle, again. In this case, however, the correlation and circular-error-probable agreements lasts only one-twentieth the flight time. After that, the linear state space covariance analysis result is drastically different from the correct Nested Integrals result. The two results would give close to the same average circular-error-probable; however, the peak values are substantially

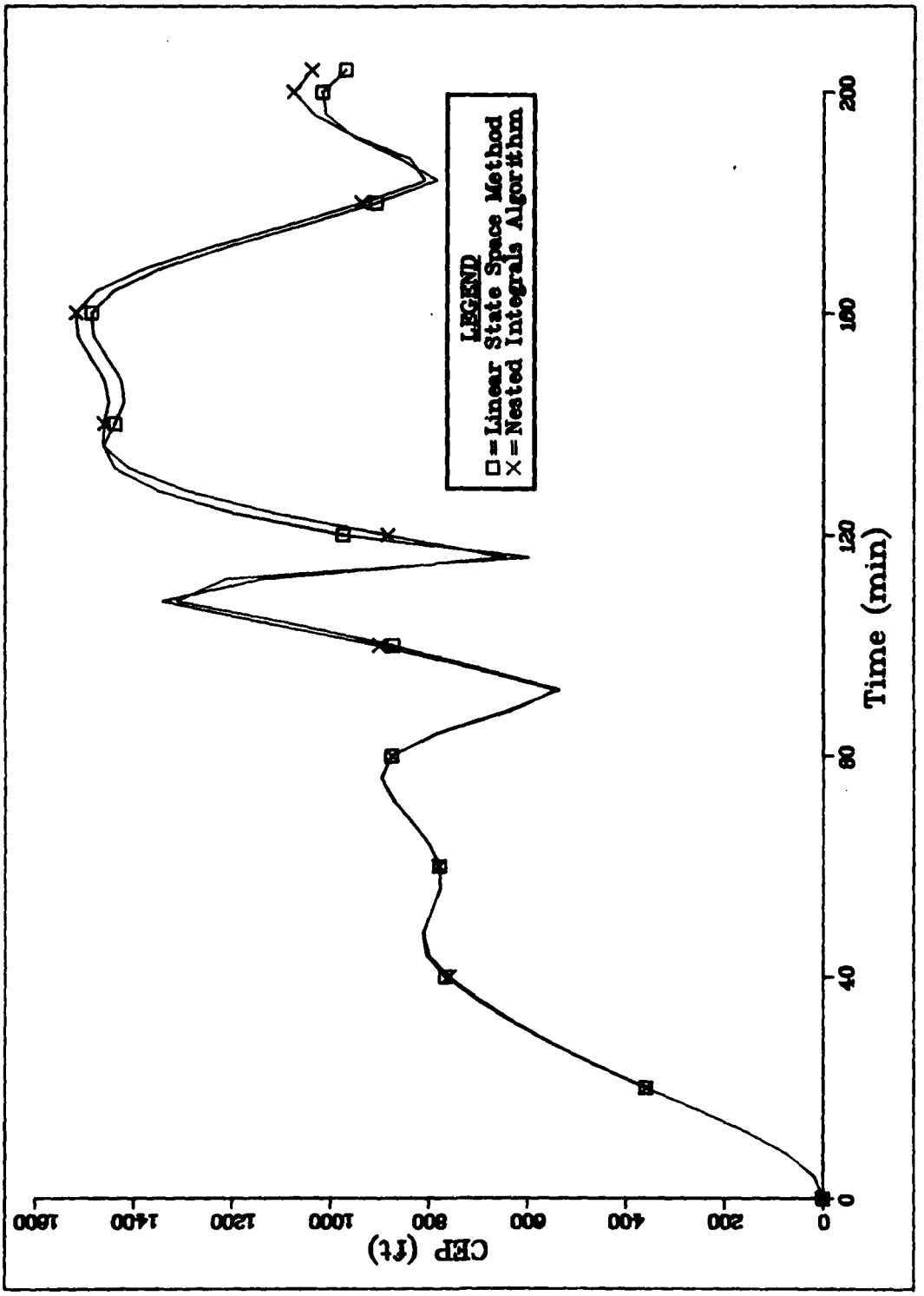

Figure 13. Circular-Error-Probable: 197 nm Minor Circle Case

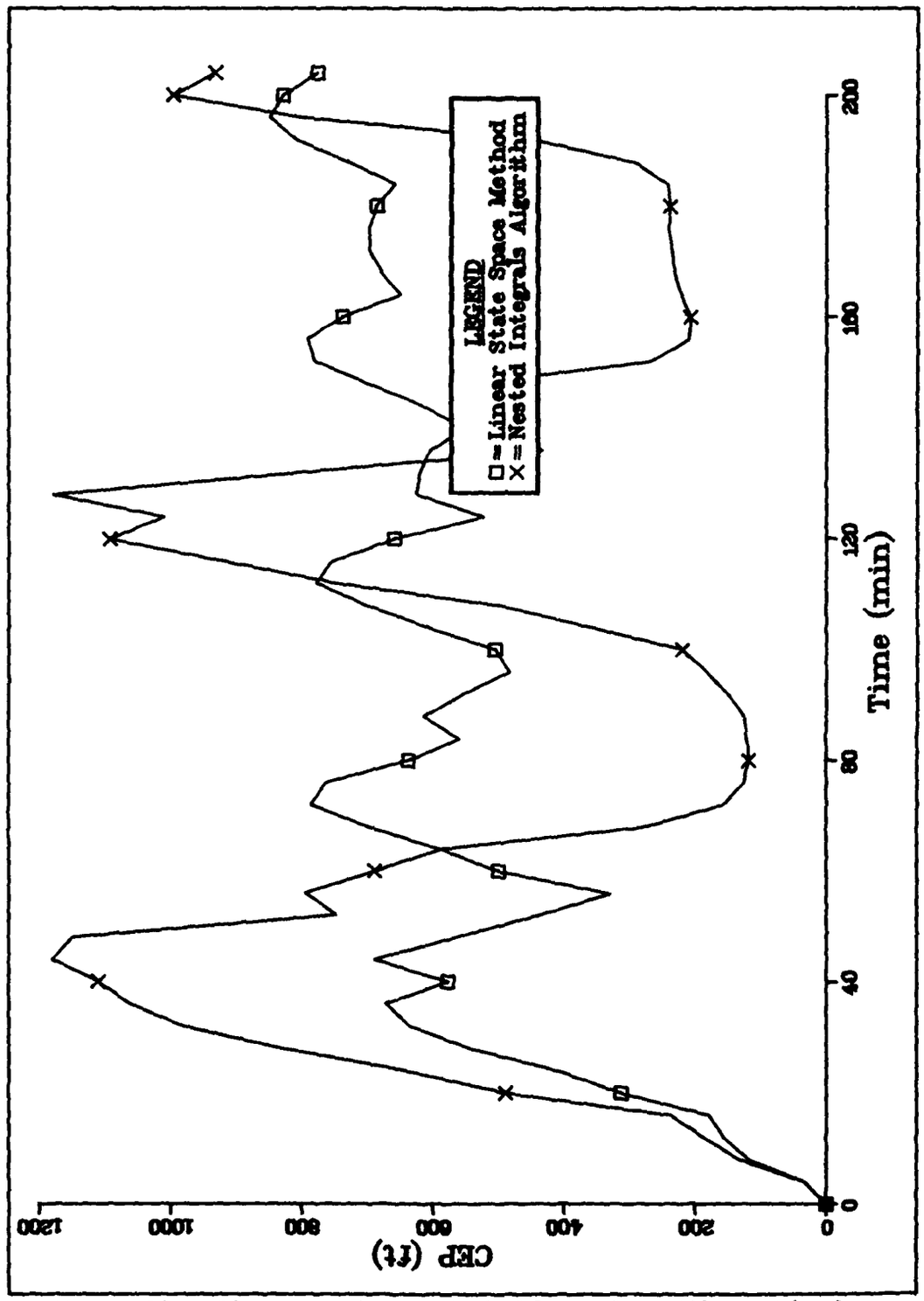

Figure 14. Circular-Error-Probable: 20 nm Minor Circle Case

different. While the linear state space results for the 197 nm case may be acceptable as an approximation, the results on the 20 nm case seem hopelessly wrong. Each analyst would find his subjective threshold of tolerable error somewhere in the span of minor circle radius. The Nested Integrals approach makes visible now the error of the linear state space covariance analysis.

Another insight afforded by Nested Integrals analysis is the effect of the trajectory on navigation errors presented in Figure 15. The Nested Integrals results are assumed to be correct due to the great circle verification. A Monte Carlo verification of these minor circle results was not performed since a more useful Monte Carlo verification is given in Section V. The three Nested Integrals results for the minor circle cases are plotted on the same scale for comparison. Note that the higher correlations on the smaller minor circles do not breed higher errors in general. In the long run, the great circle special case produces significantly higher errors.

4.4 Comparison Conclusions

The minor circle and great circle studies have proved two points and have provided some insights not previously available. First, the Nested Integrals algorithm is verified on a full-scale problem. Then, the potential error of using linear state space covariance analysis is demonstrated through trajectory variations out of the great

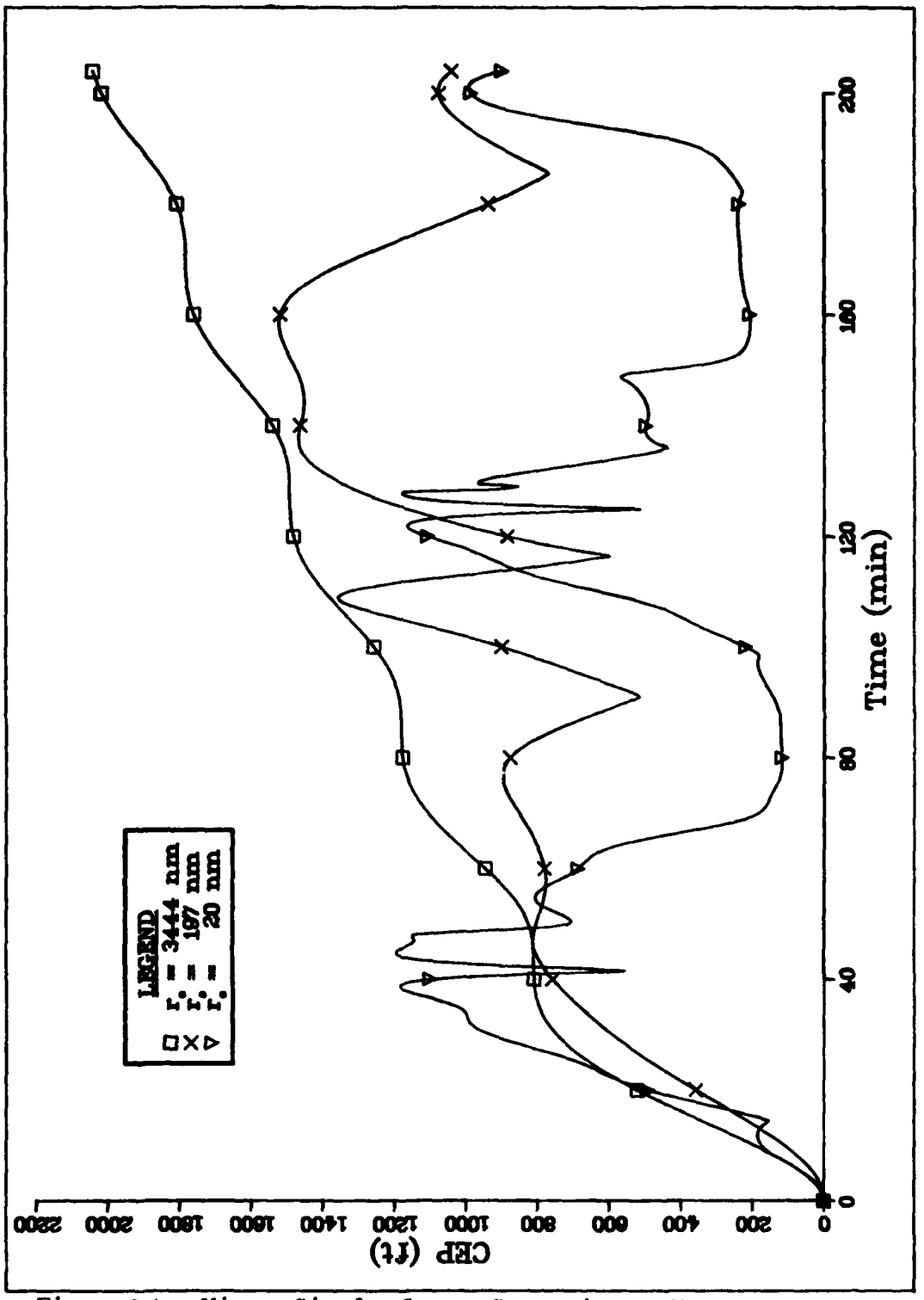

Figure 15. Minor Circle Cases Comparison, Nested Integral Results

circle restriction. This latter process gives insight into how significant these errors might be and into when the error level might be accepted in order to gain the greater computational efficiency of linear state space methods. Finally, a comparison of gravity-induced navigation errors as a function of the trajectory is provided by the Nested Integrals method. The results are interesting and provide a view of issues not seen before. The fact that Nested Integrals can correctly calculate these covariances in an efficient manner is a prime aim of this research. A needed alternative to the linear state space analysis trajectory restrictions has been presented on a full-scale problem.

V. Nested Integrals Versus Monte Carlo Analysis

The three statistical analyses discussed in Sections I and II are linear state space covariance analysis, Monte Carlo analysis, and covariance integral analysis. Nested Integrals, as a covariance integral type of analysis, was compared to linear state space analysis in Section IV. The minor circle trajectories used in Section IV while violating the linear state space restrictions still do not exercise the full range of Nested Integrals capability. Also, the question of whether this new method is more efficient than Monte Carlo must be faced. For these reasons, this section is devoted to a Nested Integrals to Monte Carlo comparison on a complex trajectory. The vehicle for this comparison is a recently completed Monte Carlo study of an air-launched strategic missile mission [Ref 10]. Nested Integrals method is used on the same problem allowing a direct comparison of results and computational costs.

The comparison of Nested Integrals to Monte Carlo method is the primary motivation for this particular study, but several other features are offered:

a. Complex trajectory. The strategic missile trajectory is significantly different from the constant-groundspeed, level-flight mission used in Section IV. While the missile trajectory stays in a great circle plane the flight profile has significant acceleration and altitude changes. Groundspeed increases some 3285 ft/sec while altitude

changes almost 80,000 feet in the initial boost and climb phases. Again, the trajectory flexibility required for studies such as this is a prime motive for Nested Integrals development.

b. Correlation model variation. The Monte Carlo analysis employed a different statistical model [Ref 21] than the previous linear state space model. For this complex altitude profile, a statistical model must, and this one does, give correlations at and between different altitude levels which are consistent with the interrelationships imposed by gravitational field theory (upward continuation). The flexibility to use a variety of statistical models is also one prime motive for the Nested Integrals development.

c. Real-world problem. The problem addressed here is not academic. Analyses of this type are typical of the exercise performed in generating an error budget for a proposed new system. In this sense, the air-launched strategic missile represents a real-world problem on which the Nested Integrals methods can be applied.

d. Independent verification. The author was the Air Force study manager for the Monte Carlo analysis, but the model selection and analysis were performed by the contractor, a separate party. These published results [Ref 10] offer an independent check on the newly developed Nested Integrals method.

The rationale for this comparison is to emulate the Monte Carlo study as nearly as possible. The Monte Carlo study is, therefore, discussed before the Nested Integrals model selection. Finally, navigation accuracy results are compared and computational costs are contrasted.

5.1 Advanced Strategic Air-launched Missile Problem

The problem is the medium through which Nested Integrals is compared to Monte Carlo analysis. The genesis of the problem was a system accuracy, error-budget exercise conducted by Aeronautical Systems Division of the Air Force Systems Command. Several trajectories were considered in an elaborate trade-off of systems and flight strategies.

The linear state space covariance analysis approach is typically used for estimating the gravity model contributions. This trajectory clearly violates the constant altitude model restriction, and some analysis considering upward continuation was desired. Geodynamics Corporation was tasked in August, 1977 to perform an analysis which would give the gravity model contribution to inertial navigation errors on this complex mission. The results of that study are recorded in Reference 10 dated August, 1978. Of the studies included in that work, the 1500-nm missile trajectory is selected as a case on which to apply Nested Integrals analysis.

5.2 Monte Carlo Study

The aspects of the Monte Carlo study which affect the course of the Nested Integrals analysis are:

a. the trajectory,

b. the navigation simulation, and

c. the statistical model.

These categories, obviously, are the three models needed for Nested Integrals analysis.

The trajectory used for the Monte Carlo study is described on page 6 of Reference10. The necessary excerpts from that description are presented in TableVI, below. The Monte Carlo trajectory generator used acceleration polynomials to match segment endpoint conditions [Ref 10:4]. The position time history, θ_o, was calculated from the resulting acceleration profile. With both acceleration and position profiles for the design mission, the specific force profile was generated using a truth model for gravity [Ref 10:4]

$$\underline{f}(t) = \underline{a}(t) - \underline{G}[\underline{r}(t)] \qquad (117)$$

where $\underline{f}(t)$ is specific force,

$\underline{a}(t)$ is total acceleration,

$\underline{G}[\,]$ is true gravitation, a vector not to be confused with the distribution matrix of the linearized navigation error propagation model, and

$\underline{r}(t)$ is from θ_o, the design mission.

The navigation simulation was whole valued and based on solving

Table VI - Missile Flight Path Data

Method	Time (min)	Groundspeed (ft/sec)	Geodetic Height (ft)	Geodetic Latitude (deg N)	Longitude (deg E)	Path* Acceleration (g's)	Tangential* Acceleration (g's)	Event
Monte Carlo	535.0	615	500	57.421	22.040			Launch/boost
	535.2	2600	500	57.386	22.090			Boost/ascent
	536.7	3900	80000	56.680	22.070			Cruise
	573.0	3900	80000	36.434	40.103			Dive
	576.1	600	500	35.233	40.759			Terminal pt.
Nested Integ.	535.00*	615*	500*	57.421*	22.040*	5.137*	0*	Launch/boost
	535.20	2600	500	57.379	22.100	0	7.0	Pitch up 16.3°
	535.33	3900	4103	57.335	22.163	5.137	0	Boost/climb
	535.46	3900	11271	57.282	22.238	0	0	Climb
	536.70	3900	79986	56.808	22.898	0	7.0	Pitch over
	575.00	3900	79986	35.323	40.752	0	0	Terminal pt.

* These quantities are specific inputs to PROFGEN [Ref 7] and are discussed in subsection 5.3.

$$\ddot{\underline{r}}(t) = \underline{a}(t) = \underline{f}(t) + \underline{G}(t) \qquad (1b)$$

Letting "^" represent navigation estimates, the navigation simulation solved

$$\hat{\ddot{\underline{r}}}(t) = \underline{f}(t) + \underline{G}_m[\hat{\underline{r}}(t)] \qquad (118)$$

where $\underline{G}_m$ is the gravitational model simulated here as

$$\underline{G}_m[\hat{\underline{r}}(t)] = \underline{G}[\hat{\underline{r}}(t)] + \delta\underline{g}[\underline{r}(t)] \qquad (119)$$

and $\delta\underline{g}[\underline{r}(t)]$ is the gravity disturbance stochastic realization from the statistical model. The navigation position error is defined as

$$\delta\underline{r}(t) = \hat{\underline{r}}(t) - \underline{r}(t) \qquad (120)$$

The Monte Carlo approach is to produce an ensemble of $\delta\underline{r}(t)$'s based on an ensemble of $\delta\underline{g}[\underline{r}(t)]$'s. The gravity disturbance ensemble is generated in such a manner that, in the limit, the correlations of the statistical model are replicated. The theory is that the ensemble of navigation error time histories is representative of those which would be produced by the population of $\delta\underline{g}$'s whence the original statistics were derived. For this study Geodynamics defined

$$\delta\underline{g}^{\ell}(t_i) = -\begin{Bmatrix} g\ell_i \\ gm_i \\ \Delta g_i + 2(g/r)N_i \end{Bmatrix} \qquad (121)^*$$

---

* This notation is maintained here for traceability to the Monte Carlo study. Crossrange deflection m is equivalent to transverse deflection μ, and ℓ to τ from Appendix F.

where

ℓ is the downrange deflection

m is the crossrange deflection

Δg is anomaly

N is geoidal height

ℓ superscript indicates the local-level downrange-crossrange-vertical coordinate frame.

The $2(g/r)N_i$ term corrects for the fact that Δg_i is not exactly δg_z. This minor correction has an insignificant effect on the results calculated in this case which is why $\delta g_z = -\Delta g$ was used as the model in Section IV. Due to computer core limitations, the desire for more dense sampling of the deflection disturbances, and an assumed altimeter-aided system, this hypothetical vertical disturbance was not even simulated [Ref 10:49] in the Monte Carlo study.

Next, a statistical model was needed on which to base the ensemble of gravity disturbance profiles. The Tscherning-Rapp anomaly degree variance model [Ref 21:43-46] number 4 was selected. The mathematical details of this model are repeated, in part, in Appendix J. This statistical model is based on a spherical harmonic representation of the anomaly autocorrelation, assumed to be spatially stationary and isotropic.

This model's coefficients explicitly represent the contribution to anomaly variance of spatial frequency terms - hence the title anomaly degree variance model. A

closed mathematical form relating harmonic coefficient to degree number is hypothesized (see Appendix J) and the resultant model fit to empirical data by a parameter identification process. Using gravitational field theory the auto- and cross-correlations of and between deflection and geoidal undulations are derived in turn using the anomaly correlation model as a basis. Throughout this derivation, the altitude coordinate information for both positions of the correlation evaluation is maintained and, thereby, provides the theoretically consistent means of upward continuing the statistics.

To employ this model, $\delta\underline{g}$ evaluations were generated for 98 position points corresponding to 25-second time increments. Let i subscripts represent t_i quantities for i=1, ..., 98. Then define

$$\delta\underline{g}_i = \delta\underline{g}(\underline{r}_i) \tag{122}$$

From the sequence $\{\delta\underline{g}_i\} = \{\delta\underline{g}_1, \delta\underline{g}_2, \ldots \delta\underline{g}_{98}\}$ define the ensemble mathematical vector

$$\overline{\delta\underline{g}} = \begin{bmatrix} \delta\underline{g}_1 \\ \delta\underline{g}_2 \\ \vdots \\ \delta\underline{g}_{98} \end{bmatrix} \tag{123}$$

Let $\overline{\phi}$ represent the correlation

$$\overline{\phi} = \mathcal{E}[\overline{\delta\underline{g}} \quad \overline{\delta\underline{g}}^T] \tag{124}$$

Equation (124) can be evaluated given the statistical model, (122), and the sequence $\{\underline{r}_i\}$. Define a square root matrix S by

$$\overline{\phi} = SS^T \tag{125}$$

Then a population having the same covariance $\overline{\phi}$ can be generated by

$$\overline{\delta \underline{g}} = S\underline{q} \tag{126}$$

where $\underline{q}$ comes from a multidimensional gaussian population with properties:

$$\mathcal{E}[\underline{q}] = \underline{0} \tag{127}$$

and

$$\mathcal{E}[\underline{q}\underline{q}^T] = I \tag{128}$$

An ensemble of 90 $\underline{q}$ vectors was used to generate an ensemble of gravity disturbance sequences using (126) and (123). The disturbance is introduced through (119) to the navigation solution of (118). The result is an ensemble of navigation error time histories, each given by (120).

From the ensemble of $\delta\underline{r}(t)$, the horizontal components were processed to yield downrange and crossrange variances at each point. Let σ_d^2 and σ_c^2 represent these variances. Then circular-error-probable (CEP) was calculated from

$$CEP = 0.562\ \sigma_{max} + 0.615\ \sigma_{min} \tag{129}$$

where

$$\sigma_{max} = \text{Maximum } \{\sigma_d, \sigma_c\} \tag{130}$$

$$\sigma_{min} = \text{Minimum } \{\sigma_d, \sigma_c\} \tag{131}$$

5.3 Trajectory Model for Nested Integrals

With the Monte Carlo results established, attention can be turned to the modeling choices for Nested Integrals. Obviously, the statistical model must be the same as for Monte Carlo. The trajectory model should be the same, but the polynomial-fit trajectory generator was not available for the Nested Integrals analysis. The trajectory was simulated using PROFGEN [Ref 7], a computer program designed to use trajectory segment definitions as input and give a complete mission time history as output. The PROFGEN segment descriptions and results are also provided in Table VI for direct comparison to the Monte Carlo trajectory data. The six segments are as follows:

a. Launch and accelerate (5.137 g's) from 615 to 2600 ft/sec groundspeed

b. Pitch-up vertical turn (7 g's) to a pitch angle of 16.3^{o}

c. Accelerate (5.137 g's) while climbing until 3900 ft/sec groundspeed.

d. Continue straight climb at constant groundspeed.

e. Pitch-over vertical turn (7 g's) level out at 80000 ft altitude.

f. Cruise at constant altitude and groundspeed.

The terminal dive phase of the last few seconds of simulated flight was not modeled for the Nested Integrals analysis.

5.4 Inertial Navigation Error Propagation Model for Nested Integrals

The inertial navigation simulation for Monte Carlo was, in essence, that of an inertial computation frame. The choice of instrument or computation frame does not change the gravity disturbance vector and Britting [Ref 8] has shown a general equivalence of error propagation models; therefore, the modified Widnall-Grundy model used in Section IV was used for this analysis as well. The vertical channel disturbance was eliminated, and the Nested Int rals step size was set at 25 seconds to be consistent with the modeling and sampling of the Monte Carlo study. Circular-error-probable was calculated from the Nested Integrals covariance results using the same downrange-crossrange rule as for Monte Carlo.

5.5 Comparison of Results

The circular-error-probable results for both the Monte Carlo and the Nested Integrals analyses are presented in Figure 16. The 95% confidence bounds for the Monte Carlo results are also repeated [Ref 10] here.

The navigation accuracies calculated by these two statistical methods differ somewhat due to modeling differences and Monte Carlo sample size limitations. The results are generally equivalent, however, and another degree of confidence in the Nested Integrals approach is warranted.

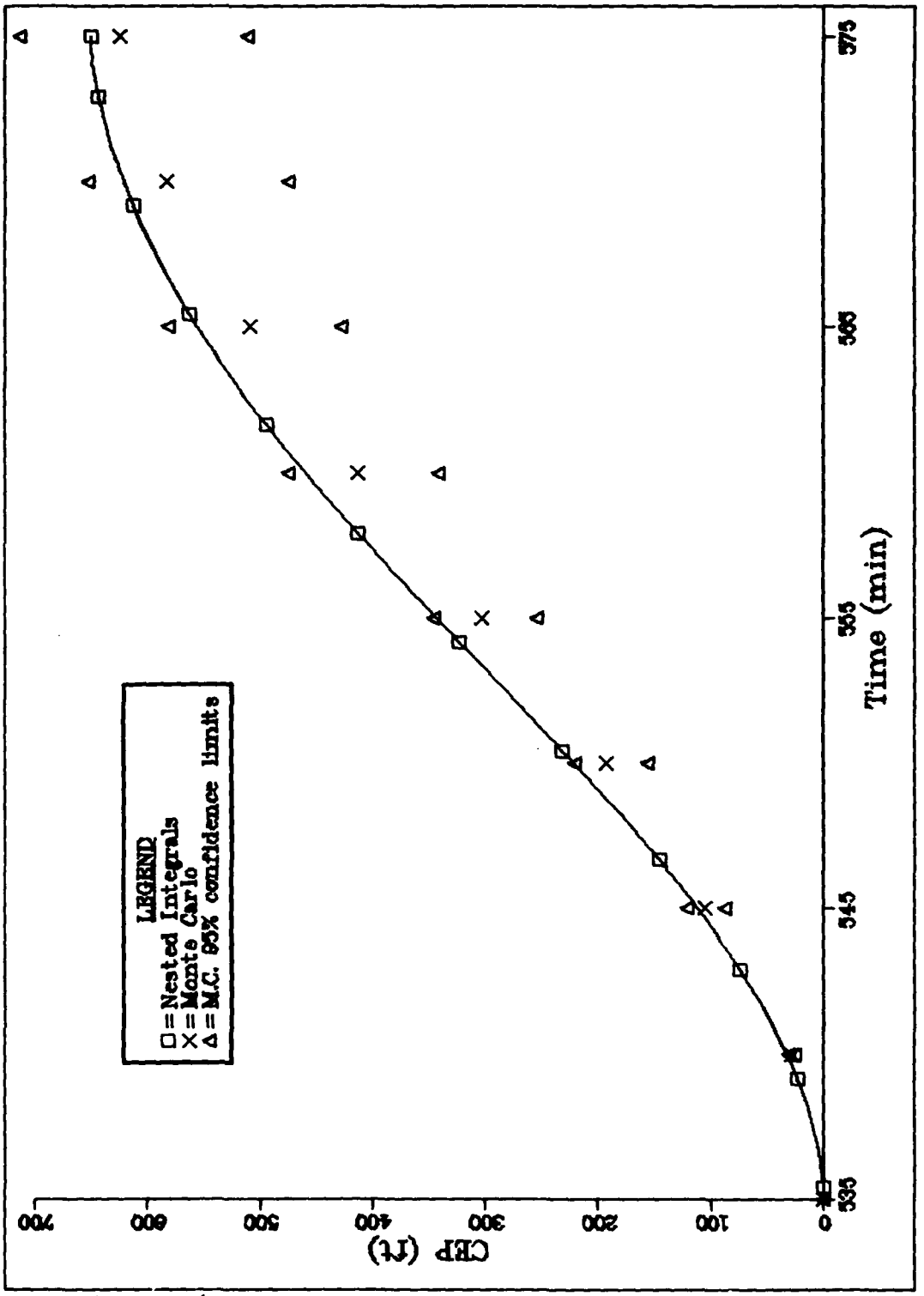

Figure 16. Circular-Error-Probable: Air Launched Strategic Missile Case

The computational costs were quite different. For the 90-case ensemble, the Monte Carlo computational time was 30 times the Nested Integrals time. That is, the entire Nested Integrals analysis was performed in the same computation time required for three of the Monte Carlo samples. Data was not available to compare post-processing time, but the Monte Carlo study requires significantly more post-processing since the sample outputs are $\delta \underline{r}(t)$, not covariance per se.

These results demonstrate that Nested Integrals has fulfilled the expectations expressed in Section II. The statistical analysis is as flexible as the Monte Carlo method, but significantly less expensive computationally. The numerical results by the two methods are equivalent; so, the Nested Integrals' computational efficiency does not entail any loss of authority in the results.

VI. Input Correlation Function Variations

In Sections IV and V, full-scale navigation error analyses were performed using Nested Integrals but based on different gravity disturbance statistical models. Nested Integrals method is, in part, motivated by the need to consider different statistical model forms. This section gives a direct comparison of results from these two models and from another fully developed model which has not been previously presented in this work. The purpose of this comparison is two-fold:

a. First, to demonstrate the capability to perform analyses with a variety of statistical model forms.

b. Secondly, the linear state space model has so dominated past studies that the existence of other models must be emphasized.

This simple comparison should demonstrate the availability of fully developed alternate statistical models.

The demonstration requires for each analysis the usual three models: trajectory, error propagation, and disturbance correlation. The disturbance correlation model, as discussed, will be varied with three separate mathematical forms considered. These three statistical models are discussed below in subsections 6.1, 6.2, and 6.3. For each correlation model, a complete Nested Integrals analysis is performed based on the same trajectory and error propa-

gation models. That is, everything in the analysis is held to a constant form except the correlation model. The benign great circle trajectory of Section IV is used along with the modified Widnall-Grundy error propagation model. The necessary data for these two models are found in Table IV of Section IV.

6.1 Linear State Space Correlation Model

This model is presented in Appendix F, and its use has been discussed in Section IV. Some additional comment is due since this model is being compared here with other model forms.

The basis of this modeling technique is a Gauss-Markov process. The gravity disturbances are represented as the outputs of a linear filter driven by white gaussian noises. The resulting disturbances quantity auto- and cross-correlations are consistent with gravitational theory except for minor approximations of the correlations between anomaly and undulation and between anomaly and downrange deflection [Ref 19:B-6]. The model used in Section IV and here is based on an eight-state filter driven by three independent noises. The resulting anomaly autocorrelation is

$$\phi_{gg}(\underline{r},\underline{r}') = \phi_{gg}(\psi) = \sigma_g^2 \, (1 + M - \tfrac{1}{2}M^2) \, e^{-M} \qquad (115)$$

where

$$M = r\,\psi/d \qquad (116)$$

and

ψ is the central angle separating $\underline{r}$ and $\underline{r}'$,
r is the reference radius value, and
d is the correlation parameter.

As it stands, this model is only valid for one altitude, so the correlation is shown as a function of central angle shift alone.

The anomaly variance level of 1800 $mgal^2$ used for this model is consistent with the worldwide anomaly variance cited in References 22 and 23. The correlation parameter of 20 nm (Table IV) is an arbitrary figure selected for the Section IV study. No one value of d will yield an overall good fit to empirical data. Several independent models of this type could be postulated, each with d_i and $\sigma_{g_i}^2$ parameters. The linear state space disturbance model used here should be viewed as a representative example, not an ultimate model. The empirical correlation function of Reference 23 has a correlation distance of 41 nm, so the 20-nm correlation parameter of this model, will yield different results on that account.

The correlation distance of the anomaly degree variance model is closer to this 20 nm parameter but the variance level is lower. The navigation error correlation results are linear with variance level, assuming the entire anomaly correlation is simultaneously scaled up or down with the variance changes. The effect of correlation parameter change is trajectory dependent. Generally one expects disturbances from a longer correlation parameter model to

appear more like a constant input to the navigation algorithm which acts as a low pass filter. The shorter correlation parameter will induce higher frequency inputs and tend to yield attenuated errors.

The linear state space correlation model example has the same trajectory, error propagation and disturbance statistical models as the great circle case of Section IV. The circular-error-probable results are identical to the Section IV study and are repeated here for comparative purposes.

6.2 Anomaly Degree Variance Correlation Model

This model was introduced in the Monte Carlo study discussed in Section V. Further details on this modeling technique are presented in Appendix J.

The anomaly correlation function is assumed to be stationary and isotropic. The function can, therefore, be expanded in spherical harmonics (i.e. Legendre functions). The symmetry of the isotropic correlation functions means the harmonic expansion can be limited to the zeroth order (i.e. Legendre polynomials).

$$\phi_{gg}(\underline{r},\underline{r}') = \phi_{gg}(r,r',\psi) = \sum_{n=0}^{\infty} c_n \left(\frac{R^2}{rr'}\right)^{n+2} P_n(\cos\psi) \tag{132}$$

The anomaly variance is given by

$$\sigma_g^2 = \sum_{n=0}^{\infty} c_n \tag{133}$$

based on setting, r=r'=R and ψ=0. A mathematical expression is hypothesized for the manner in which c_n approaches zero as n approaches infinity. Each c_n represents the contribution to the variance from the n-th degree polynomial, hence the name anomaly degree variance model. Note that the spherical harmonic mathematical form inherently gives upward continuation of the statistics without an additional integration. Closed-form mathematical expressions for (132) are developed and associated disturbance quantity correlations derived from this basis (see Appendix A).

The specific c_n model and the associated parameter set are discussed in Appendix J. The resulting model has an anomaly variance of 1795 $mgal^2$ and a correlation distance of approximately 30 nm. The circular-error-probable for the great circle trajectory for this statistical model is also presented later.

6.3 Attenuated White Noise Correlation Model

The two previously discussed models were introduced prior to this Section. Another fully developed statistical model exists and is included in this model comparison.

The attenuated white noise model is presented in Reference 23 with additional discussion in Reference 22. Some of the details are reiterated here in Appendix K. The basis of this model is a hypothetical white noise, anomalous potential process on a spherical shell at a depth

d below the earth's surface. The earth-surface anomalous potential is, therefore, the upward continuation of this white noise process. LaPlace's equation relates anomalous potential above the model noise process and the resultant earth-surface process is correlated by way of the Poisson Integral upward continuation [Ref 3].

The mathematical expressions which result from this hypothesis are quite complex and an asymptotic form is postulated. The asymptotic form maintains accuracy within an earth's radius of the surface, and this region includes all "terrestrial" navigation missions. The anomaly correlation from the asymptotic form of the attenuated white noise model is

$$\phi_{gg}(\underline{r},\underline{r}') = \phi_{gg}(\psi, h, h')$$

$$= \frac{8d^4(2d+h+h')[2(2d+h+h')^2 - 3(R\psi)^2]}{[(2d+h+h')^2 + (R\psi)^2]^{7/2}} \sigma_g^2 \qquad (134)$$

where

- ψ is central angle between $\underline{r}$ and $\underline{r}'$,
- h,h' are geocentric altitudes from $\underline{r}$, $\underline{r}'$ respectively,
- d is white noise depth,
- σ_g^2 is anomaly variance, and
- R is radius of sphere which approximates earth's surface.

Note that the model has upward continuation of statistics by the altitude data in the functional expression. To fit empirical data, three statistically independent white noise

shells were postulated each with a variance level and depth. This device allows both long and short wavelength information in the empirical function to be modeled. The final correlations are the sum of these three independent models.

With the parameter sets $\{d_i\}$ and $\{\sigma_{g_i}^2\}$ identified (Appendix K), the resulting model has an anomaly variance of 1821 mgals^2. The results using this statistical model on the great circle trajectory are also presented in Figure 17.

6.4 Comparison of Navigation Errors

The three model concepts presented above attempt to replicate empirical statistics and to conform to the strictures of gravitational field theory. The basic premise for the mathematical form is different in each case, and the result is different representations for each correlation of interest. Equations (115), (132), and (134) present the different functional forms for anomaly autocorrelation as examples. Each model employs the isotropic assumption, so only four disturbance correlations are required. These four correlations are presented in Appendix L in a comparative study of the three models above.

The circular-error-probable results for each model on the great circle trajectory are presented in Figure 17. These results are considerably different as the Appendix L comparison forbodes. Which model is correct? There is no

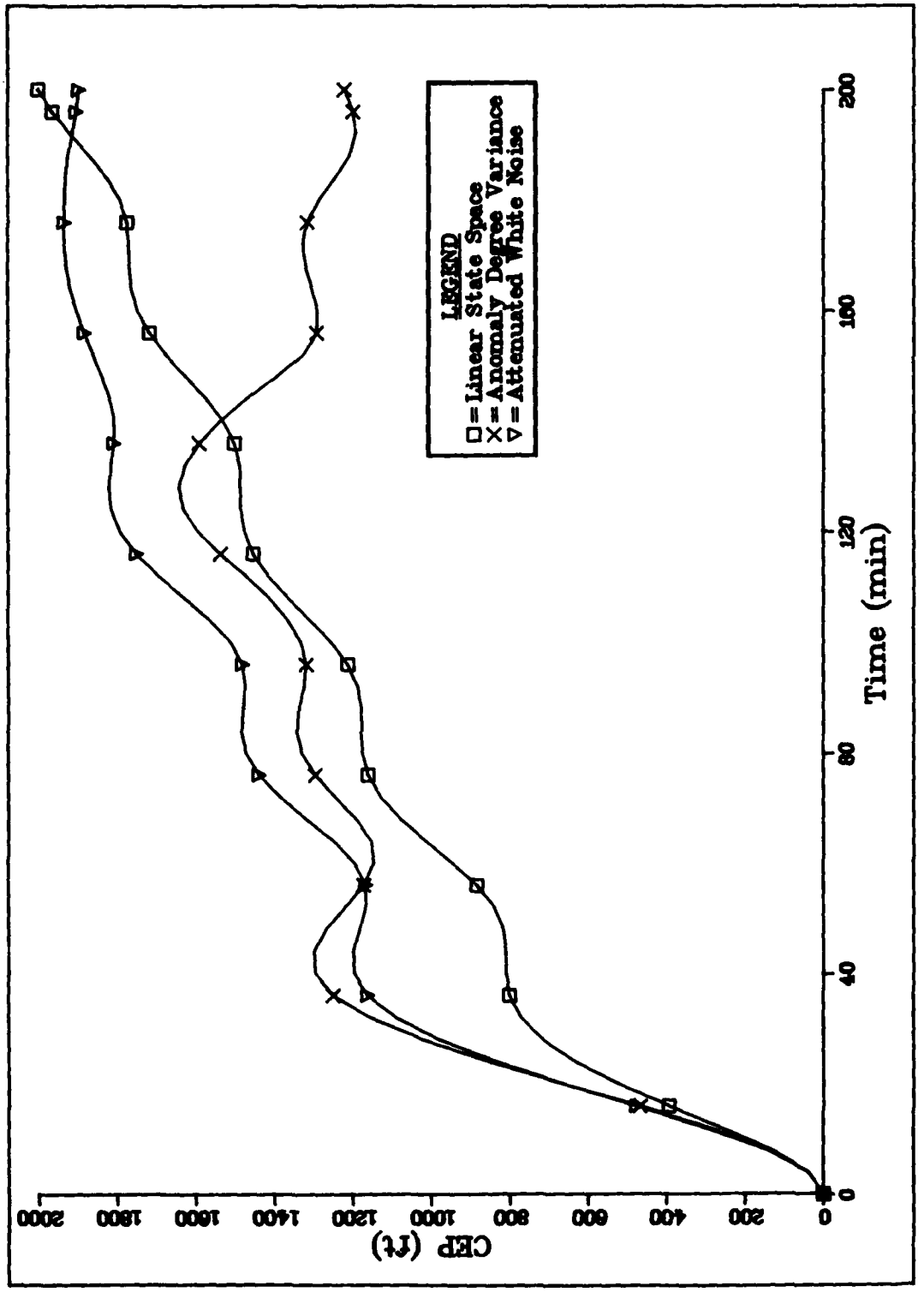

Figure 17. Circular-Error-Probable: Correlation Function Variations on the Great Circle Trajectory

general answer to that question. Each model purports to represent the same physical process, and each, being limited, fails in some way. Which model is "correct" is a subjective judgment that will depend on the mission being analyzed and the analyst's prejudices.

The attenuated white noise and the anomaly degree variance models have upward continuation of the statistics inherent in the mathematical form, a desirable general feature. These two models are also internally consistent with gravitational field theory. The linear state space model requires additional work to upward continue statistics [Ref 13] and only approximates consistency with gravitational field theory.

The outcome of this investigation will not specify a model type. This study's aims are simply to

a. Point out the existence of statistical model alternatives, and

b. To demonstrate Nested Integrals method's capability to employ any of these different mathematical forms.

The analysis results in Figure 17 provide the demonstration of Nested Integrals capability and simultaneously shows that model selection has a direct effect on analysis results.

VII. Variations in Spherical Harmonic Modeling

Inertial navigation gravity model improvements should be evaluated in terms of resulting system true accuracy. Model improvement changes the residual field statistics both in magnitude and in spectral content. If these changes can be summarized in residual field correlation models, Nested Integrals offers an evaluation technique to select the model complexity which meets mission accuracy specifications. This section demonstrates such an evaluation on a hypothetically spherical harmonic model of limited degree and order and with no error in harmonic coefficients. While such a model is unrealistic, a study based on this hypothetical model can give insight into the sensitivity of system accuracy to model complexity.

As in Section VI, this analysis will involve variations in the input correlation function. Unlike Section VI, the functional form will be constant. For this study, the model changes are seen in model parameter variations. The correlation modeling is discussed below. The great circle trajectory model and modified Widnall-Grundy error propagation model are again used as a vehicle for the statistical model variations.

7.1 Correlation Model

The gravitational model can be based on a spherical harmonic expansion of gravitational potential U [Ref 3 :342]

$$U(\underline{r}) = \frac{\mu_\oplus}{r}\left\{1 - \sum_{n=2}^{\infty} \left[\frac{a}{r}\right]^n J_n P_n(\cos\phi) - \sum_{n=2}^{\infty}\sum_{m=1}^{n} \left[\frac{a}{r}\right]^n (J_{nm}\cos m\lambda + K_{mn}\sin m\lambda)\cdot P_{nm}(\cos\phi)\right\} \tag{135}$$

$$P_{nm}(t) = 2^{-n}(1-t^2)^{m/2} \sum_{k=0}^{j} (-1)^k \frac{(2n-2k)!}{k!(n-k)!(n-m-2k)!}\, t^{n-m-2k} \tag{136}$$

$$j = \text{integer}\left[\frac{n-m}{2}\right] \tag{137}$$

$$P_n(t) = P_{no}(t) \tag{138}$$

where

$\mu_\oplus$ is earth gravitational constant

$\underline{r}$ is radius vector of

a earth semi-major axis

ϕ colatitude

λ longitude

J_n are zonal harmonic coefficients

J_{nm}, K_{nm} are tesseral harmonic coefficients

$P_n(\cdot)$ are Legendre polynomials of degree n

$P_{nm}(\cdot)$ are Legendre functions of degree n and order m

Zonal harmonic models of low degree and order are most common, but higher order models have been formed [Ref 10]. Specific values for the parameters depend on the geodetic model selected. This work does not depend on any specific model so these data are not required explicitly here. Models are based on truncated versions of (135) making use of

$$\underline{G}(\underline{r}) = \nabla U(\underline{r}) \tag{139}$$

where $\underline{G}$ is the gravitational vector. Any attempt to identify coefficients will result in errors from the following sources:

a. Measurements are limited by economics and politics, hence aliasing of higher order effects onto low order coefficients.

b. Measurement errors.

Koch [Ref 24] has pointed out rather severe aliasing at degree-and-order 12 truncation based on satellite data. A perfect spherical harmonic model of any given finite degree and order is unrealistic.

A study based on the thesis of perfect spherical harmonic modeling is a valid experiment to determine sensitivity to model improvements. On this premise, a study is proposed to determine the navigation error due to perfect spherical harmonic modeling over a range of degree-and-order truncations.

The effects of this level-of-detail variations in the gravity model must be projected onto the statistical model of the residual field. A spherical harmonic expansion of the residual field would have zero coefficients for all degrees less than the truncation number. With the anomaly degree variance model, the statistical model alteration is apparent. This model was introduced in Sections V and VI and further discussed in Appendix J. Since the anomalous field has zero coefficients in spherical harmonics

below the truncation number, it is reasonable to model the statistics similarly.

With the anomaly degree variance model, the anomaly correlation is given by an equation from Section VI

$$\varphi_{gg}(\underline{r},\underline{r}') = \varphi_{gg}(r,r',\psi)$$

$$= \sum_{n=0}^{\infty} c_n \left(\frac{R^2}{rr'}\right)^{n+2} P_n(\cos\psi) \qquad (132)$$

The coefficient c_n is determined by an algebraic rule given in Appendix J. For this study,

$$c_n = \begin{cases} 0 & n \leq 2 \quad \text{or} \quad n \leq N \\ \dfrac{A(n-1)}{(n-2)(n+B)} & n > N \quad \text{and} \quad n > 2 \end{cases} \qquad (140)$$

where N is the degree and order of the spherical harmonic truncation. The anomaly degree variance model modified by (140) is the disturbance statistical model for this study.

7.2 Navigation Error Results

Nested Integrals covariance analyses were conducted for truncation levels of 2, 36, 72, and 180. Again, these studies were based on the modified Widnall-Grundy navigation error propagation model and the great circle trajectory model. The truncation level 2 is roughly equivalent to an ellipsoidal model and represents the unmodified anomaly degree variance model. The circular-error-probable results for all cases are presented in Figure 18. The accuracy is generally better with each increment. Note,

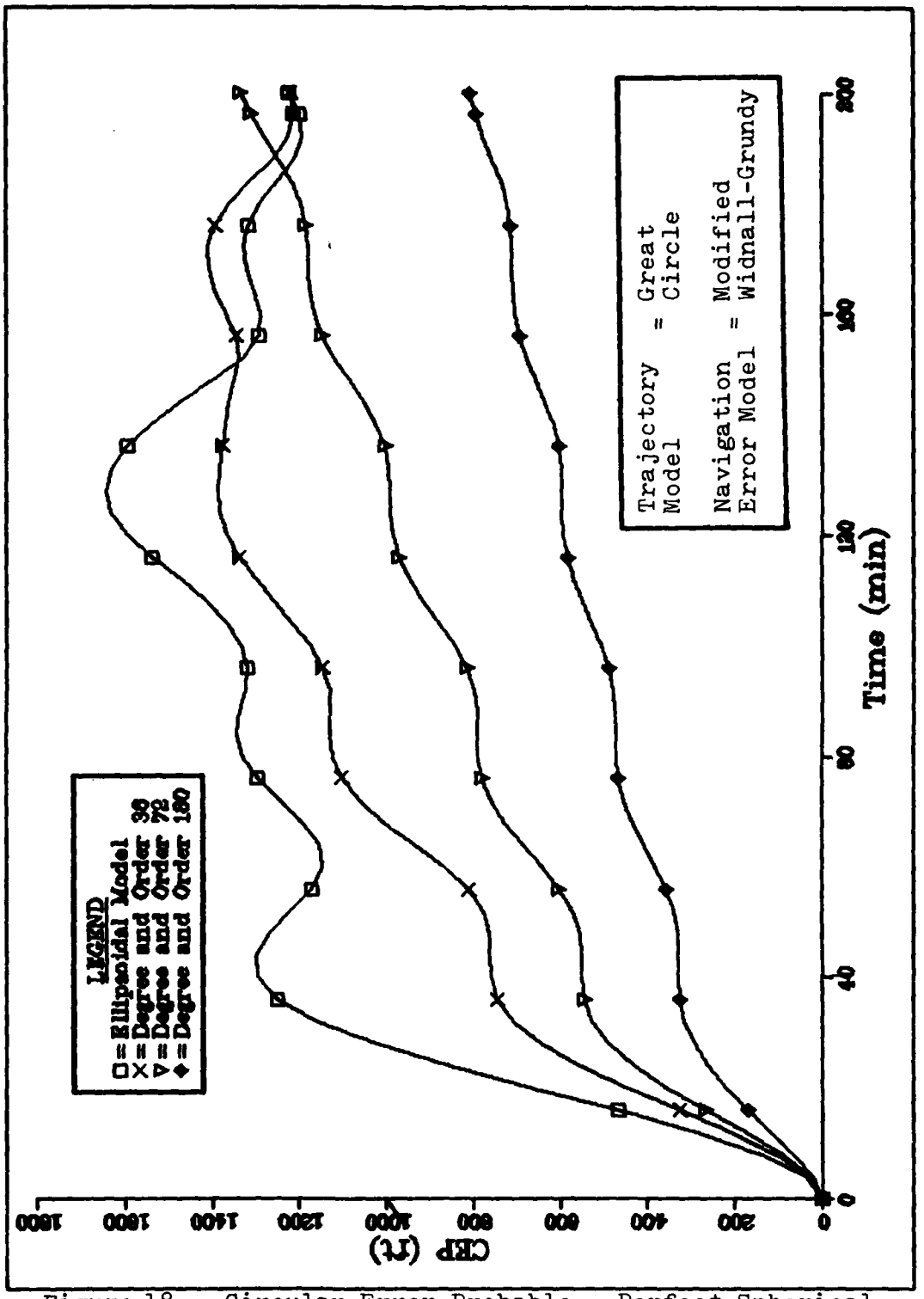

Figure 18. Circular-Error-Probable: Perfect Spherical Harmonic Models of Limited Degree and Order

however, that a more precise model does not guarantee better system accuracy at all times. The dynamics of the navigation error propagation model apparently causes the ellipsoidal model performance to be better than more detailed models near the 160 minute mission time.

The accuracy improvement implied by Figure 18 comparisons is desirable; the cost of producing the corresponding models is not. The system designer must weigh both factors in deciding on a level of model detail. Nested Integrals supplies a method to answer the model accuracy, half of the system design trade-off.

VIII. Nonstationary Statistics Demonstration

The statistical models presented in Sections IV, V, and VI are all based on an assumption of homogeneity. This assumption is instrumental in deriving the mathematical expressions for the gravity disturbance stochastic model, but the homogeneous assumption is not required for Nested Integrals analysis. Quite the contrary, the only requirement of $Q(\underline{r},\underline{r}')$ is that it be integrable. This section presents some rationale which might be used in supporting an assumption of nonstationary statistics for the gravity disturbance field. Then, a simple nonstationary example is presented to demonstrate Nested Integrals validity on this type of problem.

First, the statistics of the disturbance gravity field (after the ellipsoidal model has been removed) vary regionally. Long has shown [Ref 25] considerable variability within the United States alone. One can surmise from predominant geographic features like the mountain ranges, which run primarily along north-south lines in this country, that geodetic features are similarly distributed. The Rice data [Ref 12] from a survey along the 35-th parallel gives some insight into the residual field variations which might be anticipated on a transcontinental mission.

The mission region definition is the key to whether the nonstationary question needs to be addressed. If the mission definition is vague and worldwide in scope (e.g.

for a short-range transport mission), worldwide average statistics seem reasonable. If the mission region is restricted (e.g. for MINUTEMAN missiles), regional characteristics should not be disregarded.

Since Nested Integrals has the inherent capability to process a nonstationary model for the gravity disturbance correlations, a simple example is proposed for demonstration purposes. Again, a proper casting of the problem will yield a case for which linear state space techniques offer a crosscheck. The restrictions, then, are to allow the verification and are not required for Nested Integrals per se.

The great circle trajectory model and the modified Widnall-Grundy navigation error propagation model are again used. The Table IV data of Section IV again applies with the exception of anomaly variance level which is explained below.

8.1 Correlation Model

A nonstationary statistical model gives $Q(\underline{r},\underline{r}')$ which cannot simply be expressed as $Q(\psi)$ or $Q(\psi,\dot{\alpha})$. For this example, the nonstationary statistics are summarized as anomaly variance which varies with longitude. One could hypothesize this model as

$$\sigma_g^2(\underline{r}) = \sigma_g^2(\lambda) \qquad (141)$$

Longitude is defined by the design mission trajectory, hence can also be considered a function of time

$$\sigma_g^2(t) = \sigma_g^2[\lambda(t)] \tag{142}$$

Applying the above rule to the linear state space gravity disturbance model of Appendix E will yield a $Q_g(t)$ nonstationary temporal noise strength. For linear state space analysis, when longitude changes, the gravity disturbance model also changes from one steady-state system to another since P_g depends directly on σ_g^2. This quasi-stationary modeling was used so that $\dot{P}_g$ would not have to be calculated and integrated.

Applying the above concept in a Nested Integrals analysis requires an interpretation. When evaluating $Q(\underline{r}_n, \underline{r}_i)$ does one use λ_i or λ_n to calculate σ_g^2 ? The answer is the same as for the question of which heading α_i or α_n should be used in transforming coordinates in which Q is expressed. $D(t_n)$ represents a driving term for $\dot{P}$ at $t=t_n$, the current time. The information entering through $D(\cdot)$ at t_n concerns the correlations of $\underline{u}(t_n)$ with all past values, but as with α, the information is paired (t_n, t_i). The correct interpretation is that the gravity correlations at t_n apply, hence $\sigma_g^2(\lambda_n)$ should be used. To be rigorous, the order of arguments in Q should be interpreted by rewriting (29b) as

$$D(t) = \int_{t_o}^{t} Q[\underline{r}(t), \underline{r}(p)] G^T(p)\ \Phi^T(t,p)\ dp \tag{143}$$

and interpreting (28) modified for the nonstationary statistics of this example as

$$Q[\underline{r}(t), \underline{r}(p)] = Q[\psi, \underline{r}(t)] = Q[\psi, \lambda(t)] \tag{144}$$

The specific rule used for σ_g^2 dependence on λ is

$$\sigma_g^2(\lambda) = (1 + 10\lambda)\ 1800\ \text{mgal}^2 \qquad (145)$$

For the great circle trajectory, the anomaly variance begins at the same level as for the Section IV study. By the end of the 204-minute flight, the variance level has increased by 25 percent. This change was not selected to be realistic; rather the result should be distinct from the Section IV case (Figure 10). With this understanding, equation (145) properly interpreted gives a covariance problem which either Nested Integrals or linear state space methods can solve.

8.2 Comparison of Results

The circular-error-probable computed by both Nested Integrals and linear state space covariance analyses are presented in Figure 19 for comparison. The results again agree but not as well as the case of Section IV which had static statistics.

This case demonstrates Nested Integrals' ability to compute correctly covariance even in the case of nonstationary statistics. This example was simple and somewhat unrealistic. Considerable study would be required to generate a valid nonstationary model. If the mission definition warrants it, and if empirical data are available to support the nonstationary model, the Nested Integrals approach can be used in performing the navigation error covariance analysis.

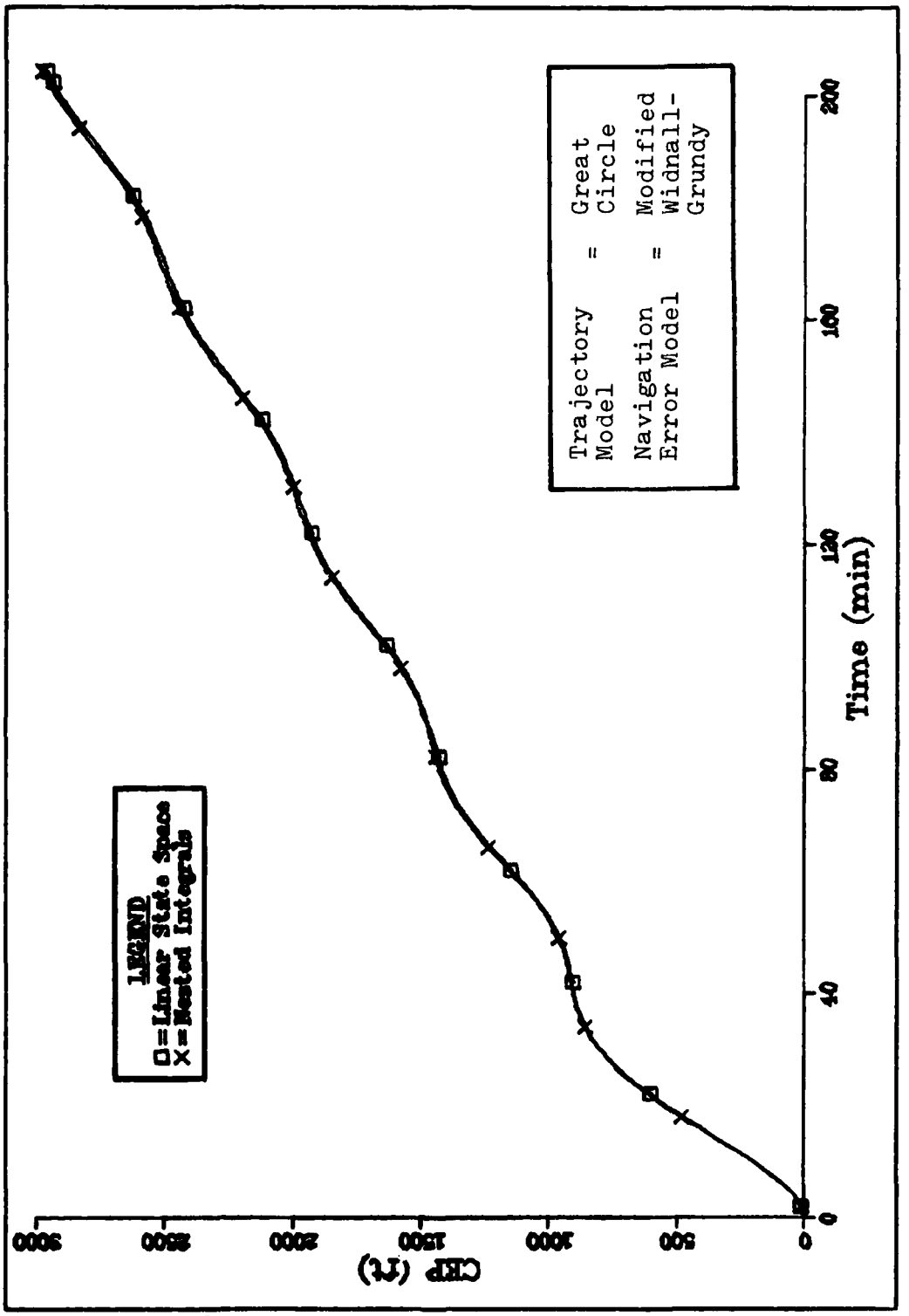

Figure 19. Circular-Error-Probable: Nonstationary Statistics Demonstration

IX. Kalman Filter Updates

Any simulation attempts to describe the response of a system to some stimuli within some environment. Nested Integrals, as a statistical simulation, gives navigation system errors due to gravity disturbances within the environment of the trajectory and navigation system. Modern navigation systems rarely use inertial instruments alone. External measurements (e.g. radar position fixes) are used to overcome the low-frequency errors to which purely inertial systems are prone. These updates are a part of the error propagation environment which was not treated in the Nested Integrals development in Section III. The purpose of this section is to develop modifications to the Nested Integrals which will properly account for the effects of measurement updates on the navigation error covariance.

The nature of the navigation update must be specified in order to embed the effects into the Nested Integrals algorithm. Some assumptions will be made on the types of systems and update methods which are most likely to be used. First, any system of high accuracy will have linear velocity or its equivalent in the system model. Secondly, the update method will either be by Kalman filter methods or by closely related schemes (extended Kalman filter for example). A set of developed theory exists [Ref 15: 325-341] concerning the evaluation of filter performance using a truth model to simulate all those environmental effects omitted from

the necessarily limited filter model. A similar line of reasoning will be followed in this development.

For Nested Integrals analysis, the truth model will include the gravity disturbance terms. Since these gravity error quantities do not generally fit the desired Markov process mold, no advantage is gained by naming them states. The $G(t)\underline{u}(t)$ driving term mode of (3) will be retained. The filter is assumed to contain states for the velocity errors, and the velocity error states will normally be driven by the gravity disturbance terms. The geoidal height N may be modeled to drive the system through the system barometric altimeter, if applicable. The point of view taken is that the filter model adequately describes the propagation of navigation errors. For an accurate navigation system, this assumption is likely to be valid. Other states can be appended to the filter model if necessary with only slight modification of the following development.

Once the algorithmic changes are derived, the question of verification must be addressed. For this case, the linear state space covariance analysis is again employed on a simple case. The trajectory and gravity disturbance models are selected to comply with the linear state space limitations. The Nested Integrals results can then be compared to the linear state space answers for verification.

9.1 Theory Review

The objective to account for Kalman filter updates can not be met without knowing the Kalman gains. The update requires a system model and a measurement model, and these models are used to calculate Kalman gains in an analysis separate and distinct from the Nested Integrals analysis. This theory must be reviewed before the algorithm changes are developed.

The filter model equivalent of (3) is

$$\dot{\underline{x}}_f(t) = F_f(t)\underline{x}_f(t) + G_f(t)\underline{w}_f(t) \tag{146}$$

where $\underline{x}_f(t)$ is an n-vector of error states which affect navigation performance,

$F_f(t)$ is the nXn state propagation matrix,

$\underline{w}_f(t)$ is an m_f-vector of white Gaussian noise, and

$G_f(t)$ is an nXm_f distribution matrix.

The noise $\underline{w}_f(t)$ satisfies the following

$$\mathcal{E}[\underline{w}_f(t)] = 0 \tag{147}$$

$$\mathcal{E}[\underline{w}_f(t)\ \underline{w}_f^T(t+\tau)] = Q_f(t)\ \delta(\tau) \tag{148}$$

The filter noise model is not limited to, indeed may not even address, gravity disturbances. The key point here is that the filter environment must be modeled as a separate entity from the Nested Integrals analysis. The model presented in (146), (147), and (148) is the standard approach in Kalman filter design [Ref 15: 291-297]. The subscripts will be omitted on most terms from here forward since the

filter model is assumed to be sufficiently detailed to serve as the Nested Integrals navigation error propagation model. Exceptions are Q_f and G_f which are different than Q and G from (28) and (3).

For the filter model of (146), it follows that

$$\dot{P}_f(t) = F(t)P_f(t) + P_f(t)F^T(t) + G_f(t)Q_f(t)G_f^T(t) \qquad (149)$$

subject to the initial condition $P_f(t_o)$. Also,

$$\dot{\Phi}(t,t_i) = F(t)\ \Phi(t,t_i) \qquad (16a)$$

Subject to the initial condition $\Phi(t_i,t_i) = I$. These equations are fundamental in describing the behavior of the filter error-covariance estimate between measurement updates. The effects of measurement updates are assumed to be discrete corrections to navigation estimates, and the discrete update of the P_f-matrix is needed to describe the filter operations. Continuous feedback of revised estimates can also be treated with a few modifications to the development here [Ref 15:333].

The Nested Integrals solution is based on a discrete solution time sequence $t_o < t_1 < \cdots < t_N$, symbolically $[t_n]$. The measurement updates are assumed to come at time points which are a subsequence of this time base. That is, measurements are at $t_{n_1} < t_{n_2} < \cdots < t_{n_M}$, symbolically $[t_{n_i}]$. At each time t_{n_i}, an r-dimensional vector measurement occurs and is described by

$$\underline{z}(t_{n_i}) = H(t_{n_i})\underline{x}(t_{n_i}) + \underline{v}(t_{n_i}) \qquad (150)$$

where

$H(t_{n_i})$ is an rXn measurement matrix, and

$\underline{v}(t_{n_i})$ is an r-dimensional discrete, white, Gaussian noise process satisfying

$$\mathcal{E}\left[\underline{v}(t_{n_i})\right] = 0 \tag{151}$$

$$\mathcal{E}\left[\underline{v}(t_{n_i})\underline{v}^T(t_{n_j})\right] = \begin{cases} R(t_{n_i}) & i=j \\ 0 & i\neq j \end{cases} \tag{152}$$

Let t_{n_i} indicate the condition of a quantity prior to the update at $t_{n_i}^-$, and let $t_{n_i}^+$ represent the post-update conditions. Then, using (149),

$$P_f(t_{n_i}^-) = \Phi(t_{n_i}^-, t_{n_{i-1}}^+)\, P_f(t_{n_{i-1}}^+)\, \Phi^T(t_{n_i}^-, t_{n_{i-1}}^+) + \int_{t_{n_{i-1}}^+}^{t_{n_i}^-} \Phi(t_{n_i}^-, p) G_f(p) Q_f(p) G_f^T(p) \Phi^T(t_{n_i}^-, p)\, dp \tag{153}$$

at t_{n_i} the Kalman gain is calculated by

$$K(t_{n_i}) = P_f(t_{n_i}^-) H^T(t_{n_i}) \left[H(t_{n_i}) P_f(t_{n_i}) H^T(t_{n_i}) + R(t_{n_i})\right]^{-1} \tag{154}$$

The update of the filter covariance matrix is given by

$$\begin{aligned} P_f(t_{n_i}^+) &= P_f(t_{n_i}^-) - K(t_{n_i}) H(t_{n_i}) P_f(t_{n_i}^-) \\ &= \left[I - K(t_{n_i}) H(t_{n_i})\right] P_f(t_{n_i}^-) \left[I - K(t_{n_i}) H(t_{n_i})\right]^T \\ &\quad + K(t_{n_i}) R(t_{n_i}) K^T(t_{n_i}) \end{aligned} \tag{155}$$

The equation set (16a), (153), (154), and (155) allow the computation of the Kalman filter gains $K(t_{n_i})$ needed to update the covariance calculated, separately, by the Nested Integrals method.

9.2 Nested Integrals Algorithm Changes

The Nested Integrals algorithm calculates the covariance between updates correctly. That is, given $P(t^-_{n_{i-1}})$ and for $t_{n_{i-1}} \leq t \leq t_{n_i}$, equation (29a) is valid

$$\dot{P}(t) = F(t)P(t)+P(t)F^T(t)+G(t)D(t)+D^T(t)G^T(t) \qquad (29a)$$

But, since $D(t)$ inherently includes the propagation of errors in its definition, the effects of updates on $D(t)$ must also be included in the Nested Integrals algorithm. Recall

$$D(t) = \int_{t_o}^{t} Q(t,p)G^T(p)\ \Phi^T(t,p)dp \qquad (29b)$$

To reflect the measurement update on both $P(t)$ and $D(t)$, the error state $\underline{x}$ is propagated across the update as

$$\underline{x}(t^+_{n_i}) = [I-K(t_{n_i})H(t_{n_i})]\underline{x}(t^-_{n_i}) + K(t_{n_i})v(t_{n_i}) \qquad (156)$$

But $v(t_{n_i})$ is zero in this gravity-error-only analysis, and, this form can be used to interpret a discrete state propagation matrix as

$$\Phi(t^+_{n_i},t^-_{n_i}) = I-K(t_{n_i})H(t_{n_i}) \qquad (157)$$

Since Nested Integrals involves geodetic errors alone, the R-matrix of (155) is not involved in the P(t) update. One should note that any altimeter errors were assumed to enter the error process through a $\underline{u}(t)$ element. One could propose altimeter updates in which case $\underline{v}$ would be correlated with $\underline{u}$; this approach is not taken here. Using equation (155) as a guide, the covariance update is

$$P(t_{n_i}^+) = \Phi(t_{n_i}^+, t_{n_i}^-)P(t_{n_i}^-)\Phi^T(t_{n_i}^+, t_{n_i}^-) \tag{158}$$

The update of D(t) must be derived since an equivalent matrix is not normally treated in Kalman filter theory. The integrand of (29b) is assumed to be finite, so the upper limit of the integration can be moved from one side of the update to the other without destroying the equality. That is, the interval (t^-, t^+) is assumed to be a set of zero measure. The resulting D(t) across updates can be found by

$$\begin{aligned}
D(t_{n_i}^+) &= \int_{t_o}^{t_{n_i}^+} Q(t_{n_i}^+, p)G^T(p)\ \Phi^T(t_{n_i}^+, p)dp \\
&= \int_{t_o}^{t_{n_i}^-} Q(t_{n_i}^-, p)G^T(p)\ \Phi^T(t_{n_i}^+, p)dp \\
&= \int_{t_o}^{t_{n_i}^-} Q(t_{n_i}^-, p)G^T(p)\left[\Phi(t_{n_i}^+, t_{n_i}^-)\Phi(t_{n_i}^-, p)\right]^T dp \\
&= \left[\int_{t_o}^{t_{n_i}^-} Q(t_{n_i}^-, p)G^T(p)\ \Phi^T(t_{n_i}^-, p)dp\right]\Phi^T(t_{n_i}^+, t_{n_i}^-) \\
&= D(t_{n_i}^-)\ \Phi^T(t_{n_i}^+, t_{n_i}^-)
\end{aligned} \tag{159}$$

This update for D(t) will force discontinuities at t_{n_i}. In solving the differential equation (29a) for the intervals between updates, the pre- or post-update D(t) must be selected with care. Let $j = n_i$; for the interval t_{j-1} to t_j, the $\dot{P}$ calculation should be based on $D(t_{j-1}^+)$ and $D(t_j^-)$. When t_j is not a measurement update time, the t_j^+ and t_j^- data are the same.

The discrete error propagation defined by (157), therefore, gives the key to the Nested Integrals Kalman filter update. Using the result of (157), P(t) is updated as specified in (158) and D(t) is updated as specified in (159). The only new information required is the Kalman gain $K(t_{n_i})$ and the measurement matrix $H(t_{n_i})$.

9.3 Verification Case

Linear state space techniques are the natural mode of Kalman filter design and analysis. A linear state space covariance analysis can be defined to include Kalman filter updates, and the results used as a benchmark to judge the modified Nested Integrals algorithm. The great circle case of Section IV will again serve as the vehicle for comparing the results from the two covariance analysis methods. The measurement model and the filter model must be specified in addition to the three models (trajectory, error propagation, and disturbance correlation) of the great circle case. Some additional explanation is required concerning how the

linear state space method is modified to incorporate the effects of the Kalman filter update.

The two new models required are described below. The linear state space covariance method is described in Section II; recall that the covariance of an augmented state is calculated. The augmented state is given by

$$\underline{x}_a(t) = \begin{Bmatrix} \underline{x}(t) \\ \cdots\cdots \\ \underline{x}_g(t) \end{Bmatrix} \tag{7}$$

The effect of the update equation above is on the $\underline{x}(t)$ states alone. Using the notation for discrete error propagation matrices,

$$\Phi_a(t_{n_i}^+, t_{n_i}^-) = \left[\begin{array}{c:c} I-K(t_{n_i})H(t_{n_i}) & 0 \\ \hdashline 0 & 0 \end{array}\right] \tag{160}$$

The linear state space augmented state covariance update is given by

$$P_a(t_{n_i}^+) = \Phi_a(t_{n_i}^+, t_{n_i}^-) P_a(t_{n_i}^-) \Phi_a^T(t_{n_i}^+, t_{n_i}^-) \tag{161}$$

For the time intervals between updates, equation (29) will describe the dynamics of P(t). The modification of the Section II described linear state space covariance analysis by (161) completely specifies the analysis by that method.

A practical note should be made before proceeding with the model definitions. The predictor-corrector integration algorithm used to solve (14) and (29a) is not designed to handle discontinuities. The discontinuities at the update times would create large predictor errors for which the

computed corrections might be erroneous. This problem is avoided if one reinitializes the integration algorithm after each update. The instructions for this initialization are a normal part of the software description with such algorithms.

9.3.1 Filter Model

To keep the verification case relatively simple, no additional states are considered other than the nine states of the modified Widnall-Grundy navigation error model. Examples of possible additional states are gyroscopic drift and accelerometer bias. The system noise model simulates the effects of such errors through white noise driving the velocity (x_4,x_5, and x_6) and attitude (x_7,x_8, and x_9) derivatives. Interpreting this filter model choice in terms of equation (146), define

$$\underline{w}_f(t) = \begin{Bmatrix} w_1(t) \\ \vdots \\ w_6(t) \end{Bmatrix} \tag{162}$$

and the asscciated distribution matrix is

$$G_f(t) = G_f = \begin{bmatrix} 0 \\ --- \\ I \end{bmatrix} \tag{163}$$

where G_f is 9X6 and the identity matrix is 6X6. The noise strength matrix associated with $\underline{w}_f$ is given by

$$Q_f = \begin{bmatrix} Q_v^2 & 0 & 0 & 0 & 0 & 0 \\ 0 & Q_v^2 & 0 & 0 & 0 & 0 \\ 0 & 0 & Q_v^2 & 0 & 0 & 0 \\ 0 & 0 & 0 & Q_\epsilon^2 & 0 & 0 \\ 0 & 0 & 0 & 0 & Q_\epsilon^2 & 0 \\ 0 & 0 & 0 & 0 & 0 & Q_\epsilon^2 \end{bmatrix} \tag{164}$$

The acceleration-level white noise is specified at a level of $Q_v = 16 \times 10^{-4}$ ft^2/sec^3, and the attitude-rate-level noise is modeled as $Q_\epsilon = 36 \times 10^{-12}$ radian^2/sec. These noise levels define an inertial navigation system of approximately one nautical mile per hour circular-error-probable growth rate.

The modified Widnall-Grundy $\underline{x}(t)$ and $F(t)$ along with (162) through (164) give the filter structure. This structure driven by the noise model above governs the filter model covariance simulation.

9.3.2 Measurement Model

A horizontal position fix is hypothesized as the measurement external to the inertial navigation system. A radar system with a 100-foot root-mean-square resolution takes east and north position coordinate measurements at intervals throughout the mission. For simplicity, the measurements are made on five-minute intervals. This rate

corresponds to once every ten Nested Integrals integration steps -- recall the 30-second step size from Table IV.

The horizontal position measurements allow the observation of east position error x_e and north position error x_n as described below:

$$x_e = r \cos\phi \, \delta\lambda = r \cos\phi \, x_1 \tag{165}$$

$$x_n = r \, \delta\phi = r \, x_2 \tag{166}$$

With (165) and (166), define

$$\underline{z} = \begin{Bmatrix} x_e \\ x_n \end{Bmatrix} \tag{167}$$

and for (150)

$$H = \begin{bmatrix} r\cos\phi & 0 & 0 & 0 & 0 & 0 & 0 & 0 & 0 \\ 0 & r & 0 & 0 & 0 & 0 & 0 & 0 & 0 \end{bmatrix} \tag{168}$$

The noise strength of (152) is modeled as

$$R = \begin{bmatrix} \sigma_r^2 & 0 \\ 0 & \sigma_r^2 \end{bmatrix} \tag{169}$$

where σ_r^2 is $(100 \text{ ft})^2$ by the above assumption.
The measurement model is complete with (168) and (169) providing the necessary components of (154) and (155).

9.4 Comparison of Results

Based on the filter and measurement models, a set of Kalman gains were calculated and stored for use in both the linear state space and Nested Integrals covariance analyses.

Then, separate results were generated using these alternative statistical methods. The circular-error-probable for both methods is plotted in Figure 20. The two curves are practically indistinguishable, and the curve markers are again offset to clarify that two curves are plotted.

The conclusion from this comparison is that the modifications to Nested Integrals can be used to account properly for the effects of Kalman filter updates throughout a mission. As in Section IV, the linear state space solution is known to be correct on this restricted trajectory. Nested Integrals has the capability to compute covariance on a wider variety of missions and with more flexibility in the choice of the gravity disturbance statistical model, and now has been extended to include the flexibility of employing Kalman filter updates on the navigation mission.

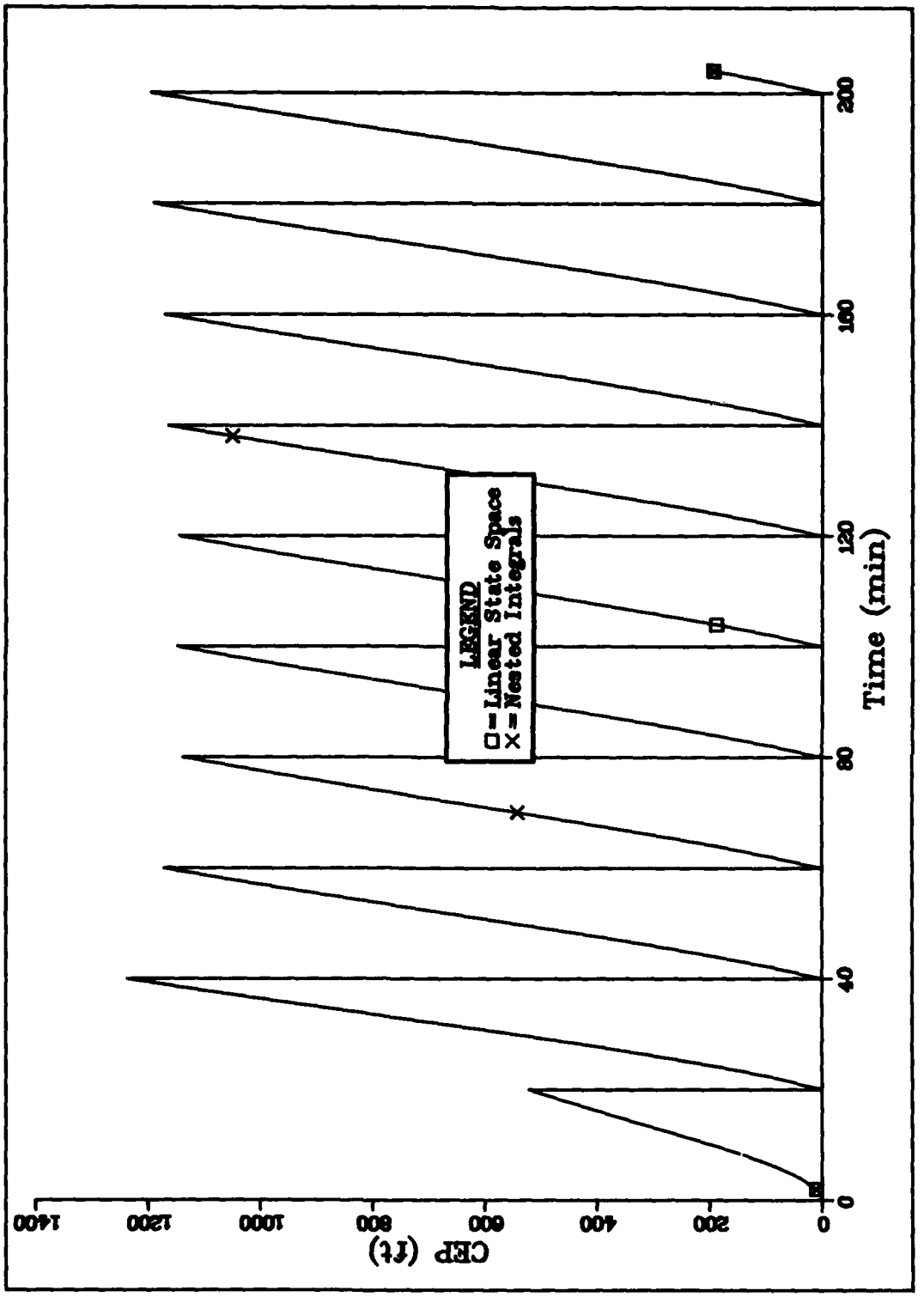

Figure 20. Circular-Error-Probable: Kalman Filter Update Comparison

X. Summary and Conclusions

The objective of this research was to develop a new computational technique which would provide a performance assessment of alternative gravity models on realistic scenarios. This section provides a summary of the development of the Nested Integrals algorithm. The verification cases and capability demonstrations are, also, recapitulated for completeness.

A navigation system accuracy measure was selected as the model comparison performance measure. Statistical methods of producing such a measure were selected since these methods admit the limitations in modeling the gravity field and permit analysis on a general mission definition. Two present statistical methods were considered and discussed: linear state space covariance analysis and Monte Carlo. The covariance integral was developed as a compromise offering more flexibility than linear state space covariance analysis but promising a savings in computational costs compared with Monte Carlo.

Numerical methods were developed to compute navigation error covariance based on an integral expression which relates the covariance to the gravity disturbance causes. Three models are required for these analyses. A linear, first-order differential equation, (3), which relates the navigation error rates to navigation errors and to the gravity disturbances. Because inertial error propagation

is trajectory dependent and because the gravity disturbance is a spatial function, a design-mission trajectory model is needed to represent the dynamics and geometry of an ensemble of missions which form the statistical sample base. Finally, the statistics of gravity disturbances encountered over this ensemble of missions must be summarized in the form of the correlation model. This correlation function is the key element in the integrand of the covariance integral.

Three separate numerical algorithms were developed to approximate the covariance integral. Two of these were direct integral approximations; one used a rectangular rule and the other trapezoidal in approximating the integral. The third algorithm was created by taking the time derivative of the covariance integral using Leibnitz' rule, equation (29). The covariance integral was, thereby, recast from a double integral into two single integrals which are nested. The outer of these Nested Integrals is in a form compatible with standard predictor-corrector numerical solution techniques.

To implement any of these three numerical methods would be computationally very costly if a naive approach were taken. To avoid the requirement to store state transition matrices between each pair of evaluation points, the semi-group property of state transition matrices was used. This reduced the data storage requirement to approxi-

mately the square root of the storage required by the straightforward approach. To accommodate this storage savings and avoid data retrieval costs, an indexed sequential file structure was selected for the required state transition matrix and position data. This approach permits relatively efficient sequential file use once the initial record is located. To exploit this feature, summations which occur in the integral approximations are run in the reverse chronological order. Together, the file structure and algorithmic form give an economically viable method of computing covariances.

Of these three methods, Nested Integrals proved to be more efficient and of equal accuracy. The analysis of an undamped Schuler loop driven by exponentially correlated noise was used as a medium for this tradeoff. This example problem demonstrated graphically the need to select integration step size small enough to meet the Shannon rate and correctly represent the frequency content of the integrand of the covariance integral. Results on the subsequent damped Schuler loop example demonstrated that the error level is lower in comparison since the system model is inherently stable.

Once the Nested Integrals method was selected, a full-scale verification study was conducted using a great circle trajectory and a shaping filter gravity disturbance model. The verification was successful, and the same comparison

format was used to demonstrate the errors in linear state space covariance analysis on more complex trajectories. Minor circle trajectories were used to demonstrate that linear state space results, while correct on a great circle case, are increasingly in error as the circle radius is decreased.

Next, the Nested Integrals method was verified against an independent Monte Carlo study of a highly-dynamic air-launched missile. This study represents a real-world application of Nested Integrals. The Monte Carlo study models were emulated in the Nested Integrals analysis. For this study, a different functional form for the correlation model was specified in the Monte Carlo analysis, and the statistical model flexibility inherent in the Nested Integrals formulation was required. The results from both methods compared well and offer an additional validation of Nested Integrals. For this problem, Nested Integrals demonstrated a 30:1 computational time advantage over Monte Carlo. This efficiency was a prime objective of the Nested Integrals method.

Clearly, Nested Integrals meets the original expectations: it is a more flexible analysis technique than linear state space covariance analysis, and it is computationally more efficient than Monte Carlo. Three demonstrations were performed to give further examples of specific Nested Integrals capabilities. Three different correlation

models were analyzed using the same trajectory and error propagation model for each study. This study demonstrated the correlation model flexibility of Nested Integrals and, simultaneously, demonstrated the variability in results possible with existing, supposedly equivalent, correlation models. Next, the ability to compare gravity models was demonstrated using perfect spherical harmonic modeling as a case study. The final demonstration verified the capability of Nested Integrals to account properly for non-stationary statistics, a correlation model nuance which might have application on some missions.

In a final development, modifications to Nested Integrals algorithm were made to accommodate Kalman filter updates. This capability is needed to analyze most modern navigation missions. A linear state space covariance analysis on the great circle trajectory was used to verify the modified Nested Integrals method.

With these developments, demonstrations and verifications, a new statistical analysis technique has been presented. This technique offers a more flexible alternative to the common linear state space method while being more computationally efficient than Monte Carlo. The Nested Integrals algorithm is a general method for producing the navigation system accuracy statistical performance index by which gravity models can be compared.

XI. Recommendations for Future Research

This research has produced a gravity model evaluation method which can be applied on general mission scenarios. This section contains some suggestions to improve this statistical method and suggestions of possible implementations which require additional research.

First, to develop this method further, it is suggested that the Nested Integrals algorithm be developed for automated variable step size selection. The trajectory model would have to interact directly with Nested Integrals. Since approximation error is usually proportional to a power of integration step size on simple, one-dimensional integration rules, one might calculate the coefficient at each point and select the next step size based on the reciprocal of this norm. This time-step calculation would tend to give constant potential for approximation error. Large time steps would be allowed when the coefficient is small, and during highly dynamic regions the coefficient would be large forcing smaller time steps. The end result could be a substantial increase in efficiency since computational costs are roughly quadratic with number of points.

A comprehensive study of the accuracy bounds of the Nested Integrals algorithm would be useful in future applications. One approach would be to treat this as a frequency response problem. The correlation function could be cos $\omega\psi$ where ω is the frequency parameter. Using this correlation

analyses can be conducted over a range of ω values. The trajectory and error propagation models must be given. A single error quantity, like maximum circular-error-probable, plotted versus ω would be the form of output. Another parameter in this study would be integration step size. These results would be trajectory dependent, and the true covariance would be required to make algorithm error observable.

The batch-processing nature of Nested Integrals will limit its use in real-time applications. As a post-mission analysis tool, it offers some attractive features. For test flights of navigation systems, Nested Integrals can be used to account statistically for gravity induced errors on complex trajectories. Better estimates of instrument errors would be the motivation for this analysis. Research is required to incorporate Nested Integrals into the post flight smoothing and error identification processes.

Along a similar line, Nested Integrals should prove useful in gravity surveys conducted with inertial navigation for position reference. The algorithm should prove useful in post-survey data processing. With adaptation, the method developed here should also be a useful tool in survey design.

Another application is to evaluate different gravity modeling techniques. The example presented in Section VII is simple; any realistic comparison would pose a distinct

problem for the analyst. How does one account for gravity model effects on the residual field? Models can be of different functional form (e.g. global spherical harmonics versus local Chebychev polynomial functional fits) and of different levels of detail within one model type (e.g. different order Chebychev polynomials within the same region). Finding a general framework within which both types of problems can be solved is a substantial research task. The residual field is treated as an error field with first-order approximations throughout the theory. Perhaps the gravity model improvements can be represented, to first-order, as a bounded linear operator over this error field. Symbolically

$$T'(\underline{r}) = \mathcal{A}\{T(\underline{r})\}$$

where T' is the residual potential field after the improved gravity model and $\mathcal{A}$ operates on T, the residual field from the ellipsoidal model. The covariance of the residual field would be given by

$$\phi'_{TT}(\underline{r}_1,\underline{r}_2) = \mathcal{A}_1\{\phi_{TT}(\underline{r}_1,\underline{r}_2)\}\mathcal{A}_2^T$$

where the operator subscripts indicate which position vector would be involved. This idea would require a substantial research effort to bring it to fruition.

Research is needed on two issues concerning the statistical model for gravity disturbance correlations.

First, although all three of the modeling methods studied in Section VI are intended to approximate the empirical correlation function, there is no mention of completeness of the underlying approximations. That is, "can any of the available modeling options replicate the empirical correlation function within some arbitrarily small norm?" Second, the analyses conducted herein assumed the residual field statistics can be "upward continued" [Appendix A and Ref 13] from some reference surface. What if the inertial navigation system (equivalent if not explicit) gravitation model is not harmonic? Such approximations exist in less precise inertial systems than addressed herein. With these existing non-harmonic models, how can correlations of gravity errors aloft be surmised from reference surface statistics? For both of these potential research areas, the first question to be answered is whether or not these statistical modeling questions are important in terms of the potential impact on answers. That is, what is the sensitivity of navigation error statistics to empirical correlation function approximation errors or to non-harmonic gravitation model effects.

Kalman filter effects were included in the Nested Integrals algorithm in Section IX. The measurement update tends to sever the correlation of present navigation errors to past gravity field errors. The effects of mis-modeling the long-time-range gravity disturbance

correlations in $Q(\underline{r},\underline{r}')$ should be less important because of the update. A navigation system with frequent updates might be adequately treated by the more efficient linear state space method even with trajectory restriction violations. Numerical studies, such as the minor circle parametric study of Section IV, could give insight into this issue. A comprehensive study would be useful in planning the statistical analysis of future systems and missions.

These research areas seem the most promising extensions and applications of Nested Integrals. Any number of small studies similar to Sections VI, VII, and VIII of this work would contribute to understanding the uses and limits of Nested Integrals. Additional comparisons between Nested Integrals and linear state space analysis would be useful in further defining the accuracy limits of the efficient linear state space method.

APPENDIX A

Comments on Gravity Correlation Models

A gravity disturbance correlation model is required in order to perform the analyses which are the subject of this research. This model conveys, in an average sense, the interrelationships of all gravity disturbance terms which affect the navigation accuracy. The choice of trajectory and navigation error propagation models is straightforward in comparison to the choice of this statistical model. No panacea exists in this case. A universally accepted model which can be used in all cases has not been, and probably cannot be, defined. The cases which might create problems for a general model include geographically restricted missions and gravity model improvements. In either of these examples, a correlation model must be formed in a manner peculiar to the problem being addressed. The purpose of this appendix is to illuminate some of the issues which should be considered in choosing the gravity disturbance correlation model.

The first problem an analyst faces when surveying model concepts is language. The fact that few orderly threads weave through this labyrinth of model types compounds the confusion. No clear taxonomy classifies these models for the novice, so a few of the labels applied to models are defined as follows:

a. Homogeneity. [Ref 4:85] The statistics are not a function of position (i.e. spatially stationary statistics). Obviously, gravity quantities change with altitude, so this term describes the behavior at one altitude level.

b. Isotropicity. [Ref 4:85] The statistics are independent of direction or heading in the horizontal plane.

c. Global. The statistics are worldwide averages or expectations as opposed to local or regional.

d. Anomaly.* The statistics are based on gravity anomaly Δg. The symbol $\varphi_{gg}(\cdot)$ is used in this work for anomaly correlation. Moritz [Ref 4:83] and others in Geodesy use $C(\cdot)$ for this function.

e. Potential.* The statistics are of or based on anomalous potential T. The symbol $\varphi_{TT}(\cdot)$ is used herein; others [Ref 4:86] use $K(\cdot)$ for this function.

f. Undulation.* The statistics are of or based on undulation N of the geoid (also known as geoidal height). This quantity is directly related to anomalous potential T by Brun's formula [Ref 3]

$$T(\underline{r}) = g\, N(\underline{r}) \tag{A-1}$$

Therefore, the correlations are related by

$$\varphi_{TT}(\cdot) = g^2\, \varphi_{NN}(\cdot) \tag{A-2}$$

---

* Definitions for Δg, N, T, and other gravity disturbance quantities are given in Reference 3.

g. k-th order. This term states the order of Markov process used in the model. For example, a third-order undulation model is based on undulation correlation and structured as a third-order Markov process.

h. Upward Continuation. Not a classification per se, this term refers to the extrapolation of statistics aloft from the datum surface. Some models (e.g. the Tscherning-Rapp anomaly degree variance model [Ref 21] in Sections V and VI) have this inherent capability; other models do not (e.g. the linear state space model [Ref 13] introduced in Section IV).

i. Self-consistent. The model generates gravity disturbance term statistics (e.g. auto- and cross-correlations) which are consistent with respect to the gravitational field theory from which interrelationships of these terms can be derived.

These terms and more await the researcher delving into this modeling issue. The three full-scale models discussed in Section VI [Refs 19, 20, 21, and 22] offer a starting point at least. References 2, 4, and 12 offer some tutorial assistance, also. In the end, whether or not a model is adequate will be the subjective judgment of the analyst, made either consciously or by default.

Consider now a scenario of how a model might be formed. Empirical correlation functions can be generated from gravity

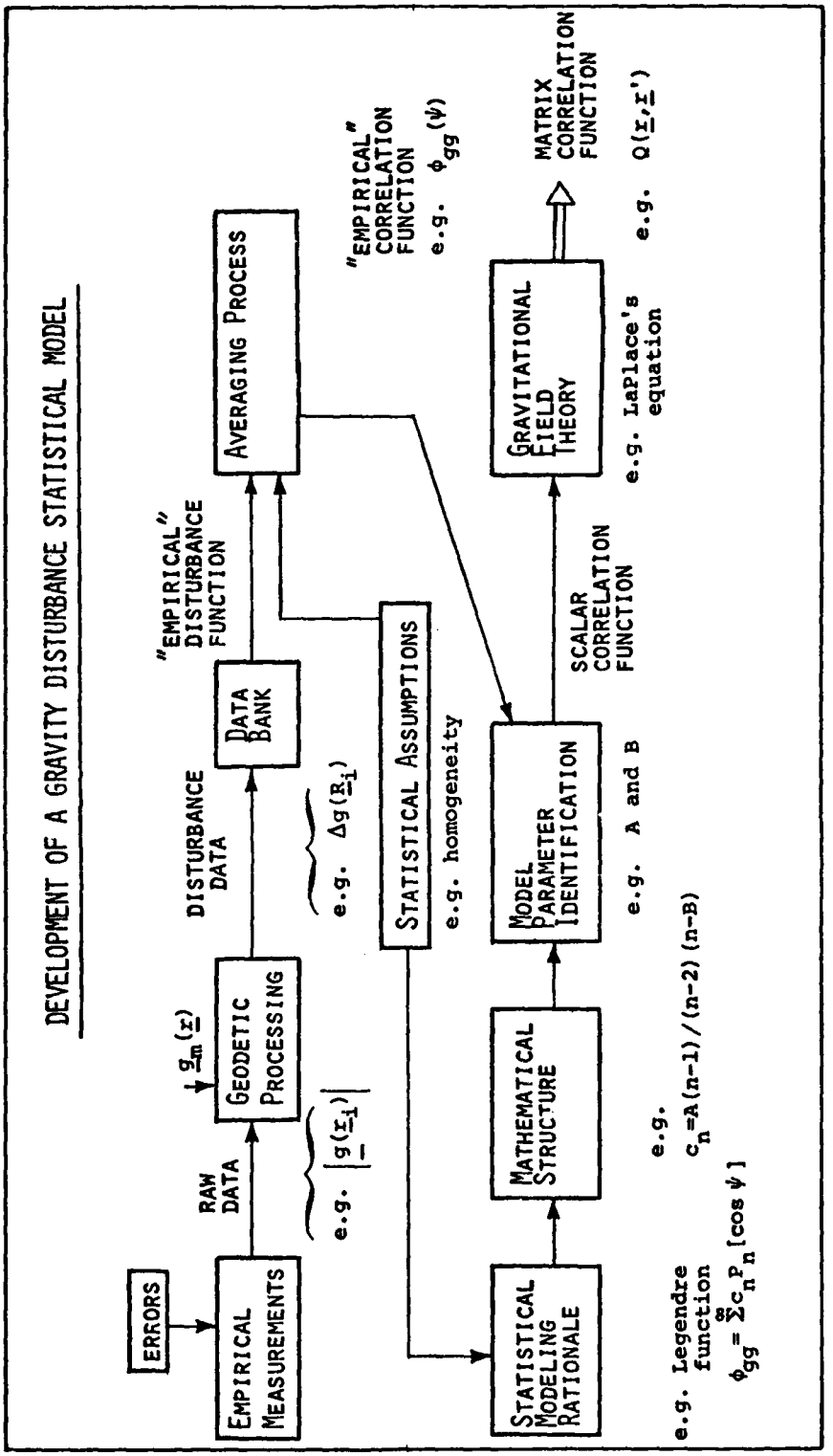

Figure A-1. Development of a Gravity Disturbance Statistical Model

(or gravity related) measurements. A model structure is next either selected from existing examples or derived on some new rationale. The model parameters are selected to replicate the empirical function. And finally, the mathematical structure and the data parameters of the model are programmed as a subroutine which accepts position pairs as input and which yields the required correlations as outputs. The correlations or at least representatives should be compared to the empirical function for validation.

The first step assumes gravity data is available. The primary data available for such analysis are gravity magnitude measurements. These data are converted to free air anomaly and referenced to the geoid. So, any averages formed from these data apply to the geoid or an approximating, analytical surface like the Bjerhammer sphere [Ref 3 :321]. These geodetic data processing steps introduce error through the models [Ref 3] used to produce the anomaly and to estimate the value on the geoid. The data produced by such processing is no longer truly "empirical". Correlation models based on these processed data will be referred to as "empirical", but the reader should be aware of these possibly corrupting influences.

Deflections of the vertical have been measured by astro-geodetic means and geoidal undulations by satellite altimetry. These data could also be processed to form empirical correlation functions. Indeed, heterogeneous

types of data can be used, if coverage is adequate, to produce cross-correlations as well. Such steps need not be taken for, as will be shown later, only one correlation function is needed. The other auto- and cross-correlations can be derived from this base function using interrelationships from gravitational theory which is assumed to correctly represent the physics of this problem.

Data for model development is limited by economics and by politics; therefore, compromises must be made in representing the correlation function. The manner in which the empirical correlation is formed makes a statement about the type of model it will support. If the correlation is calculated by averaging data over the earth's surface, the resulting correlation function will represent global statistics. If the independent variables for the averaging are relative position quantities, the average represents a model based on the homogeneous assumption [Ref 4 :85]. If the independent variable is central angle (or equivalent surface arc distance) shift with the average being over all headings, the resultant empirical correlation is consistent with the isotropic assumption [Ref 4 :85]. With all of this structure, the reality of the data availability is that global high frequency coverage does not exist due to the magnitude of the task implied. The homogeneous and isotropic assumptions will undoubtedly be made just to bring more data points into the empirical formulation.

Assuming that the empirical correlation exists, the model structure must be defined. The examples in Section VI are fully-developed and appear adaptable. Whether these models can fit an arbitrary empirical correlation function with arbitrarily small error is a question worthy of attention. For now, assume the model can be fit to the empirical function with acceptable veracity. Then, one merely transforms the mathematical model into a computer subroutine and proceeds with the analysis.

The question may be raised, "Why go to these mathematical forms when the empirical function is the desired correlation?" Obviously, a table look-up approach can be used on the basic correlation function. The $Q(\underline{r},\underline{r}')$ matrix function of (28) requires a set of auto- and cross-correlation functions, however, and this set should be consistent. Data does not exist to produce adequate empirical models for all of these gravity disturbance terms, so producing them indirectly from a basic model is required. The number of $Q(\underline{r},\underline{r}')$ evaluations is great on even a modest analysis. The cases in Section IV were based on 409-point Nested Integral analysis, and each case required 83,845 $Q(\underline{r},\underline{r}')$ evaluations, for instance. A closed mathematical expression is a practical necessity in such analyses.

Fortunately, a closed mathematical expression is only required for the basic correlation function. The other correlations can be derived from this source. The

anomaly or the anomalous potential correlation is sufficient [Ref 4:94-98] as a base for this derivation. To see this fact, consider the following.

The gravity disturbance vector is related to potential by

$$\delta\underline{g}(\underline{r}) = \frac{d}{d\underline{r}} T(\underline{r}) = \nabla T(\underline{r}) \qquad \text{(A-3)}$$

where T is the scalar anomalous potential. For navigation studies, $\delta\underline{g}$ and T are the most likely candidate elements in $\underline{u}$ of (3). The disturbance vector represents the driving terms in the inertial navigation velocity error derivative. The anomalous potential is related to geoidal undulation N by (A-1). The geoidal undulation could be considered an error term in a barometric altimeter used to stabilize the vertical channel.

For discussion then, define

$$\underline{u}(\underline{r}) = \begin{Bmatrix} \delta\underline{g}^{a}(\underline{r}) \\ \cdots\cdots \\ N(\underline{r}) \end{Bmatrix} \qquad \text{(A-4)}$$

where the a-frame is an arbitrary orthogonal frame with coordinates x, y, and z.

Using (A-1), (A-3) can be rewritten as

$$\underline{u}(\underline{r}) = \begin{Bmatrix} \frac{\partial}{\partial x} \\ \frac{\partial}{\partial y} \\ \frac{\partial}{\partial z} \\ \cdots \\ 1/g \end{Bmatrix} T(\underline{r}) \qquad \text{(A-5)}$$

AD-A082 494 AIR FORCE AVIONICS LAB WRIGHT-PATTERSON AFB OH F/G 17/7
GRAVITY MODEL EVALUATION FOR PRECISE TERRESTRIAL INERTIAL NAVIG--ETC(U)
DEC 79 R M EDWARDS
UNCLASSIFIED AFAL-TR-79-1231 NL

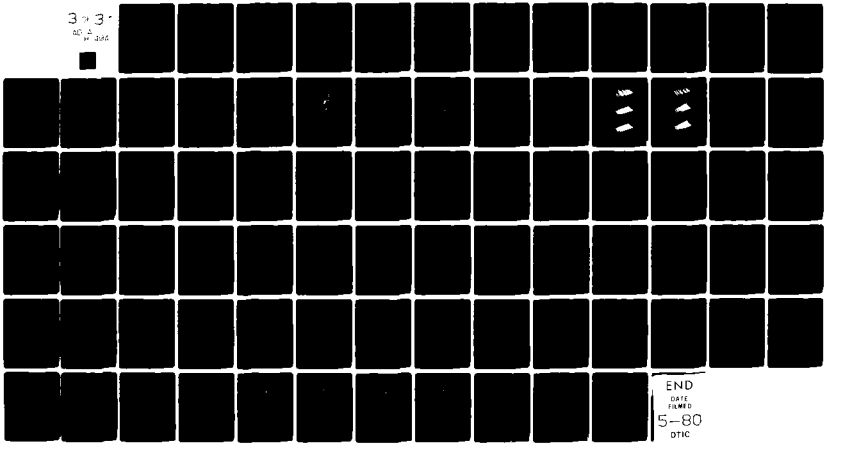

END
DATE FILMED
5-80
DTIC

Now the Q-matrix function of (8) can be written

$$Q(\underline{r}_1,\underline{r}_2) = \mathcal{E}\{\mathcal{B}_{1,2}[T(\underline{r}_1)\ T(\underline{r}_2)]\} \qquad (A\text{-}6)$$

where

$$\mathcal{B}_{1,2} = \begin{bmatrix} \frac{\partial^2}{\partial x_1 \partial x_2} & \frac{\partial^2}{\partial x_1 \partial y_2} & \frac{\partial^2}{\partial x_1 \partial z_2} & \frac{1}{g} & \frac{\partial}{\partial x_1} \\ \frac{\partial^2}{\partial y_1 \partial z_2} & \frac{\partial^2}{\partial y_1 \partial y_2} & \frac{\partial^2}{\partial y_1 \partial z_2} & \frac{1}{g} & \frac{\partial}{\partial y_1} \\ \frac{\partial^2}{\partial z_1 \partial x_2} & \frac{\partial^2}{\partial z_1 \partial y_2} & \frac{\partial^2}{\partial z_1 \partial z_2} & \frac{1}{g} & \frac{\partial}{\partial z_1} \\ \frac{1}{g}\frac{\partial}{\partial x_2} & \frac{1}{g}\frac{\partial}{\partial y_2} & \frac{1}{g}\frac{\partial}{\partial z_2} & 1/g^2 & \end{bmatrix} \qquad ((A\text{-}7)$$

where the subscripts on the x, y, and z partials identify the $\underline{r}$ term involved (e.g. $\partial/\partial x_1$ means $\partial/\partial x$ for the $\underline{r}_1$ terms).

Physical principals assure that, the partial derivatives in (A-5) are uniformly bounded. The partial derivative operations of (A-5) are, therefore, bounded and linear, so the order of these operations may be interchanged with the linear expectation operator. Then, (A-5) becomes

$$Q(\underline{r}_1,\underline{r}_2) = \mathcal{B}_{1,2}[\phi_{TT}(\underline{r}_1,\underline{r}_2)] \qquad (A\text{-}8)$$

where

$$\phi_{TT}(\underline{r}_1,\underline{r}_2) = \mathcal{E}[T(\underline{r}_1)\ T(\underline{r}_2)] \qquad \text{(A-9)}$$

With (A-8) and (A-9), it is clear that the Q-matrix function can be produced from an anomalous potential correlation function basis. The gravity disturbance quanties of $Q(\underline{r},\underline{r}')$ are related to anomaly through the Stoke's integral [Ref 3:89] and the Vening-Meinesz integrals [Ref 3;114]. So, a similar line of reasoning can be followed to yield $Q(\underline{r},\underline{r}')$ as a function of $\varphi_{gg}(\underline{r},\underline{r}')$. The linear operators of (A-8) are integrals rather than derivatives in this case.

With this demonstration complete, attention can be given to the two cases which are likely to require model development. These are:

a. Mission space geographical restrictions to a region known to have a residual field statistically different from the global averages, or

b. Gravity model improvements which change the magnitude and the spectrum of the residual field statistics.

Even in these events, the functional forms presented in Section VI may, yet, be adequate. The model parameters would need to be re-identified to reflect the new residual field of interest. The references given for the three functional forms [Refs 19, 21, 22, and 23] present some rationale for the parameter identification for the original models, and these suggestions should be useful in identi-

fying parameters for the new situation, either geographic or gravity model.

For the geographically restricted mission, a geographically restricted, empirical correlation function could be used to identify the model parameters on the basis correlation function. Where model improvements are considered, the effects of the improved gravity model can be used to form a new empirical data base. Consequently, a new empirical correlation function can be generated for subsequent model parameter identification. Either method requires that a gravity data base be at the disposal of the analyst.

The required data may not be available. Even if it is, the calculations over all empirical data would be expensive. An alternative might be considered when studying the effects of a gravity model improvement. The model improvement can be viewed as a transform $\mathscr{A}(\cdot)$ over the ellipsoidal model's residual field:

$$T'(\underline{r}) = \mathscr{A}[T(\underline{r})] \qquad \text{(A-10)}$$

where T' is the residual field of the improved gravity model. Note that $\mathscr{A}(\cdot)$ transforms one function into another function, not just one value of the scalar $T(\cdot)$ into another scalar value. A suggestion for future research based on this operator concept is given in Section XI.

This appendix has presented some of the statistical model selection issues. A categorical answer to the gravity disturbance correlation model is not available, but several examples are developed [Refs 19, 21, 22, and 23] and are amenable to adaptation.

APPENDIX B

Conversion of a Spatial, Linear State Space, Statistical Gravity Disturbance Model to a Temporal Model

The time history of mission position converts the gravity disturbance from a function of position into an implicit function of time. The statistical model for gravity disturbances undergoes a similar transformation. For the linear state space statistical model, this transformation can be continued to form an equivalent temporal statistical model for a restricted class of trajectories. This conversion to the time domain is mentioned in Sections I through IV, and this appendix provides a derivation to explain the assertions.

The linear state space gravity disturbance model attempts both to approximate an empirically derived correlation function and to yield auto- and cross-correlations of all disturbance quantities produced which are consistent with gravitational field theory. If, for example, $\phi'_{gg}(\psi)$ is the empirical function, we have

$$\phi'_{gg}(\psi) \approx \underset{(\underline{r}_1,\underline{r}_2)\,\in\,\Upsilon}{\mathcal{E}}[\Delta g(\underline{r}_1)\,\Delta g(\underline{r}_2)] \tag{B-1}$$

where

$$\Upsilon = \{(\underline{r}_1,r_2)\,|\,\underline{r}_1\cdot\underline{r}_2 = r^2\cos\psi\} \tag{B-2}$$

The Gauss-Markov model is based on a state vector $\underline{x}_g$ which satisfies the shift invariant relationship

$$\frac{d}{d\psi}[\underline{x}_g(\psi)] = F_g\,\underline{x}_g(\psi) + G_g\,\underline{q}(\psi) \tag{B-3}$$

where $\underline{q}$ is a vector of white gaussian noise sources satisfying

$$\mathcal{E}[\underline{q}(\psi)\ \underline{q}^T(\psi+\Delta\psi)] = Q_g\ \delta(\Delta\psi) \tag{B-4}$$

The anomaly is an output of this process

$$\Delta g(\psi) = C_g \underline{x}_g(\psi) \tag{B-5}$$

The model's anomaly correlation, $\phi''_{gg}(\psi)$, is given by

$$\phi''_{gg}(\Delta\psi) = C_g P_{xg}(\Delta\psi)\ C_g^T \tag{B-6}$$

where

$$P_{xg}(\Delta\psi) = \mathcal{E}[\underline{x}_g(\psi)\ \underline{x}_g(\psi+\Delta\psi)] \tag{B-7}$$

which can be produced from (B-3) and (B-4). The difficulty of performing this task should not be underestimated. The modeler must form F_g, G_g, Q_g, and C_g in order to produce $\phi''_{gg}(\psi)$. These model elements are used in producing a model for which

$$\phi''_{gg}(\psi) \approx \phi'_{gg}(\psi) \tag{B-8}$$

Other disturbance quantities produced by extension of (B-5) should have auto- and cross-correlations consistent with field theory. A chronicle of this model's development is provided in Reference 11 for the interested reader.

The model can be viewed as

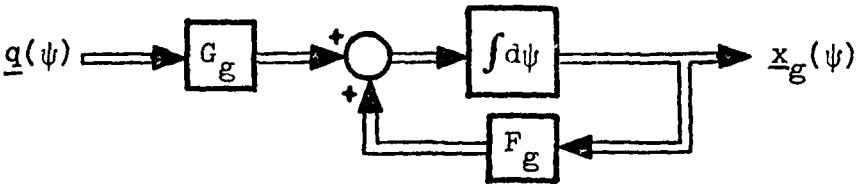

The error state transition matrix for (B-1) is

$$\Phi(\psi-\psi_o) = e^{(\psi-\psi_o)F_g} \tag{B-9}$$

Then,

$$\underline{x}_g(\psi) = \Phi(\psi-\psi_o)\ \underline{x}_g(\psi_o) + \int_{\psi_o}^{\psi} \Phi(\psi-v)G_g\underline{q}(v)\,dv \qquad \text{(B-10)}$$

Using the statistical independence of $\underline{q}(\psi)$ and $\underline{x}_g(\psi)$ with (B-4), yields the result

$$P_g(\psi) = \mathcal{E}[\underline{x}_g(\psi)\ \underline{x}_g^T(\psi)]$$

$$= \Phi(\psi-\psi_o)P_g(\psi_o)\ \Phi^T(\psi-\psi_o)$$

$$+ \int_{\psi_o}^{\psi} \Phi(\psi-v)G_gQ_gG_g^T\ \Phi^T(\psi-v)\,dv \qquad \text{(B-11)}$$

The statistical process is typically modeled to be at steady state, so

$$P_g(\psi) = P_g(\psi_o) = P_g \qquad \text{(B-12)}$$

Since the derivative of P_g with respect to ψ is zero, it follows that

$$G_gQ_gG_g^T = -F_gP_g - P_gF_g^T \qquad \text{(B-13)}$$

Solution for Q_g in (B-13) is not unique in general since G_g^{-1} could only exist for cases where $\underline{x}_g$ and $\underline{q}$ have the same number of elements. The two Schuler loop cases of Section III provide convenient examples for (B-13) application.

To convert this spatial model to the time domain, assume ψ changes according to the rule

$$\psi(t) = \psi_o + \int_{t_o}^{t} [V(t)/r(t)]dt = \psi_o + \int_{t_o}^{t} \omega(t)\,dt \qquad \text{(B-14)}$$

where

$V(t)$ is horizontal velocity magnitude and non-negative,

$r(t)$ is position radius magnitude, and

$\omega(t)$ is central angular velocity.

For this transformation to be valid simultaneously between all points on the trajectory, the path has to lie in one

plane with a total change of less than 180^{o}. Using (B-14)

$$d\psi = [V(t)/r(t)]dt = \omega(t)\ dt \tag{B-15}$$

Employing the chain rule, (B-3) can be converted to

$$\dot{\underline{x}}_g[\psi(t)] = [\omega(t)F_g]\ \underline{x}_g[\psi(t)] + G_g\ \underline{w}(t) \tag{B-16}$$

where

$$\underline{w}(t) = \omega(t)\underline{q}[\psi(t)] \tag{B-17}$$

The new noise correlation is

$$\mathcal{E}[\underline{w}(t)\underline{w}^T(t+\tau)] = \omega^2(t)Q_g\ \delta[\psi(t+\tau) - \psi(t)] \tag{B-18}$$

With the monotonic assumptions above, the argument of the dirac delta function can be replaced by the Taylor series, first-order approximation

$$\psi(t+\tau) - \psi(t) \leftarrow \tau\omega(t)$$

It can be shown that

$$\omega(t)\ \delta[\tau\omega(t)] \equiv \delta(\tau) \tag{B-19}$$

So, (B-18) can be rewritten as

$$\mathcal{E}[\underline{w}(t)\ \underline{w}^T(t+\tau)] = \omega(t)\ Q_g\ \delta(\tau) \tag{B-20}$$

which completes the temporal model of (B-16)

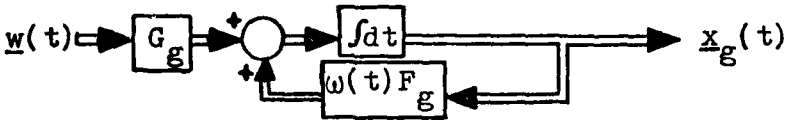

Note that for $V(t)=0$, $\dot{\underline{x}}_g(t)=0$, since the noise strength and the feedback term have $\omega(t)$ factors. This result is intuitively satisfying. That is, when position is constant, the gravity disturbance is constant as expected.

In order for the temporal model to emulate the correlations of the spatial model, some restrictions must be placed on the type of trajectory used. Specifically, the

trajectory must be a great circle of less than 180°, and the central angle must be monotonic nondecreasing. These trajectory restrictions are further discussed at the end of Section II.

APPENDIX C

Undamped Schuler Case, Graphical Results

This appendix presents the graphical results of the undamped Schuler loop study of Section III. The table below gives a convenient cross reference for the plots.

Table C-I

Undamped Schuler Loop Graphical Results
Cross Reference

Type of Error Plot	Rectangular		Trapezoidal		Nested Integrals	
	Figure	Page	Figure	Page	Figure	Page
Position Variance	C-1	192	C-2	193	C-3	194
Pos.-Vel. Covariance	C-4	195	C-5	196	C-6	197
Velocity Variance	C-7	198	C-8	199	C-9	200
% Position Variance	C-10	201	C-11	202	C-12	203
Composite Position Variance	C-13	204	C-13	204	C-13	204
Composite Velocity Variance	C-14	205	C-14	205	C-14	205

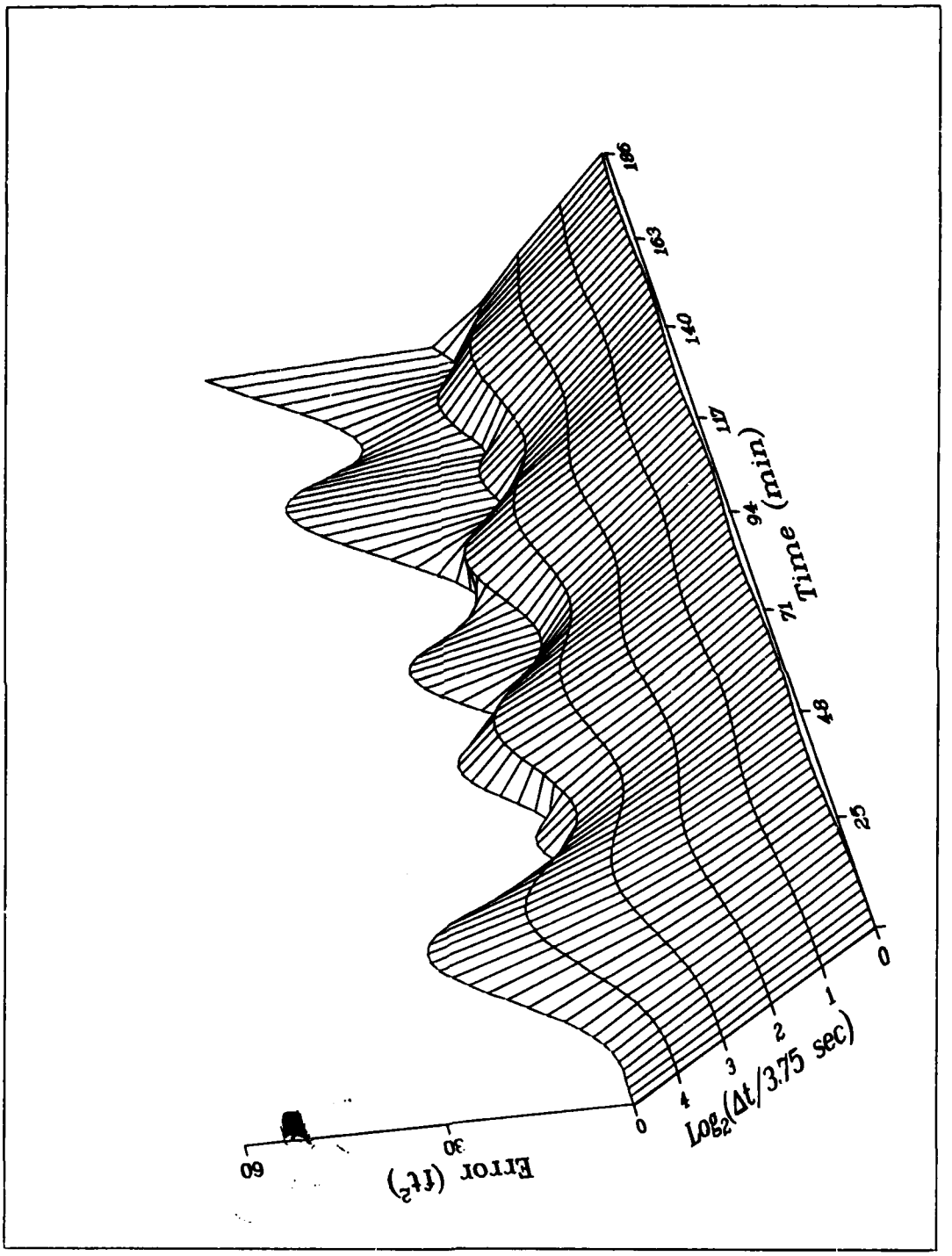

Figure C-1. Error in Position Variance, Undamped Schuler Case, Rectangular Algorithm

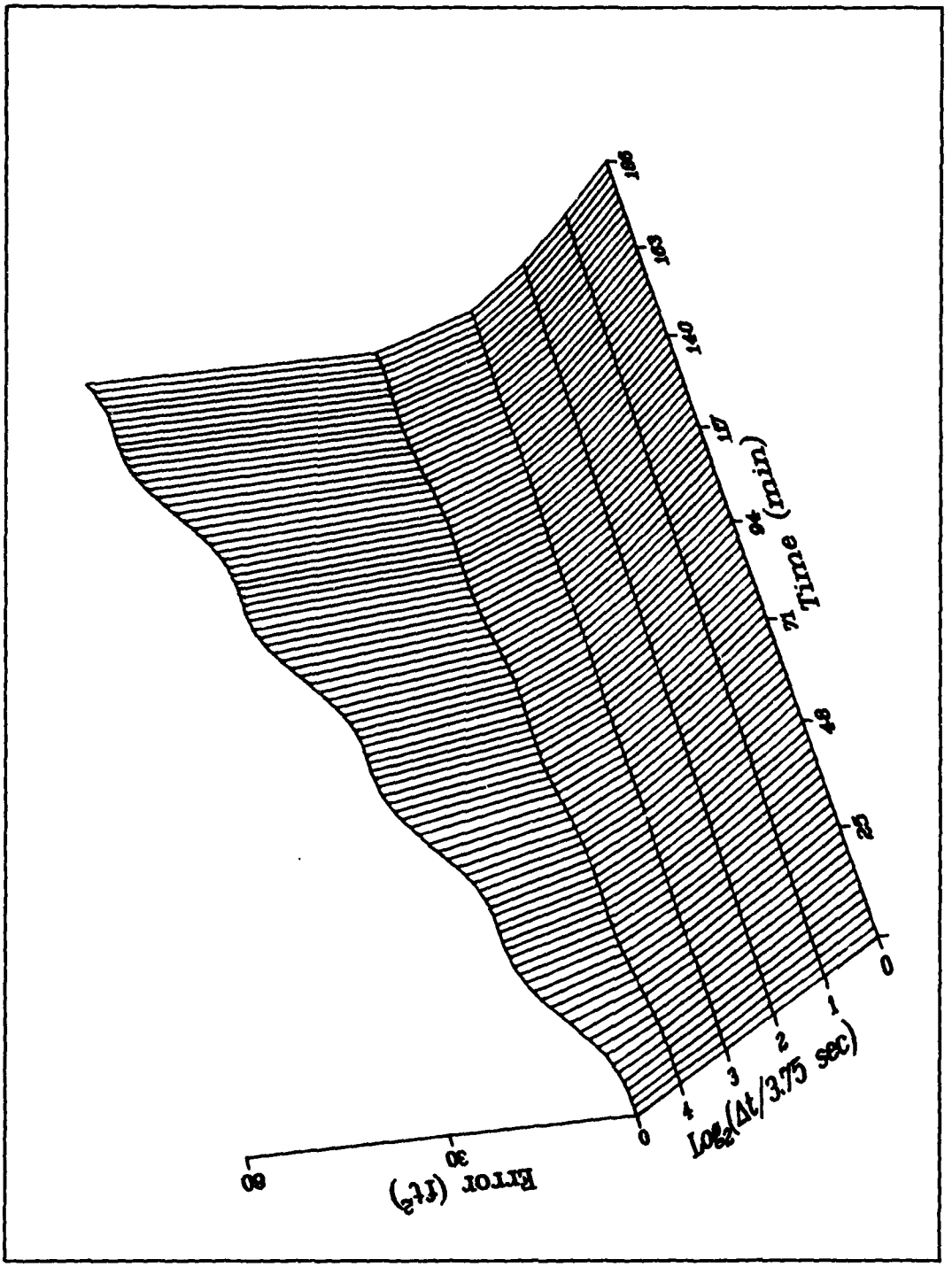

Figure C-2. Error in Position Variance, Undamped Schuler Case, Trapezoidal Algorithm

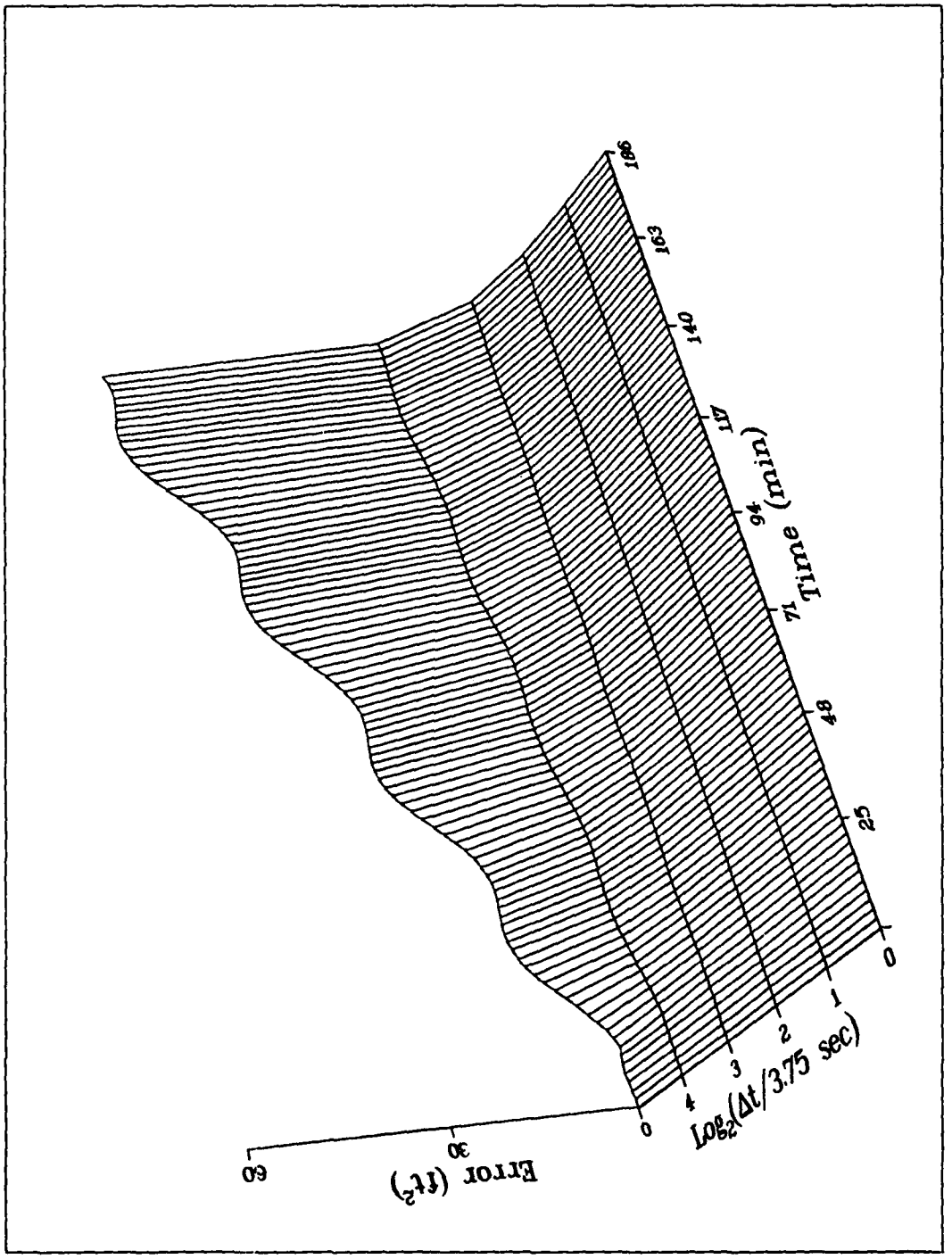

Figure C-3. Error in Position Variance, Undamped Schuler Case, Nested Integrals Algorithm

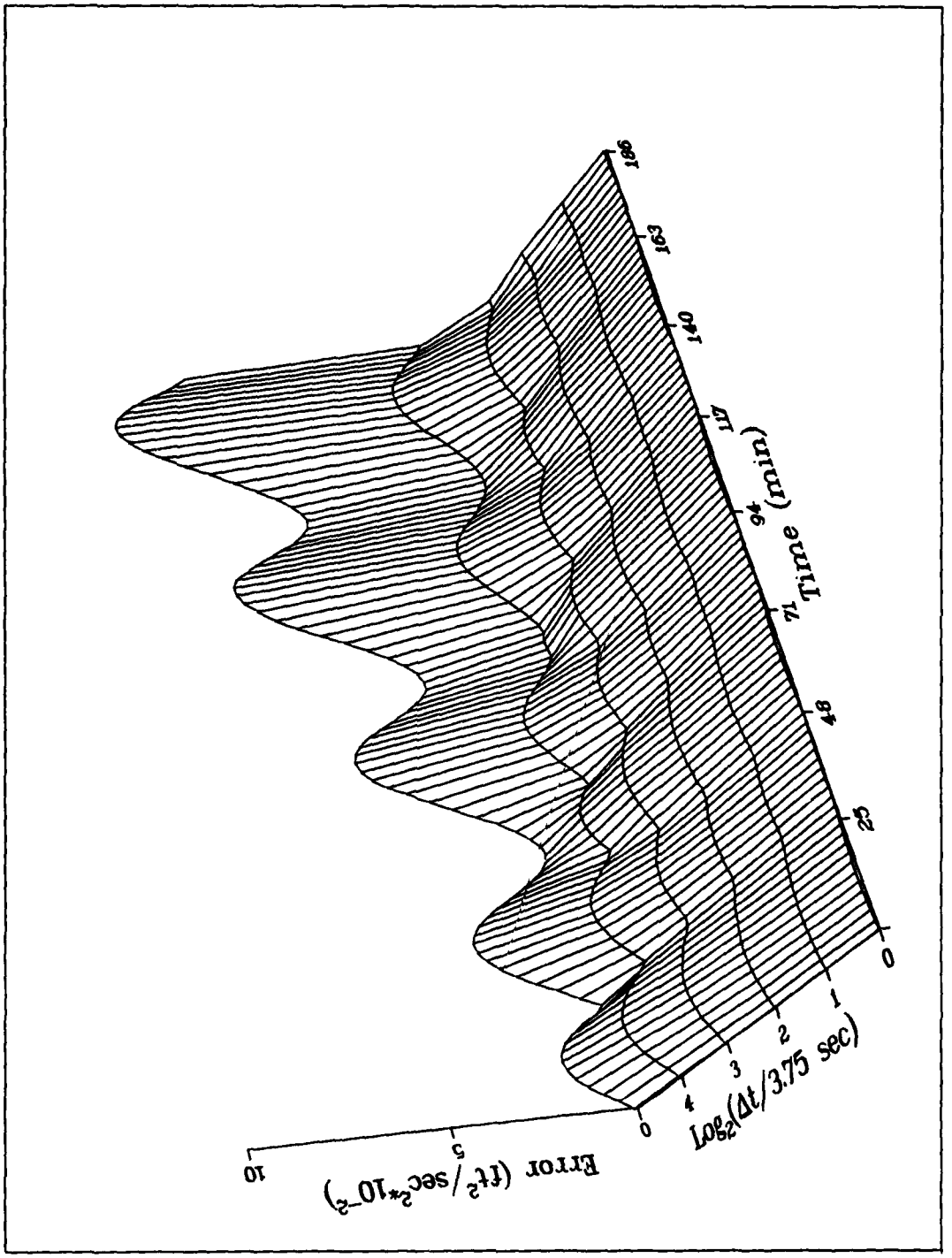

Figure C-4. Error in Velocity Variance, Undamped Schuler Case, Rectangular Algorithm

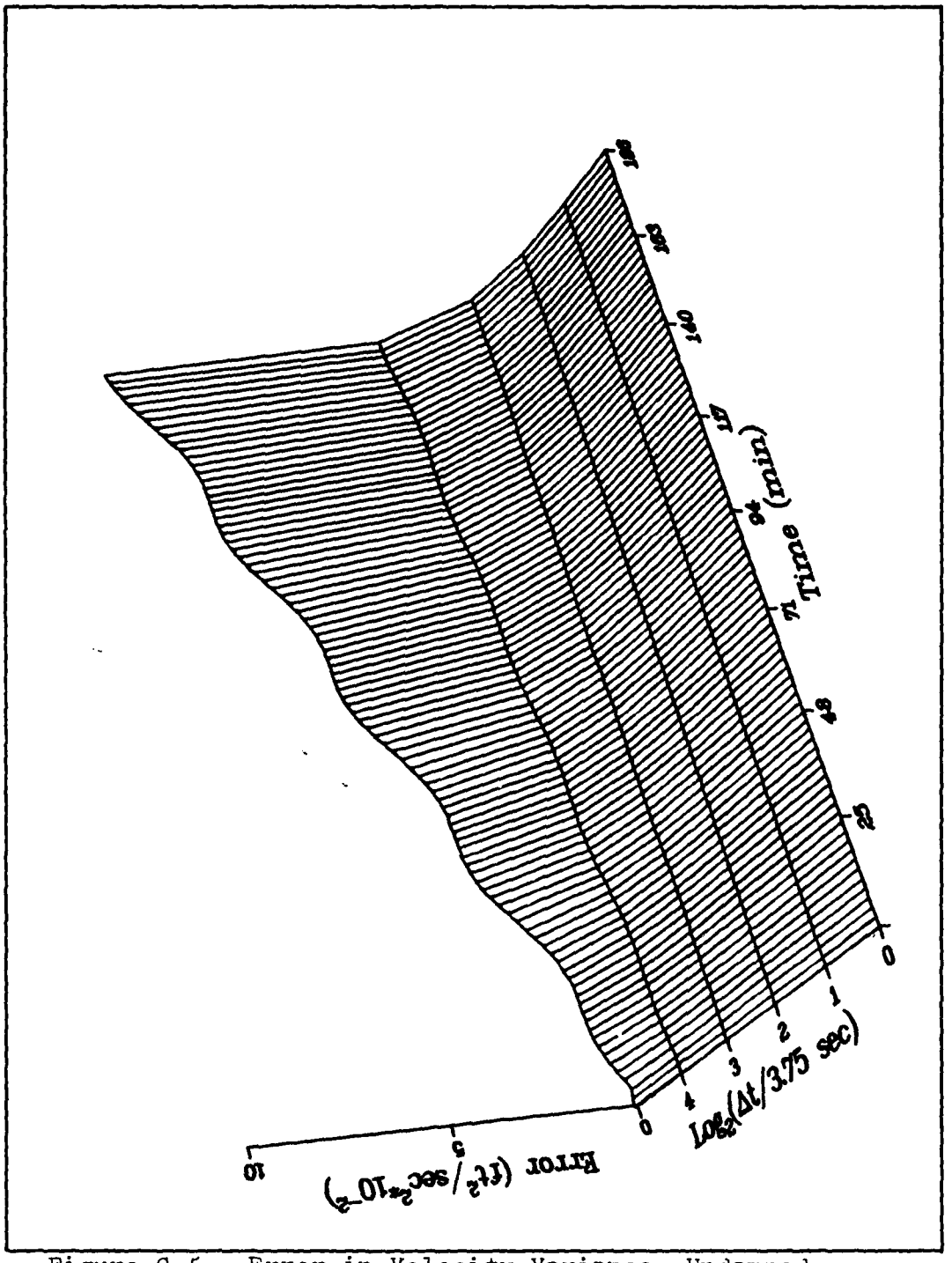

Figure C-5. Error in Velocity Variance, Undamped Schuler Case, Trapezoidal Algorithm

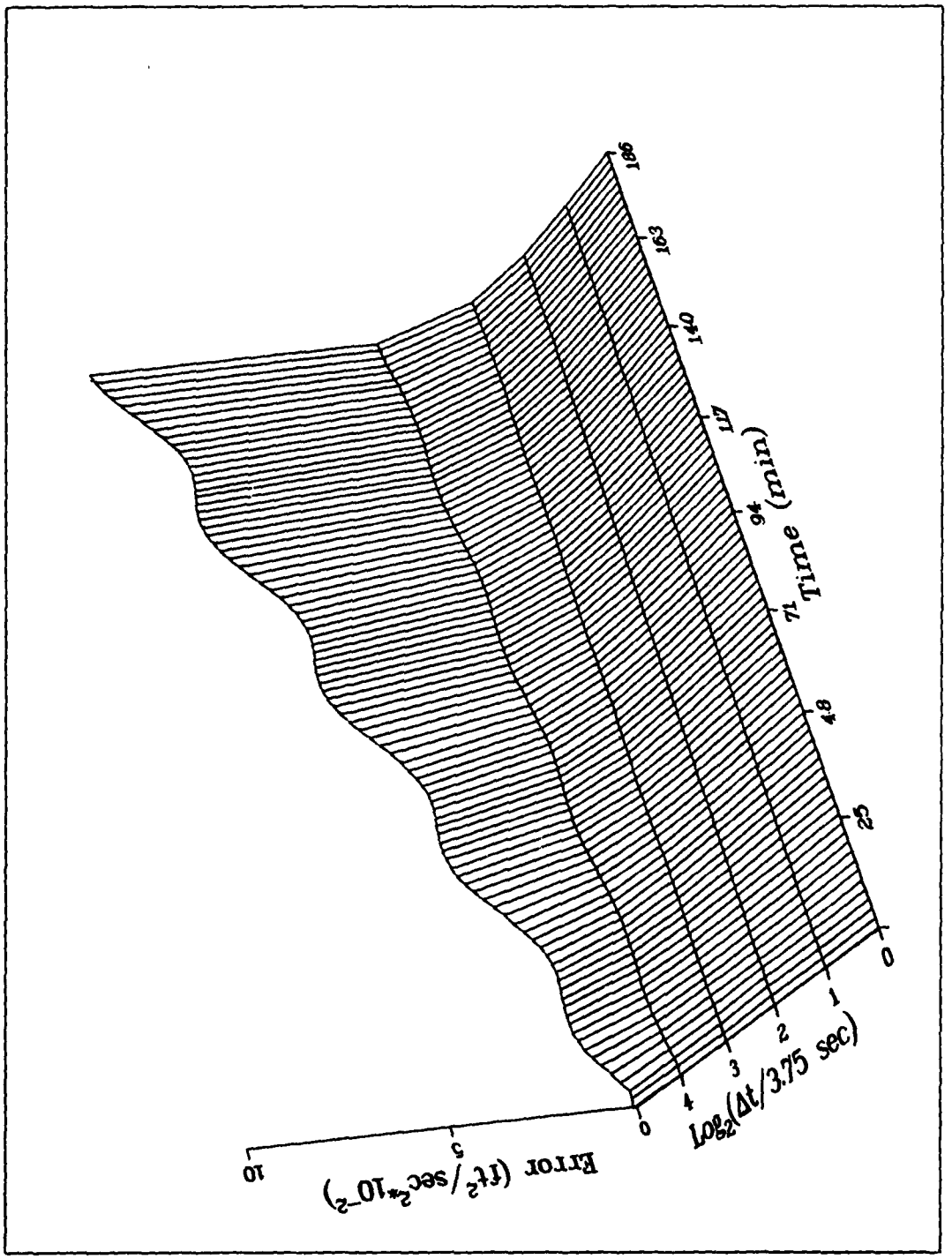

Figure C-6. Error in Velocity Variance, Undamped Schuler Case, Nested Integrals Algorithm

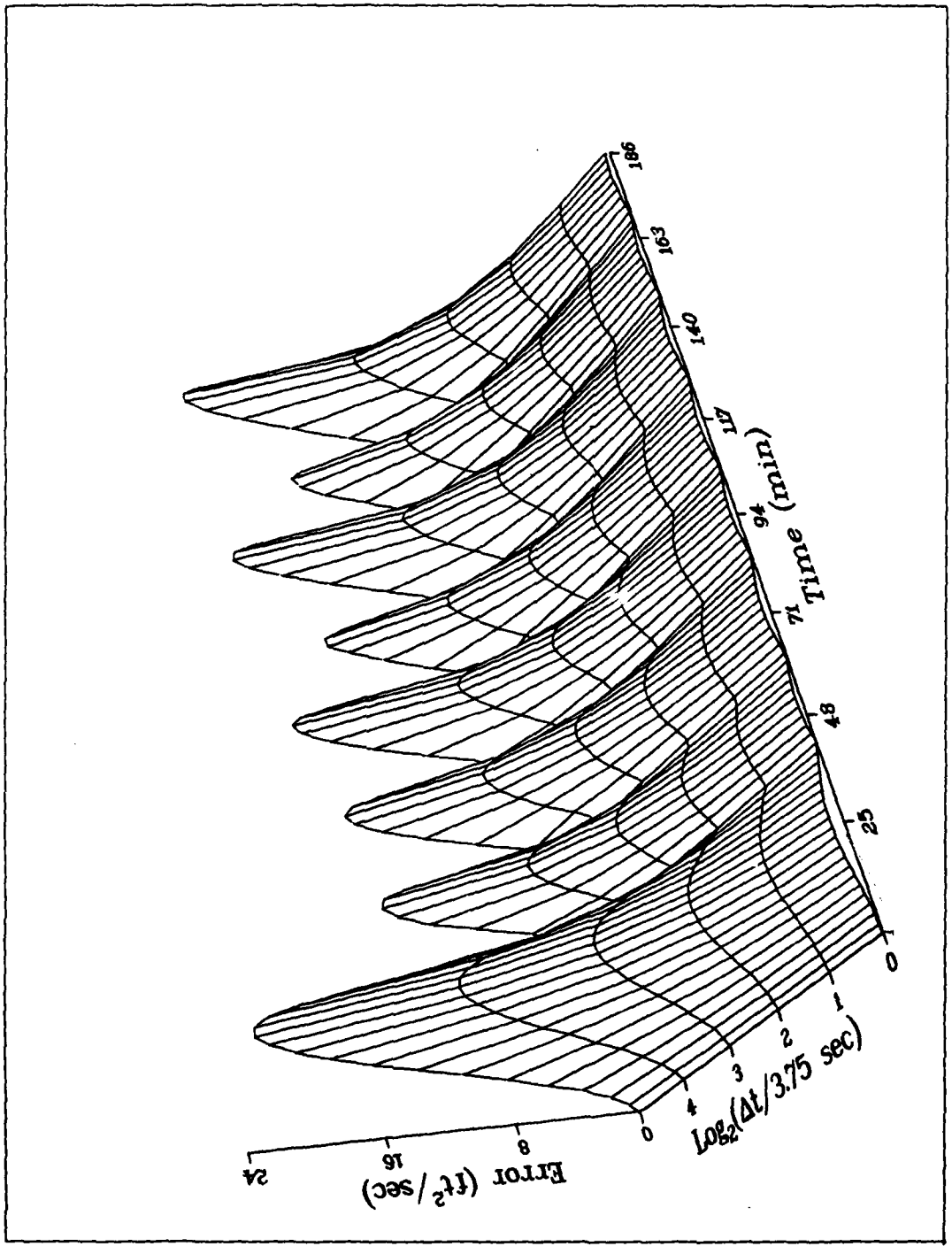

Figure C-7. Error in Position-Velocity Covariance, Undamped Schuler Case, Rectangular Algorithm

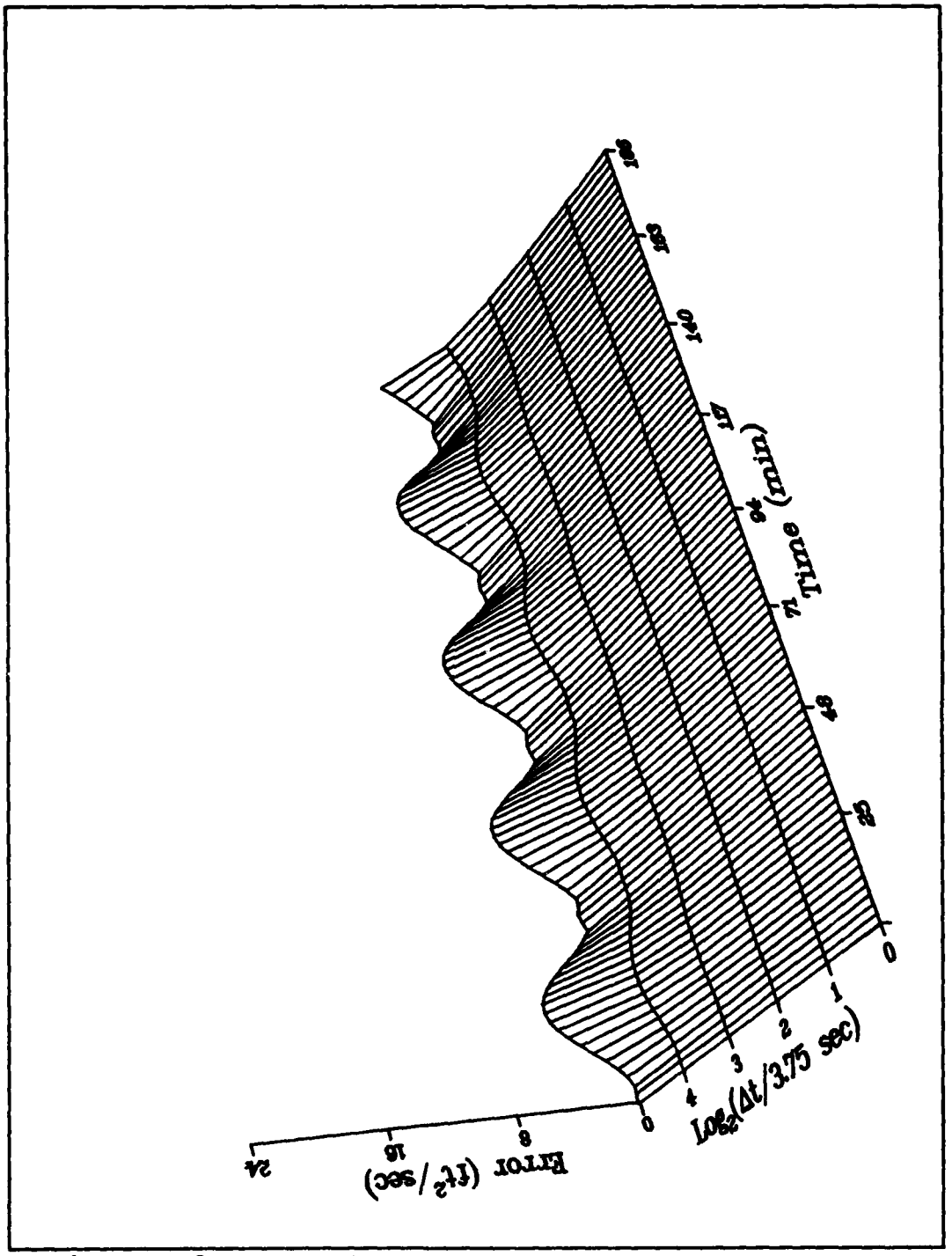

Figure C-8. Error in Position-Velocity Covarinace, Undamped Schuler Case, Trapezoidal Algorithm

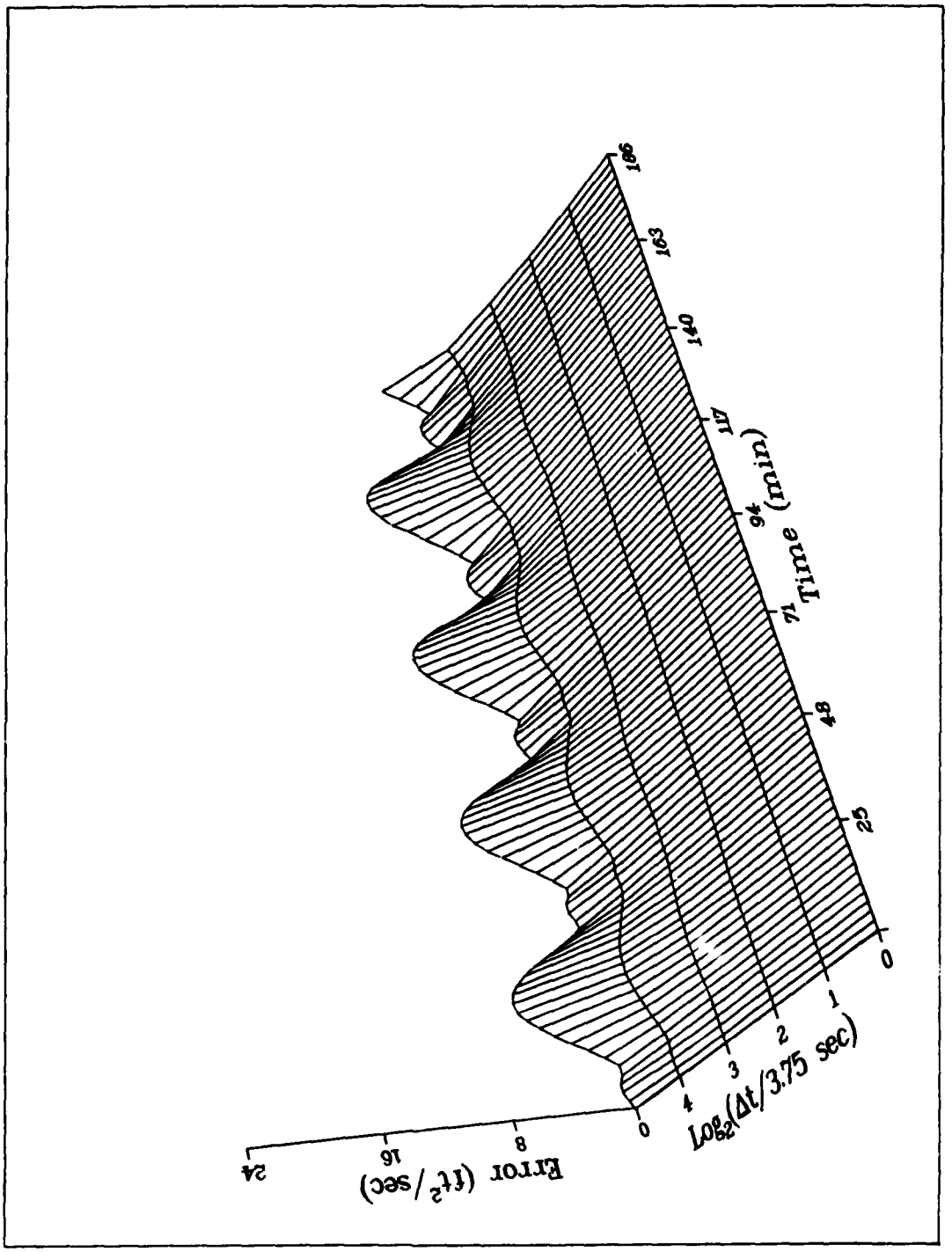

Figure C-9. Error in Position-Velocity Covariance, Undamped Schuler Case, Nested Integrals Algorithm

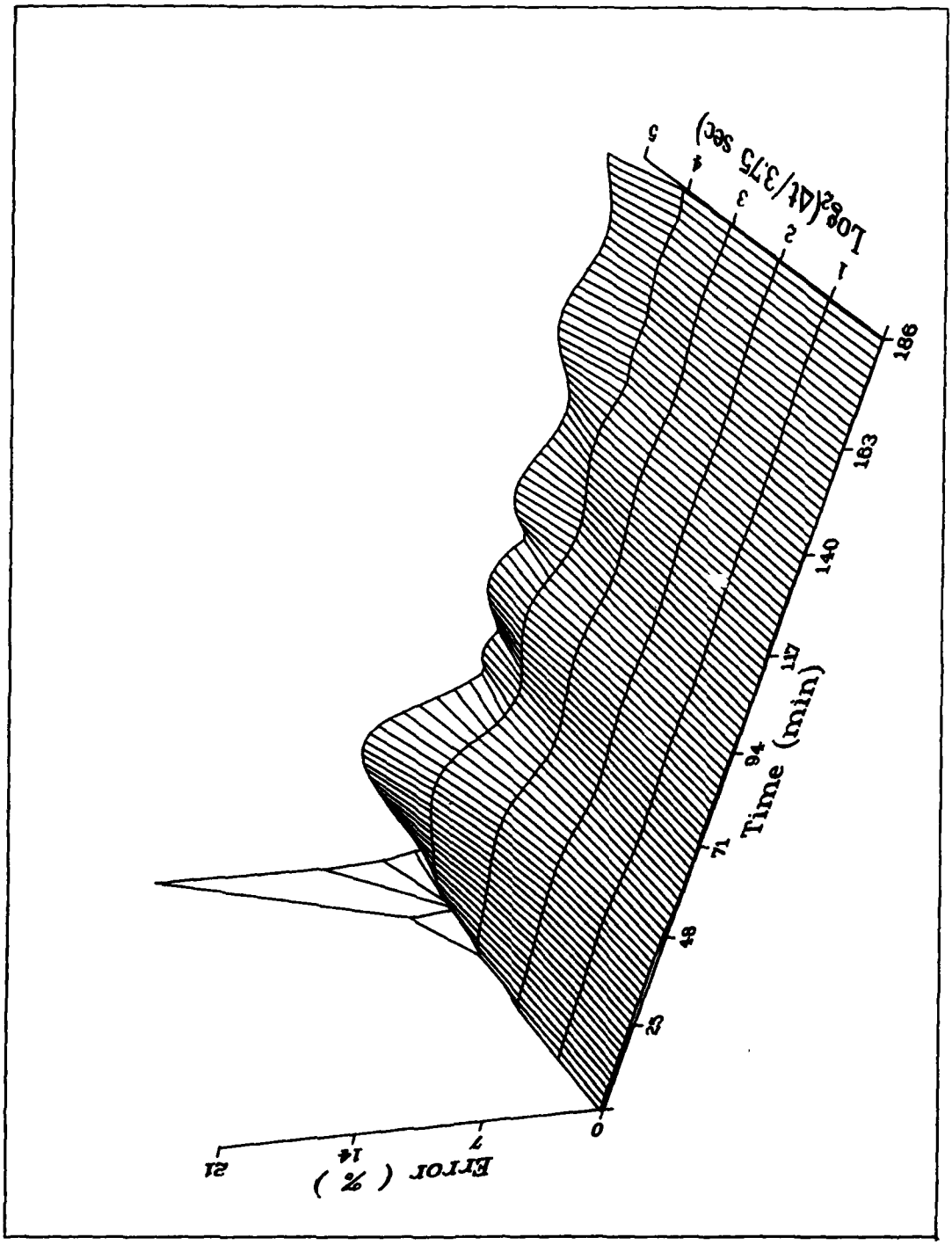

Figure C-10. Percent Error in Position Variance, Undamped Schuler Case, Rectangular Algorithm

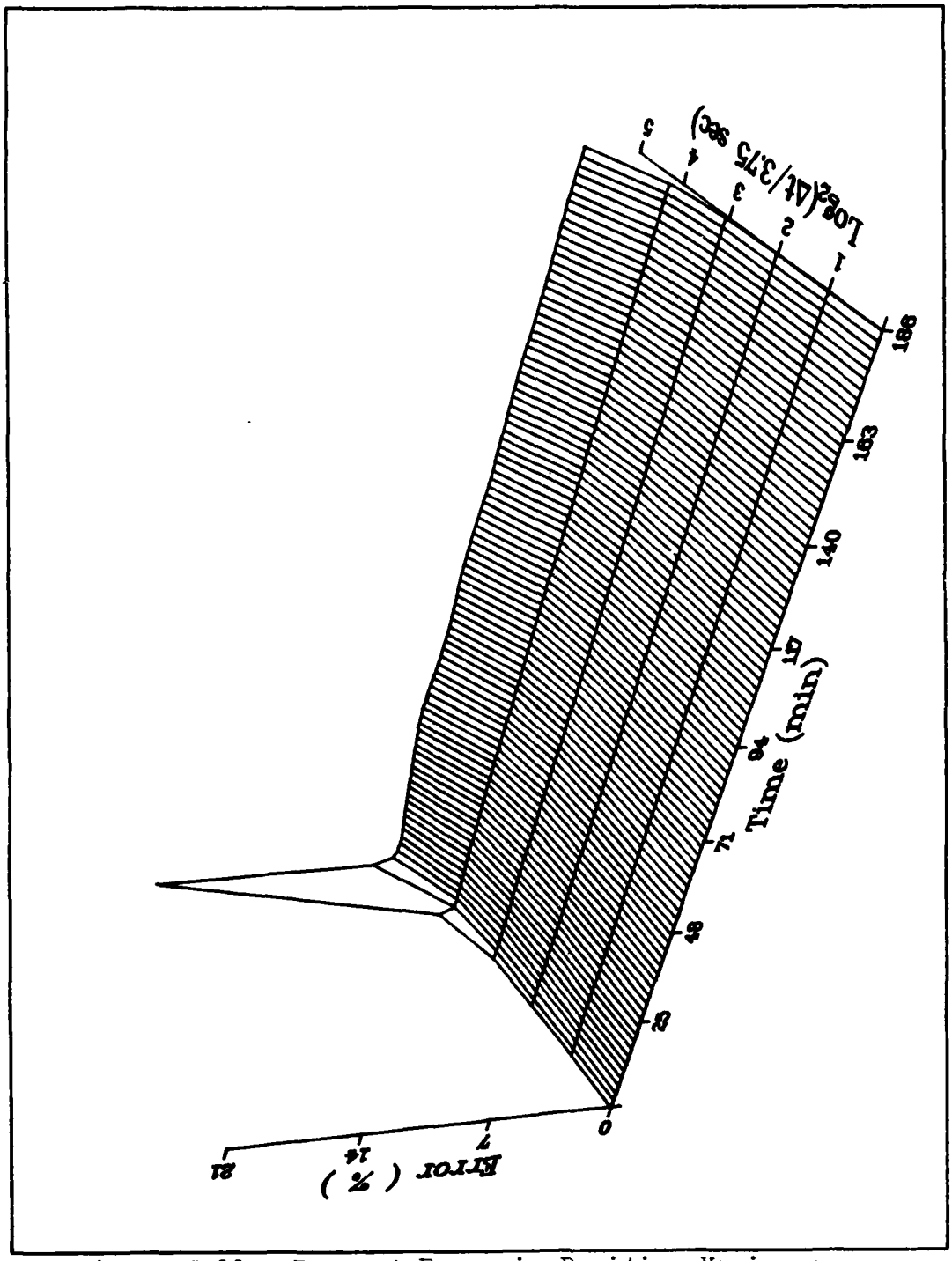

Figure C-11. Percent Error in Position-Variance, Undamped Schuler Case, Trapezoidal Algorithm

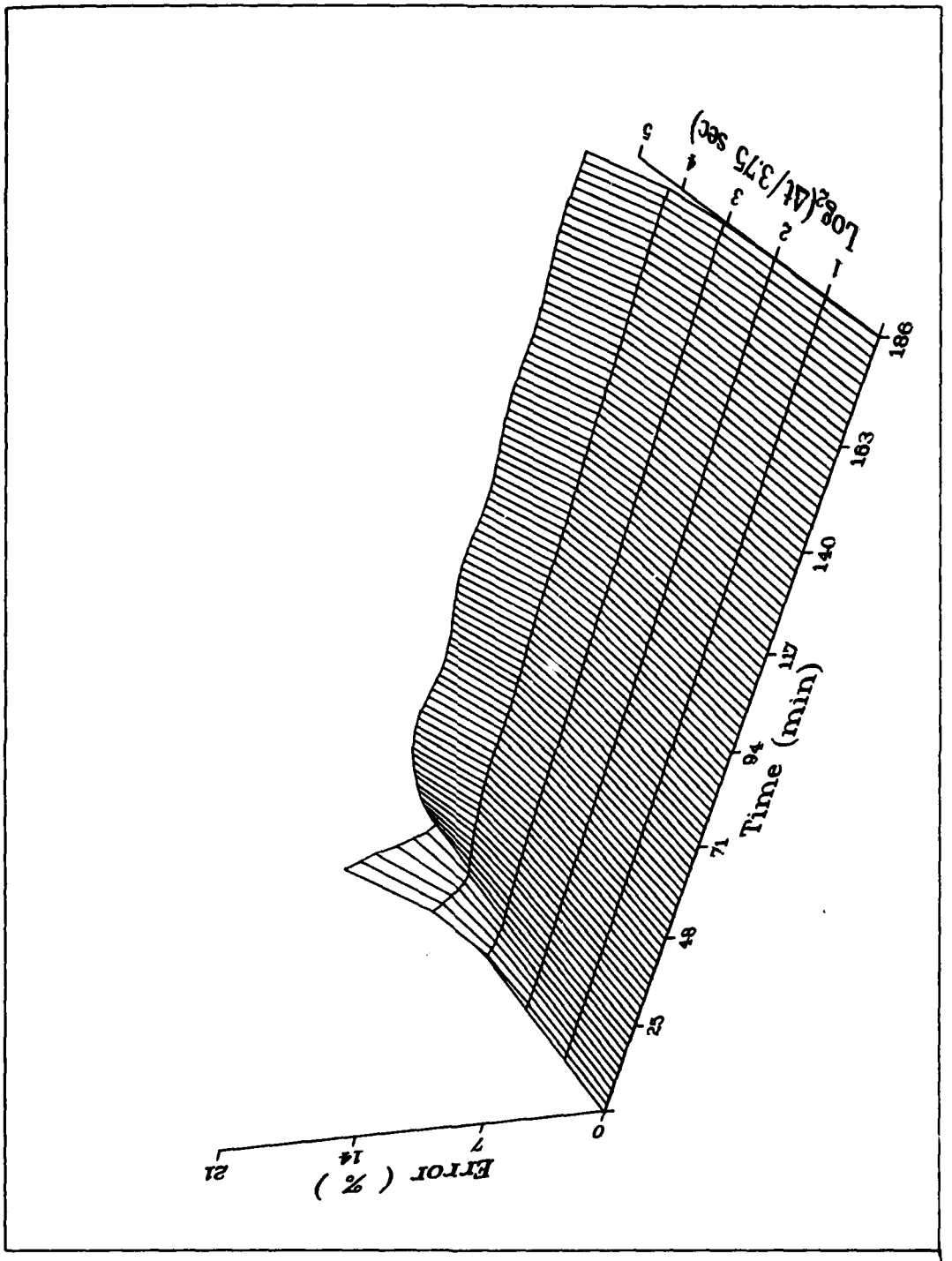

Figure C-12. Percent Error in Position Variance, Undamped Schuler Case, Nested Integrals Algorithm

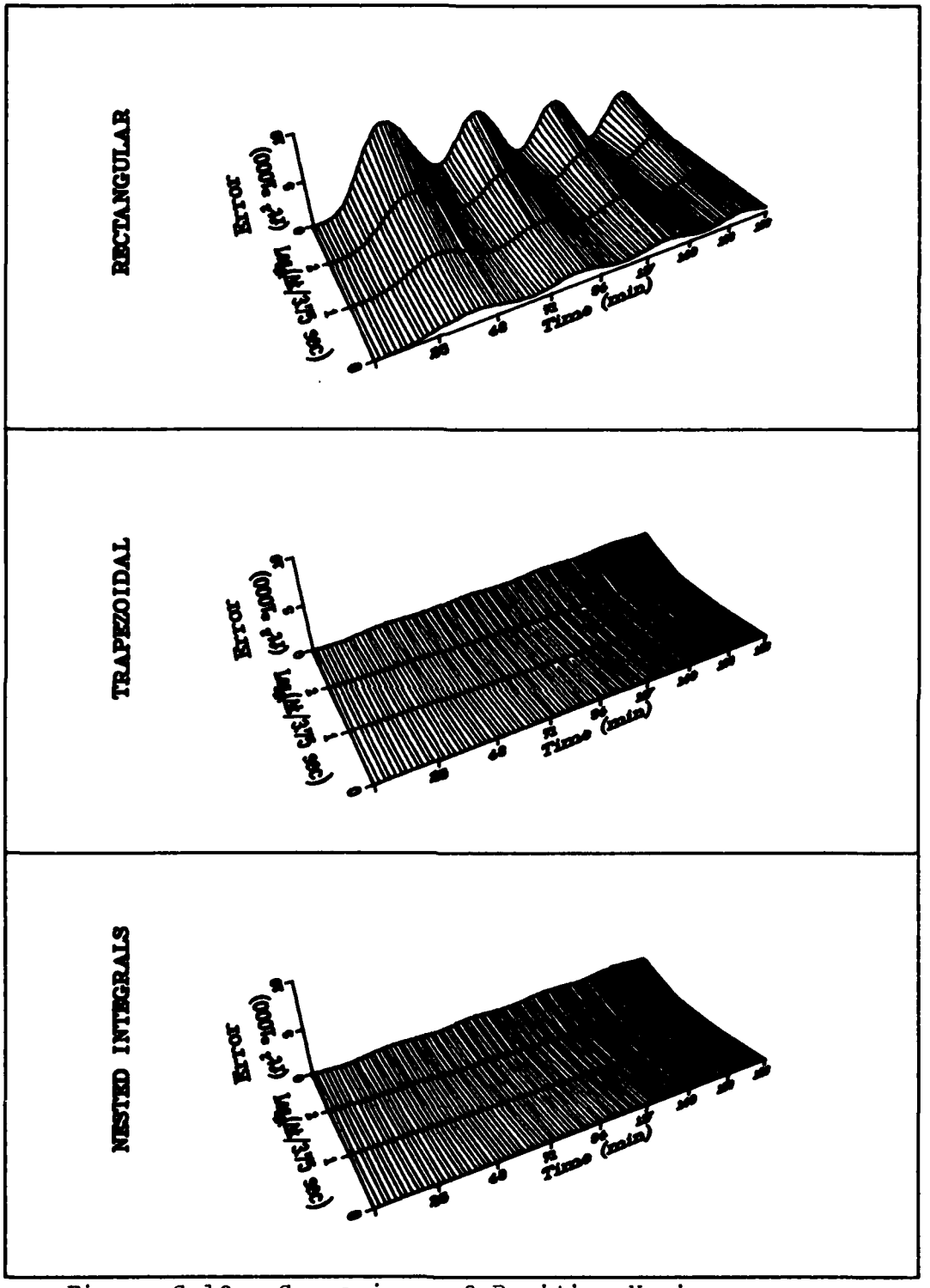

Figure C-13. Comparison of Position Variance Errors for the Undamped Schuler Case

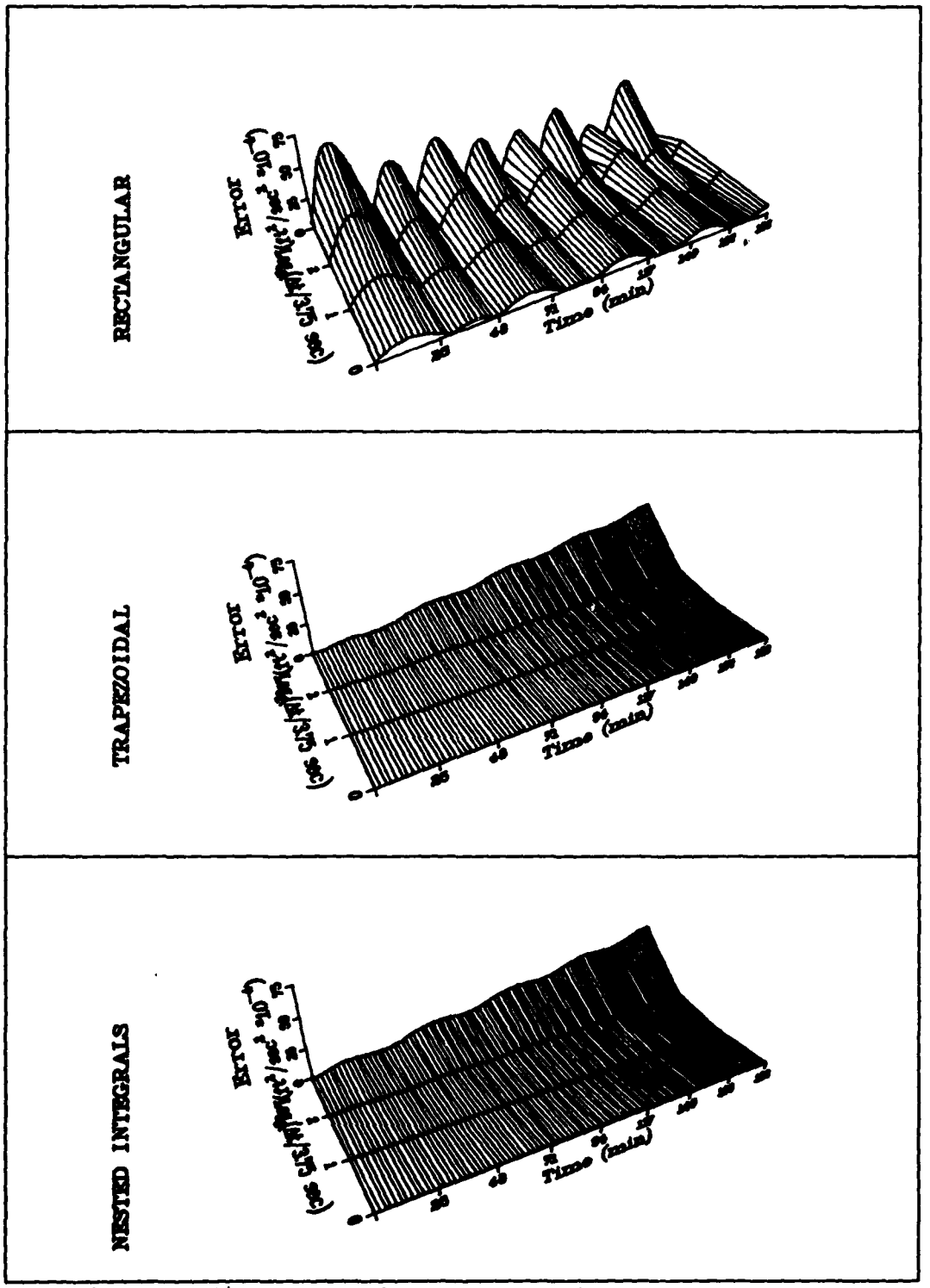

Figure C-14. Comparison of Velocity Variance Errors for the Undamped Schuler Case

APPENDIX D

Damped Schuler Case, Graphical Results

This appendix presents the graphical results for the Nested Integral algorithm on the damped Schuler loop case discussed in Section III.

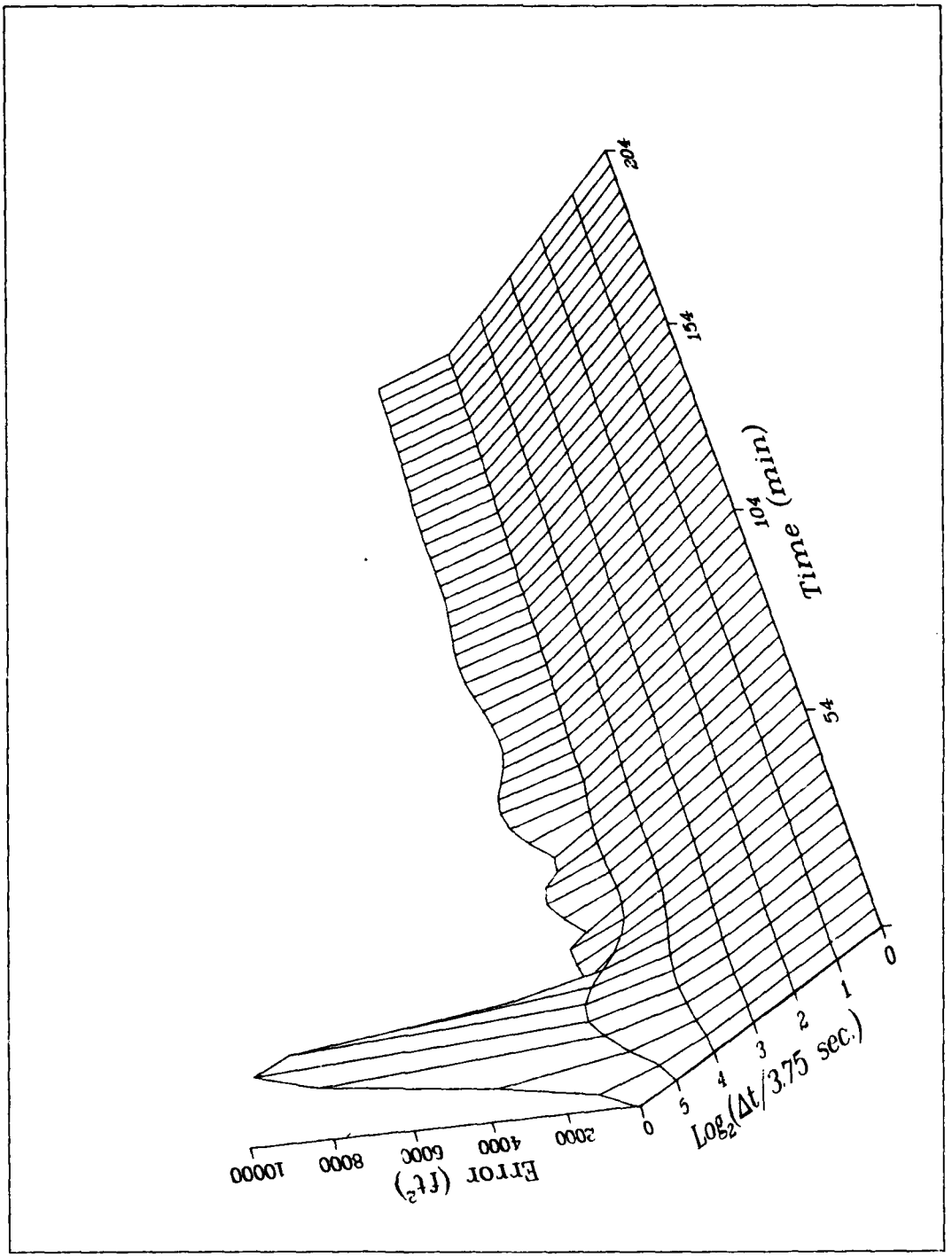

Figure D-1. Error in Position Variance, Damped Schuler Case

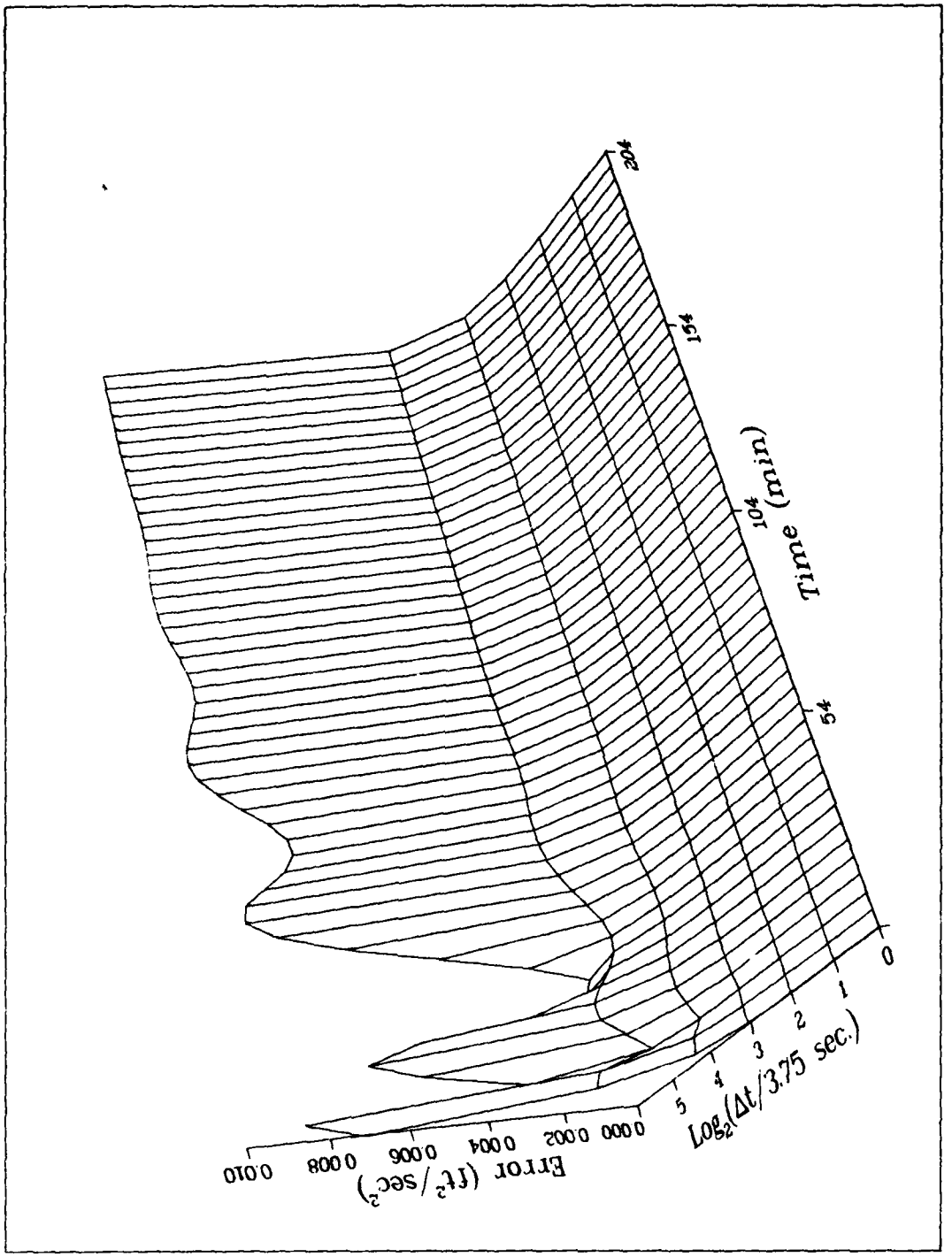

Figure D-2. Error in Velocity Variance, Damped Schuler Case

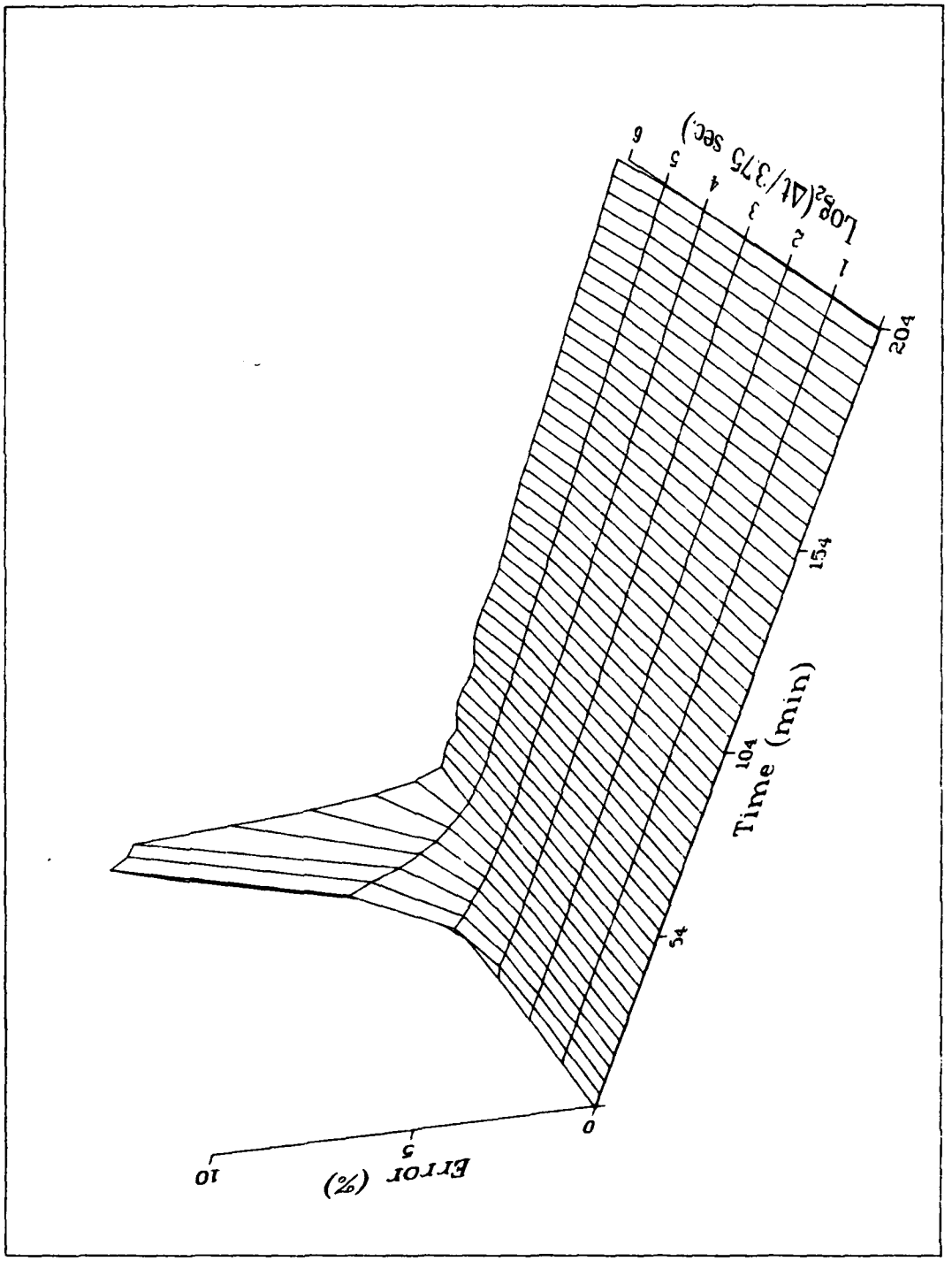

Figure D-3. Percent Error in Position Variance, Damped Schuler Case

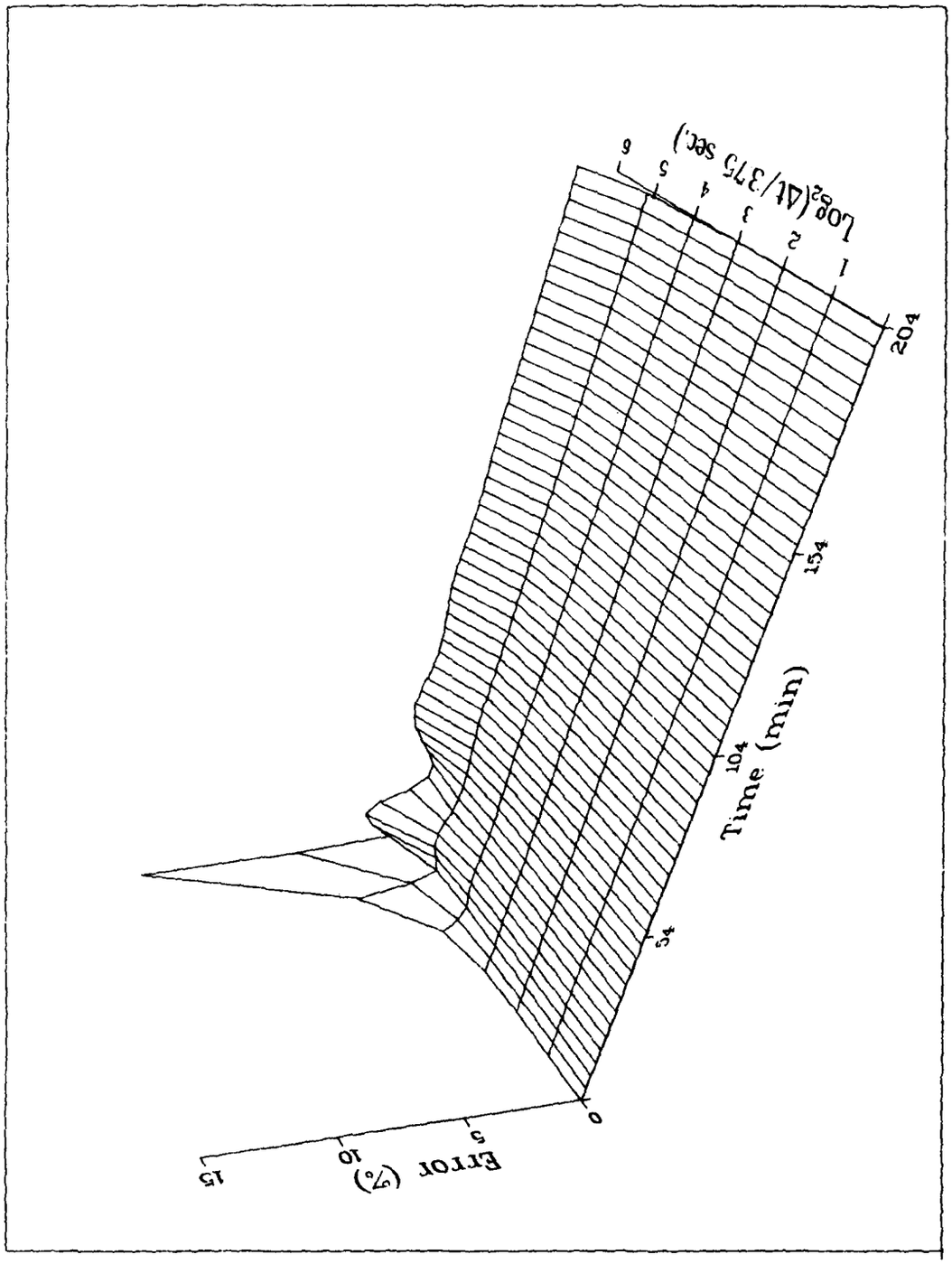

Figure D-4. Percent Error in Velocity Variance, Damped Schuler Case

APPENDIX E

Modified Widnall-Grundy Inertial Navigation Error Propagation Model

The Widnall-Grundy inertial navigation error propagation model [Ref 9:26-27] is used in several examples in this study. A modification of the vertical channel feedback is made to simulate a damped vertical channel. This appendix presents the specific equations used to model the F-matrix.

The nine error state vector elements are defined in Section IV. The following additional terms are defined for use in this appendix.

ϕ ~ design mission latitude
r ~ design mission radius magnitude
g ~ magnitude of gravity vector
e,n,z ~ subscripts indicate east, north, or vertical component respectively
v_e, v_n, v_z ~ earth relative velocity
f_e, f_n, f_z ~ specific force
ω_{ie} earth rotation rate

The following computations are required to form the F-matrix:

$$\Omega_n = \omega_{ie} \cos \phi \qquad \text{(E-1)}$$

$$\Omega_z = \omega_{ie} \sin \phi \qquad \text{(E-2)}$$

Components of local level, fixed azimuth platform angular velocity with respect to the east-north-up frame are

$$\rho_e = -v_n/r \tag{E-3}$$

$$\rho_n = v_e/r \tag{E-4}$$

$$\rho_z = v_e \tan \phi/r \tag{E-5}$$

And components of angular rate with respect to inertial space are

$$\omega_e = \rho_e \tag{E-6}$$

$$\omega_n = \rho_n + \Omega_n \tag{E-7}$$

$$\omega_z = \rho_z + \Omega_z \tag{E-8}$$

For later reference, also, define

$$k_z = v_z/r \tag{E-9}$$

Let F_{ij} represent an element of F. All elements of F are zero except the following 40 elements:

$$F_{12} = \rho_z/\cos \phi \tag{E-10}$$

$$F_{13} = -\rho_n/r \cos \phi \tag{E-11}$$

$$F_{14} = 1/r \cos \phi \tag{E-12}$$

$$F_{23} = \rho_e/r \tag{E-13}$$

$$F_{25} = 1/r \tag{E-14}$$

$$F_{36} = 1. \tag{E-15}$$

$$F_{42} = 2(\Omega_n v_n + \Omega_z v_z) + \rho_n v_n/\cos^2 \phi \tag{E-16}$$

$$F_{43} = \rho_z \rho_e + \rho_n k_z \tag{E-17}$$

$$F_{44} = -\rho_e \tan \phi - k_z \tag{E-18}$$

$$F_{45} = \omega_z + \Omega_z \tag{E-19}$$

$$F_{46} = -\omega_n - \Omega_n \tag{E-20}$$

$$F_{48} = -f_z \tag{E-21}$$

$$F_{49} = f_n \tag{E-22}$$

$$F_{52} = -v_e(2\Omega_n + \rho_n/\cos^2 \phi) \tag{E-23}$$

$$F_{53} = \rho_n \rho_z - \rho_e k_z \quad \text{(E-24)}$$

$$F_{54} = -2\omega_z \quad \text{(E-25)}$$

$$F_{55} = -k_z \quad \text{(E-26)}$$

$$F_{56} = \rho_e \quad \text{(E-27)}$$

$$F_{57} = f_z \quad \text{(E-28)}$$

$$F_{59} = -f_e \quad \text{(E-29)}$$

$$F_{62} = -2\Omega_z v_e \quad \text{(E-30)}$$

$$F_{63} = -(g/r + \rho_n^2 + \rho_e^2) \quad \text{(E-31)}$$

$$F_{64} = 2\omega_n \quad \text{(E-32)}$$

$$F_{65} = -2\rho_e \quad \text{(E-33)}$$

$$F_{67} = -f_n \quad \text{(E-34)}$$

$$F_{68} = f_e \quad \text{(E-35)}$$

$$F_{73} = -\rho_e/r \quad \text{(E-36)}$$

$$F_{75} = -1/r \quad \text{(E-37)}$$

$$F_{78} = \omega_z \quad \text{(E-38)}$$

$$F_{79} = -\omega_n \quad \text{(E-39)}$$

$$F_{82} = -\Omega_z \quad \text{(E-40)}$$

$$F_{83} = -\rho_n/r \quad \text{(E-41)}$$

$$F_{84} = 1/r \quad \text{(E-42)}$$

$$F_{87} = -\omega_z \quad \text{(E-43)}$$

$$F_{89} = \omega_e \quad \text{(E-44)}$$

$$F_{92} = \omega_n + \rho_z \tan \phi \quad \text{(E-45)}$$

$$F_{93} = -\rho_z/r \quad \text{(E-46)}$$

$$F_{94} = \tan \phi/r \quad \text{(E-47)}$$

$$F_{97} = \omega_n \quad \text{(E-48)}$$

$$F_{98} = -\omega_e \quad \text{(E-49)}$$

The F_{63} term above gives the coupling of δh into $\delta \dot{v}_z$. In an uncompensated system, this element is predominated by a $+2g/r$ term which accounts for the vertical loop instability. For this study, altimeter feedback was simply modeled [Ref 8] as a $-g/r$ term. This modification represents a stable vertical loop.

In summary this appendix provides the equations that form an F-matrix for the example navigation studies. Equations (E-1) through (E-49) supply all the non-zero elements for the Widnall-Grundy navigation error state propagation model with a modification to simulate a damped vertical channel. The required inputs to these equations are ω_{ie}, g, r, ϕ, v_e, v_n, v_z, f_e, f_n, and f_z. These data come primarily from the trajectory model and yield F(t) for equation (3).

APPENDIX F

Linear State Space Gravity Disturbance Model

A linear state space gravity disturbance model and its associated correlation function are required for several of the examples. An eight-state shaping filter driven by three independent white, gaussian noise sources* has been developed [Ref 19] and gives all three gravity disturbance terms needed for these studies. The statistical interrelationships of this model are consistent with gravitational field theory except for minor approximations. This appendix presents the equations required for both linear state space and Nested Integral covariance analysis. An overall input-output list is provided in the summary.

Figure F-1 shows the shaping filter block diagram and output matrix with

$$\underline{q}(t) = \begin{Bmatrix} q_1(t) \\ q_2(t) \\ q_3(t) \end{Bmatrix} \tag{F-1}$$

Recall

$$\mathcal{E}[\underline{q}(t)\ \underline{q}^T(p)] = Q_g(t)\ \delta(p-t) \tag{22}$$

The noise strengths and correlation parameter for this model were selected to match an empirical anomaly correlation function [Ref 19]:

$$Q_g(t) = \frac{2\beta^3\ \sigma_g^2}{g^2} \begin{bmatrix} 1 & 0 & 0 \\ 0 & 4 & 0 \\ 0 & 0 & 20 \end{bmatrix} \tag{F-2}$$

* This model is sometimes referred to as "third order" due to the three levels of integration separating noise sources from outputs. This structure forms a third order Markov process.

where σ_g^2 is the anomaly variance at the flight altitude. For the studies which use this model, flight altitude and velocity were constant; therefore, neither σ_g^2 nor β are varied. Recall,

$$\beta = \frac{V}{d} \tag{85}$$

where V is the horizontal earth-relative velocity and d is the correlation parameter. Note: d is not the distance at which anomaly correlation is $1/e$ of anomaly variance. The term correlation parameter will be used with the understanding that this distance applies to the underlying model's individual feedback gains, not the resultant filter correlation distance.

The filter states in Figure F-1 are named x_{10} through x_{17}, since, in this study, x_1 through x_9 are navigation error states defined in Section IV.

$$\underline{x}_g(t) = \begin{Bmatrix} x_{10}(t) \\ \vdots \\ x_{17}(t) \end{Bmatrix} \tag{F-3}$$

The filter outputs are

τ ~ in plane deflection angle,
μ ~ transverse deflection angle,
N ~ geoidal undulation (not used here), and
Δg ~ gravity anomaly

For a flight path heading angle α, the relationship of prime, η, and meridional, ξ, deflections to the inplane-transverse pair is shown in Figure F-1. Since

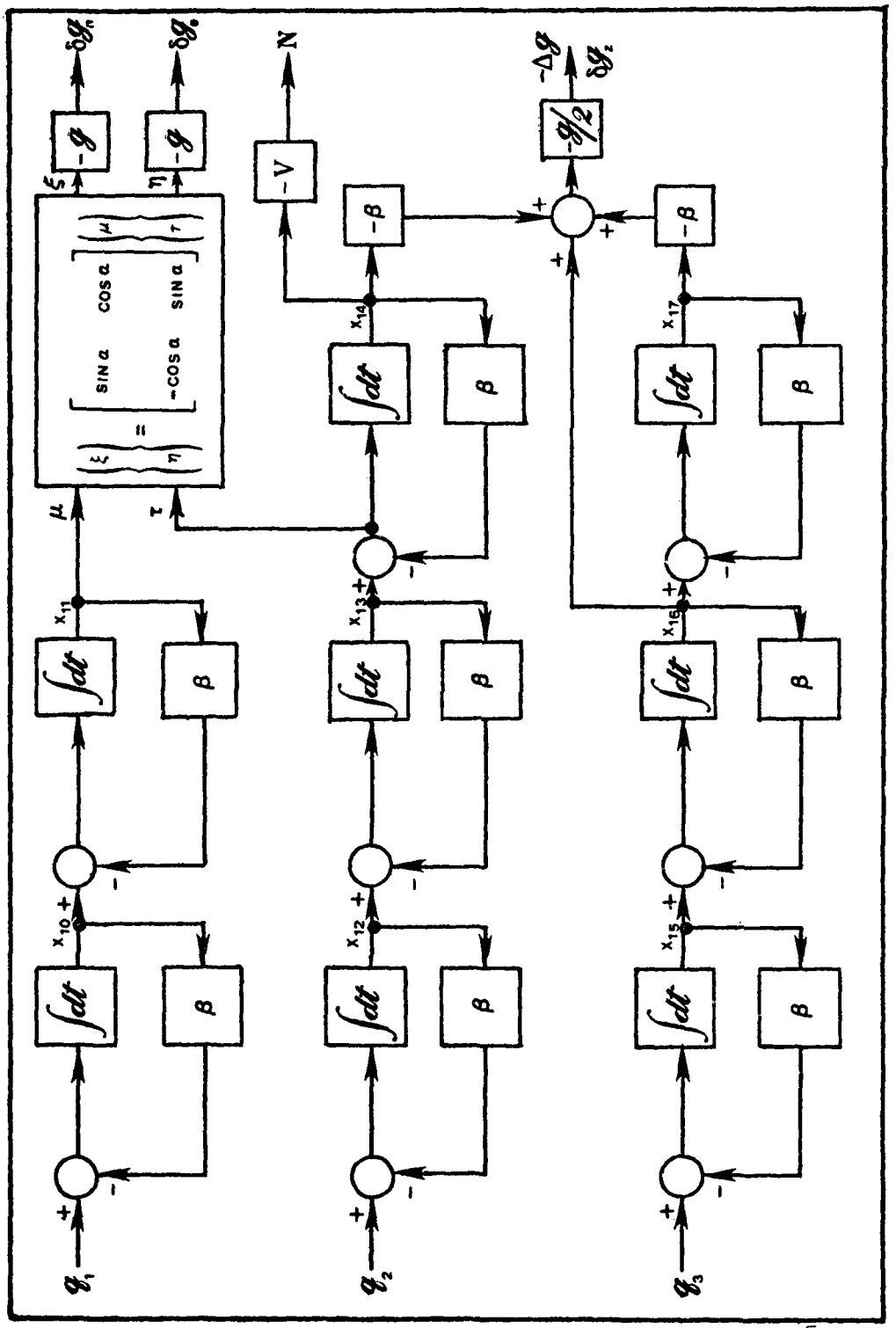

Figure F-1. Gravity Disturbance Shaping Filter [Ref 19]

$$\underline{u}(t) = \begin{Bmatrix} \delta g_e \\ \delta g_n \\ \delta g_z \end{Bmatrix} \tag{94}$$

Horizontal elements are given by using g to scale the deflection angles, and the vertical component is modeled as gravity anomaly.

$$\begin{aligned} \delta g_e &= -g\eta = g\mu \cos\alpha - g\tau \sin\alpha \\ &= g \cos\alpha \; x_{11} - g \sin\alpha(x_{13}-\beta x_{14}) \end{aligned} \tag{F-4}$$

$$\begin{aligned} \delta g_n &= -g\xi = -g\mu \sin\alpha - g\tau \cos\alpha \\ &= -g \sin\alpha \; x_{11} - g \cos\alpha(x_{13}-\beta x_{14}) \end{aligned} \tag{F-5}$$

$$\delta g_z = -\Delta g = -g/2(x_{16}-\beta x_{14}-\beta x_{17}) \tag{F-6}$$

From this, the output matrix for (21) and (25) is

$$C_g(t) = \begin{bmatrix} 0 & g\cos\alpha & 0 & -g\sin\alpha & \beta g \sin\alpha & 0 & 0 & 0 \\ 0 & -g\sin\alpha & 0 & -g\cos\alpha & \beta g \cos\alpha & 0 & 0 & 0 \\ 0 & 0 & 0 & 0 & \beta g/2 & 0 & -g/2 & \beta g/2 \end{bmatrix} \tag{F-7}$$

Since the gravity disturbance process does not begin at t_o, the filter is modeled at steady state. P_g is zero at steady state which yields

$$P_g(t) = \mathcal{E}[\underline{x}_g \underline{x}_g^T] = \left[\begin{array}{c:c:c} P_\mu & 0 & 0 \\ \hdashline 0 & P_\tau & 0 \\ \hdashline 0 & 0 & 5P_\tau \end{array}\right] \tag{F-8}$$

where

$$P_\mu = \frac{\sigma_g^2}{2g^2} \begin{bmatrix} 2\beta^2 & \beta \\ \beta & 1 \end{bmatrix} \tag{F-9}$$

and

$$P_\tau = \frac{\sigma_g^2}{2g^2} \begin{bmatrix} 8\beta^2 & 4\beta & 2 \\ 4\beta & 4 & 3/\beta \\ 2 & 3/\beta & 3/\beta^2 \end{bmatrix} \tag{F-10}$$

The shaping filter state propagation matrices, F_g and G_g of (4), can be defined from Figure (F-1) as

$$G_g = \begin{bmatrix} 1 & 0 & 0 & 0 & 0 & 0 & 0 & 0 \\ 0 & 0 & 1 & 0 & 0 & 0 & 0 & 0 \\ 0 & 0 & 0 & 0 & 0 & 1 & 0 & 0 \end{bmatrix} \tag{F-11}$$

and

$$F_g = \begin{bmatrix} F_\mu & 0 & 0 \\ 0 & F_\tau & 0 \\ 0 & 0 & F_\tau \end{bmatrix} \tag{F-12}$$

where

$$F_\mu = \begin{bmatrix} -\beta & 0 \\ 1 & -\beta \end{bmatrix} \tag{F-13}$$

and

$$F_\tau = \begin{bmatrix} -\beta & 0 & 0 \\ 1 & -\beta & 0 \\ 0 & 1 & -\beta \end{bmatrix} \tag{F-14}$$

With this last set of equations, the gravity disturbance model for linear state space analyses is complete. The resulting correlations need to be expressed for Nested Integrals. These correlations will first be expressed in the transverse-inplane-down coordinate τ-frame of Ref 18. Then, the correlation matrix function will be converted by a similarity transform to the east-north-vertical n-frame in which the navigation analysis is conducted.

Since the anomaly correlation is isotropic in heading, cross correlations of transverse deflection with the other terms are zero. This result can be deduced from Figure F-1 where μ is produced by a statistically independent shaping filter. The Q-function has the form for $\underline{r}_1$ and $\underline{r}_2$ separated by ψ central angle

$$Q^{\tau}(\underline{r}_1,\underline{r}_2) = \begin{bmatrix} \phi_{\mu\mu}^{(\psi)} & 0 & 0 \\ 0 & \phi_{\tau\tau}^{(\psi)} & \phi_{g\tau}^{(\psi)} \\ 0 & \phi_{\tau g}^{(\psi)} & \phi_{gg}^{(\psi)} \end{bmatrix} \tag{F-15}$$

where the superscript τ indicates the coordinate frame and where, for example,

$$\phi_{\mu\mu}^{(\psi)} = \mathcal{E}[\mu(\underline{r})\ \mu(\underline{r}')] \tag{F-16}$$

the expectation is over all $(\underline{r},\underline{r}')$ pairs in the sample space which are separated by ψ central angle.

For brevity define

$$M = \frac{r|\psi|}{d} \tag{116}$$

Then,

$$\phi_{\mu\mu}^{(\psi)} = \frac{\sigma_g^2}{2g^2}\ (1 + M)\ e^{-M} \tag{F-17}$$

$$\phi_{\tau\tau}^{(\psi)} = \frac{\sigma_g^2}{2g^2}\ (1 + M - M^2)\ e^{-M} \tag{F-18}$$

$$\phi_{gg}^{(\psi)} = \sigma_g^2\ (1 + M - \tfrac{1}{2}M^2)\ e^{-M} \tag{115}$$

$$\phi_{\tau g}^{(\psi)} = \frac{\sigma_g^2}{4g} \cdot \frac{r\psi}{d} \cdot (1 + M)\ e^{-M} \tag{F-19}$$

$$\phi_{g\tau}^{(\psi)} = -\phi_{\tau g}^{(\psi)} \tag{F-20}$$

$$\phi_{\tau\mu}^{(\psi)} = \phi_{\mu\tau}^{(\psi)} = \phi_{g\mu}^{(\psi)} = \phi_{\mu g}^{(\psi)} = 0 \qquad \text{(F-21)}$$

Using (116) through (F-21), $Q(r,n)$ can be formed with (F-15). This correlation function satisfies a need of Nested Integral analysis. $Q(\underline{r}_1,\underline{r}_2)$ is formed in the τ-frame, inplane-transverse-down, coordination and the navigation error terms are in an n-frame, east-north-vertical. An arbitrary vector $\underline{Z}$, expressed in n-frame coordinates is written $\underline{Z}^n$. Define $C_{\tau n}$ as the coordinate transformation matrix. Then

$$\underline{Z}^n = C_{\tau n}\,\underline{Z}^\tau \qquad \text{(F-22)}$$

Recall that heading angle α separates the north and inplane axes in the horizontal plane, but note that α, here, is not defined by $\underline{V}$.

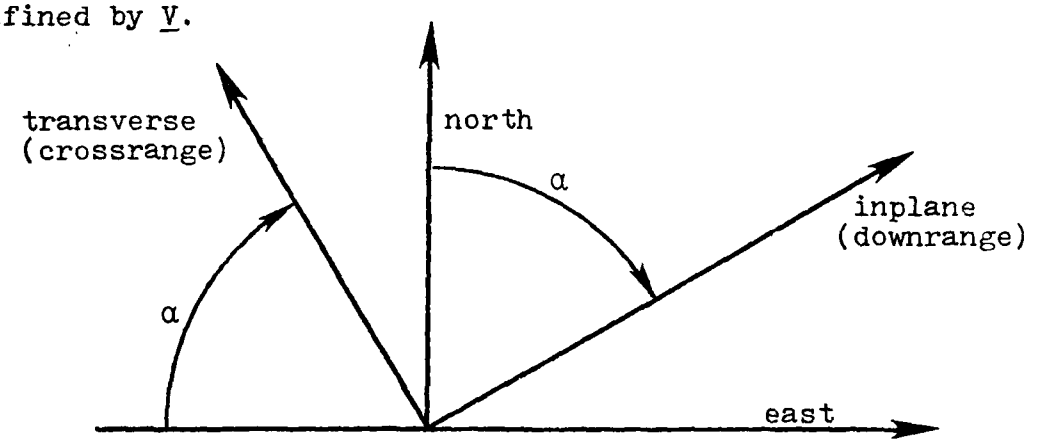

$C_{\tau n}$ is given by, paraphrasing (F-22),

$$\begin{Bmatrix} \text{east} \\ \text{north} \\ \text{vertical} \end{Bmatrix} = \begin{bmatrix} -\cos\alpha & \sin\alpha & 0 \\ \sin\alpha & \cos\alpha & 0 \\ 0 & 0 & -1 \end{bmatrix} \begin{Bmatrix} \text{transverse} \\ \text{inplane} \\ \text{down} \end{Bmatrix} \qquad \text{(F-23)}$$

Since,

$$C_{n\tau} = C_{\tau n}^{-1} = C_{\tau n}^{T} \qquad \text{(F-24)}$$

$$Q^n(\underline{r}_1,\underline{r}_2) = C_{n\tau}\, Q^\tau(\underline{r}_1,\underline{r}_2)\, C_{n\tau}{}^T \qquad \text{(F-25)}$$

This $Q(\underline{r}_1,\underline{r}_2)$, then, is the form required to interface correctly with the Widnall-Grundy navigation error model. The coordinate transformation performed here could have been performed in the G-matrix with a redefinition of $\underline{u}$ in (110) to the τ-frame rather than the present n-frame coordinates.

The heading angle, α, of (F-23) must correspond to the navigation coordinates in effect at that time. The arguments of $Q(\underline{r}_1,\underline{r}_2)$ are two positions, $\underline{r}(t_1)$ and $\underline{r}(t_2)$. The great circle arc from $\underline{r}(t_1)$ to $\underline{r}(t_2)$ has heading α_1 at the $\underline{r}(t_1)$ end and α_2 at the $r(t_2)$ end. In the Nested Integrals approach, for $t_i \le t_n$, $Q(t_n, t_i)$ evaluations are $\underline{r}(t_n)$ and $\underline{r}(t_i)$. α_n must be used since $t=t_n$ when these calculations are performed in these evaluations. If position coordinates are given in longitude λ, latitude ϕ, and altitude h, the heading angle needed is

$$\alpha_n = \tan^{-1}\left\{\frac{\sin(\lambda_n-\lambda_i)\cos\phi_i}{\cos\phi_i \sin\phi_n \cos(\lambda_n-\lambda_i) - \sin\phi_i \cos\phi_n}\right\} \qquad \text{(F-26)}$$

The central angle between $\underline{r}(t_i)$ and $\underline{r}(t_n)$ is

$$\psi_{in} = \cos^{-1}\left[\cos\phi_i \cos\phi_n \cos(\lambda_n-\lambda_i) - \sin\phi_i \sin\phi_n\right] \qquad \text{(F-27)}$$

These complete the requirements for Nested Integrals analysis.

In summary, this appendix has presented a previously developed [Ref 19] eight-state, linear shaping filter model for the gravity disturbance process. For the linear state

space covariance analysis method, inputs are V, d, g, σ_g^2, and α. The outputs are

$P_g(t)$ of (4) and (9) given by (F-12) through (F-14) and (85)

$G_g(t)$ of (4) and (10) given by (F-11)

$C_g(t)$ of (5) and (9) given by (F-7)

$Q_g(t)$ of (6) and (14) given by (F2)

Part of the initial condition for (14) is given as $P_g(t_o)$ in (F-8) through (F-10).

The Nested Integrals method inputs are g, d, σ_g^2, cos ϕ_n, cos ϕ_i, sin ϕ_n, sin ϕ_i, λ_i, and λ_n; the output is

$Q(\underline{r}_n, \underline{r}_i)$ in n-frame coordinates using (115), (116), and (F-17) through (F-25) where

central angle ψ_{in} is given by (F-27) and

arc heading α_n is given by (F-26).

APPENDIX G

Great Circle Flight Path

The trajectory generator is required to yield position, velocity and specific force throughout the interval of study. A general trajectory generation program [e.g., Ref 7] could be used for this purpose; however, computer resources can be conserved for this study by programming the following closed-form solutions. An input-output list is provided in the summary to this appendix.

A spherical earth of radius R_e is assumed. Two sets of earth-centered, earth-fixed coordinates facilitate the development. The a-frame is defined by x-axis through the equator where the great circle crosses while the path is moving north. The z-axis is along the north polar axis (parallel to ω_{ie}), and the y-axis, in the equatorial plane, completes the right-handed coordinate set. The b-frame has the same x-axis but the y-axis lies in the great circle plane. Figure G-1 shows this basic geometry.

The basic angles of interest in Figure G-1 are

i - the earth relative inclination of the path

λ - the longitude from x_a

ϕ - geocentric latitude

Λ - great circle, earth central angle

For brevity, time arguments are not given. The radius magnitude, r, at constant altitude, h, is

$$r = R_e + h \qquad \text{(G-1)}$$

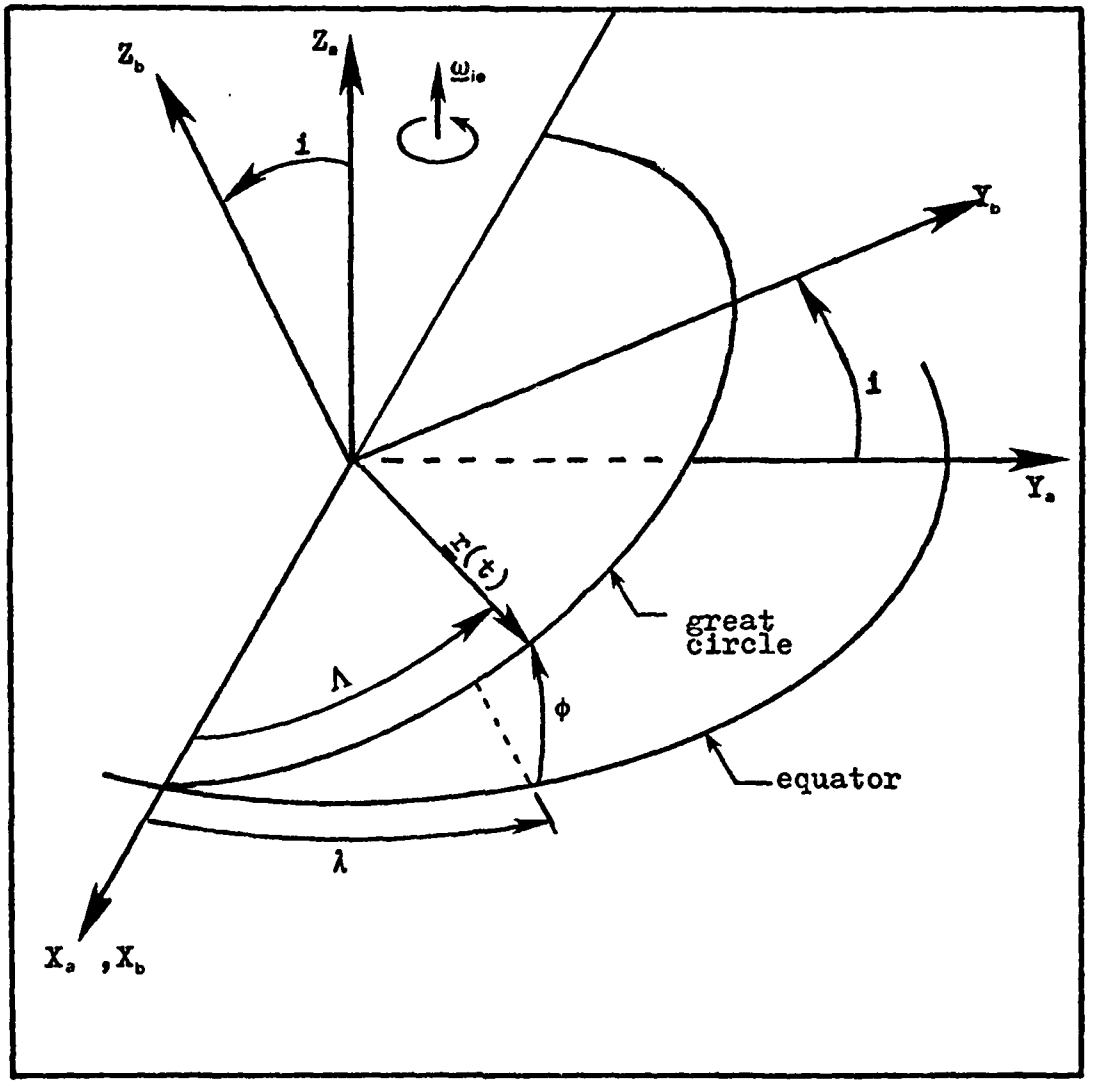

Figure G-1. Great Circle Geometry: Earth-Centered, Earth-Fixed Coordinates

Since h is constant, r is constant. Now since V and h are constant

$$\Lambda = \frac{V}{r}\,(t-t_o) + \Lambda_o \qquad \text{(G-2)}$$

The central angle $\psi(t_2, t_1)$ between $\underline{r}(t_1)$ and $\underline{r}(t_2)$ is simply

$$\psi(t_2, t_1) = |\Lambda(t_2) - \Lambda(t_1)| = \frac{V}{r}\,|\,t_2 - t_1| \qquad \text{(G-3)}$$

$$\underline{r}^b = r \begin{Bmatrix} \cos\Lambda \\ \sin\Lambda \\ 0 \end{Bmatrix} \tag{G-4}$$

The coordinate transformation from b-frame to a-frame is

$$C_{ba} = \begin{bmatrix} 1 & 0 & 0 \\ 0 & \cos i & -\sin i \\ 0 & \sin i & \cos i \end{bmatrix} \tag{G-5}$$

So,

$$\underline{r}^a = r \begin{Bmatrix} \cos\Lambda & \\ \cos i & \sin\Lambda \\ \sin i & \sin\Lambda \end{Bmatrix} \tag{G-6}$$

$$\lambda = \tan^{-1}(y_a/x_a) = \tan^{-1}(\cos i \ \tan\Lambda) \tag{G-7}$$

$$\cos\phi = \sqrt{x_a^2 + y_a^2}/r = \sqrt{\cos^2 + \cos^2 i \sin^2} \tag{G-8}$$

$$\sin\phi = \frac{z_a}{r} = \sin i \ \sin\Lambda \tag{G-9}$$

From Figure G-2, the heading angle α is defined. For a great circle

$$\cos i = \sin\alpha \cos\phi \tag{G-10}$$

$$\sin\alpha = \cos i/\cos\phi \tag{G-11}$$

$$\cos\alpha = \begin{cases} +\sqrt{1-\sin^2\alpha} & -90^\circ \le \Lambda \le 90^\circ \\ -\sqrt{1-\sin^2\alpha} & 90^\circ \le \Lambda \le 270^\circ \end{cases} \tag{G-12}$$

Since the velocity vector is of magnitude V and lies α radians clockwise from the north axis in the horizontal plane,

$$v_n = V \cos\alpha \tag{G-13}$$

and

$$v_e = V \sin\alpha \tag{G-14}$$

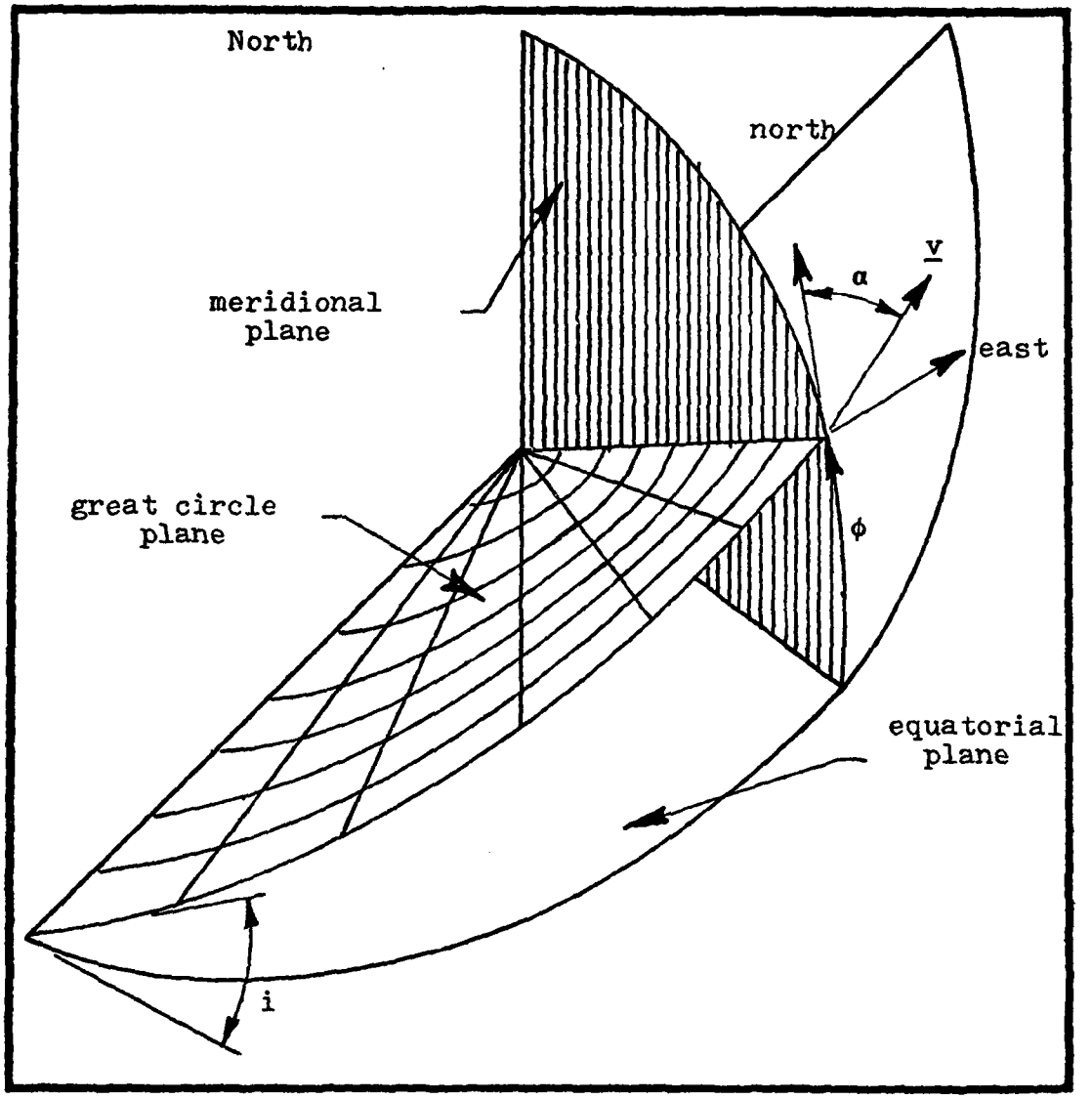

Figure G-2. Great Circle Heading Angle

Since h is constant

$$v_z = 0 \tag{G-15}$$

$$\underline{a}|_i = \underline{f} + \underline{g} + \underline{\omega}_{ie} \times \underline{\omega}_{ie} \times \underline{r} \tag{G-16a}$$

and

$$\underline{a}|_i = \underline{a}|_e + 2\underline{\omega}_{ie} \times \underline{V} + \underline{\omega}_{ie} \times \underline{\omega}_{ie} \times \underline{r} \tag{G-16b}$$

where

$\underline{V}$ = earth relative velocity

i - subscript means with respect to inertial frame

e - subscript means with respect to earth-fixed frame

$\underline{f}$ - is specific force vector

$\underline{g}$ - is gravity vector

$\underline{\omega}_{ie}$ - is earth rotation vector

Using

$$\underline{g}^n = \begin{Bmatrix} 0 \\ 0 \\ -g \end{Bmatrix} \tag{G-17}$$

$$\underline{\omega}^a_{ie} = \begin{Bmatrix} 0 \\ 0 \\ \omega_{ie} \end{Bmatrix} \tag{G-18}$$

$$\underline{f} = \dot{\underline{V}} + 2\underline{\omega}_{ie} \times \underline{V} - \underline{g} \tag{G-19}$$

$$\underline{f}^n = \begin{Bmatrix} f_e \\ f_n \\ f_z \end{Bmatrix} = \begin{Bmatrix} -2V\omega_{ie} & \sin\phi & \cos\alpha \\ 2V\omega_{ie} & \sin\phi & \sin\alpha \\ g-\frac{V^2}{r} & -2V\omega_{ie} & \cos i \end{Bmatrix} \tag{G-20}$$

Equation (G-1), (G-7), (G-8), (G-9) provide the position coordinates needed for Nested Integrals correlation evaluation. Latitude ϕ need not be found directly since only sin ϕ and cos ϕ are required for the ψ and α_n calculations. For F-matrix evaluation, these equations are supplemented by the relative velocity, (G-13) through (G-15), and specific force (G-20).

In summary, a great circle trajectory has been modeled in sufficient detail to support the covariance analyses of this study. Inputs are t, t_o R_e, h, V, Λ_o, i, ω_{ie}, and g.

Outputs are r, λ, cos ϕ, sin ϕ, $\underline{v}^n$, sin α, cos α, and $\underline{f}^n$. These outputs interface with other models and analyses as follows:

1) g, r, cos ϕ, sin ϕ, $\underline{v}^n$, and $\underline{f}^n$ for F-matrix evaluation of Appendix E
2) cos α and sin α for C(t) evaluation of (F-7) in Appendix F
3) λ, cos ϕ and sin ϕ for Nested Integrals position data to be used in α_n and ψ_{in} calculations of (F-26) and (F-27) in Appendix F.
4) h for $Q(\underline{r}_1, \underline{r}_2)$ evaluations for the Tscherning-Rapp, and the Heller-Thomas correlation models used in Sections V and VI (see also Appendices J and K).

APPENDIX H

MINOR CIRCLE FLIGHT PATH

The minor circle flight path trajectory model is presented in this appendix. Based on input data which shall be summarized later, this model provides the position, velocity and specific force information required for the covariance analyses used in this study.

The basic geometry and the earth-centered, earth-fixed coordinates (a-frame) are pictured in Figure H-1. In this figure

λ is longitude from x_a

ϕ is geocentric latitude

Λ is minor circle angle

$\underline{r}$ is radius vector

$\underline{r}_c$ is minor circle radial vector

$\underline{V}$ earth relative velocity

$\underline{r}_b$ fixed radial vector to center of minor circle

The radius magnitude is constant

$$r = R_e + h \tag{H-1}$$

where R_e is earth radius and h is the constant altitude. The minor circle constant angular velocity is

$$\omega = \frac{V}{r_c} \tag{H-2}$$

Now the minor circle angle is given by

$$\Lambda = \omega(t-t_o) + \Lambda_o \tag{H-3}$$

where t_o is initial time and Λ_o is initial angle. Note that time arguments are dropped for brevity.

Now given

$$r_c = |\underline{r}_c|$$

$$r_b = |\underline{r}_b| = \sqrt{r^2 - r_c^2} \tag{H-4}$$

and

$$\underline{r}_b^a = r_b \begin{Bmatrix} 1 \\ 0 \\ 0 \end{Bmatrix} \tag{H-5}$$

Also,

$$\underline{r}_c^a = r_c \begin{Bmatrix} 0 \\ \sin\Lambda \\ \cos\Lambda \end{Bmatrix} \tag{H-6}$$

So,

$$\underline{r}^a = \underline{r}_c^a + \underline{r}_b^a = \begin{Bmatrix} r_b \\ r_c \sin\Lambda \\ r_c \cos\Lambda \end{Bmatrix} \tag{H-7}$$

$$\underline{v}^a = r_c\dot{\Lambda}\begin{Bmatrix} 0 \\ \cos\Lambda \\ -\sin\Lambda \end{Bmatrix} = V \begin{Bmatrix} 0 \\ \cos\Lambda \\ -\sin\Lambda \end{Bmatrix} \tag{H-8}$$

The coordinate transformation from the a-frame to the east-north-vertical n-frame is

$$C_{na} = \begin{bmatrix} -\sin\lambda & \cos\lambda & 0 \\ -\sin\phi\cos\lambda & -\sin\phi\sin\lambda & \cos\phi \\ \cos\phi\cos\lambda & \cos\phi\sin\lambda & \sin\phi \end{bmatrix} \tag{H-9}$$

Now, the required earth relative velocity components are given by

$$\underline{v}^n = \begin{Bmatrix} v_e \\ v_n \\ v_z \end{Bmatrix} = C_{na}\,\underline{v}^a$$

$$= V \begin{Bmatrix} \cos\Lambda & \cos\lambda \\ -\cos\Lambda & \sin\phi\sin\lambda - \sin\Lambda\cos\phi \\ \cos\Lambda & \cos\phi\sin\lambda - \sin\Lambda\sin\phi \end{Bmatrix} \tag{H-10}$$

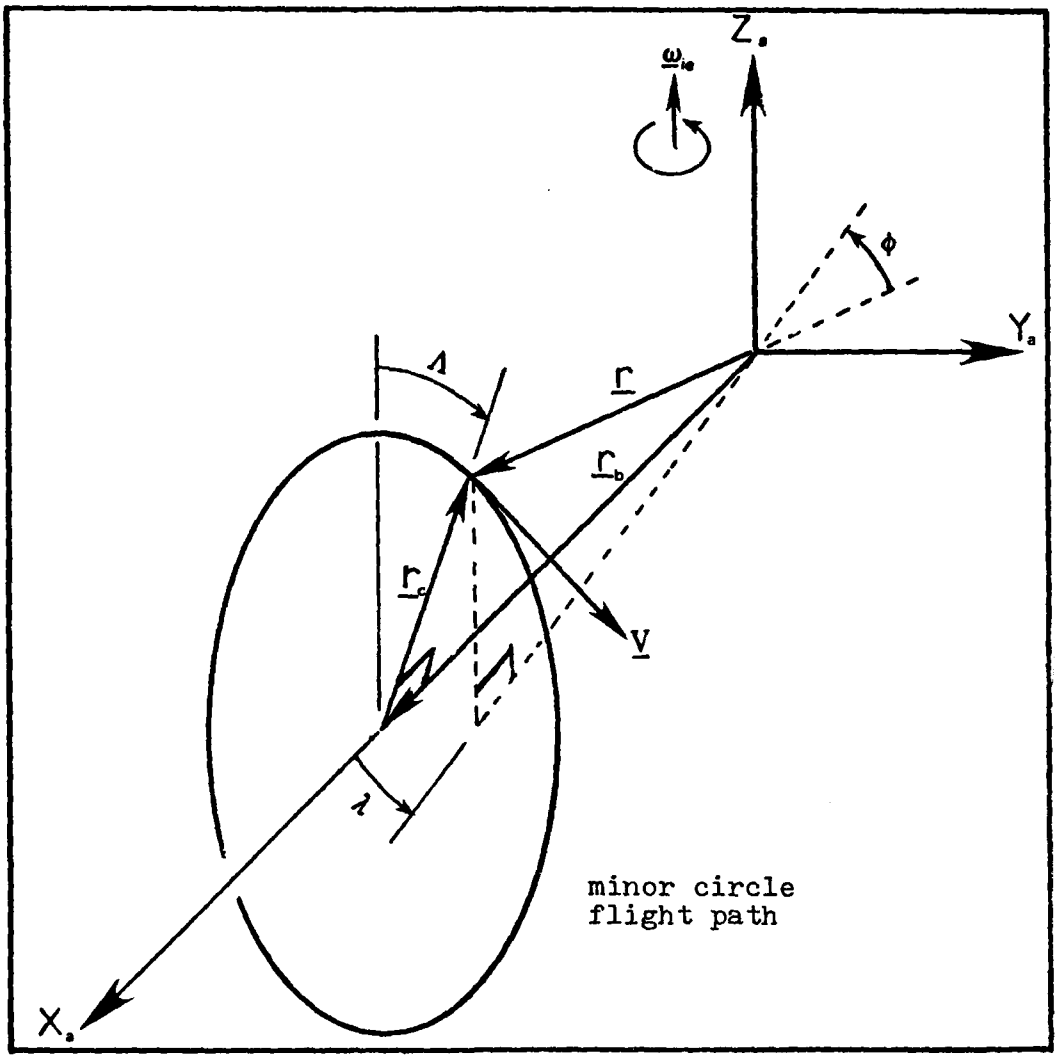

Figure H-1. Minor Circle Geometry

To express these latitude and longitude forms define

$$r_{xy} = \sqrt{x_a^2 + y_a^2} = \sqrt{r^2 + r_c^2 \cos^2 \Lambda} \qquad \text{(H-11)}$$

$$\sin \lambda = y_a / r_{xy} = r_c \sin \Lambda / r_{xy} \qquad \text{(H-12)}$$

$$\cos \lambda = x_a / r_{xy} = r_b / r_{xy} \qquad \text{(H-13)}$$

$$\lambda = \tan^{-1} (y_a / x_a) = \tan^{-1} [r_c \sin \Lambda / r_b] \qquad \text{(H-14)}$$

$$\sin \phi = z_a/r = r_c \cos\Lambda/r \tag{H-15}$$

$$\cos \phi = r_{xy}/r \tag{H-16}$$

Substituting $\cos\Lambda$, $\sin\Lambda$, $\cos \phi$, and $\sin \phi$ back into (H-10) yields the expected

$$v_z = 0 \tag{H-17}$$

$$v_e = V\sqrt{r^2 - r_c^2}\ \cos\Lambda/r_{xy} \tag{H-18}$$

$$v_n = -V\ r \sin\Lambda/r_{xy} \tag{H-19}$$

Now specific force

$$\underline{f} = \dot{\underline{V}} + 2\underline{\omega}_{ie} \times \underline{r} - \underline{g} \tag{G-19}$$

So with

$$\underline{\omega}_{ie}^{a} = \begin{Bmatrix} 0 \\ 0 \\ \omega_{ie} \end{Bmatrix} \tag{G-18}$$

$$\underline{g}^{n} = \begin{Bmatrix} 0 \\ 0 \\ -g \end{Bmatrix} \tag{G-17}$$

$$\underline{f}^{n} = \begin{Bmatrix} f_e \\ f_n \\ f_z \end{Bmatrix} = \begin{Bmatrix} V\ \sin\Lambda(2\omega_{ie}\ r_c \cos\Lambda - \omega r_b)/r_{xy} \\ V\ r_b \cos\Lambda\ (2\omega_{ie}\ r_c \cos\Lambda - \omega r_b)/(r \cdot r_{xy}) \\ g - V(2\omega_{ie}\ r_b \cos\Lambda + V)/r \end{Bmatrix} \tag{H-20}$$

These results complete the minor circle trajectory. The required inputs are t, t_o, R_e, h, r_c, V, Λ_o, g, and ω_{ie}. The outputs are as follows: g, r, $\cos \phi$, $\sin \phi$, $\underline{v}^n$, and $\underline{f}^n$ for F-matrix calculations; α for C(t) calculation in (G-7) for linear state space covariance analysis; and $\cos \phi$, $\sin \phi$, h, and λ for Nested Integrals.

The equation, (113), for central angle presented in Section IV can be derived by using

$$\psi_{1,2} = \cos^{-1}[|\underline{r}_1 \cdot \underline{r}_2|/(r_1 r_2)] \qquad \text{(H-21)}$$

where $\underline{r}_1$ is $\underline{r}(t_1)$ and $\underline{r}_2$ is $r(t_2)$

when (H-7) is used for both $\underline{r}_1$ and $\underline{r}_2$, the result is

$$\psi_{1,2} = \cos^{-1}\left\{\frac{r^2 - r_c^2[1-\cos\{\frac{V}{r_c}(t_2-t_1)\}]}{r^2}\right\} \qquad \text{(H-22)}$$

APPENDIX I

Circular-Error-Probable Computation

The analyses performed in Sections IV through IX used a nine-state navigation error model and, therefore, produced an 81-element covariance matrix. Since this matrix is symmetric, only 45 elements need to be considered in any comparative study. In the verification study of Section IV, all 45 independent elements are presented for the great circle case comparison. Such an exhaustive comparison is rarely necessary since the primary interest is in position, and perhaps velocity, statistics. The desire for a more compact performance index can be met with some second order statistic of position.

Several alternatives are available, but circular-error-probable (CEP) is the most common. This statistic gives the horizontal-plane radius which, when centered on the mean, encompasses one-half the population. This appendix presents the method used to calculate CEP in the studies of Sections IV through IX.

CEP can be calculated by two meth ds. The entire population can be accounted for by the instructions above, or the frequency function can be integrated until the radius is found, which gives a probability of one-half. Neither the population nor the frequency function are known in general. Since the navigation error propagation is a linear process, the cases which employed the gaussian noise models

will have multidimensional gaussian distribution for the error states. In these instances, a rather straightforward method is available to estimate CEP.

The population is not known for the other cases, but the errors which drive the navigation covariance are numerous. That is, the distributed earth mass nonuniformity can be construed as millions of error sources, and the gravity disturbances are the sum of these errors. Appealing to the Central Limit Theorem [Ref 15:109], the error population is probably well-approximated by a gaussian distribution. If the gaussian distribution is used as an approximation for cases of unknown population, then the same method can be used to calculate CEP in all instances.

Of the 45 independent elements of the navigation error covariance matrix, only three are required in the CEP calculation. These elements are the latitude and longitude error covariances. The ultimate CEP answer will be in linear measure, so these angular errors must be converted to linear. The east component of position error is

$$\delta x_e = r \cos \phi \, \delta\lambda \tag{I-1}$$

and the north component is

$$\delta x_n = r \, \delta\phi \tag{I-2}$$

Let P_p be the position covariance. Then,

$$P_p = \mathscr{E}\begin{bmatrix} \delta x_e^2 & \delta x_e \delta x_n \\ \delta x_e \delta x_n & \delta x_n^2 \end{bmatrix} \tag{I-3}$$

and

$$P_p = \begin{bmatrix} r^2 \cos^2\phi & \mathcal{E}(\delta\lambda^2) & r^2 \cos\phi\, \mathcal{E}(\delta\lambda\ \delta\phi) \\ r^2 \cos\phi & \mathcal{E}(\delta\lambda\ \delta\phi) & r^2 \cdot \mathcal{E}(\delta\phi^2) \end{bmatrix} \qquad \text{(I-4)}$$

The three expectations needed to evaluate (I-4) come directly from the navigation error covariance matrix for the state vector definition used in Sections IV through IX.

For the bivariate, normal distribution described by P_p from (I-4), CEP was approximated using the following procedure [Ref 20]:

Define,

$$\sigma_e^2 = \mathcal{E}(\delta x_e^2) = r^2 \cos^2\phi\ \mathcal{E}(\delta\lambda^2) \qquad \text{(I-5)}$$

$$\sigma_n^2 = \mathcal{E}(\delta x_n^2) = r^2\ \mathcal{E}(\delta\phi^2) \qquad \text{(I-6)}$$

$$= \frac{1}{\sigma_e \sigma_n}\ \mathcal{E}(\delta x_e\ \delta x_n) = \frac{r^2 \cos\phi}{\sigma_e \sigma_n}\ \mathcal{E}(\delta\lambda\ \delta\phi) \qquad \text{(I-7)}$$

A new coordinate frame, x-y, is defined by rotating γ from the east-north frame until the correlation coefficient is zero:

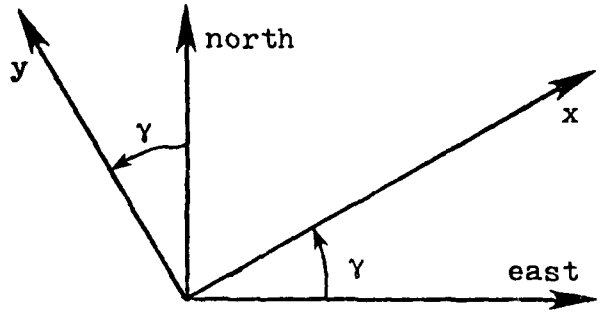

$$\mathcal{E}(\delta x\ \delta y) = 0. \qquad \text{(I-8)}$$

For this condition,

$$\gamma = \begin{cases} 45^\circ & \sigma_e = \sigma_n \\ \tan^{-1}\left[\dfrac{2\,\sigma_e\,\sigma_n}{\sigma_e^2 - \sigma_n^2}\right] & \sigma_e \neq \sigma_n \end{cases} \qquad \text{(I-9)}$$

Then,

$$\sigma_x^2 = \sigma_e^2 \cos^2\gamma + \sigma_e\sigma_n \sin 2\gamma + \sigma_n^2 \sin^2\gamma \qquad \text{(I-10)}$$

$$\sigma_y^2 = \sigma_e^2 \sin^2\gamma - \sigma_e\sigma_n \sin 2\gamma + \sigma_n^2 \cos^2\gamma \qquad \text{(I-11)}$$

Next, the maximum and minimum variances are identified.

$$\sigma_{max} = \text{Maximum } \{\sigma_x, \sigma_y\} \qquad \text{(I-12)}$$

$$\sigma_{min} = \text{Minimum } \{\sigma_x, \sigma_y\} \qquad \text{(I-13)}$$

Finally the estimate is made by

$$CEP = 0.562\ \sigma_{max} + 0.615\ \sigma_{min} \qquad \text{(I-14)}$$

In essence, (I-5) through (I-7) transform the statistic to linear measure. Next, (I-9) gives the resolvent angle with which prime variances are calculated by (I-10) and (I-11). Then, the prime variances are ordered by (I-12) and (I-13), and, finally, the CEP calculation performed by (I-14). The input data for these calculations are r, cos ϕ, $\mathcal{E}(\delta\lambda^2)$, $\mathcal{E}(\delta\phi^2)$, and $\mathcal{E}(\delta\lambda\ \delta\phi)$. The output of these computations is an estimate of circular-error-probable.

An exception to the above rule is the CEP calculation for the Nested Integrals results of Section V. The Monte Carlo results cited in Section V were based on downrange and crossrange variances. The above procedure can be used to yield the desired comparable result if (I-9) is not applied. For a downrange - crossrange resolution of the data, simply use the complement of the heading angle in place of the (I-9) result. For Section V, then, the heading angle is an additional required input.

APPENDIX J

Anomaly Degree Variance Correlation Model

The statistical analysis of navigation errors induced by gravity disturbances can be based on a disturbance correlation model as discussed in Sections I and II. Correlation models are also used in smoothing and predicting problems, and geodesists have used this approach in processing gravity measurements. These gravity measurements come in many forms (e.g., anomaly and vertical deflections), and all measurements cannot be made on a convenient surface. Therefore, some advanced statistical models for geodetic data processing have the capability to produce all the needed correlations for navigation analysis.

The Tscherning-Rapp anomaly degree variance model [Ref 21] was developed for a geodetic application. This correlation model was used in the Monte Carlo analysis [Ref 10] and is used in Sections V, VI and VII of this work. This appendix provides some background on this model and on the manner in which it was used in these navigation analyses.

The anomaly correlation function from the geodesist's viewpoint is the mean over some region of anomaly products. The ensemble of missions which gives the sample space basis for inertial navigation studies is not the geodesist's perspective. To him

$$\varphi_{gg}(\underline{r},\underline{r}') = \underset{(\underline{r},\underline{r}') \in T}{\mathcal{M}}[\Delta g(\underline{r})\ \Delta g(\underline{r}')] \qquad \text{(J-1)}$$

where

$\mathcal{M}$ is the mean operator over the set $\mathbb{T}$ which restricts $(\underline{r},\underline{r}')$ pairs (e.g., to a ψ central angle separation).

For continuous data over a spherical surface and central angle as the shift variable,

$$\mathbb{T} = \{(\underline{r},\underline{r}') | \underline{r}\cdot\underline{r}' = r^2 \cos\psi\} \tag{J-2}$$

and

$$\varphi_{gg}(\psi) = \frac{1}{4\pi} \int_{\lambda=0}^{2\pi} \int_{\phi=-\pi/2}^{\pi/2} \frac{1}{2\pi} \int_{\alpha=0}^{2\pi} \Delta g(\phi,\lambda)\, \Delta g(\phi',\lambda') \cos\phi \, d\phi \, d\lambda \, d\alpha \tag{J-3}$$

where

ϕ is geocentric latitude

λ is longitude

α is heading at $\underline{r}$ of the great circle to $\underline{r}'$.

This difference in approach in defining the correlation is artificial. In fact, the statistics defined by (J-3) are precisely the sort which "represent" the anomalous field over which the navigation mission occurs.

The form of (J-3) does define a function with both homogeneous and isotropic features (see Appendix A). The integrals over all ϕ and λ produce a global average consistent with a homogeneous assumption. The integral over all α gives a function which represents an average for all headings - isotropic assumption [Ref 4:85].

Global data is required to approximate the integrals in (J-3). Reference 21 discusses the problems encountered in estimating $\varphi_{gg}(\psi)$ from a restricted data base, but empirical correlation functions have been produced in spite of diffi-

culties. The modeling approach is to create a closed-form mathematical model which is capable of approximating this empirical correlation function. Then, one derives other needed auto- and cross-correlations from this basis (see Appendix A).

The correlation function of (J-3) can be expanded into a series of (zonal spherical harmonics) Legendre polynomials as [Ref 4:85]

$$\varphi_{gg}(\psi) = \sum_{n=0}^{\infty} c_n P_n (\cos \psi) \qquad \text{(J-4)}$$

where

$P_n(\cdot)$ is the Legendre polynomial

c_n is the associated coefficient.

The name "anomaly degree variance" comes from the observation that each c_n represents a contribution to the anomaly variance. This form can be generalized to points off the reference surface by defining

$$s = \frac{R^2}{rr'} \qquad \text{(J-5)}$$

where

R is the spherical surface used as a datum (Bjerhammer sphere [Ref 21:52]).

Whereas anomaly is not harmonic (satisfies LaPlace's Equation), the product $r \cdot \Delta g$ is harmonic [Ref 3:90]. So, the general form for (J-4) is

$$\varphi_{gg}(\psi) = \sum_{n=0}^{\infty} c_n s^{n+2} P_n(\cos \psi) \qquad \text{(J-6)}$$

Note that altitude information enters (J-6) through the radius magnitudes in (J-5). The statistics of (J-6) are therefore nonstationary with respect to altitude change, but for a fixed altitude, the statistics are stationary.

Low frequency coefficients of (J-6) can be identified using the empirical data base. The high frequency terms must at some point be approximated. All c_n are non-negative [Ref 4:85] and some are positive giving a positive definite variance

$$\sigma_g^2 = \sum_{n=0}^{\infty} c_n \qquad \text{(J-7)}$$

This equation demonstrates that c_n represents the anomaly variance contribution from the n-th degree.

One approach to modeling the anomaly correlation is to create a mathematical form which will fit the low ordered c_n's and prescribe the manner in which high frequency coefficients approach zero. Tscherning and Rapp propose five such rules in Reference 21 and develop models for four of these. These complete models include auto- and cross-correlations for anomaly, deflection angles, and geoidal undulation. Each of these models is based on an algebraic expression relating c_n to n.

The fourth rule was completely developed and programmed for computer application. That model is, also, recommended in the conclusion [Ref 21:30]

$$c_n = \begin{cases} 0 & \text{for } n \leq 2 \\ \dfrac{A(n-1)}{(n-2)(n+B)} & \text{for } n > 2 \end{cases} \qquad \text{(J-8)}$$

where A and B are constants identified to approximate the empirical correlation. Then,

$$\varphi_{gg}(\psi) = \sum_{n=3}^{\infty} \frac{A(n-1)}{(n-2)(n+B)} \left(\frac{R^2}{rr'}\right)^{n+2} P_n(\cos\psi) \qquad \text{(J-9)}$$

The values for A, B, and R were determined from empirical data and are presented in Table J-I, below.

Table J-I

Model 4 Data

Symbol	Value	Units
A	425.28	$mgal^2$
B	24 (exact)	
R	6369.8 *	km

* based on a 6371.0 km mean earth radius

Equation (J-9) is obviously not a simple, computationally efficient, closed-form mathematical expression. One property of Legendre polynomials redeems this modeling choice. Consider the triangle formed by $\underline{r}$ and $\underline{r}'$:

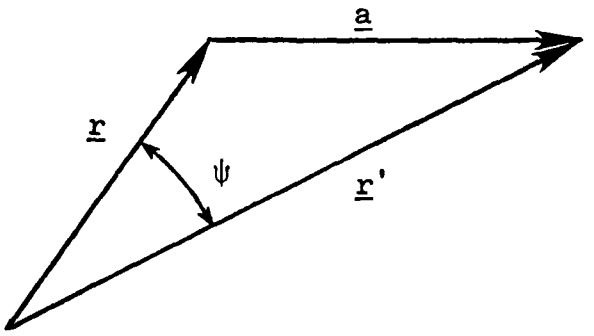

By the law of cosines

$$a^2 = r^2 + r'^2 - 2rr' \cos \psi \tag{J-10}$$

$$\frac{1}{a} = \frac{1}{\sqrt{r^2 - 2rr' + r'^2}} = \frac{1}{r\sqrt{1 - 2bs + s^2}} \tag{J-11}$$

where, for now,

$$s = r'/r \tag{J-12}$$

and

$$b = \cos \psi \tag{J-13}$$

Expanding the right hand side of (J-11) as a power series in s gives [Ref 3:32-33]

$$\frac{1}{r\sqrt{1 - 2bs + s^2}} = \frac{1}{r} \sum_{n=0}^{\infty} s^n P_n(b) \tag{J-14a}$$

$$\frac{1}{\sqrt{1 - 2s \cos \psi + s^2}} = \sum_{n=0}^{\infty} s^n P_n(\cos \psi) \tag{J-14b}$$

Now (J-9) can be written as

$$\varphi_{gg}(\psi) = s^2 A \sum_{n=0}^{\infty} \frac{(n-1)}{(n-2)(n+B)} s^n P_n(\cos \psi) \tag{J-15}$$

where

$$s = \frac{R^2}{rr'} \tag{J-16}$$

By partial fraction expansion

$$\frac{n-1}{(n-2)(n+B)} = \frac{1/(B+2)}{n-2} + \frac{(B+1)/(B+2)}{n+B} \tag{J-17}$$

So a closed-form expression for φ_{gg} can be found if

$$\sum_{n=0}^{\infty} \frac{s^n}{n+i} P_n(\cos \psi)$$

can be given in closed form using (J-14b). Expressions for these terms are derived in Reference 21 by using the fact that

$$\int_0 s^{n+i-1}\, ds = \frac{s^{n+i}}{n+i}\ ,\ n+i > 0 \qquad \text{(J-18)}$$

The derivations are presented in Reference 21, pages 30 through 46, and will not be repeated here. The above discussion shows the general approach taken.

A computer subroutine COVA was developed and documented in Reference 21, pages 85 through 89. This subroutine uses Model 4 and the data in Table J-I to produce the following correlations as a function of central angle:

a. Anomaly autocorrelation,

b. Anomaly and downrange deflection cross-correlation,

c. Anomaly and geoidal height cross-correlation,

d. Downrange deflection autocorrelation,

e. Crossrange deflection autocorrelation,

f. Downrange deflection and geoidal height cross-correlation, and

g. Geoidal height autocorrelation.

Of these a, b, d, and e are used in Nested Integrals analyses of Sections V, VI, and VII.

Since the intent of this model is to provide high frequency c_n's, provision was made to specify up to the first 300 coefficients. The closed form expression for the infinite summation is altered by removing the effects of each coefficient to be replaced and adding in the

effects of the user-supplied coefficients. This feature is used in the spherical harmonic modeling study of Section VII.

In performing the Monte Carlo study discussed in Section V, Geodynamics discovered minor errors in COVA [Ref 10:18] and these changes should be made before the subroutine is used on a trajectory with altitude variations. The subroutine used in this study was, in fact, programmed by Geodynamics. The subroutine was verified by recreating Table 10 of Reference 21.

The anomaly degree variance correlation model developed by Tscherning and Rapp offers an alternate form of statistical model for use in the analysis of navigation errors induced by gravity disturbances. The corrected subroutine COVA offers a convenient useful tool for direct use of this model in gravity model performance evaluations.

APPENDIX K

Attenuated White Noise Correlation Model

For long range missions such as intercontinental ballistic missiles, the effects of earth curvature must be considered in navigation performance analyses. The linear state space gravity disturbance correlation model is based on a tangent-plane, flat-earth approximation. Such flat-earth models are of questionable validity on long-range mission analysis. The attenuated white noise correlation model was developed to provide a round-earth alternative. This appendix provides a partial summary of this development and lists the correlation functions used in the attenuated white noise case of Section VI.

The gravity disturbance process on the earth's surface can be statistically summarized in the form of the anomalous potential correlation function (see Appendix A).

$$\phi_{TT}(\underline{r},\underline{r}') = \mathcal{E}[T(\underline{r})\ T(\underline{r}')] \qquad \text{(K-1)}$$

The anomalous potential is a spatially correlated process. A ploy used in modeling a temporally correlated process is to view the random occurrences as the output of a linear system driven by white gaussian noises. Symbolically,

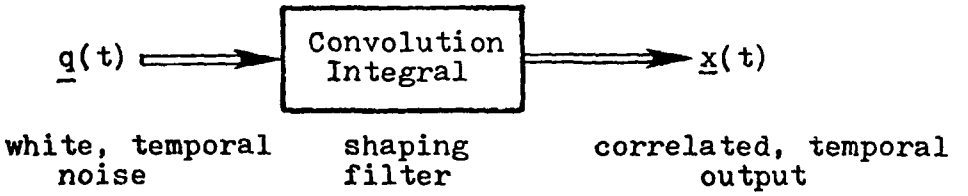

The approach used by Heller [Ref 23] in producing the attenuated white noise was to model the earth-surface anomalous potential as the upward continuation of a white noise process over a subterranean sphere [Ref 4:4-5]. Symbolically,

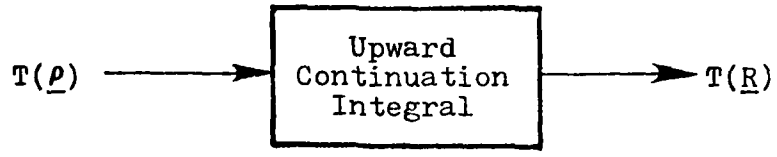

white, spatial noise — Laplace's Equation — correlated, spatial output

where

$\underline{\rho}$ is radius vector on the sphere, and

$\underline{R}$ is radius vector on the earth's surface.

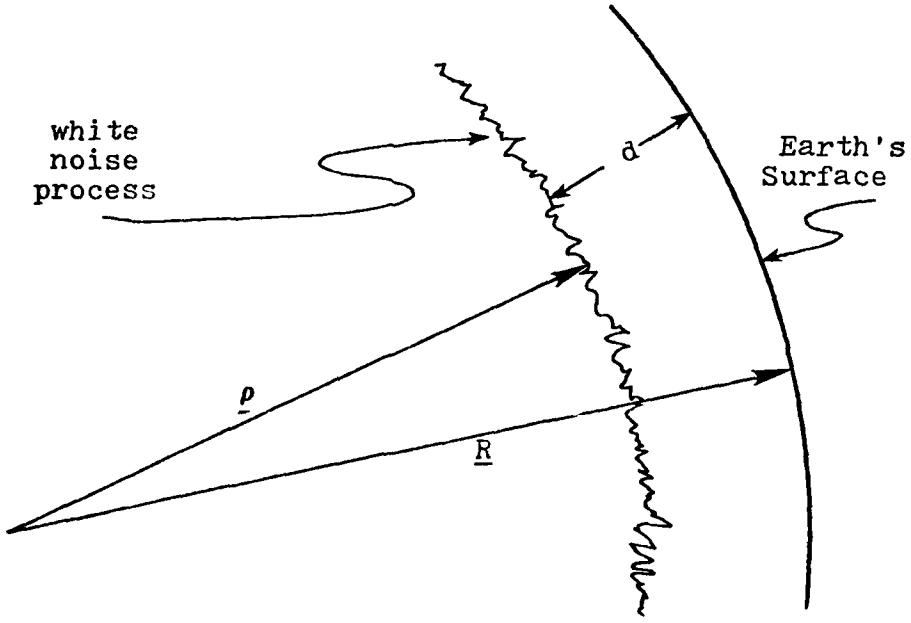

The $T(\underline{\rho})$ process is white noise on the sphere with a constant variance given by

$$\phi_{TT}(\underline{\rho},\underline{\rho}') = \phi_{TT}(\psi) = A\, f(\psi) \qquad \text{(K-2)}$$

and $f(\psi)$ is the unit impulse function on the sphere satisfying

$$2\pi\rho^2 \int_0^{\pi} f(\psi) \sin\psi \, d\psi = 1 \qquad \text{(K-3)}$$

or

$$f(\psi) = \frac{\delta(\psi)}{2\pi\rho^2 \sin\psi} \qquad \text{(K-4)}$$

The anomalous potential above the noise source is given by upward continuing (K-2). An extensive derivation is given in Appendices A through F of Reference 23. The result is

$$\phi_{TT}(\underline{r},\underline{r}') = \phi_{TT}(rr',\psi) = \frac{d^3(2R-d)^3[(rr')^2 - (R-d)^4]\,\sigma_T^2}{[R^4-(R-d)^4][(R-d)^4+(rr')^2-2rr'(R-d)^2\cos\psi]^{3/2}} \qquad \text{(K-5)}$$

where σ_T^2 is the earth surface variance level (let r=r'=R and ψ=0). A complete set of disturbance terms and auto- and cross-correlations were derived from (K-5) by methods outlined in Appendix A of this work. The key benefit of this model is that (K-5) correctly accounts for altitude changes in $\underline{r}$ or $\underline{r}'$ without requiring a new integral evaluation [Ref 23:4-6].

The depth parameter d acts in a similar manner to the feedback gain in the linear state space model. Correlation distance is directly related to d. For a d of 10 nm, the earth surface arc correlation distance is 11.15 nm. When d is 500 nm, correlation distance is 468 nm [Ref 23: pF-13].

Asymptotic forms of these round-earth correlation models were also developed in Reference 23. These asymptotic forms come from first order expansions in ψ and in d/R [Ref 23:

4-9 through 4-11]. These mathematically simpler expressions were used in the Section VI study.

The asymptotic version of (K-5) is

$$\phi_{TT}(r,r',\psi) = \frac{4d^2(2d+h+h')}{[(2d+h+h')^2 + R^2\,\psi^2]^{3/2}}\ \sigma_T^2 \qquad \text{(K-6)}$$

where

$$h = r-R$$

and

$$h' = r' - R.$$

For this study ϕ_{TT} was not required. The associated model correlations which were used are as follows:

Define σ_g^2 the earth surface gravity anomaly variance value as

$$\sigma_g^2 = \frac{3\sigma_T^2}{2d^2} \qquad \text{(K-7)}$$

Let,

$$\tau = R\psi \qquad \text{(K-8)}$$

$$A = 2d + h + h' \qquad \text{(K-9)}$$

$$B = 8d^4\sigma_g^2/(A^2+\tau^2)^{3/2} \qquad \text{(K-10)}$$

$$C = A \cdot B \qquad \text{(K-11)}$$

Then the transverse disturbance autocorrelation is

$$\phi_{\mu\mu}(r,r',\psi) = C(A^2+\tau^2) \qquad \text{(K-12)}$$

The inplane disturbance autocorrelation is

$$\phi_{\tau\tau}(r,r',\psi) = C(A^2-4\tau^2) \qquad \text{(K-13)}$$

The inplane and radial disturbances cross-correlation is

$$\phi_{\tau g}(r,r',\psi) = \tau B(4A^2-\tau^2) \qquad \text{(K-14)}$$

The radial disturbance autocorrelation is

$$\phi_{gg}(r,r',\psi) = C(2A^2-3\tau^2) \qquad \text{(K-15)}$$

Given (K-15), the modeler has two parameters, σ_g^2 and d, to use in approximating an empirical correlation function. A more flexible model can be created, however, by simply viewing the white noise shell which gave (K-15) as one of a set of statistically independent processes. With a σ_{g_i} and a d_i for each of n shells, the modeler has 2n parameters with which to build an overall correlation model: For example,

$$\phi_{gg}(r,r',\psi) = \sum_{i=1}^{n} \phi_{gg_i}(r,r',\psi) \qquad \text{(K-16)}$$

The other auto- and cross-correlations are summed in the same manner. A three-level model was proposed and parameters identified in the Reference 23 study. These parameters were used in the Section VI example and are given in Table K-I.

Table K-I

Parameters for the Three-Level Attenuated White Noise Gravity Disturbance Correlation Model

i	d_i n.m.	σ_{g_i} mgal^2	Percent of Total Variance
1	1002	175	9.6
2	179	284	15.6
3	39.7	1362	74.8

The percent of total variance is also provided in this table. Clearly the high frequency terms dominate the spectrum.

The correlations required in the Section VI study can be calculated with Table K-I data and equations (K-8) through (K-15). Other than the model parameters above ψ, h, and h' are the only required inputs. Appendix F explains the calculation of ψ and the transformation of the Q-matrix from the transverse-inplane-down coordinates to the east-north-up coordinates of the navigation error propagation model.

APPENDIX L

Gravity Disturbance Statistical Models Comparison

This appendix presents a graphical view of the auto- and cross-correlations of gravity disturbance components. The correlations are calculated using three different functional forms:

a. Linear State Space. This shaping filter model is presented in Appendix F with additional discussion in Sections IV and VI.

b. Anomaly Degree Variance. This Legendre polynomial form of representation is presented in Appendix J with additional discussion in Sections V and VI.

c. Attenuated White Noise. This model, based on a subterranean white noise anomalous potential, is presented in Appendix K with additional comments in Section VI.

The altitude level was zero for this comparison. The coordinate frame in which gravity disturbances are assumed to be expressed is a local-level, transverse-inplane-down (crossrange-downrange-down) frame used in References 19, 21, and 23. Since all three models are isotropic, the transverse component cross-correlations with both inplane and down components are zero, hence are not plotted.

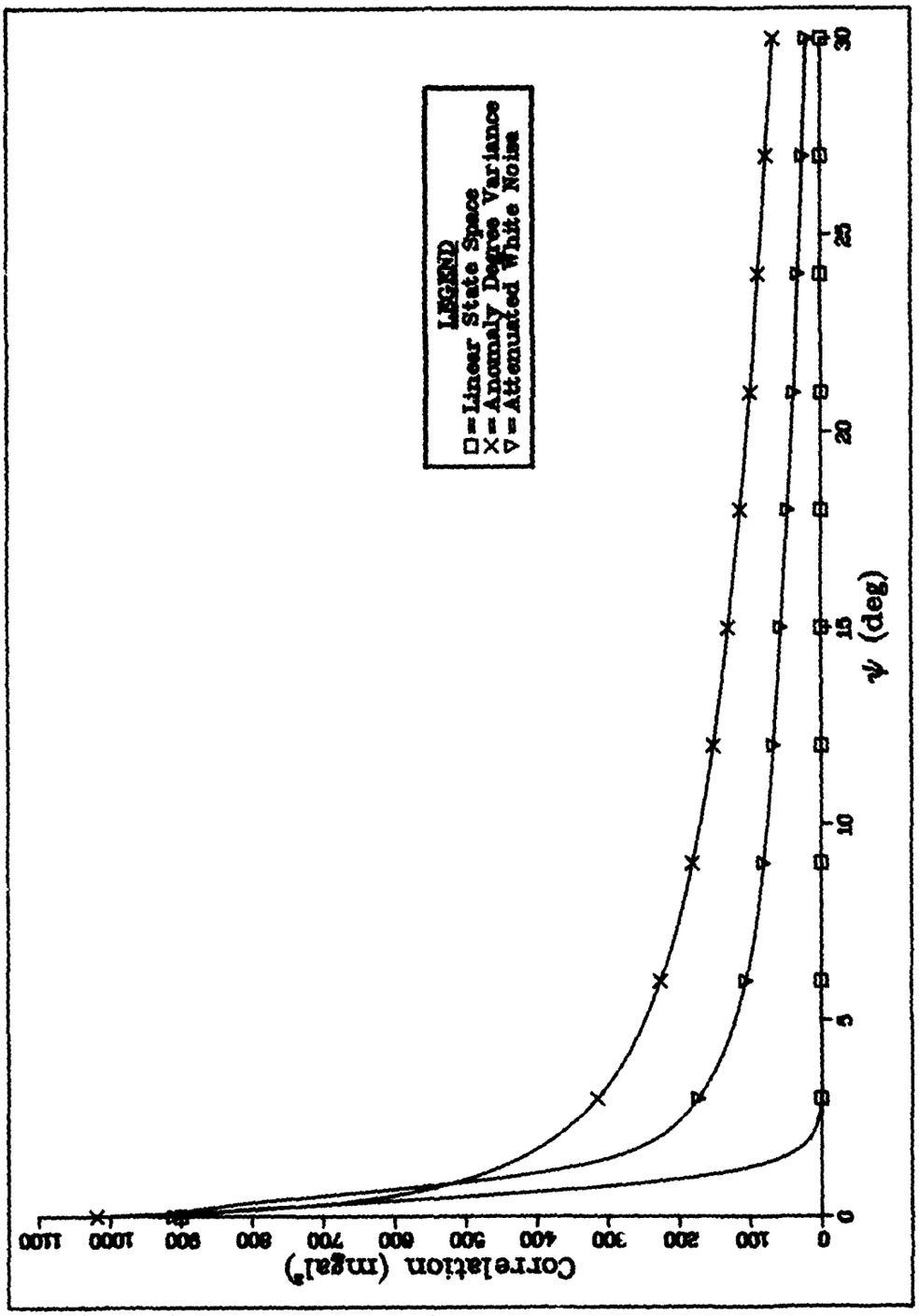

Figure L-1. Transverse (Crossrange) Gravity Disturbance Autocorrelations

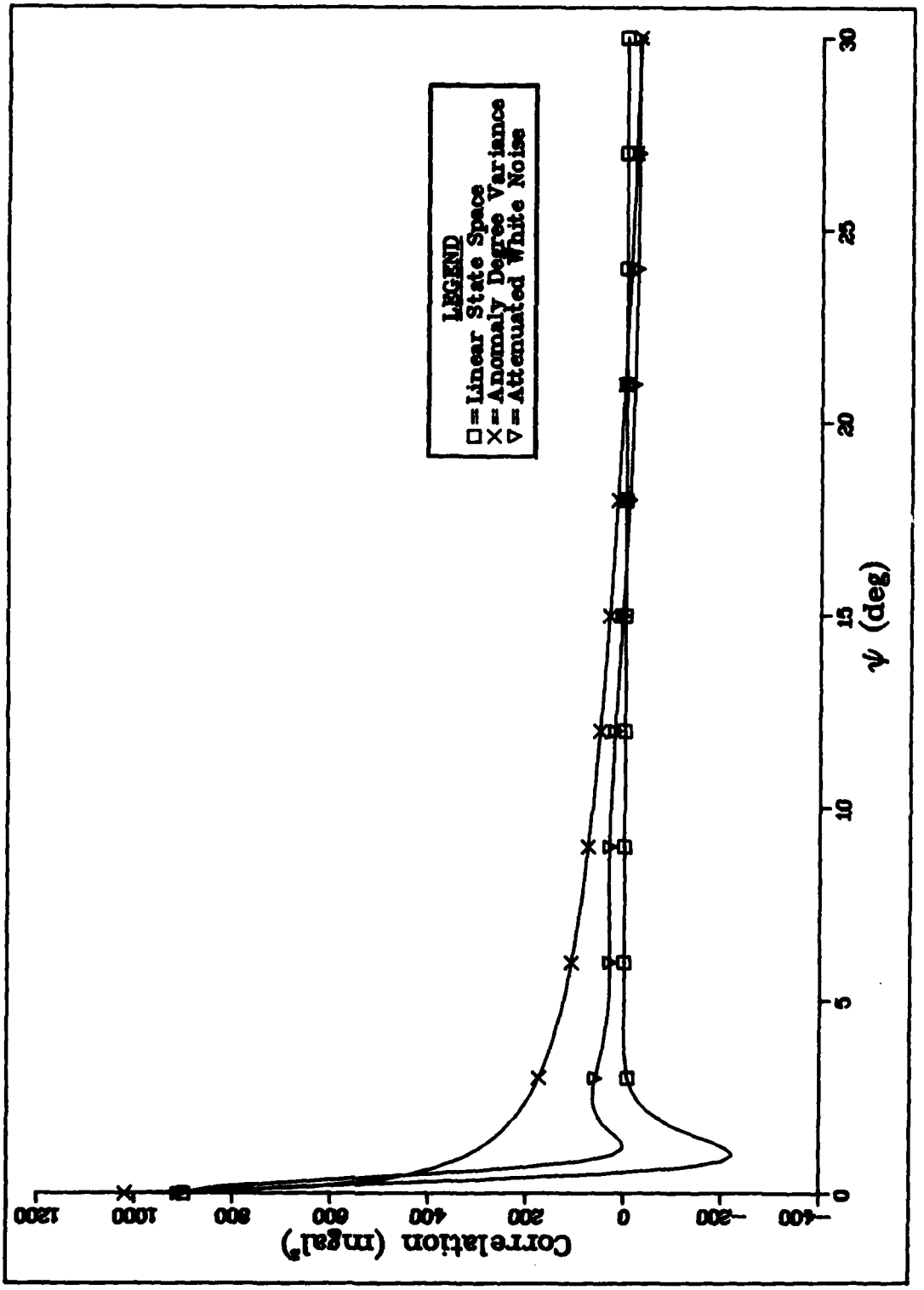

Figure L-2. Inplane (Downrange) Gravity Disturbance Autocorrelations

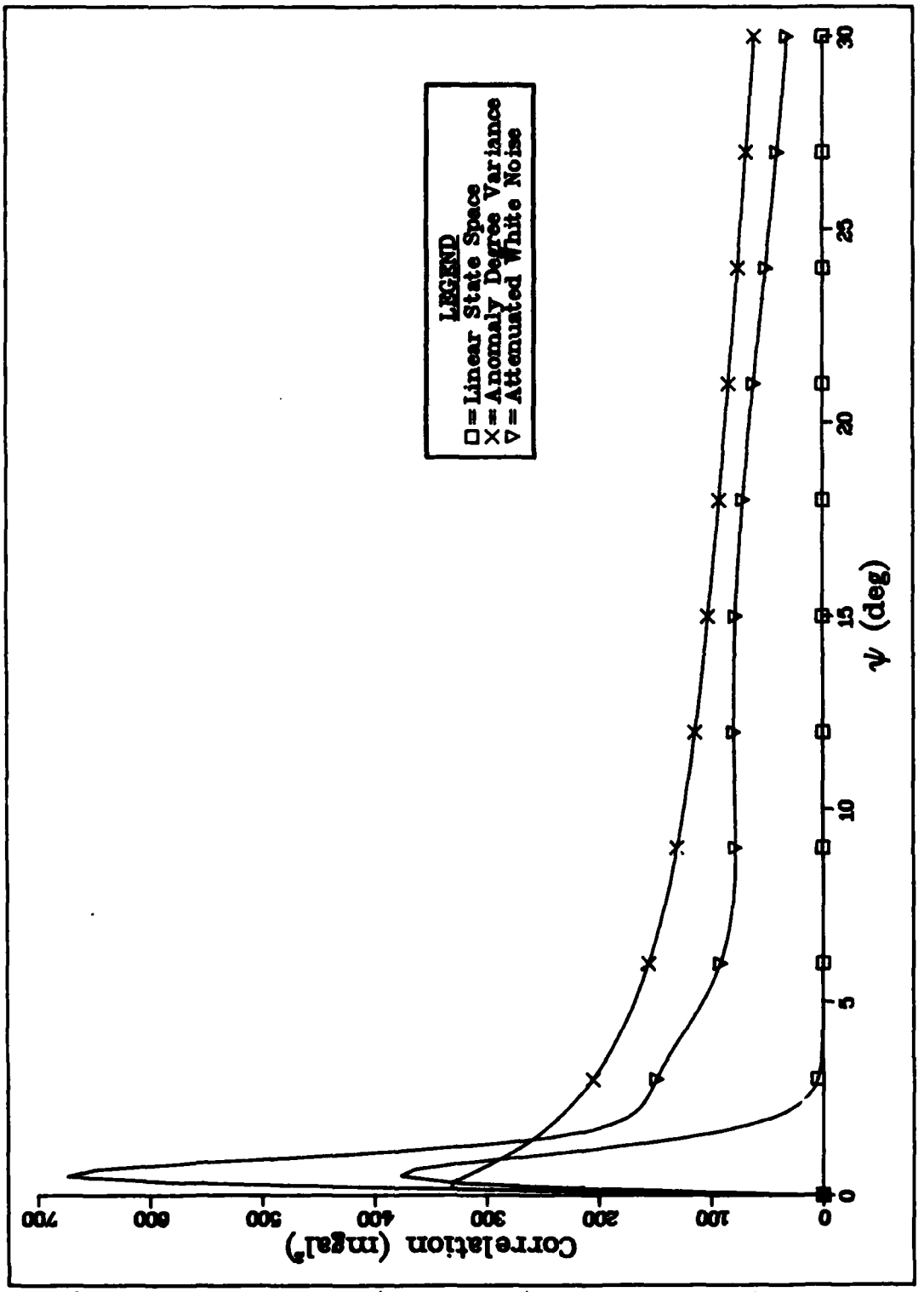

Figure L-3. Inplane (Downrange) and Down Gravity Disturbances Cross-Correlations

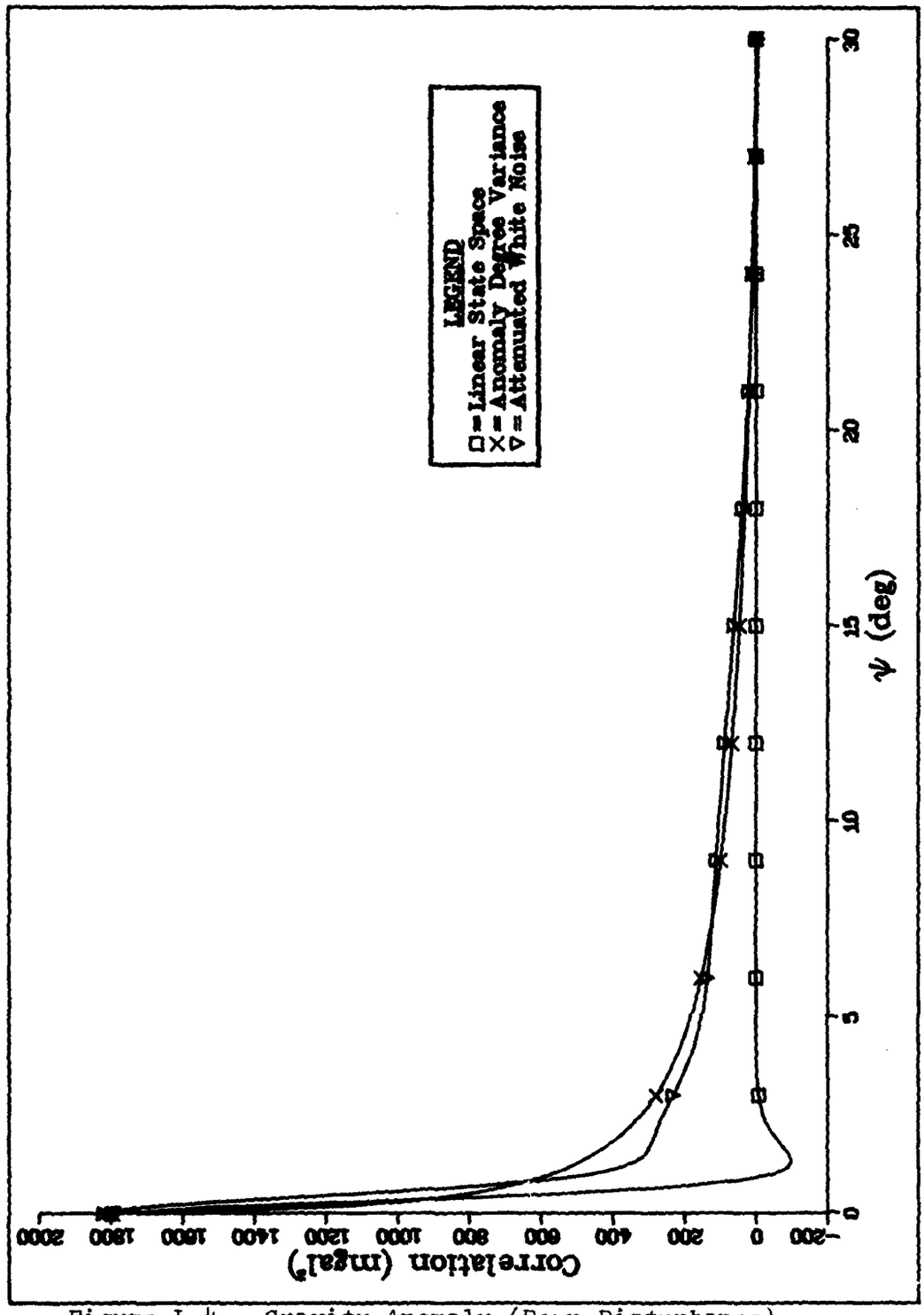

Figure L-4. Gravity Anomaly (Down Disturbance) Autocorrelations

REFERENCES

The following reference list gives the cited works for this dissertation. An additional bibliography is given in Reference 2, and Reference 12 has an extensive list of pertinent sources. Defense Documentation Center (DDC) or National Technical Information Service numbers are given for many references. Where a contractor report has been redesignated as a government laboratory report, that number is also given.

1. Kayton, M. Coordinate Frames in Inertial Navigation, (PhD dissertation), Report T-260 (two volumes), MIT Instrumentation Laboratory, Cambridge, Mass., 1960.

2. Edwards, Robert M. Gravity Modeling for Precise Terrestrial Inertial Navigation, (PhD dissertation prospectus), Air Force Institute of Technology, Wright-Patterson AFB, Ohio 45433, June 1977 (AD A042419).

3. Heiskanen, W. A. and H. Mortiz, Physical Geodesy, W. H. Freeman and Company, 1967.

4. Moritz, H. Advanced Least-Squares Methods, Report No. 175, Ohio State Univ. Dept. of Geodetic Science, Columbus, Ohio 43210, June 1972. Also, AFCRL-72-0363 (AD 749873).

5. Junkins, J. L. "Investigations of Finite-Element Representations of the Geopotential." AIAA Journal, Vol 14, No 6, pp 803-808, June 1976.

6. Bennett, M. M. and P. W. Davis, "MINUTEMAN Gravity Modeling." AIAA Paper No. 76-1960 presented at AIAA Guidance and Control Conference, San Diego, August, 1976.

7. Musick, S. H. PROFGEN - A Computer Program for Generating Flight Profiles, Report No. AFAL-TR-76-247, Air Force Avionics Laboratory, Wright-Patterson AFB, Ohio 45433, November 1976. (AD A034993)

8. Britting, K. R. Unified Error Analysis of Terrestrial Inertial Navigation (PhD dissertation). Report No. TE-42, MIT Instrumentation Laboratory, Cambridge, Mass, 1970. Alternate Source: Inertial Navigation Systems Analysis, Wiley Interscience, a Division of John Wiley & Sons, Inc., 1971.

REFERENCES

9. Widnall, W. S. and P. A. Grundy, Inertial Navigation System Error Models, Report TR-03-73, Intermetrics Inc., 701 Concord Avenue, Cambridge, Mass 02138, 11 May 1973. Also, AGSWC-TR-73-26

10. Chatfield, A. B. Initial Estimates of the Gravity Model Contributions to Strategic Missile Errors. Report No. CDR0514 (WP678u)-1, Geodynamics Corporation, Santa Barbara, CA., August 1978. Also, ASD-TR-78-30

11. Levine, S. A. and A. Gelb. "Geodetic and Geophysical Uncertainties - Fundamental Limitations on Terrestrial Inertial Navigation." AIAA Paper No. 68-847 presented at the AIAA Guidance Control, and Flight Dynamics Conference, Pasadena, Ca., 12-14 August 1968. Also see, "Effects of Deflections of the Vertical on the Performance of a Terrestrial Navigation System." AIAA Journal of Spacecraft, Vol 6, No 9, pp 978-984, September 1969.

12. Nash, R. A., Jr. and S. F. Jordan, "Statistical Geodesy - An Engineering Perspective", Proceedings of the IEEE, Vol 66, No 5, pp 532-550, May 1978.

13. Bellaire, R. G. "Statistics of the Geodetic Uncertainties Aloft", presented at the American Geophysical Union Fall Annual Meeting, San Francisco, Ca., December 1971.

14. Shampine, L. F. and M. K. Gordon, Computer Solution of Ordinary Differential Equations, W. H. Freeman and Company, San Francisco, 1975. Also see, Nikolai, P. J. and D. S. Clem, Solution of Ordinary Differential Equations on the CDC 6600/Cyber 74 Processors. Technical Memorandum AFFDL-TM-76-130-BR, Air Force Flight Dynamics Laboratory, Wright-Patterson AFB, Ohio 45433, January 1977.

15. Maybeck, P. S. Stochastic Models, Estimation, and Control - Volume I, Academic Press, 1979.

16. Hornbeck, R. W. Numerical Methods, Quantum Publishers, Inc., 1975.

17. Blum, E. K. Numerical Analysis and Computation: Theory and Practice, Addison-Wesley Publishing Company, 1972.

REFERENCES

18. Hildebrand, F. B. Introduction to Numerical Analysis, Second Edition, McGraw-Hill Book Company, 1974.

19. Heller, W. G. Models for Aided Inertial Navigation System Sensor Errors, Report No. TR-312-3, The Analytic Sciences Corporation, Six Jacob Way, Reading, Mass 01867, (Section 3.3.2 and Appendix B) 8 February 1975.

20. Musick, S. H. Computing CEP for a Bivariate Normal Distribution having a Nonzero Correlation Coefficient, Technical Memorandum, AFAL-TM-78-32, Air Force Avionics Laboratory, Wright-Patterson AFB, Ohio 45433, 27 September 1978.

21. Tscherning, C. C. and R. H. Rapp, Closed Covariance Expressions for Gravity Anomalies, Geoid Undulations, and Deflections of the Vertical by Anomaly Degree Variance Models, Report No. 208, Ohio State Univ Dept of Geodetic Science, Columbus, Ohio 43212, May 1974. Also, AFCRL-TR-74-0231 (AD 786417).

22. Thomas, S. and W. G. Heller, Efficient Estimation Techniques for Integrated Gravity Data Processing, Report No. TR-680-1, The Analytic Sciences Corp., Six Jacob Way, Reading, Mass 01867, 30 September 1976. Also, AFGL-TR-76-0232 (AD A034055).

23. Heller, W. G. Self-Consistent Statistical Geodetic and Geophysical Error Models for Land-Based ICBMs, Report No. TR-573-1, The Analytic Sciences Corp., Six Jacob Way, Reading, Mass 01867, 15 July 1977.

24. Koch, D. W. GRAVSAT/GEOPAUSE Covariance Analysis Including Geopotential Aliasing, NASA-TM-X-71057, Goddard Space Flight Center, Greenbelt, MD, October 1975 (NTIS N76-17685).

25. Long, L. T. Determination and Statistical Studies of Gravimetric Deflections, Georgia Institute of Technology, School of Geophysical Sciences, Atlanta, Ga., 30 November 1973. Also, Army Engineer Topographic Laboratories Report ETL-CR-74-8 (AD A003 271).

*U.S.Government Printing Office: 1980 — 657-084/495